Institut für
Sicherheitstechnologie
(ISTec) GmbH

Modeling of Reactive Transport in Salt and Claystone as Host Rock for a Radioactive Waste Repository by using Code TOUGHREACT- Adaptation, Development, Qualification and Comparison

Modellierung des reaktiven Stofftransports in Salz und Ton als Wirtsgesteine eines Endlagers für radioaktive Abfälle mit dem Code TOUGHREACT – Anpassung, Weiterentwicklung, Qualifizierung und Vergleich

BMWi-02E10467

H. Alkan
W. Müller

ISTec - A - 1733

November 2010

Dieser Bericht ist im Auftrag des Bundesministeriums für Wirtschaft und Technologie unter der Auftragsnummer 474421 erstellt worden

CONTENT

LIST OF THE FIGURES

LIST OF THE TABLES

ZUSAMMENFASSUNG

Das hier vorgestellte Vorhaben liefert einen qualitativen und quantitativen Beitrag zur Modellierung gekoppelter Transportprozesse in Salz- und Tonformationen unter Endlagerungsbedingungen. Ziel dieser Arbeiten ist es, das Verständnis der Wechselwirkungen bei der gekoppelten Modellierung von hydraulischen, thermischen, mechanischen und chemischen Prozessen zu vertiefen im Hinblick auf den reaktiven Stofftransport unter hoch-salinaren Bedingungen. Da mit dem Code TOUGHREACT in voraus gegangenen Studien umfangreiche positive Erfahrungen erzielt wurden, wurde er für die numerischen Anwendungen ausgewählt. Es handelt sich dabei um einen ausgereiften, validierten und vielfach angewandten Code für unterschiedliche Modellierungsfälle.

Als Ausgangspunkt der Untersuchungen und zur Dokumentation des Standes von Wissenschaft und Technik wird vorab eine detaillierte Literaturübersicht bereitgestellt.

Die Sicherheitsanalyse eines Endlagers muss die Analyse der Wirksamkeit verschiedener Barrieren einschließen, die zur Isolation der Abfälle von Wasser (Grundwasser, Laugen) in Anspruch genommen werden, und/oder die Freisetzung langlebiger Radionuklide aus den Abfallgebinden verhindern, die andernfalls zu unzulässigen Strahlenexpositionen führen. Nach dem Verschluss eines Endlagers für radioaktive Abfälle in geologischen Formationen stellen sich kurzfristig (innerhalb weniger hundert Jahre) anaerobe Bedingungen ein. Unter diesen Bedingungen bilden sich Gase, vorwiegend Wasserstoff aus der anaeroben Korrosion des Eisens bzw. Stahls der Abfallbehälter und ihres Inhalts sowie in geringerem Umfang CO_2 aus der Zersetzung organischer Abfallbestandteile. Diese Gase können sich in den versetzten Einlagerungsbereichen akkumulieren und unter Umständen einen signifikanten Einfluss auf die Langzeitsicherheit des Endlagers ausüben.

Weiterhin sorgen die Wärmeentwicklung der HLW, die geomechanischen Wechselwirkungen, sowie die geochemischen Ausgangsbedingungen des Nahfelds und des Fernfelds im Endlager für ein hochkomplexes System gekoppelter Prozesse von thermo-, hydraulischen, geomechanischen und geochemischen Einflussgrößen. Die ersten drei dieser Prozesse wurden und werden seit Jahrzehnten untersucht, sowohl separat, als auch gekoppelt hinsichtlich experimenteller Befunde und numerischer Modellierungsansätze. Zahlreiche geochemische Reaktionen beschreiben die Mobilisierung und den Transport radioaktiver Stoffe entlang der gestuften Barrieren, als die das Endlager bei der Sicherheitsanalyse verstanden wird. Möglicherweise werden neue feste Reaktionsprodukte gebildet, die unter den gegebenen Randbedingungen thermodynamisch begünstigt sind. Die so entstandenen Phasen halten unter Umständen einen Anteil spezifischer Radionukliden zurück. Die Umsetzung und die Intensität dieser Prozesse können sich in der Realität je nach den Gegebenheiten des Einzelfalls unterscheiden. Die Prognose dieser Prozesse und Abläufe erfordert den Einsatz numerischer Modelle, die anhand von experimentellen Daten geeicht und validiert sind. Eine Übersicht publizierter Lösungsansätze und ihrer Prognosen wird bereitgestellt.

Die Modellierung wird in der vorliegenden Studie mit dem Code TOUGHREACT durchgeführt. TOUGHREACT ist ein Code zur numerischen Modellierung des reaktiven Stofftransports. Er wurde entwickelt am Lawrence Berkeley National Laboratory (LBNL), University of California, USA als eine Erweiterung des Codes TOUGH2. TOUGHREACT ist anwendbar für ein-, zwei-, oder dreidimensionale geologische Bereiche einschließlich physikalischer und

chemischer Heterogenitäten. Temperaturen im Bereich zwischen 0°C und 300°C können modelliert werden. Die Obergrenze von 300°C ergibt sich aus der Tatsache, dass die am häufigsten verfügbaren und eingesetzten geochemischen Datenbanken wie z.B. EQ3/6 ebenfalls bis 300°C einsetzbar sind. Der Druck kann von 0,1 MPa (Atmosphärendruck) bis einige zehn MPa reichen (in mehreren tausend Meter Tiefe). Die Wassersättigung kann zwischen vollkommen trockenen bis zu vollständig gesättigten Systemen reichen. In seiner ursprünglichen Version ist das implementierte Modell geeignet für schwache Ionenstärken und weist folgende wichtigen Eigenschaften auf im Hinblick auf die Beschreibung fluider Strömungen und geochemischer Transportvorgänge: (1) Die Gasphase berücksichtigt Mehrphasenströmungen, Stofftransport und chemische Reaktionen; (2) es werden nicht nur poröse Medien, sondern auch reaktive Strömungs- und Transportvorgänge in klüftigem Gestein modelliert; (3) der Einfluss von Wärme wird berücksichtigt, einschließlich Wärme getriebener Strömungsvorgänge und der Temperaturabhängigkeit thermophysikalischer und geochemischer Eigenschaften (z.B. Fluiddichte und –viskosität, sowie thermodynamische und kinetische Daten). Die Aktivitätskoeffizienten von Ionen in Elektrolytlösungen werden in der ursprünglichen TOUGHREACT-Version mit einer erweiterten Debye-Hückel-Gleichung und den zugehörigen Parametern berücksichtigt. Dabei wird angenommen, dass Natrium bzw. Chlor die dominierenden Kationen und Anionen in der Lösung sind, so dass die Debye-Hückel-Gleichung direkt angewandt werden kann. Jedoch unterscheiden sich konzentrierte wässrige Lösungen signifikant von verdünnten Lösungen nicht nur in Bezug auf das geochemische Verhalten (z.B. Aktivitätskoeffizienten von Wasser und ionale Aktivitätskoeffizienten stark unterschiedlich von 1), sondern auch hinsichtlich Strömung und Transport wegen der erhöhten Dichte und Viskosität. Es ist bekannt, dass der Debye-Hückel-Ansatz das Aktivitätsverhalten solcher Lösungen nicht angemessen beschreibt.

Um verlässlichere Ergebnisse für hoch salinare Lösungen zu erhalten, wurde das Pitzer-Modell ionaler Wechselwirkungen in TOUGHREACT implementiert. Das Pitzer-Modell ermittelt die ionale Aktivität einer Lösung als Funktion der ionalen Stärke der Lösung (weit reichende Wechselwirkung), von weiteren Wechselwirkungstermen (kurz reichende Wechselwirkungen) sowie von Temperatur und Druck. Das Modell wird formuliert als ein System von Virial-Gleichungen, auch bekannt als Wechselwirkungsgleichungen, Pitzer-Gleichungen, oder phänomenologische Gleichungen. Die Implementierung des Pitzer-Modells erfolgte auf der Basis der HWM-Formulierung, einer allgemein akzeptierten Form des Pitzer-Modells. Das implementierte Modell wurde anhand vorhandener experimenteller Daten kalibriert und validiert.

Ferner wurde auf der Grundlage früherer ISTec-Arbeiten ein mechanisches Konvergenz-Modell in TOUGHREACT installiert Die dazu gehörigen Porositäts-, Permeabilitäts- und Kapillardruckbeziehungen wurden kritisch überprüft. Im Ergebnis wurde festgestellt, dass ein bereits früher getestetes Modell bessere, besser anwendbare und robustere Ergebnisse lieferte. Es wurde daher für die Implementierung bevorzugt. Die für eine Fallstudie erforderlichen materialspezifischen Parameter liegen vor. Die Validierung der Ergebnisse erfolgte ebenfalls auf der Grundlage der entsprechenden ISTec-Untersuchungen.

Für die Modellierung des Schwellungsverhaltens von Bentonit oder Bentonit-Sand-Gemischen als Versatzmaterialien für Endlager in tiefen geologischen Formationen finden sich in der Literatur verschiedene Modelle. Eine Methode, die den Einfluss der Porenwasser-

chemie und der Temperatur beschreibt und zur Prognose des Schwellungsverhaltens von kompaktiertem Bentonit geeignet ist, wurde 1996 von Komine und Ogata publiziert. Diese Methode kann auch zur Modellierung des Schwellungsverhaltens von Bentonit-Sand-Gemischen herangezogen werden. Sie erlaubt die detaillierte Auswertung der Effekte austauschbarer Kationengemische. Die Methode wurde hierbei zur Modellierung des Schwellungsverhaltens von Bentonit herangezogen. Das implementierte Modell wurde als erstes an einem japanischen Bentonit getestet, dessen Daten aus der Literatur entnommen wurden. Ein zweiter Qualifizierungsschritt wurde mit einer Anwendung des Modells auf den Bentonit MX-80 unternommen, der in Deutschland verschiedentlich eingesetzt wurde.

Für generische Anwendungen wurden realitätsnahe Modelle für HLW in Ton und Salzgestein sowie für ILW in Salz erstellt. Die Eigenschaften individueller Systemkomponenten wurden ausgewählt auf der Grundlage verfügbarer und veröffentlichter Daten. Besonderer Wert wurde dabei auf die Einfachheit der ausgewählten Parameter gelegt. Zwei Endlagerungskonzepte wurden untersucht. In dem ersten wurden HLW Container in vertikalen Bohrlöchern eingelagert. Im zweiten Konzept werden ILW in Strecken gelagert.

Das Bohrlochkonzept wurde separat für Ton und Salzgestein mit den jeweils angepassten Systemkomponenten angewandt. Das gesamte Bohrloch ist unterteilt entsprechend der Länge des aktiven Teils des Bohrlochs von 15 m. Der Abstand zwischen der Streckensohle der Zufahrt und dem oberen Ende der Abfallgebindesäule beträgt 2 m, der entsprechende Abstand am unteren Ende 0,5 m. Der Abstand zwischen den Abfallgebinden ist 1,80 m unter der Annahme, dass 6 Abfallgebinde entlang des Bohrlochs eingelagert werden. Der Bohrlochdurchmesser von 1,75 m setzt sich zusammen aus dem Durchmesser des Abfallgebindes und dem des Versatzmaterials. Für die Diskretisierung wird ein axialsymmetrisches zweidimensionales Modell verwendet. Die Bohrlochachse ist die Symmetrieachse in Übereinstimmung mit dem Konzept der Bohrlochlagerung.

Das Modellgitter für die Streckenlagerung besteht aus 38x204 Blöcken. Das bedeutet, dass insgesamt 7752 Blöcke verwendet werden mit wechselnden geometrischen Parametern in einer r-z Geometrie. Die Modellierung der Einlagerung in Strecken erfolgt nach ähnlichen Prinzipien. Hierzu wird ein vereinfachtes rechtwinkliges 2D-Gitter eingesetzt. Eine feinere Diskretisierung erfolgt für die Einlagerungskammern und den Nahbereich. Das Volumen des Versatzmaterials wird mit 40 m³ angenommen. Jeweils vier Wärmequellen sind in einer Einlagerungskammer angeordnet. Für die Festlegung der Quellstärke wird ein Abfallvolumen von 60 m³ unterstellt, entsprechend einem Volumenverhältnis von 0,6 zwischen Abfall und gesamten Hohlraumvolumen.

Auf der Basis früherer Untersuchungen wurde die Wärmeerzeugung eines HAW-Abfallbehälters festgelegt. Die Wärmeerzeugung ist am größten bei Einlagerungsbeginn mit ca. 2500 W//m². Nach ungefähr 200 Jahren sinkt sie unter 10 W/m². Das bedeutet, dass sie nach dieser Zeit bei der numerischen Modellierung nicht mehr berücksichtigt werden muss. Zur Modellierung der Gasbildung wird eine durch experimentelle und in-situ-Daten gestützte Korrelation abgeleitet. Die Korrelationsparameter wurden für verschiedene Pufferungsbedingungen getrennt eingegeben.

Für die Initialisierung des Modells wurden verschiedene grundsätzliche Annahmen getroffen. Die Rechenläufe wurden bis maximal 5000 Jahre durchgeführt. Die numerischen Eingabeda-

ten wurden nach den Vorgaben der Code-Entwickler von TOUGH2 in LBNL gewählt. Die für die Initiierung der eingebauten Verbesserungen erforderlichen Eingabedaten wurden zu den Standardeingabedateien hinzugefügt. Der Output wurde überwiegend mit dem Code TECPLOT ausgewertet, der zur Darstellung zwei- und drei-dimensionaler Ergebnisse geeignet ist. Als EOS-Modul wurde in de Regel das Modul EWASG verwendet. Die chemischen Parameter sind in TOUGHREACT-kompatiblen Dateien gespeichert. Um die Auswirkungen der chemischen Kopplung besser isoliert betrachten zu können, wurden in den Rechenläufen die mechanischen und chemischen Modelle schrittweise den thermohydraulischen Rechnungen zugeschaltet.

Aus ersten grundlegenden Rechenläufen für HLW in Salz resp. Ton als Wirtsgestein wird abgeleitet, dass die maximale Temperatur im Endlager an der Abfallgebindeoberfläche nach einem Jahr 190 °C beträgt, während sie nach 1000 Jahren in der Umgebung der HLW-Behälter auf weniger als 50°C abfällt. Die Temperatur im Versatzmaterial erreicht in der Nähe der Abfallgebinde maximal 130°C nach einem Jahr. Die Temperatur sinkt mit wachsendem Abstand von den Abfallgebinden. Die maximalen Werte treten nach einem Jahr auf. Im zweiten beginnen die Temperaturen zu fallen. Die berechneten Werte stehen im Einklang mit experimentellen Arbeiten zur Ermittlung der Wärmeverteilung in der Umgebung Wärme entwickelnder radioaktiver Abfälle. Ein wesentliches Ergebnis der Rechnungen war, dass sowohl die maximale Höhe der Temperatur als auch der Temperaturverlauf stark von den thermischen, aber auch den hydraulischen Eingangsparametern abhängen.

In einer zweiten Serie von Simulationsrechnungen wurde die Gasbildung (H_2) eingeschaltet. um die Auswirkungen der Gasbildung auf thermohydraulische Fragestellungen zu ermitteln. Hierbei wurde ein Diffusionskoeffizient von 5.10^{-9} m^2/s für die Diffusion von Gas in Wasser verwendet. Es entwickelt sich keine freie Gasphase. Vielmehr wird das gesamte gebildete Gas instantan in Wasser gelöst. Aus diesem Grund werden keine signifikanten Änderungen hinsichtlich des Druckaufbaus im Endlager erwartet. Auch für chemische Auswirkungen der Gasbildung werden keine wesentlichen Beiträge prognostiziert. Das Druckaufbauverhalten wird vorrangig kontrolliert von den petrophysikalischen Daten, d.h. vor allem von der Permeabilität der eingesetzten Materialien.

Eine der Auswirkungen des Schwellens von Bentonit als Puffermaterial ist die abnehmende Porosität und damit die Verringerung der Permeabilität. Die Veränderung der petrophysikalischen Parameter bewirkt offensichtlich zusätzliche Einflüsse auf das mechanische Verhalten der Endlagerbarrieren. Einige weitere Rechenläufe wurden daher durchgeführt, um Extremfälle des Druckaufbaus und ihrer mechanischen Auswirkungen auszuwerten. In den Modellrechnungen wurde die Gasbildung berücksichtigt. Die Permeabilität des Wirtsgesteins wurde nicht verändert in der Erwartung, dass diese Annahme gleichzeitig realistisch und konservativ ist.

Die reaktiven Elemente wurden in das Modell eingebracht durch die Aktivierung des chemischen Modellteils. In der Praxis wurden dazu die vorhandenen Eingabemöglichkeiten ergänzt und modifiziert entsprechend der Zielsetzung und dem Arbeitsprogramm dieses Vorhabens. Viele Rechenläufe wurden zu Beginn durchgeführt mit dem Ziel, ein besseres Verständnis für die Phänomene des reaktiven Stofftransports in einem Endlager mit Ton als Wirtsgestein zu gewinnen.

Wie zu erwarten ist der Temperaturgradient eine Funktion von Ort und Zeit. In Anbetracht des gegebenen Temperaturgradienten und der langfristigen Entwicklung des Systems werden mineralogische Transformationen als bedeutsamer angesehen als Oberflächen- oder Ionentauscher-Reaktionen. Daher wurden Oberflächen- oder Ionentauscher-Reaktionen in den meisten Rechenläufen vernachlässigt.

Die wichtigste Schlussfolgerung der unter “CLAY_plus_reactive” zusammengefassten Rechenläufe mit Berücksichtigung des Schwellens ist der starke und schnelle Abfall der Porosität um die Abfallbehälter herum. Der Verlauf der Porosität wird zum einen bestimmt vom Schwellen und zum anderen durch die Ausfällung und das wieder in Lösung gehen von Mineralien. Dabei ist das Schwellen ein schnellerer Prozess, der die Reduktion des Porenvolumens bewirkt. Der schwellende Bentonit wird zu Beginn als mit einer Gleichgewichtslösung gesättigt angenommen. Es wird beobachtet, dass chemische Parameter wie z.B. der pH-Wert sich stark verändern. Die Konsequenzen für die Mineralogie sind signifikant und der Bentonitpuffer verliert seine anfängliche thermodynamische Stabilität. Der pH-Wert sinkt insbesondere in der Umgebung der Abfallbehälter mit steigender Temperatur. Dies beeinflusst den Korrosionsprozess erheblich. Um die Veränderung des Bentonits bei Kontakt mit Stahl modellieren zu können, wird in einer Zelle die Eisenkorrosion simuliert. In dieser Zelle werden nur Siderit- und Magnetit-Bildung kinetisch betrachtet. Die Konversion von Na/Ca–Montmorillonit zu Illit wird als mögliche Reaktion mit einer Bentonitbarriere in einem Endlager für radioaktive Abfälle angesehen, weil in der anstehenden geologischen Lösung eine hohe Kaliumkonzentration vorliegt.

Auch die Konversion von Na/Ca–Montmorillonit-zu Chlorit wurde als ein möglicher chemischer Prozess mit einer Bentonitbarriere in einem Endlager für radioaktive Abfälle untersucht wegen der Eisenkonzentration in der anstehenden geologischen Lösung, aber auch wegen des Eisenüberschusses durch die Behälterkorrosion. Wie erwartet begünstigen hohe Eisenkonzentrationen die Auflösung des Na/Ca–Montmorillonits.

Aus den Modellierungsuntersuchungen mit Salz als Wirtsgestein ergibt sich ein offensichtlicher Vorteil für den Einsatz von Brucit als Puffer gegenüber Q-Lösung in Hinblick auf die Korrosion von Eisen. Die Korrosionsstabilität dieser Pufferkombination ist sogar höher als die im Fall Bentonit-NaCl. Nach 1000 Jahren erreicht die Eisenauflösung im Schutzfluid 0,4 % der anfänglichen Eisenkonzentration in einem Modellblock. Der pH-Wert steigt kurz nach Beginn der Simulationsrechnung auf 7,3 und bleibt konstant auf diesem Wert. Eine Veränderung tritt erst ein, wenn der Magnesiumpegel nicht mehr ausreicht, den pH-Wert zu puffern, und Brucit ($MgOH_2$) ausfällt. Die Ausfällung von Mineralstoffen in der Umgebung der Abfallbehälter spielt insgesamt eine wesentliche Rolle.

Ziel der Entwicklung und Installation des Modells für die Streckenlagerung ist die Untersuchung der Gasbildung und des damit verknüpften Radionuklidtransports als Folge der mikrobiellen Zersetzung von organischen Komponenten des ILW. Mit diesen Untersuchungen werden frühere Arbeiten wieder aufgenommen mit dem entscheidenden Unterschied, dass in der vorliegenden Studie das Pitzer Aktivitätsmodell verwendet wird.

Der radioaktive Abfall wird in dem aufgefahrenen Hohlraumvolumen abgelegt. Der verbleibende offene Hohlraum wird mit Versatzmaterial aufgefüllt. Das Porenvolumen wird als gesättigt in einer geeigneten Salzlösung unterstellt. Das Versatzmaterial B wird eingesetzt, um

zu untersuchen, wie ein auf Brucit beruhender Versatz sich auswirkt auf das geochemische Milieu und seine Stabilität. Dieser Fall spielt eine große Rolle für die Stabilität des pH-Werts im System. Die Veränderung des Karbonatvolumens wie etwa von Kalzit und Magnesit ist signifikant. Kalzit fällt schlagartig aus wegen seiner hohen Reaktionsrate bei den lokalen Gleichgewichtsbedingungen. Aber nach wenigen Stunden sinkt die Ausfällrate stark ab und Kalzit geht wieder in Lösung. Als Ergebnis lässt sich eine nachhaltige Rückkopplung des Auflösungs- und Fällungsprozesses mit dem das Transportverhalten radioaktiver Stoffe erwarten.

SUMMARY

The main objective of the study is a qualitative and quantitative contribution on modeling studies of coupled processes in salt and clay formations as underground radioactive repository. The study aims at providing a feedback on the coupled modeling of hydraulic, thermal, mechanical and chemical processes for the definition of the reactive transport at high salinity conditions. As the previous studies make a significant amount of experience available, the code TOUGHREACT was used for the numerical application. The code was improved, validated and applied for selected modeling cases.

A detailed literature research is provided firstly. The safety assessment for a repository has to cover the performance of different barriers supposed to isolate waste from contact with water or to prevent a release of long-lived radionuclides from waste containments and hence to remove/reduce the cause of intolerable radiation exposures. After the closure of an underground nuclear waste repository, anaerobic conditions are reached rapidly in the repository (within a few hundred years) and gases mainly H_2 form by anoxic corrosion of the steel canister. Corrosion of Fe and degradation of waste canisters leads to the generation and accumulation of H_2 gas in the backfilled emplacement tunnels, which may significantly affect long-term repository safety. On the other hand the heat generation from HLW and the geomechanical issues as well as the initial hydrogeochemical conditions of the near and far field of the repositories create a very complex problem for the safety analysis; a coupled process of thermal-hydraulic-mechanical and chemical issues. The first three of these processes have been studied since many decades separately as well as coupled in terms of experimental and numerical works. Various geochemical reactions govern the generation of radionuclide species and their transport throughout cascade like repository system. New solid reaction products are formed, which may thermodynamically be favoured under given geochemical conditions. These phases may retain a certain quantity of specific radioelements. The realisation and intensity of these processes might be different for the cases studied. The prediction of these processes is due to the use of numerical modeling tools validated and calibrated with experimental data. The geochemical processes that can be expected in the near field of a HLW repository and the efforts of their prediction are summarized referring on published studies.

The quantitative definition of the software development and improvement works are given in the following chapters. The study was performed based on numerical simulation using TOUGHREACT, a numerical reactive transport modeling code developed by the scientists of Lawrence Berkeley National Laboratory (LBNL), University of California, USA as an extension of TOUGH2. TOUGHREACT is applicable to one-, two-, or three-dimensional geologic domains with physical and chemical heterogeneity. Temperature ranges from 0 °C to 300 °C, because the present most available geochemical database is up to 300 °C such as EQ3/6. Pressure can be from 1 bar (atmospheric pressure) to several hundred bars (at several thousand meter depth). Water saturation can range from completely dry to fully water saturated. In its original form, the model can deal with low ionic strength and has three important features in terms of fluid flow and geochemical transport: (1) the gas phase is active for multiphase fluid flow, mass transport and chemical reactions, (2) not only porous media, but also reactive fluid flow and transport in fractured rocks is considered, (3) the effects of heat are

considered, including heat-driven fluid flow, and temperature-dependent thermophysical and geochemical properties (such as fluid density and viscosity, and thermodynamic and kinetic data). The activity coefficients of charged aqueous species are computed in original TOUGHREACT using an extended Debye-Hückel equation and parameters. The assumption is made that the dominant cation and anion in solution are sodium and chloride, respectively, so that the Debye-Hückel equation can be used directly. However, concentrated aqueous solutions are significantly different from dilute solutions not only in terms of geochemical behavior (e.g., water activity and ionic activity coefficients far from unity), but also in terms of flow and transport because of elevated density and viscosity and it is well known that the Debye-Hückel model may not model the activity behaviour of such solutions.

The Pitzer ion-interaction model was implemented in TOUGHREACT for more reliable calculations of the high salinity solutions. The Pitzer model evaluates the ionic activity of a solution as a function of solution ionic strength (long-distance interaction), interaction terms (short-distance interaction), temperature, and pressure. The model formulation consists of several virial equations, sometimes called specific interaction equations, Pitzer equations, or phenomenological equations. The implementation of Pitzer model was performed based on the HWM formulation which is a generally accepted form of the Pitzer model. The implementation was calibrated and validated via available experimental data.

A mechanical convergence model was implemented into TOUGHREACT based on previous ISTec studies and related porosity-permeability-capillary pressure changes were also revisited. A previously tested model exhibiting better and more applicable, robust results was preferred for the implementation. For a case study material specific parameters are available. The implementation performed was also validated based on corresponding ISTec studies.

Several methods are published to model the swelling behaviour of the bentonit or bentonite-sand mixtures to be used as backfill material in geological repositories. A prediction method dealing with the influences of pore-water chemistry and temperature that can be applied to the swelling characteristics of compacted bentonite was only presented by Komine and Ogata (1996). This new method for predicting the swelling characteristics of the sand–bentonite mixtures which can evaluate the effects of exchangeable-cation compositions in detail was selected in this project to model the swelling of bentonite. The implemented model was tested first for a Japanese bentonite as given in available literature. A second validation effort was made based on the properties of MX-80 bentonite which is used for German applications.

Generic models for HAW in clay and salt rocks as well as for MWL repository in salt rock were created based on related studies. The properties of individual components of the system were selected due to published data with a special care to simplicity. Two concepts were considered; in the first one the HWL waste containers emplaced in a borehole and in the second one MLW/LWW emplaced in a drift.

The borehole model was applied for salt and clay host rock separately with related components. The total of the borehole is divided as the active borehole of 15 m, with a distance of 2 m to the gallery to the top, an additional distance to the bottom is also considered. The distance between the containers is equal to 1,80 m assuming 6 containers disposed along the borehole. The borehole diameter consists of the container diameter and buffer material

being equal to 1,75 m. For the discretisation an axisymmetric, two dimensional model is applied. The symmetry axis is the borehole axis. This is consistent to the repository concept applied.

The model grid network consists of 38x204 blocks; this means a total of 7752 blocks is applied with various geometry in an r-z geometry. Similar principles were also applied for modeling the drift repository model. A simplified rectilinear 2D grid model was used; finer discretization was applied for the emplacement chamber and near field. A total volume of 40 m^3 was assigned for backfill material, and four source terms were located in the model chamber. For the determination of the source term, a waste volume of 60 m^3 was assumed, based on a volume ratio of 0,60 for waste to total excavated volume.

A heat source representing the heat generating from HAW containers was introduced based on previous studies. The heat generation is due to HAW waste and exhibit higher heat activity at the beginning of the repository time being equal to approximately 2500 W/m^2 and after about 200 years the heat generation decreases below 10 W/m^2 that means no more relevance for the numerical modeling. For modeling the gas generation a correlation supported by experimental and field results was used. The parameters of the correlation were introduced for various buffering conditions separately.

For the initiation of the models some general assumptions were made. The runs were performed for maximum 5000 years. The input data were prepared based mainly on the related facilities disseminated by the developers of TOUGH2, LBNL. The keywords necessary for the improvements performed in this study were added to the standard input files. The evaluation of the outputs was performed mainly by using the Software “Tecplot” for two and three dimensional description of the results. The EOS module EWASG was mainly used for the runs. The chemical parameters are assumed as being given in data files of TOUGHREACT-Pitzer. To investigate a better isolation of the chemical coupling the simulation runs were performed by adding the mechanical and chemical options successively to thermal-hydraulic computations.

In basic runs for HLW in both clay and rock salt as host, it is concluded that the temperature is as high as 190 °C in the repository after one year whereas it decreases beyond 50 °C in the vicinity of the containers after 1000 years. It should be noted that the maximum temperatures indicates the temperatures on container blocks. The temperature in the buffer near the container reaches approximately 130 °C after one year and decreases with increasing distance from the container. As expected the maximum temperature is calculated in the first years and after approximately 2 years the temperature begins to decrease. This thermal behaviour conforms to experimental/laboratory studies to investigate the temperature distribution around the heat generating radioactive wastes. It is worth to note that the maximum temperature reached after the disposal as well as the temperature profile is strongly dependent on the thermal as well as hydraulic parameters assumed for the model. As a second simulation series the gas generation (H_2) was switched on to observe the effect of the gas generation on thermo-hydraulic issues. In this run named a diffusion coefficient of 5.10^{-9} m^2/s is used for the diffusion of gas in liquid. No free gas phase is observed; all of the gas generated dissolves in water instantaneously, therefore no significant changes are expected in pressure built-up behaviour. The H_2 generation case is expected to make no relevant impact

on the chemical issues. It should be repeated that the pressure behaviour is strongly related to the petrophysical data most of all on the permeability of the materials used.

One of the impacts of the swelling of the bentonite buffer is the decrease on the porosity and therefore on the permeability. The variation of the petrophysical parameters has obvious additional effects on the mechanical response of the repository barriers. Some additional runs were performed in order to evaluate extreme cases in terms of pressure built-up and its effect on mechanical behaviour. In all models gas generation was also considered. The permeability of the host rock was not changed considering that this is realistic and conservative at the same time.

The reactive issues were introduced in the model by the activation of the chemical part of the model. This was realized by using the necessary data input provided and modified in the framework of this work. Many successive runs were performed to have a better understanding of the reactive transport phenomena in the systems where clay is assigned as host rock. As expected the temperature gradient must be a function of time and space. Considering the temperature gradient given and the long term evolution of the system, the mineralogical transformations have been considered as being more important than the surface and ion exchange reactions. As a consequence, these reactions were neglected in most of the runs. The most important conclusion of the “CLAY_plus_reactive” which takes the swelling into account is the strong and rapid decrease of the porosity around the container. The variation in porosity is due to firstly swelling and secondly to the precipitation/dissolution of the minerals where the swelling is a more rapid process causing the reduction in pore volume. The swelling bentonite buffer is considered as initially saturated with an equilibrated solution. It is observed that chemical parameters like pH are significantly changed. The consequences on mineralogy are significant and the buffer loses its initial thermodynamic stability. The pH decreases particularly in the vicinity of the container with increasing temperature influencing the corrosion process considerably. In order to model the bentonite alteration in contact with the steel, a cell simulates the iron corrosion. In that cell, only siderite and magnetite formations are kinetically processed. The Na/Ca–montmorillonite-to-illite conversion is observed as a potential chemical process for a bentonite barrier in the radioactive waste repository because of high concentration potassium in the geological fluid. The montmorillonite-to-chlorite conversion was observed also as a potential chemical process for bentonite barrier in the radioactive waste repository because of the iron concentration in the geological fluid and also because of the iron excess by the container corrosion. As expected high iron concentration favors the Na/Ca–montmorillonite dissolution.

In the modeling attempts using salt rock as host it is concluded that the advantage of using brucite buffer with Q solution is obvious in terms of corrosion. The corrosion stability of this buffer combination is higher than bentonite+NaCl case. After 1000 years the dissolution of iron in the protection fluid reaches 0,4 % of the initial iron concentration in the block. The pH increases shortly after the simulation start to a level of 7,30 and remains at this value constant. This value stay constant as long as Magnesium level is sufficiently high for buffering the pH and brucite $MgOH_2$ precipitates. The mineral precipitation around the container is of significant level.

The aim of creating and studying the drift model is to investigate the gas generation and related radionuclide transport as a result of microbial degradation of organic components of

MLW's. This is a revisitation of a similar previous study with the important difference of using Pitzer activity model. The radioactive waste is emplaced within the excavated volumes. The remaining portion of the volume is consumed with a backfill material, and the pore volume is assumed to be saturated with a suitable brine solution. Backfill B was introduced to investigate how the brucite-based backfill would affect the geochemical environment of the system and its stability. This case is relevant with its effect on stabilizing the pH of the system. The variation of carbonate volumes such as calcite and magnesite is significant. Calcite precipitates rapidly, because of its high reaction rate at local equilibrium, but after a few hours, the precipitation rate decreases strongly and the calcite may dissolve. The effect of the dissolution/precipitation on the transport properties may be significant.

1 INTRODUCTION

A prediction for the year 2040 shows that in Germany a total of approximately 273.000 m^3 of conditioned radioactive waste with negligible heat generation and about 6000 m^3 of heat generating radioactive waste will be accumulated /BRE 08/. Radioactive wastes from research, industrial and medical activities have to be collected first in defined collection sites from where they are then disposed to deep geological sites as final repository. Waste from nuclear industry is to be stored directly in geologic repository with interim storage only taking place on site of the nuclear facility. The safe disposal of all these wastes has to be analyzed and demonstrated.

The design of a deep geological repository for permanent storage of high-level nuclear wastes requires the consideration of a set of engineered barriers (the waste product itself e.g. vitrified waste, metal canisters, bentonite backfill, etc.) and natural barriers (geological formations). The role of all these barriers is to ensure the long term stability of the waste, and to avoid the radionuclide transport to surface. Effective isolation should be assured by a totally ‘‘passive’’ repository system of optimized engineered and natural barriers with limited groundwater access to the radioactive substances, their long-term containment in waste packages and retardation of transport to the biosphere. The key criterion for a safe disposal strategy is therefore the capability of isolating long-lived radionuclides.

The associated risk of the disposal system depends not only on the quantity of radioactive elements stored in a repository, but also on whether these elements can be mobilized in case groundwater (brine) intrusion to the repository. The analysis of this risk can be assessed only with numerical modeling of the related transport processes. However the transport process is not an independent issue but is a function of various coupled effects of thermal, geomechanical and geochemical aspects. This requires a coupled numerical modeling taking all scenarios into consideration. The so-called THMC modeling is the most actual subject of most of the related research of repository issues as well as all geosciences. However, this is neither an easy task nor a routine.

Various geochemical reactions govern the generation of radionuclide species and their transport throughout cascade like repository systems. Primarily wastes become corroded by groundwater and radionuclides are leached. New solid reaction products are formed, which are thermodynamically favoured under given geochemical conditions. These phases may retain a certain quantity of specific radionuclides.

In conjunction with systematic and iterative development of scenarios related to near field geochemistry in various disposal systems, safety relevant properties of actinides are currently analysed and modelled according to a general scheme given in Figure 1-1 which shows the interrelation of mobilizing and immobilizing processes /KIM 99/. The rates of radionuclide release by dissolution of the waste packages ($R1_{mobile}$) are compared with retention effects by sorption, precipitation or coprecipitation ($R1_{immobile}$) on corrosion products from waste forms and containers. The net-mobility of both rates constitutes the source term I for radionuclide (RN) release from the engineered barrier system. Reprecipitation or sorption of RN at surfaces of the backfill materials, i.e. the geo-engineered barriers ($R2_{immobile}$) and redissolution ($R2_{mobile}$) has to be considered in the formulation of a source term (II) for the geo-engineered barrier system. Finally, for calculating potential exposures in the biosphere, the

colloid assisted RN-migration ($R3_{mobile}$) in aquifers and sorption on minerals and rocks in the geosphere ($R3_{immobile}$) have to be considered.

These calculations provide adequate results if the physical and numerical modeling leaves a correct and validated basis and a sound understanding of the processes and their developments in space and time. However, to fulfil these conditions is not an easy task especially for extreme cases. A saline repository might be such an extreme case if some brine inflow has to be considered yielding a solution of high activity. The modeling of this case requires the use of Pitzer activity model implemented in an already validated reactive transport modeling tool.

This project aimed at more realistic evaluation of radionuclide/contaminant transport by implementing and using the Pitzer activity model instead of conventional activity model used in TOUGHREACT reactive transport modeling code. Some variations in order to take the geomechanical changes like swelling and compaction into account were also initiated. The new code was validated and tested with some generic models and the results are discussed.

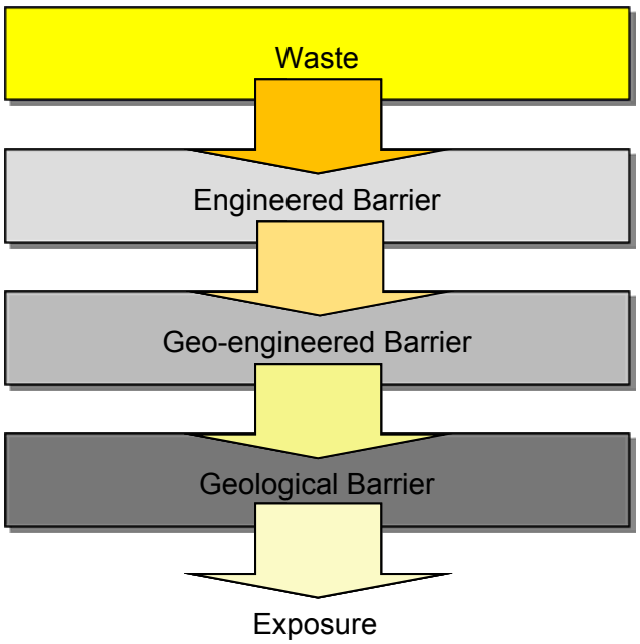

Figure 1-1 Mobilizing and immobilizing processes in a geological repository (modified after /KIM 99/)

2 OBJECTIVES AND METHODOLOGY

The main objective of the study is a qualitative and quantitative contribution on modeling studies of coupled processes in salt and clay formations as underground radioactive repository. The study aims at providing a feedback on the coupled modeling of hydraulic, thermal, mechanical and chemical processes for the definition of the reactive transport at high salinity conditions. As the previous studies make a considerable amount of experience available, the code TOUGHREACT is used for the numerical application. The code is developed, improved, validated and applied for selected modeling cases.

2.1 Reference to the research politics

The project is expected to contribute to the following supporting objectives of the executive organisations:

B6 Development of Methods and Computer Programs for Safety Analyses (Methodenentwicklung und Rechenprogramme für Sicherheitsbewertungen)

- Improvement and actualization of methods and computer programs for long term safety analyses on the basis of modified disposal concepts and actual expertise from R&D works considering international works.
- Investigation and modeling of migration behaviour of radionuclides under the hydrogeochemical conditions in host rock, geotechnical barriers and cap rock (coupled transport models)

B7 Validation of Models, Safety Analyse (Validierung von Modellen, Unsicherheitsanalyse)

- Application of existing or development of new methods and procedures for the validation of the models for the characterization of geomechanical, hydrologic and geochemical effects in the vicinity and host rock.
- Investigation of geochemical and geomechanical natural analogies for the analysis of long term barrier behaviour of salt, granite and claystone.

2.2 Scientific Objectives

The study addresses to the permanent disposal of HAW (also HLW for high activity-level waste) and heat producing MAW (medium activity waste) in salt and/or clay formations. The repository corresponds to the requirements of a safe closing. This means that the possibility for an unlimited solution influx needs not to be considered. Some locale accumulations or limited influx of solution can be expected due to migration through geological barriers.

The wastes are disposed in CASTOR respectively POLLUX-Containers (burned fuel elements, vitrified HAW). Heat generating MAW are compacted and packed in CSD-C-container. The dimensions of CDS-C-Containers correspond to the dimensions of HAW containers. Parts of the packing materials as well as part of the wastes (CSD-C, technological waste) consist of organic material which can produce gas as the result of the radiation or microbial degradation. A limit of 10 g organic material is given as the actual limit per container for technological waste in CSD-C-Containers. The validity period of this limiting value is

open to discussion. The CSD-C- containers are equipped with a sinter metal filter in the internal cap in order to avoid a pressure increase in the containers, all other packaged wastes are gas tight sealed.

/RÜB 07/ estimated that the water saturation in crushed salt buffer material and in the excavated damaged zone of a HAW repository is always high enough to support the chemical reactions generating gas from the disposed wastes. Some other assumptions for a safety analysis of a HAW are:

- A pressure built up over the dilatancy boundary is possible
- The generation of CO_2, CH_4 and small chain alkanes is due to the degradation of the organic materials in the wastes and/or to the interaction between the carbon content of the liquid and solid phases of the fuel materials with water
- The interactions of the generated gases (H_2, CO_2, CH_4) with the chemical conditions take place in the near field
- The generation and transport of the radioactive gas components from the wastes, especially $^{14}CO_2$ und $^{14}CH_4$ is plausible

The same scenario is valid for the disposal of HAW in clay. The mentioned effects can appear partially in an isolated volume as well as coupled each other in the total of the near field. In all cases the definition of the chemical interactions and their dependency on time is required as the resulting effects on gas generation and transport, on the solubility of the radionuclides and gas generation. The dimension of these effects is dependent on the thermodynamic, hydrodynamic, geomechanical as well as geometrical/petrophysical parameters dominating the repository conditions.

Assuming disturbed conditions of the repository, limited inflow of solution or groundwater into the repository may cause negative effects on the safety conditions. Such extreme conditions require additionally the examination of the fracture and pathways through which the flow of the gas-solution mixtures takes place. In such a case a two-phase flow can be expected.

The corrosion behaviour of the HAW glass containers is investigated in many recent projects /LUC 04/. It is confirmed that the long term corrosion behaviour in solution from clay formations (Boom, Opalinus) exhibit a similar behaviour compared to granite fluids and NaCl solutions. Although during the long term corrosion in concentrated solutions in salt formations only few reactions take place, during the corrosion of glasses in clay formations significant chemical interactions and transport mechanisms between the solution and rock minerals are reported. This is expected to influence the corrosion behaviour considerably. However, the high carbonate concentration (HCO_3^-/CO_3^{2-}) especially in Boom Clay solution may decrease the solubility of the actinides at high pH because of carbonate complexation. The same interactions may take place also in clay based buffer materials (bentonite).

Under these conditions geochemical modeling may provide information on gas generation conditions and retention of the generated gases. This also results in interplay with the pressure increase because of the convergence and changes in stress distribution. On the other hand the geochemistry of the solutions is affected by the dissolved gases (f.i. CO_2) causing pH changes as well as changes in thermophysical properties of the solution. The effects on

the transport behaviour of all phases should be computed as function of pressure as well as of the temperature as all of the described parameters are dependent on the temperature.

The importance and significance of the coupled geochemical modeling is even higher if the considered system contains CO_2. The unconventional physical and chemical properties of CO_2 and CO_2 containing water contributes to the modeling complexity largely. Higher solubility and reactivity of CO_2 in brine, non-conventional density behaviour of CO_2-water systems as well as higher compressibility and volumetric properties of CO_2 as gas phase are additional numerical challenges. Although many numerical tools exist for modeling and prediction of the phase and transport behaviour of the geological systems, only a limited number of these tools are suitable for the two-phase flow of complex CO_2 containing fluids systems.

The interplay of the above described processes and their synergetic effects can be predicted only with coupled modeling. This is valid for all geological system that exhibit similar complexities. As the coupled processes and their prediction with numerical modeling have a vital importance for the safety analysis of radioactive repositories, information exchanges on the subject was started at earlier times of investigations on nuclear repository safety /f.i. NEA 91/. The first approaches began with coupling the fluid dynamic with geomechanic preferring integral assessment with strong assumptions /DAV 95/.

The numerical coupling of the geochemical processes with THM processes is one of the most revisited actual research themes. However these efforts to improve the reactive transport modeling is at its initial phase and there are still many problems to solve in reaching a modeling tool coupling the chemical phenomena to the hydraulic,-thermal and mechanical issues as needed by modeling the engineering- and natural barrier systems being imposed to the storage of radioactive waste for assuring the safety requisites.

The present project aims at improvement, validation and application of the code TOUGHREACT for modeling the reactive transport as the result of interactions between disposed waste and surrounding engineering and geo-materials in nuclear repositories. This code has been applied for various engineering and scientific cases and was also used for German decommissioning works. Because of the good and validated experience of ISTec with TOUGH2 and based on the first successful application on repository problems with TOUGHREACT, TOUGHREACT is selected for further improvement to fulfil the modeling needs of salt as well as of clay formations. The code was improved through new implementations, qualified and applied in terms of some generic repository models considering the high salinity of formation or synthetic water as a part of the repository system.

2.3 Methodology

The study was performed based on numerical simulations using TOUGHREACT. In this framework code development, implementation, calibration, validation and application stages were applied. All these stages were performed based on a previously conducted literature survey. Published experimental work was used to calibrate and validate the numerical work. The validated numerical tool was used for investigating and commenting the reactive transport issues of above given repository conditions.

3 LITERATURE SURVEY - BACKGROUND

The safety assessment for a repository has to cover the performance of different barriers supposed to isolate waste from contact with water or to prevent a release of long-lived radionuclides from waste containments and hence to remove/reduce the cause of intolerable radiation exposures. After the closure of an underground nuclear waste repository, anaerobic conditions are reached rapidly in the repository (within a few hundred years) and gases mainly H_2 form by anoxic corrosion of the steel canister. Corrosion of Fe and degradation of waste canisters leads to the generation and accumulation of H_2 gas in the backfilled emplacement tunnels, which may significantly affect long-term repository safety. On the other hand the heat generation from HLW and the geomechanical issues as well as the initial hydrogeochemical conditions of the near and far field of the repositories creates a very complex problem for the safety analysis; a coupled process of thermal-hydraulic-mechanical and chemical issues. The first three of these processes have been studied since many decades separately as well as coupled in terms of experimental and numerical works. Various geochemical reactions govern the generation of radionuclide species and their transport throughout cascade like repository system. New solid reaction products are formed, which may thermodynamically be favoured under given geochemical conditions. These phases may retain a certain quantity of specific radioelements. The realisation and intensity of these processes might be different for the cases studied. The prediction of these processes is due to the use of numerical modeling tools validated and calibrated with experimental data. The geochemical processes that can be expected in the near field of a HLW repository and the efforts of their prediction are summarized in the following referring on published studies.

3.1 Chemical Interactions in a Radioactive Repository

The geochemical conditions in the near-field of a radioactive waste repository are determined mainly by the host rock, the groundwater, the disposal concept, the waste product and its packaging. For HLW it is obvious that the temperature development already provides an effect on geochemistry. For L/MLW this is not evident. In most cases a differentiation is made only for aerobic and anaerobic conditions corresponding to an open or sealed repository. The constant geochemical setting may, however, be disturbed by competing reactions. E.g. the degradation of organic materials by microbes produces acidic reaction products. On the other hand the large quantities of Portland cement-based grouts and iron oxides e.g. from corrosion may have a buffering effect. The deterioration of a cemented waste product by saline waters may lead to lower pH levels. As a consequence gas generation rate may change. If such cases cannot be excluded it may be appropriate to assign constant geochemical conditions within certain time periods. This means that corrosion or microbial degradation rates may have to be adjusted to two or more geochemical environments. Thus more than one gas generation rate per metal or organic may have to be assigned, depending on the results of the evaluation of chemical conditions over time.

The mobility of radionuclides depends strongly on the chemical nature and stability of species in groundwater and the geochemical characteristics of various surfaces of minerals, rocks and engineered barrier materials. The various geochemical reactions which govern the generation of mobile radionuclide species and their migration are shown schematically in Figure 3-1. Key factors for the relation between the chemical state of radioelements and var-

ious mobility controlling reactions are charge differences between surfaces and solution species and specific chemical interaction affinities. In contact with groundwater most mineral surfaces are negatively charged. Radionuclide mobility is highest if the solution species has the same charge (negative) as the surface. All cations tend to surface sorption. The geochemical stability of positively charged species decreases with increasing charge. The charge of the bare ion depends strongly on the oxidation state of each element. Elements in higher oxidation states form oxo-ions turning over to lower charges. Positive ions can decrease their charge and increase their mobility by complexation or colloid formation. Complexation increases with pH and carbonate concentration owing to the formation of hydroxo- and carbonato complexes. Colloid formation increases with the humic acid content and the chemical nature of groundwater. The oxidation state of many radioelements (so-called redox-sensitive elements) depends on the redox state of the geochemical environment. At low redox potentials expected in the near field, the elements Np, U, Pu and Tc will all be reduced to a tetra-valent state, becoming rather low in solubility, but with a high tendency for colloid formation. Systematic experimental and modeling investigation of the thermodynamic behaviour of actinides and long-lived fission products in the natural environment is in progress. Studies focuses mainly on heptavalent Tc, hexavalent U and Pu, pentavalent Np tetravalent U, Pu, Np and Tc, and trivalent Am and Cm considering complexation with respect to hydroxide, chloride and carbonate ions behaviour, effects of ionic strength, pH and redox potential /KIM 99/.

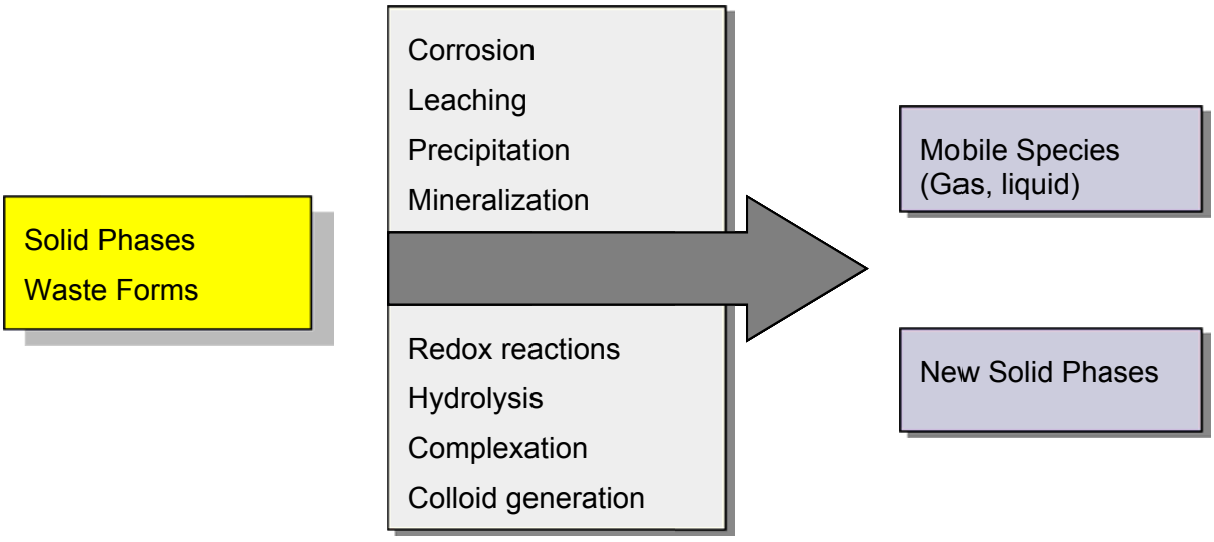

Figure 3-1 Effect of the geochemical processes on radionuclide mobility (after /KIM 99/)

Corrosion of waste packages and radionuclide mobility are directly related to the geochemistry of intruding brines such as brine composition, pH, redox potential and partial pressures of carbon dioxide. Compositions of naturally occurring saline solutions are variable for concentrations of main components and controlled by temperature dependent salt/solution equilibrium within the six component Na–K–Ca–Mg–Cl–SO4 system of oceanic salts. Most salt brines are saturated with halite (NaCl). The relationship between the stability fields of various

salt minerals in the composition range of saturated solutions at 25°C is described in Figure 3-2 using the so-called Janecke representation. Halite is not shown owing to its omnipresence. Included in this diagram are the Mg-rich brines found during the underground investigation of the Gorleben site.

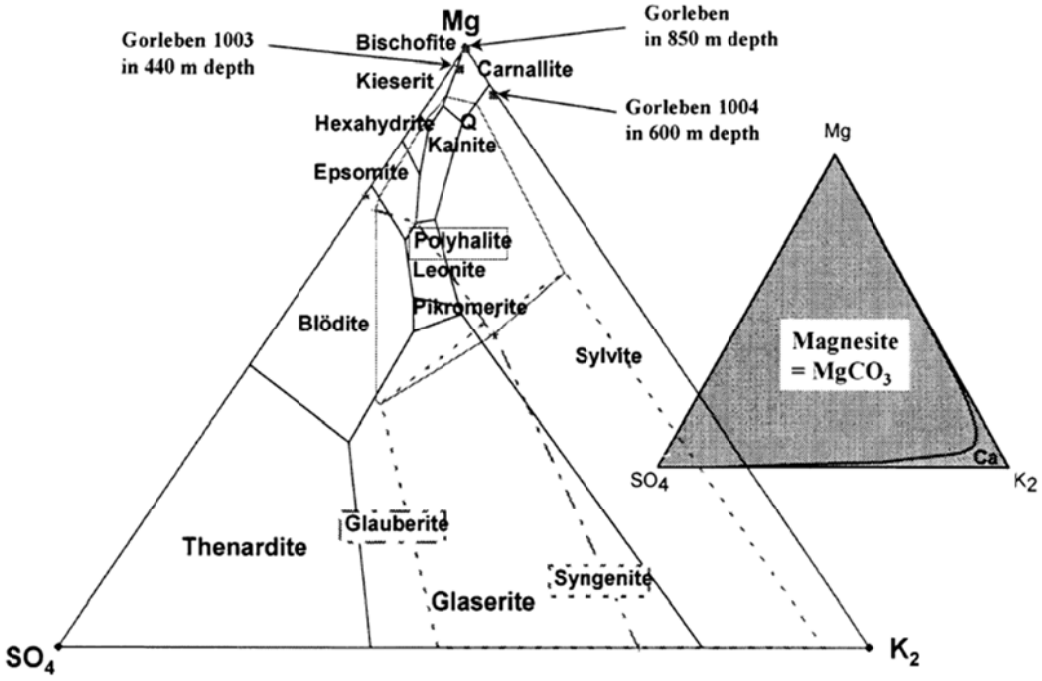

Figure 3-2 Janecke representation of Na–K–Ca–Mg–Cl–SO4 system of oceanic salts at 25°C /KIM 99/

As can be seen in the second triangle in Figure 3-2 carbonate concentrations are mainly controlled by magnesite. Natural saline solutions generally have low buffer capacity for pH and redox potential (Eh). In case of intrusion of saline solutions to the waste forms the pH and Eh values are altered by corrosion of waste packages and by radiolysis. Radiolysis will lead to production of H_2 and O_2 gases and dissolved oxidizing chlorine species. As H_2 is rather mobile the net effect of radiolysis will be oxidizing. On the other hand, resulting from hydrogen formation by corroding canisters, ‘‘redox fronts’’ can be balanced. Reducing conditions create a beneficial effect on radionuclide mobility by establishing low solubilities of safety relevant nuclides such as Np, Pu, U, Tc and Se. Corrosion of waste packages leads also to changes in pH, with the lowest pH of about 3–4 resulting from glass corrosion in Mg-containing brines /GRA 90/ and the highest pH (9–10) occurring in NaCl-dominated brines, tetravalent U, Pu, Np and Tc, and trivalent Am and Cm /FAN 98/ considering complexation with respect to hydroxide, chloride and carbonate ions behaviour, effects of ionic strength, pH and redox potential. Considerable research is still necessary, in particular on understanding the behaviour of tetravalent carbonate concentrations that are mainly controlled by elements.

3.2 Corrosion of Waste Containers in Salt/Salt Solutions

Figure 3-3 shows a schematic description of a repository system in a salt dome as given in /ROT 10/. The emplacement takes place either in deep boreholes or in drifts. Figure 3-3 also depicts the processes, modelled to represent a near-field in a salt formation in an emplacement chamber or drift containing radioactive waste (container) capsulated in a multi-barrier system. In case of an altered evolution of the repository system, water can access the emplaced waste, and the following processes have to be considered: corrosion of the steel containers, waste matrix corrosion, gas production, release of contaminants, transport processes for fluids and contaminants, retardation of contaminants, creep (convergence) of surrounding salt rock, etc. The combination of all these processes results in transport of radionuclides through the entire near-field and potentially from there to the far-field.

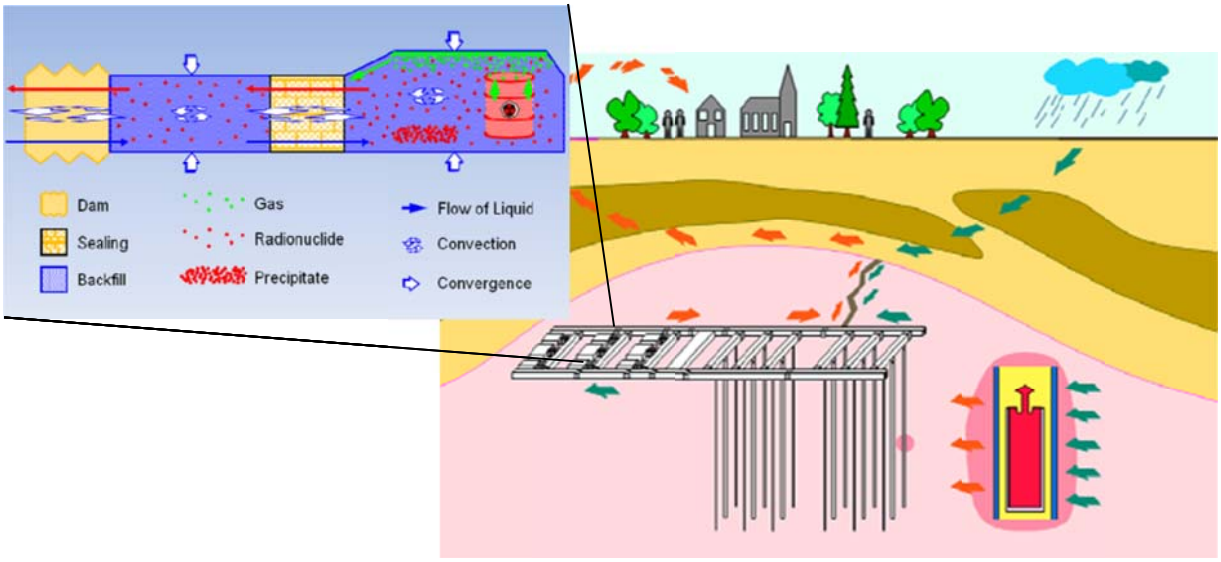

Figure 3-3 Schematic description of a repository system in salt (after /ROT 10/)

The waste container as a part of the multi-barrier system contributes to the safety disposal of HLW/Spent Fuel in geological formations by protecting the waste forms against radionuclide mobilization by attack of salt brines or groundwater. The main requirement on the container materials is long-term corrosion resistance under normal operating and accident conditions in the repository.

A collection of the studies on the corrosion of cemented wastes by 1998 is given in /KIE 98/. Most of the properties of the cemented wastes are affected by the producing conditions. The cement type (high oven cement or portland cement) the composition of the waste concentrates, the hydration behaviour, the volume changes and the mechanical properties of the cement play important roles. It is observed that the cement type has a minor effect on the cement suspension. The technical definitions and the average chemical composition as well as the hydration reactions of the cements used are given in the same reference.

The definition of the stability of the concrete in sea water and other brine solutions were investigated with numerous experimental studies /KIE 98/. Some of these works had the main investigation subject with the transport of the radionuclides. Due to contact with water with various salt concentrations, between the solution and the solution filling the pore volume of the cement, there is a concentration gradient. Therefore a diffusion based transfer process takes place. After the theory and the experimental works following mechanisms determines the behaviour of the cement products:

- Corrosion through leaching: This mechanism affects f.i. the element like Caesium, which is partly solved in pore water that can be mobilised very quickly from the cement. The portlandite is solved which results in the pore volume increase. In the case of water or NaCl solution the pH is increased.
- Corrosion of low solubility components f.i. calcium and magnesium through exchange reactions and leaching
- Corrosion through forced processes, caused by the adhesion of the new phases with increased specific volume in cement. This kind of corrosion is formed especially with the effect of sulphate on cement.

The experiments that are conducted with cement samples in NaCl solution and $MgCl_2$ (Q solution) are reported everywhere /SMA 02/. The results are generalised as follows:

With the contact to corroded solution Cl^- penetrate into the cement. The leaching of less soluble portlandite, waste salts (f.i Nitrate) and radionuclides (Cs) begin with diffusion controlled transport process. The pH of the Q solution increases with contact with various cements and stabilizes between 6 and 7 after some weeks of contact time. This value stays constant as long as Magnesium level is sufficiently high for buffering the pH and brucite $MgOH_2$ precipitates. In the case of NaCl solution following is observed: any buffering effect is lacking and the pH increases within a very short time (few days) up the values 12. In other experimental process the high oven cements exhibit higher corrosion stability against Q brine. The corrosion stability of the cement is dependent on the microporosity, this means on the pore volume. The measures to reduce the pore volume had no effect on the cement corrosion.

After the influence of $MgCl_2$ rich Q brine, the presence of Friedel salt, magnesium hydroxochloride (Mg_2OH_3, 4 H_2O) and various Gips phases are observed. It is expected that the magnesium hydroxochlorid and the gips phases may plug the pores delaying the corrosion steps. In a further step it is demonstrated that higher specific volumes of Gips phases may result in the mechanical degradation of the cement. In microscopical observation zones with various contrasts could be differentiated that can be commented as possibly high and low corroded zones. Figure 3-4 shows the profile of various elements of Portland cement in Q brine after 48 weeks as function of the distance from the surface of the cements. As can be concluded from the surface to the deep inside of the cement, the calcium concentration decrease first until a minimum is reached then increases rapidly having a maximum value and after this point decreases moderately until the corrosion medium. The curve for Mg is in contrast to Ca, first increases than decreases and remains constant after a minimum is reached. The same occurs as Ca is followed by Na. The Silicium on the other hand follows a different, an increasing profile with increasing distance from the inner to the surface of the cement, stay approximately constant after reaching to a value. The experiments show a strong temperature dependency.

In the corrosion experiments using Q brine, some traces of quartz as well as ettringit and portlandite are found at the surface of the cement. In these experiments main phases are CSH phases and Friedel salts. At the inner parts of the corrosion layer, portlandite, Friedel salt and Klinker phases are observed. The phase content is changed up to fully corrosion of the cement product. It is observed that at high pressures (100 bar) the ratio of crystalline phases is smaller as the case in 1 bar.

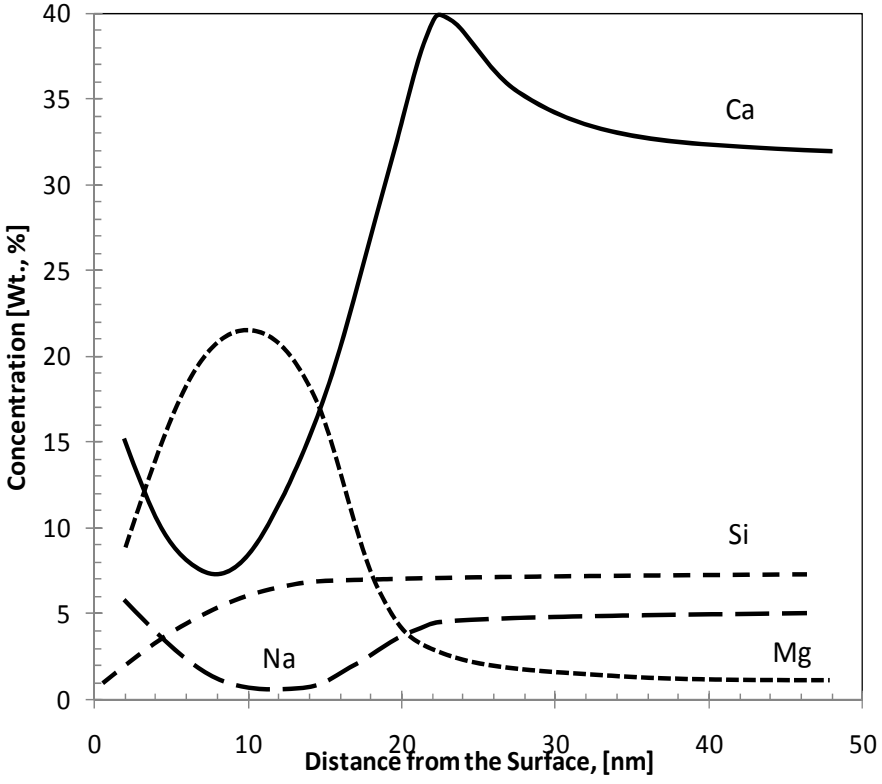

Figure 3-4 Profile of the elements from the corrosion distance in Q brine after 48 weeks /KIE 98/

To determine the influence of essential parameters (e.g., composition of the medium, temperature etc.) on corrosion, to gain a better understanding of corrosion mechanisms, and to provide more accurate data for modeling the corrosion of the containers over hundred of years an extended study was conducted /MOO 02/. To achieve the objectives of the project, a combination of chemical experiments (long-term immersion tests), electrochemical studies and stress corrosion cracking studies were performed in the EU-partner laboratories. FZK.INE considered both disposals in rock salt and in granite. Work of GNF.IUT concentrated on disposal in rock salt, ENRESA/INASMET considered disposal in granite, and SCK.CEN covered disposal in clay. The whole programme was coordinated by FZK.INE /SMA 02/.

The corrosion results obtained from these studies are used to develop material degradation models in order to predict the lifetime of the containers over very many years. A container corrosion model can be combined with other models (e.g. spent fuel and HLW glass models)

to describe the source term in the near field in the framework of safety analyses for a repository. Some relevant results are provided in the following:

Long-term immersion studies on candidate container materials

Long-term immersion studies were performed on the candidate container materials Ti99.8-Pd, Cu-base materials and carbon steel in disposal-relevant salt brines at 150°C.In these studies the galvanic corrosion behaviour of between the preselected TStE355 carbon steel and Ti99.8-Pd, the long-term corrosion behaviour of Cu-base materials such as Cu, Cu-Ni 90-10 and Cu-Ni 70-30 and the galvanic corrosion between Cu-Ni alloys and TStE355 carbon steel were investigated. All materials were evaluated for general corrosion and local corrosion by using gravimetry, measurements of pit depths, surface profilometry and metallography.

Influence of welding and thermal stress relief treatment of welds on corrosion of TStE355 steel in brines

To examine the effect of electron beam (EB) and tungsten-inert-gas (TIG) welding (potential container closure techniques), and thermal treatment of welds on corrosion of the preselected TStE355 steel, the steel was investigated in three material conditions: unwelded (parent material), only-welded, and welded plus stress-relief thermal treated. The steel was examined at 150°C in NaCl-rich brine (25,9 wt% NaCl) without gamma radiation, and in $MgCl_2$-rich brine (Q-brine, 26 wt% $MgCl_2$) in the presence of a gamma radiation field of 10 Gy/h. The results indicate that the unwelded steel is resistant to pitting corrosion in the sense of an active-passive corrosion element and its general corrosion rates (15,3 µm/a in NaCl-brine and 72,6 µm/a in $MgCl_2$-brine) imply corrosion allowances acceptable for thick-walled containers. The only-welded specimens suffer in this brine from severe local corrosion attacks in the welds and in the heat-affected zone (HAZ). However, the stress relief thermal treatment of the welds improves the corrosion resistance of the welded material in the $MgCl_2$-rich brine, so that the thermal treated welded steel is resistant to pitting corrosion, as does also the unwelded material. In view of these results, the TStE355 carbon steel continues to be considered promising for long-lived containers. To avoid local corrosion problems in the region of the welded container cover, a stress-relief thermal treatment of the welds is recommended.

Galvanic corrosion between TStE355 carbon steel and Ti99.8-Pd in brines

In NaCl-rich-brine both with and without gamma radiation and in $MgCl_2$-rich brine in the absence of gamma radiation no galvanic corrosion occurs on the coupled material pair Ti99.8-Pd/TStE355 carbon steel because both materials form protecting corrosion layers. However, in $MgCl_2$-rich brine and in the presence of gamma radiation field of 10 Gy/h a significant galvanic corrosion occurs which leads in the case of the coupled steel in strong local corrosion attacks and in a high increase in the corrosion rate (370 µm/a) compared to the value of the uncoupled steel specimens (72 µm/a). This is attributed to the fact that the oxidants (mainly O_2) formed by the radiolysis of water are reduced at the Ti99.8-Pd alloy which results in an increase of the oxidation rate of Fe analog to a local element.

Long-term corrosion behaviour of Cu-base materials and galvanic corrosion between Cu base materials and TStE355 carbon steel

Cu and the alloys Cu-Ni 90-10 and Cu-Ni 70-30 are potential materials for long-lived HLW/Spent Fuel disposal containers. They are resistant to pitting corrosion in salt brines and their corrosion rates (in NaCl-brine: 3-12 µm/a, in $MgCl_2$-brine: 24-46 µm/a) determined imply corrosion allowances reasonable for long-lived containers. In the NaCl-rich brine with and without gamma radiation (10 Gy/h) the coupled material pairs Cu-Ni 90-10/TStE355 carbon steel and Cu-Ni 70-30/TStE355 carbon steel form stable corrosion protective surface layers, and, therefore, no galvanic corrosion occurs. In $MgCl_2$-rich brine, however, both in irradiated and unirradiated brine environment, galvanic corrosion occurs due to local break down of the corrosion surface layer of the steel. This results in localized corrosion on the less noble coupled carbon steel and significant increase in its general corrosion rate (123- 564 µm/a) compared to the value of the uncoupled steel specimens (47-72 µm/a). For the more noble coupled Cu-Ni alloys a clear decrease in corrosion rate (6-6,2 µm/a) is observed in the unirradiated $MgCl_2$-rich brine compared to the values of the uncoupled specimens (37-46 µm/a). This means that in this brine the Cu-Ni alloys are cathodically protected by the carbon steel.

Electrochemical corrosion studies and surface analytical investigations on candidate container materials in salt brines

Electrochemical investigations into the corrosion behaviour of TStE355 carbon steel, Ni, Cu and Cu-Ni-alloys in the $MgCl_2$-rich Q-brine and in NaCl-rich brine were performed by applying potentiostatic and potentiodynamic measurements, measurements at rest potentials (free corrosion potentials) and at galvanic potentials at 25°C and at 80°C.

The results obtained demonstrate that among the materials investigated theTStE355 carbon steel is the less resistant material in Q-brine and in NaCl-rich brine, due to its negative potential with respect to its oxidant H_3O^+, which is reduced to H_2.The corrosion rates of carbon steel are higher in Q-brine than in NaCl-rich brine. The higher corrosivity of the Q-brine is attributed to its higher Cl^- concentration and lower pH (pH=4,5 at 25°C) compared to the NaCl-rich brine (pH=6,5 at 25°C), and to the Mg^{2+} containing in the Q-brine, which influence the formation of the corrosion surface layer. In general higher temperatures enhance the corrosion rates of all the materials under investigation. At 25°C the corrosion rate of Ni is only R_{Ni} = 8 µm/a in Q-brine due to its being passivated by a NiO surface layer. At this temperature the corrosion rate of Cu is significantly higher, R_{Cu} = 24 µm/a in this medium, because its potential is shifted more to the negative range due to the $[CuCl_2]^-$-complex formation. On the other hand, at 80°C in NaCl-rich brine it is R_{Ni} = 215 µm/a and R_{Cu} = 105 µm/a. This behaviour is caused by the passive range of Ni being shortened at higher temperature due to the disruption of the passivating NiO surface layer. At 80°C the oxidant of Ni and Cu in brines is O_2 to be reduced to H_2O or OH^- , respectively. At 80°C the O_2 concentration of the brines is smaller than at 25°C, which causes the shift of the relevant rest potentials of Ni and Cu to more negative values, because the cathodic potential current density is decreased. In case of galvanic coupling of carbon steel with Cu, Ni and Cu-Ni alloys, respectively, carbon steel is the anode in the two brines at both temperatures. The galvanic potentials are near to the relevant rest potentials of carbon steel which acts as a cathode protector. In accordance with the theory, the corrosion rates of the cathodic materials are decreased. From the contact pair Cu/Ni, which is of importance from the theoretical point of view, it was demonstrated that Cu is the anode and Ni the cathode in brine due to the existence of the $[CuCl_2]^-$-complex and the NiO layer.

The relevant thermodynamic data (Reaction Free Enthalpy $\Delta_R G$; Reaction Enthalpy $\Delta_R H$ and Reaction Entropy $\Delta_R S$) were calculated from Gibbs-Helmholtz and the dependence of the EMF on temperature, assuming $\Delta_R H$ to be independent from T. The reasonable data obtained confirm the assumptions made. They represent the few data which have been calculated for brines until now. Referring to all the corrosion data obtained by applying electrochemical methods it always must be kept in mind that only the starting period of the relevant corrosion processes and, therefore, the initial corrosion rate of the materials could be determined. The long-term corrosion behaviour and the final corrosion rate of the materials, which are needed for the evaluation of the suitability of the materials as container materials, were determined from the long-term immersion experiments. The most important advantage of the electrochemical studies compared to the chemical immersion experiments, however, is the possibility to study the corrosion mechanisms in detail, which allows a better interpretation of the corrosion results obtained from the long-term immersion experiments. The surface analytical investigations of corroded material specimens have shown that in the case of the electrode couples Cu/steel and Ni/steel in Q-brine, the steel electrode corrodes very strongly. A thick layer (μm-range) arises on the surface, which consists of crystallites of (Fe,Mg)-oxides, -hydroxides and -chlorides. The corrosion of the Cu and the Ni partner, respectively, is comparatively small. In the case of the electrode couple Cu/Ni in Q-brine at 26 °C, the corrosion of copper is very high, whereas the corrosion of Ni is small due to its strong passivation by an oxide/hydroxide layer. Besides the element composition and morphology being already analyzed, first investigations were undertaken and further investigations are urgently needed to determine also the phase composition and the structure of the surface layers by means of diffraction methods. The results from the investigation into the element composition and the morphology of the corroded surfaces of the Cu, Ni and steel electrodes by means of EPMA/EDX (Energy Dispersive X-ray Analysis) and SEM prove to be a valuable addition as well as a confirmation of those obtained electrochemically.

3.3 Geochemical Evolution of HAW in Clay

The repository concept proposed for Opalinus clay in Switzerland consists of containers that are placed on bentonite sockel and the rest pore volume filled with clay in form of pellets. In Nagra concept the fully compacted bentonite pellets should be disposed. The bentonite clay swells when it contacts with solutions and becomes tight limiting the further solution transport. On the other hand, the French repository concept proposes the placement of 8 HAW glass containers in horizontal or vertical wellbores (Figure 3-5). The horizontal wellholes will be filled up with clay buffers which at the end framed with steel liners. The ends of the repository tunnels will be sealed with clay based closure plugs. The maximum temperature of the repositories would not exceed 100 °C /LUC 04/.

The repository concept in Belgium is described in SAFIR reports. In the framework of these studies, the high and middle activity wastes should be deposited in various tunnels of the repository /SAF 03/. The diameter of the tunnels is given as 4 m and of the shafts as 6 m (Figure 3-6). The concrete is planned to be used for the preparation of the tunnels. The wastes are planned to be disposed in metal containers. The containers are designed so that they produce minimum hydrogen during the anaerobe phase of disposal. The pore space

between the containers and concrete frame will be filled with compacted Ca-bentonite, sand and graphite.

In French and Belgium concepts the buffer material consists of a mixture of 60% clay with swelling property, 35% quartz and 5% graphite. The graphite should serve for increasing the heat conduction properties independent of saturation.

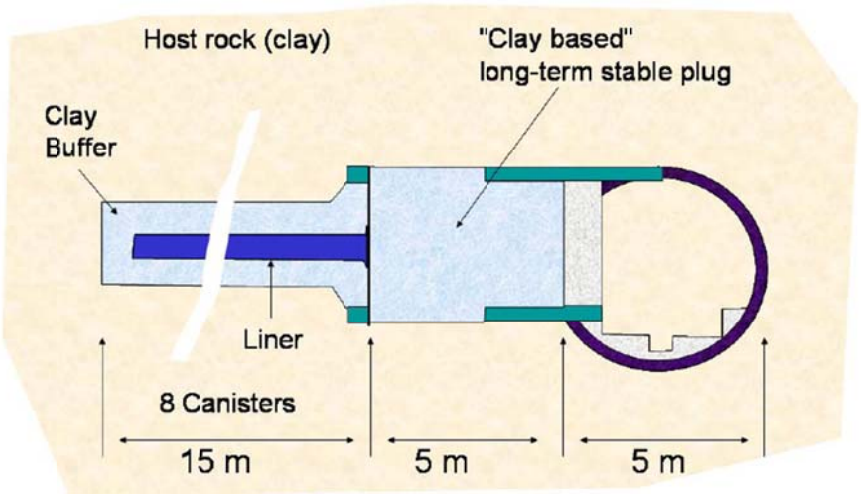

Figure 3-5 Disposal concept for HAW products in Callovo Oxford clay formation in France /LUC 04/

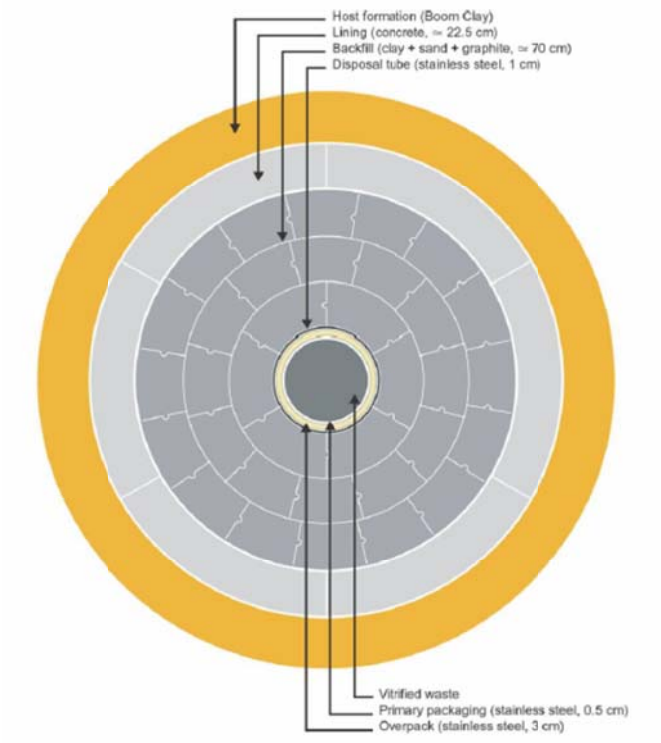

Figure 3-6 Cross section of a repository tunnel for HAW glasses in Boom clay /LUC 04/

The relevant parameters of a clay formation as geological repository determined by the various EU research programs is given in the Table 3.1 giving the initial and boundary conditions for a clay geological barrier. This also serves input data for modeling studies.

Table 3.1 Characteristics of the conditions of clay formations with clay as geotechnical barrier and metal containers /LUC 04/

Parameter	Definition	Variation Interval
Temperature, °C	T	25 - 60
Diffusion coefficient, m^2/s		10^{-13} – 10^{-10}
Solubility limit mol/l		1.10^{-7} (pessimistic) 3.10^{-9} (reference) 5.10^{-7} (pessimistic)
Porosity, percent		0,4
Sorption coefficient, m3/kg		Up to 1
compression strength, MPa		4 - 10 (bentonite buffer)
pH		7 - 10
Eh, mV		-130 (pH 7) to – 300 (pH 8)
Bicarbonate mol/l,	$HCO3^-$	10^{-4} – 6. 10^{-2}
Dominating cations, mol/l	Na^+	2.10^{-3} – 0.4
	K^+	10^{-4} – 10^{-3}
	$Ca2^+$	10^{-4} – 10^{-2}
	$Mg2^+$	10^{-5} – 2.10^{-3}
Relevant species for redox conditions	P(H2)	<1 to 10 MPa
	Fe(II)	1.10^{-7} – 3.10^{-4}
Anion, mol/l	Cl^-	3.10^{-2} – 0,2
	$SO4^{2-}$	10^{-5} – 0,14
Other species	Al3+	1.10^{-8} – 5.10^{-5}
	Si (total)	1.10^{-4} –1.10^{-3}
	HPO42+	
	Organic	?

3.3.1 Geochemical interactions of Metals with Clay formations

There are only a few experimental analyses on the possible corrosion products of container materials in a repository of clay formations. Some investigations for Boom clay results in following corrosion products of carbon steel (Table 3.2):

Table 3.2 XRD analysis of the composition of corrosion layers of carbon steel in Boom Clay /LUC 04/

Phase		16 °C	90 °C	170 °C
Magnetit	Fe3O4	x	x	x
Haematit	a-Fe2O3	?	?	?
Lepidocrocite	g-Fe2O3.H2O	??	?	-
Maghemite	g-Fe2O3	-	?	x
Goethit	a-FeOOH	??	?	?
Quartz	SiO2	x	x	
Calcite	CaCO3	-	-	
Pyrrhotit	Fe(1-x)S	-	-	

3.3.2 Interactions of Clay with Cement

The subject is intensively investigated. Clay is considered as host rock or buffer material. Cement is applied in various repository concepts as a medium for the fixation of the radioactive waste and in concrete as structure element. The influx of water can results in the alteration of the cement which also result in alkaline solutions with high pH values (12,5-13,6). The solution composition should be dominated in the first line the alteration through NaOH and KOH. In relation with this first reaction phase the solution composition will be controlled through portlandite ($Ca(OH)_2$ – pH 12) and at a further reaction step by the silicat-hydrat (CSH – pH -10).

If smectite comes in contact with alkaline solutions the smectite as plat forms big aggregates. From the point of view of crystal chemistry an increase of layer can be observed that layer charge is increased. The smectite contains with that no more swelling capacity, but produces more aluminium in its tetrahedral layers. The layer charge of smectite increases continuously and at the end results in the irreversible collapse of the layers. This collapse also named as illitisation results in the irreversible production of potassium.

The reaction with alcaline solutions results in with the dissolution of kaolinit and related precipitation of the illit. This follows the precipitation of various mineral phases. After the formation of illt, zeolite and phillipsit can be formed in the same system. In the smectite samples the crystallisation of quarts and kallifeldspat is formed, in the kaolinit the formation of kalifeldspat is observed.

The conditions in the vicinity of a clay repository is investigated in /TAU 00/ with Opalinus clay and Hammerschmiede Smektit. A solution which can be assumed as a first step of the cement alteration is applied. The applied clay exhibits very low alteration layers only in the first centimeters. In the opalinus clay the chloride layer could not be observed in the röntgen diffraktogramm. Apparent differences exist on the development of the permeabilities. Because of the dissolution process some new flow path are observed being developed. Because of its mineralogical composition Opalinus clay shows very low swelling properties which means that the newly formed flow paths could not be closed. In the case of Hammerschmiede smectite the permeability reduces apparently because of the swelling and the precipitation of the secondary phases (Brucite, Portlandite, Calcite, etc.).

The effect of the alcalien solutions on the clay is investigated by Claret et al. /CLA 02/. From the dominating phases smectite, illit and illit/smectite interplay phase demonstrated only smectite an indication of a reaction. A very important result of the investigations of Claret is the higher dissolved content (concentration) of organic carbon (<250 mg/l).

3.3.3 Corrosion of HAW Glasses

The very important difference between the corrosion of glasses in salt solutions and in solution of clay formations consists of the fact that the corrosion in saturated salt formations i.e. in salt formations the long-term corrosion is influenced at very low degree as only few reactions take place between the salt formation and the solution and these reactions has a very limited effect on the composition of the salt solutions. Contrary, the corrosion of glasses in clay formations can results in very strong interactions and material interchanges between the solutions and minerals of the rock such as sorption, ion changes, sorption and precipitation. These interactions affect the corrosion rate significantly. The same is valid in the case of using clay based buffer (bentonite) materials. A list of the experiments to investigate these interactions is given in /MOO 02/. The results of these experiments being conducted in a variety of conditions are difficult to be used directly to describe the interactions in the real repository units /LUC 04/.

Clay Environment

The resistance of eight preselected container materials to pitting corrosion was investigated under conditions representative for underground disposal in clay. These materials are: carbon steel (TStE 355), stainless steels (AISI 316L, AISI 316L hMo, AISI 316Ti, UHB 904L), nickel-base alloys (Hastelloy C-4, Hastelloy C-22), and the titanium alloy Ti/0.2Pd (Ti99.8-Pd). The influence of four environmental parameters on the pitting corrosion of the materials was investigated, namely the oxygen level, the temperature, the chemical composition of the underground disposal environment (chloride, sulphate, and thiosulphate), and the presence of the most important rad olytic product hydrogen peroxide (H_2O_2). The oxygen content reflects the aerobic and anaerobic phases of the disposal. The tests were conducted at three

temperatures, namely 16°C, 90°C, and 140°C. The chloride concentration was varied up to 50,000 mg/l. The influence of thiosulphate was investigated in the range 20- 200 mg/l. Experiments were performed in solutions containing 0.2, 216, 1700, and 5400 mg/l sulphate. The influence of hydrogen peroxide, which occurs as a radiolytic product from the interaction of gamma radiation with the aqueous surroundings, was studied in the range 8.10^{-3}-8.10^{-1} mol/l.

The long-term susceptibility to pitting corrosion was evaluated by comparing the critical potential for pitting (E_{NP}) and the protection potential (E_{PP}), which were determined from CPP-measurements, to the actual corrosion potential, which was determined by monitoring the free corrosion potential as a function of time. The results indicate that among the materials investigated only the alloy Ti/0.2Pd was completely resistant to pitting corrosion under all experimental conditions applied. The results obtained for the other materials under the various experimental conditions are also given /LUC 04/.

3.3.4 Secondary Phase in Boom and Opalinus Clay

Experiments on the behavior of HAW glasses in Boom Clay system are mainly concentrated on the degradation of the glass materials in wet milieu at various temperatures. Because of the composition of the pore fluid of Boom and Opalinus clay no significant differences were observed on the corrosion behavior of the HAW glasses. This also means that no variation is expected on the release of the radionuclides with comparison to the experiments of granit-water and NaCl solutions. Actually the higher carbonate concentrations (HCO_3,CO_3) especially in Boom clay solution may increase the solubility of actinides because of higher pH as the result of carbonate-complexation /LUC 04/.

The reactions between the solution and the clay result in the immobilization of Si and decrease of the Si concentration in the solution. This decrease is due to various mechanisms:

i. Nucleation in pore fluid, this is the precipitation of the Si in various forms
ii. Si use for the growth of the existing Si phases.
iii. Si growth with the adsorption of phyllosilicates and a homogeneous nucleation on the surface
iv. Transformation or recrystallisation of the initial clay in Si rich clay
v. Si retention in the interlayer of clay minerals

It is very difficult of differing between sorption and generation of Si in already existing and newly precipitated phases. Secondary phases were examined in only few experiments at 90 °C. The formed secondary phases are probably too small to be observed with conventional measurements. The term “immobilisation” will be applied for sorption and/or precipitation. For some of the corrosion tests can the whole immobilized Si amount can be calculated from the mass loss of the glass samples.

A generalized description of the concentration of the phases adsorbed to the solid phases as function of the concentration is given in Figure 3-7. After all available sorption sites are filled, the concentration remains constant and the concentration of the species in the solution increases strongly. After the concentration in the solution reaches to the saturation limit precipitation begins. Some diffusion and adsorption tests were reported; the adsorption of Si is reversible but the sorption mechanisms and sorption kinetic could not be exactly determined.

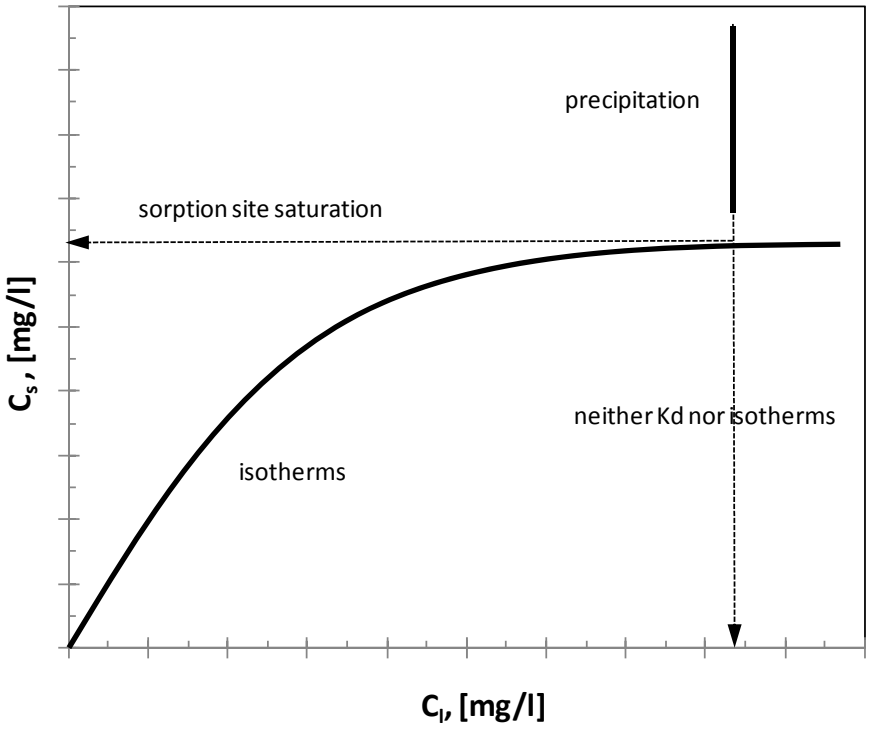

Figure 3-7 Generalized evolution of the concentration of the adsorbed and dissolved species

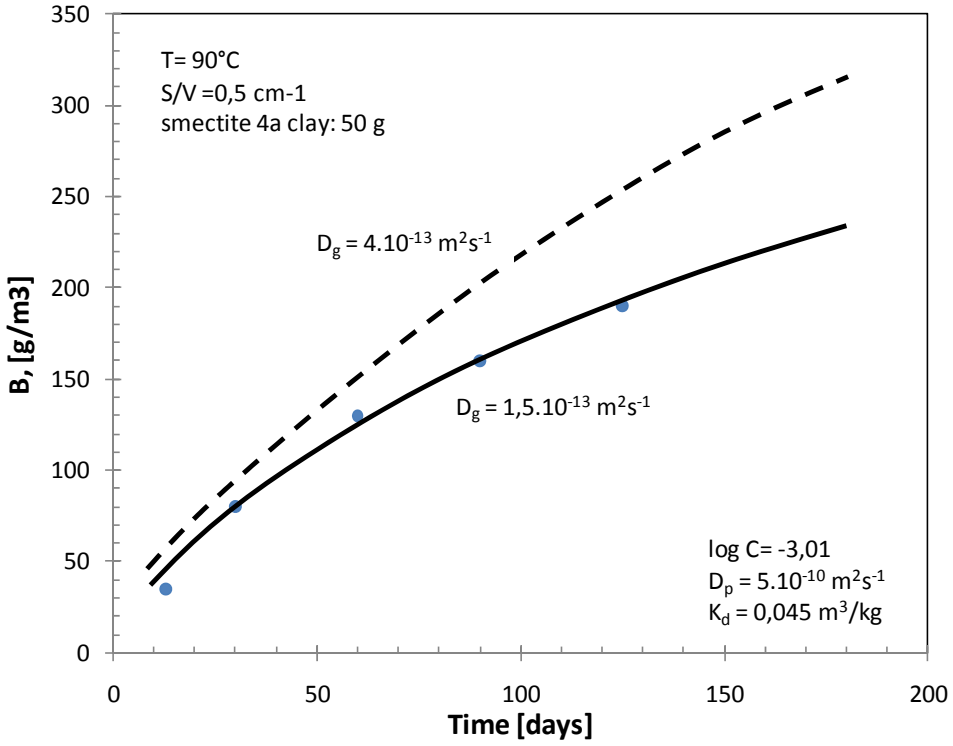

Figure 3-8 Experimental and calculated corrosion of glasses under static conditions /LUC 04/

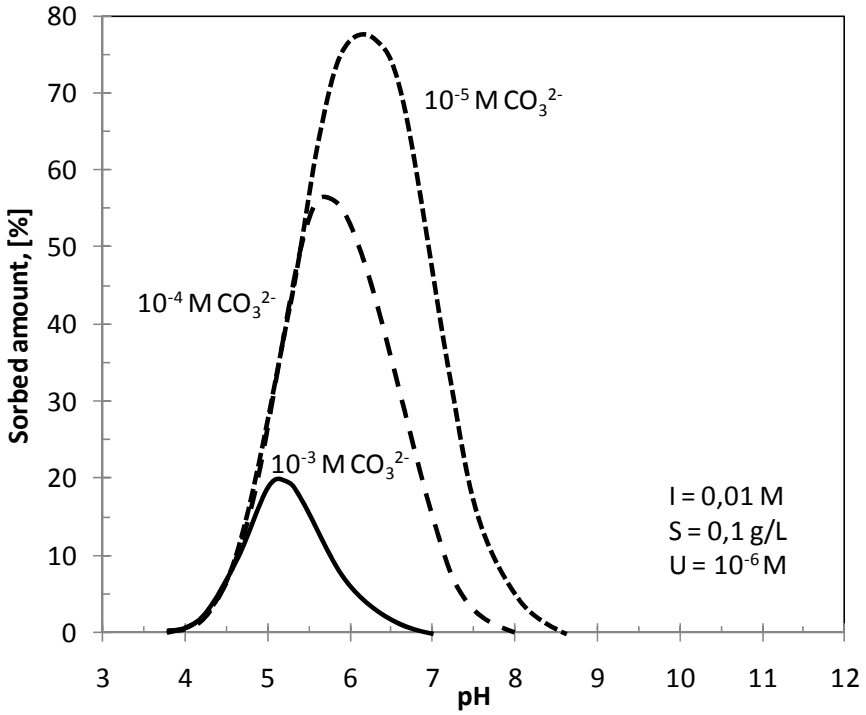

Figure 3-9 Effect of carbonate concentration on the U sorption on corrensit /LUC 04/

3.4 Chemical Interaction Buffer Material (Bentonite) in Saline Solution

The isolation properties of the bentonite buffer depend on several properties. The bentonite contains small amounts of sulphides (mainly in the form of pyrite) and residue organics. The pyrite and organics function as redox buffering material to ensure a reducing environment in the vicinity of the canister. In a reducing environment, solubilities of most of the radionuclides in groundwater are extremely low. Their transport in groundwater is therefore very low. Sorption capacity of bentonite, on the other hand, in reducing conditions is much higher than under oxidising conditions.

In addition to interlayer cations like Na^+, K^+, Ca^{2+} and/or Mg^{2+} both the tetrahedral and octahedral sheets of montmorillonite contain OH groups at the sheet surfaces which under neutral and alkaline conditions can be deprotonised to give the sheet extra negative charges to give the sheet extra charges . These negatively charged sites have a large tendency to bind cations. The sorption capacity of the compacted bentonite is quite high, with a cation exchange capacity (CEC) of on the order of 100 meq/g. Many released radionuclides from the canister will first be sorbed onto clay /FER 06/.

Several mechanisms can be responsible for changing the long-term properties and thus degrade the isolation properties of the bentonite buffer /KAU°09/ /ARC 03/. The first one is the oxidation mechanism. Oxygen trapped in the galleries and deposition caverns during the excavation and construction of the repository is considered to be very small and to be depleted either by the reducing components of the near field or by mass transport. Radiotically generated oxidants can however last for a longer time and possibly react (oxidise) the pyrite

and the organics in the bentonite either directly or by first oxidising uraninite in the spent fuel to give hexa-valent uranium as an oxidant. The radiotically generated oxidant will not be released until the container is damaged which seems to be not high probable. The oxidation mechanism has been studied /ROM 95/.The model calculations were based on mass balance of the reducing capacity of the bentonite clay and the diffusive mass transport of the radiolytically generated oxidant through clay. Detailed chemical reactions have not been considered. Studies of chemical reactions of bentonite with groundwater in the literature have been limited to several specific types of reactions. Kinetics of chemical reactions of the oxidation mechanism has been considered by some authors. It has been applied to study the time evaluation of entrapped oxygen concentration and redox conditions in the bentonite buffer after the repository is sealed.

Another mechanism that affects the long-term properties of bentonite is the alteration to other minerals. Montmorillonite in the bentonite can be altered to non-expanding hydrous mica (illite). The conversion yields a dramatic drop in swelling pressure and stiffness and an increase in hydraulic conductivity; there are two kind of conversion: high temperature beidellitisation and low temperature dissolution alteration. In a final repository, the maximum temperature is about 80°C, the beidellitisation is not likely to occur. The dissolution alteration, however, must be considered.

The third mechanism is the ion-exchange mechanism. The bentonite used in the buffer material will be Na-bentonite. Sodium cations incorporated in the interlamellar sites of montmorillonite can be replaced by calcium cations through cation-exchange. Some investigations showed that this mechanism does not significantly alter the physical properties of smectite buffer of high density. In some studies on the other hand, it is affirmed that the ion exchange of sodium for calcium is considered to be probably the most important chemical alteration of the bentonite buffer, resulting in a loss of plasticity and to a limited extent of swelling ability.

3.5 Modeling of Reactive Transport

Three-dimensional geological transport codes are applied nowadays in various fields of engineering and sciences for calculating the time and location dependent transport of various phases as well as components of these phases. One of the general assumptions of using such codes is to neglect the chemical reactions between the existing phases including the minerals of the solid phase.

For the long-term safety analysis of nuclear repositories, the application of the reactive transport codes taking the effect of the temperature, generation and transport of the gases and contaminants is necessary. In the near field of the transport process is influenced mainly by the chemical milieu which defines the solubilities as well as the sorption characteristics. As the thermodynamic conditions changes continuously as the result of the transport processes a coupled thermodynamic package should calculate the unstationary chemical equilibrium continuously.

The modeling of the geochemical conditions and its time dependent changes in a geological milieu started with static modeling efforts that means calculating the chemical conditions and concentrations of the species in a solution for various time steps and/or with the addition of new species /MOO 07/. The first documented code for the modeling of geochemical changes

was the EQ3/6 which permitted the evaluation of the geochemical condition coupling implicitly to the transport processes /WOL 92/.

EQ3/6 is a software package for geochemical modeling of aqueous systems. The software deals with the concepts of thermodynamic equilibrium, thermodynamic disequilibrium and reaction kinetics. The basic purpose of EQ3/6 is to make two kinds of calculations pertaining to aqueous solutions and aqueous systems. The first kind is called a speciation solubility calculation and the purpose is to describe the chemical and thermodynamic state of the solution using as input analytical data and/or theoretical assumptions such as of partial equilibrium with specified minerals. Such a calculation uses the concept of thermodynamic equilibrium, activity coefficients and ion pairing and complexation along with the corresponding mathematical descriptions and model parameters. It is possible to introduce some elements of thermodynamics disequilibrium in such a calculation so it is not necessarily a pure equilibrium calculation. That must be paid is the requirement of additional analytical data. The output of a speciation-solubility calculation consists of two parts. One of these is the speciation: the concentration and thermodynamic activity of each individual chemical species. The other the solubility part, consists of the saturation indices:

$$SI = \log(Q / I) \tag{3-1}$$

where Q is the activity product and K the equilibrium constant for the various reactions not in a state of partial equilibrium. Most of these reactions pertain to mineral dissolution and often speaks of the saturation index of a given mineral. Many aspects of such calculations can be inverted so that an output and an input to the problem can change the roles.

An important next step was the development of the reaction path models that captured the sequence of chemical/mineralogical states resulting from such irreversible processes as chemical weathering and hydrothermal alteration. Early versions of the reaction path models, pioneered by Helgeson and coworkers, did not include an explicit treatment of real time kinetics, quantifying the system evolution instead as a function of reaction progress /HEL 68/, /HEL 69/. These models provided a way of interpreting quantitatively the sequence of minerals observed in nature as the natural consequence of the dissolution of some primary phase (e.g., feldspar), which is itself out of equilibrium due to either the initial state of the system, or more commonly, due to the flux of reactive constituents. In general the boundary conditions of a system are modified stepwise obtaining for each case a new equilibrium. In a further variance of this modeling concept is to eliminate the introduced solid phase at the end of each step obtaining a new local equilibrium model.

The reaction path approach can be used to describe chemical processes in a batch or closed system (e.g., a laboratory beaker) however; such systems are of limited interest in the geosciences where the driving force for most reactions is transport. Lichtner clarified the application of the reaction path models to water–rock interaction involving transport by demonstrating that they could be used to describe pure advective transport through porous media /LIC 88/. By adopting a reference frame which followed the fluid packet as it moved through the medium, the reaction progress variable could be thought of as travel time instead. This approach has now been generalized to heterogeneous, multi-dimensional flow fields, using both deterministic and stochastic approaches /YAB 98/ /MAL 04/. Multi-component reactive transport models that could treat any combination of transport and biogeochemical process-

es date back to the mid-1980s. Lichtner outlined much of the basic theory of a continuum model for reactive transport /LIC 85/. Yeh and Tripathi also presented the theoretical and numerical basis for the treatment of reactive contaminant transport /YEH 89/. Steefel and Lasaga presented a reactive flow and transport model for non-isothermal, kinetically controlled water–rock interaction and fracture sealing in hydrothermal systems based on simultaneous numerical solution of both reaction and transport /STE 94/. These studies were largely focused on developing the theoretical and numerical tools for simulating reactive transport in a range of environments. A number of seminal studies have explored the use of transport theory in interpreting spatial patterns in geologic environments. In groundwater aquifers, the studies of Valocchi and co-workers /VAL 81/ and Appelo /APP 94/ demonstrated that ion exchange could be used to interpret the spatial and temporal patterns of dissolved species in groundwater systems. In the case of contaminant plumes developed from organic rich landfills, it is showed that the spatial zonation of redox zones in an aquifer downstream from an organic-rich waste plume could be rigorously interpreted as the result of the natural sequence of microbially mediated redox reactions as the system gradually becomes less reducing /ENG 96/ /BRU 02/. Beginning with the seminal work of Berner, reactive transport modeling helped to make sense of the redox zonation found in marine sediments in terms of a coupling of transport processes and microbially mediated oxidation of organic matter. Reactive transport theory has also been applied to the interpretation of isotopic spatial patterns in soils and groundwater /BER 80//JON 94/, although only very recently have these models developed explicit accounting of the various reaction mechanisms that control isotopic exchange /MAH 04/.

The application of transport theory to the interpretation of mineralogical, chemical, and isotopic spatial patterns in metamorphic rocks is an example of where reactive transport modeling has had profound impact. The types of problems that can be treated with reactive transport modeling has grown, and now includes multi-phase flow, heat transport, and multicomponent reaction in fractured media and flow and reaction in highly resolved, heterogeneous porous media. The recent advances appear to have had the most impact in the groundwater and contaminant transport, but are likely to have much broader impact in the near future on many other situations where water–rock interaction is important. Following items can be cited as the important feedbacks considered as coupled processes in reactive modeling /STE 05/:

- Coupling between energy and fluid flow (conservation of momentum), primarily through the advection of heat and the effect of temperature on the fluid density,
- Coupling between the conservation of momentum and the conservation of fluid or solid mass, typically treated by solving the two together to obtain the flow field or the deformation of the solid phase,
- The effect of dissolution or precipitation of minerals on concentrations of solutes and the mass of minerals,
- Coupling between fluid flow and solute concentrations, primarily through the advection of solutes and/or colloids and the effect of concentration on fluid density and coupling between the deformation of the solid matrix and solute concentrations through the effect of stress on reactions (i.e., pressure solution)and through modifica-

tions in the porosity and permeability as a result of mineral dissolution or precipitation, and

- Coupling between temperature (conservation of energy) and solute concentrations through the effects of temperature on the thermodynamics and on reaction rates and the effect of chemical reactions on the thermal regime where heats of reaction are significant.

The efficient and applicable coupling of a transport code with a geochemical program has been long time a challenge because of the theoretical as well as numerical difficulties. The complexity of the coupled processes especially the effect of the solid precipitation and computing time have been the principal negative factors. The computation of the chemical equilibrium in most of the cases has taken place not directly but indirectly resulting in a discontinuity thus a numerical process inefficiency.

With the developments on computer science and the chronic need for modeling of the reactive transport processes increased the intensity of the works at the latest decades resulted in the release of various reactive transport codes. As most of them are still in validation stage they are available free as in the case of MODFLOW from USGS, CHEMTARD from NEA and HYTEC from ENSMP. For the assessment of long-term safety of underground waste repositories the program-package EMOS is used in the GRS /MOO 02/. EMOS that is an integral simulation package for module-specific transport processes for various types of repository was linked with CHEMAPP, a commercially available, pre-compiled library of routines for the calculation of thermodynamic equilibrium. A new database was established containing data from the above mentioned sources. While radioactive decay, temperature evolution, etc. are taken into account in all modules, diffusion and sorption are considered in far-field modules; while in near-field modules, advection, dispersion, diffusion, and convection are considered as transport processes besides other effects. However EMOS is reported to model the one-phase flow and does not take the effect of any free gas on transport.

In the near field the transport process is influenced mainly by the chemical milieu which defines the solubilities as well as the sorption characteristics. As the thermodynamical conditions changes continuously as the result of the transport processes a coupled thermodynamical package should calculate the instationary chemical equilibrium. Various cases were studied by modeling in repository conditions coupled with chemical issues. Latest publications give interesting applications of reactive transport modeling for nuclear repositories.

In the case of using cement and concrete in conjunction with bentonite the potentially negative effects of cement degradation on the performance of the geological barrier in the near-field should be evaluated. Saturation of cementitious materials with groundwater produces a hyperalkaline pore fluid with a pH in the range 10–13,5 /BER 92/. These hyperalkaline pore fluids have the potential to react chemically with bentonite affecting its physical and chemical properties and react with canisters. On the other hand, mineral alteration in the engineered barriers could also affect the potential migration of radionuclides from the repository. There are great concerns that the mineralogical composition of the bentonite will not be stable under the hyperalkaline pore fluid infiltration and its properties may degrade over long time periods Whether such interactions could impact long-term repository performance is one of the questions that must be answered. The effect of these interactions on the composition of water that could potentially seep into emplacement drifts is of particular importance to the as-

sessment of corrosion rates of waste containers and other in-drift engineered systems. Reactions of bentonite clays with hyperalkaline fluids have been studied from a very wide perspective, including radioactive waste disposal /SAV 02/, /STE 98/. Previous modeling studies of the interaction of clays with hyperalkaline fluids in engineered barriers for a HLW repository suggest that mineral dissolution/precipitation will be important in defining the alteration zones and porosity evolution which will be intrinsic to governing the degree to which bentonite may be altered. In /SAV 02/ a 1-D numerical model to simulate the interaction of bentonite with hyperalkaline fluids is presented. In the model, hyperalkaline fluids were considered as infiltration of boundary water into the bentonite where minerals were allowed to dissolve and precipitate using kinetic (time-dependent) reaction mechanisms. However, their models only simulate the geochemical processes in the bentonite induced by the infiltration of hyperalkaline fluids from the boundary. A numerical model to simulate geochemical evolution in a multibarrier system for a potential HLW disposal in a clay formation is presented in /YAN 08/. The multibarrier system consists of bentonite buffer, concrete and the host clay formation. The model is used to study the interactions of hyperalkaline pore fluids with rock a long time period (around 1 Ma) and evaluate the chemical evolution of pore water composition, mineral alteration patterns, and resulting rock-porosity changes in the multi-barrier system using a multicomponent reactive transport code, $CORE_{2D}$ V4 (/SAM 03/). Codes of CORE series have been extensively used to model laboratory and in situ experiments including CERBER-US Experiment in Boom clay /SAM 06a/ interpretation of the Redox Zone Experiment in a fracture zone of the Aspo site /MOL 06/, inverse reactive transport of laboratory experiments and coastal aquifers /DAI 06/, evaluation of oxygen consumption in a HLW repository /YAN 08/ and stochastic cation exchange and reactive transport in aquifers /SAM 06b/.

A fracture network makes always a part of a radioactive repository whatever the type of the geological media and the modeling of transport in fractured rock is a challenging issue because of the unconventional flow and thermodynamic behavior of the existing phases that are present in the fractures. The natural fractured system that may be typical for the transport through crystalline host rocks, or dilatancy induced fracture network at the excavation damaged zones and the secondary flow paths in compacted clay buffers are typical for repository concepts. Some efforts to study the reactive flow in fracture network of repository systems can be found in the literature /NOV 93/, /SPY 03/, /KER 05/.

In the literature conceptual models are provided for far-field movement of redox fronts in crystalline rock to identify the required capabilities of a multi-component reactive transport model suited to test these conceptual models. These conceptual models focus primarily on geochemical processes, and to a lesser degree on transport processes. The model requirements are discussed in the framework of a state-of-science review of existing reactive transport models in /KER 05/. In particular, the capabilities and limitations of existing models are addressed. It is focused on the use of multi-component reactive transport models suitable for the investigation of the evolution of redox conditions. The effect of salinity changes are required additional model features, which is also briefly discussed.

An interesting study in terms of modeling the reactive transport in fractured rocks as nuclear repository is published on Yucca Mountain /SPY 03/. The potential repository in Yucca Mountain host-rocks consist of fractured, welded volcanic tuffs located several hundred meters above the regional water table. These geologic units are unsaturated, with total water-

moisture content typically around 10% (by volume). Most of this water resides in the rock matrix (liquid saturation near 0,9), whereas fractures are thought to contain little water (saturation typically < 0,1). Fracture permeability is several orders of magnitude greater than that of the rock matrix. After the studies on the potential effects of thermal loading upon heating to boiling conditions (approximately 95 °C at Yucca Mountain), water moisture in the rock boils, and a dry zone develops around the drift (Figure 3-10). In this zone, the water saturation in fractures declines to zero, whereas the rock matrix may still contain water if the vapour pressure in the tight matrix is significantly lowered by capillary pressure or if the total pressure increases. This zone of dry fractures expands outward for several hundred years, impeding seepage into the drift. It then recedes as the repository cools down, until some point in time when water eventually wets fractures at the drift wall again. After tens of thousands of years, following the nearly complete decay of short-lived radionuclides, temperature eventually returns to ambient values. During the boiling period, mobilized water vapour travels more rapidly in fractures and condenses in cooler areas away from the drift. The condensate flows back towards the boiling zone mostly by gravity (drainage) but also through the effect of capillary suction (imbibition), and then boils again. These areas of continuous condensate refluxing are anticipated to be the most affected by water–gas–rock interactions. In contrast, if the rock moisture does not boil, much less water is mobilized. Significant evaporation still takes place such that the processes described for the boiling conditions occur, but to a much lesser extent. However, fractures may never completely dry out. Also, as noted earlier, mineral reaction rates are slower at low temperatures than at high temperatures (by one to two orders of magnitude in the present study). For these reasons, variations in water compositions and mineral precipitation or dissolution amounts are expected to be less pronounced at low temperatures. Water–rock interactions in the subsurface are strongly affected by the CO_2 dissolved in most natural waters. The effects of heating, boiling, and condensation on CO_2 chemical behavior and its effect on water chemistry and mineral alteration in geothermal systems have been understood for some time. However, in such studies, the coupled effects of fluid flow and reaction were not considered, and the modelled systems were liquid- saturated. Only a few investigators have attempted to model coupled THC processes in an evolving, boiling, unsaturated system /XUT 01a/. These simulations captured most of the coupled processes discussed here, including reactive CO_2 transport around a heater-test drift at Yucca Mountain. In /LIC 96/ such processes around a potential repository at Yucca Mountain are simulated and pH trends (caused by CO_2 transport) are predicted similar to those discussed below. Their study considered a simple model (one-dimensional, single porosity) with a limited number of minerals and chemical components. In /NIT 97/ another modeling study of coupled THC processes around a repository drift (two-dimensional, dual porosity) that included only silica phases and ignored the effect of reactive CO_2 transport is presented. In /SPY 03/ a two-dimensional, unsaturated dual-continuum model including all major host-rock minerals, several possible secondary solid phases, and reactive CO_2 transport are considered. Two underground thermal tests at Yucca Mountain have provided the basis to further evaluate the coupled effects of thermal and hydrological processes on water chemistry and mineral alteration, including CO_2 transport, in a boiling unsaturated environment. The Drift Scale Test, and to a lesser extent the Single Heater Test, have provided a significant amount of water chemistry and mineralogical data to understand and model coupled THC processes

around a heated drift /SON 01/. From this and earlier studies, the following important processes affecting water and gas compositions have been observed:

- Upon heating (before boiling), pore water evaporates and CO_2 from dissolved inorganic carbonate species naturally present is volatilized. This is typically accompanied by calcite precipitation (i.e., $Ca_{2+} + 2HCO_3^{-2} + CaCO_{3(s)} + CO_{2(g)} + H_2O$) and generally also a pH increase in the remaining solution (e.g., $HCO_3^- + H^+ \; CO_{2(g)} + H_2O$). Eventually, evaporative concentration results primarily in the precipitation of amorphous silica and gypsum (or anhydrite) in addition to calcite.
- Upon boiling, the effects are similar to, but more pronounced, than those described above, with increased mobilization of steam and CO_2. Also, upon continuous boiling, steam displaces air and CO_2 in the gas phase.
- In condensation zones, dilution of ambient pore waters is typically accompanied by a pH decrease resulting from the dissolution of CO_2 gas mobilized with steam (e.g., $CO_{2(g)} + H_2O \; Z \; HCO_{3\_} + H_{+}$). This causes aluminosilicate phases and calcite in fractures to dissolve.

Although these processes are noticeable over the relatively short time scales of the thermal tests (1–4 years), additional interactions are likely to affect water compositions around waste emplacement drifts over thousands of years. For example, the precipitation of small amounts of secondary minerals such as clays or zeolites could have a significant effect on water chemistry, although precipitated amounts are too small to be discernable in a short timeframe experiment. To fully understand and predict interactions over longer time frames, numerical models then become a necessity.

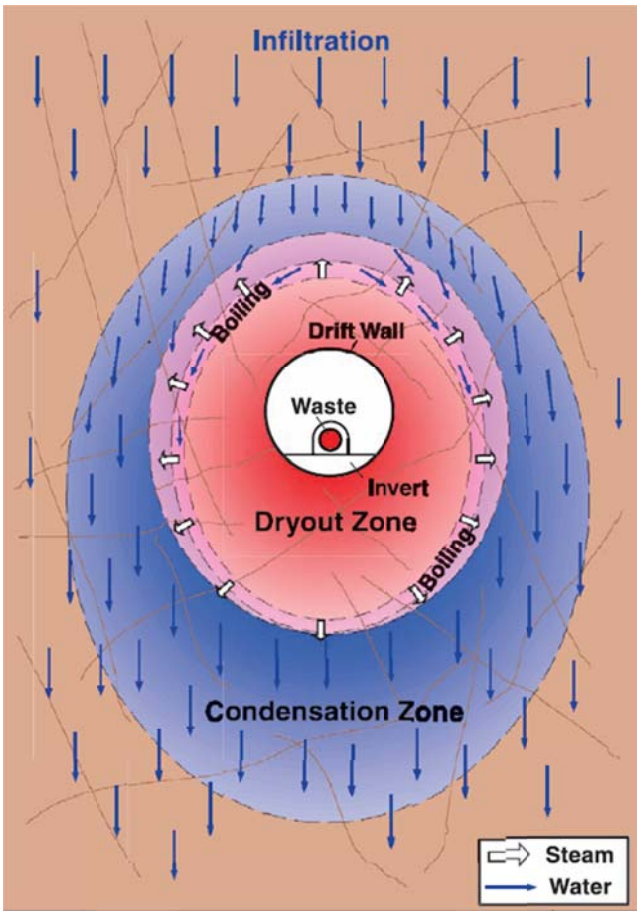

Figure 3-10 Conceptual model fro the numerical study applied in /SPY 03/

In /KER 05/, the conceptual model is based on the fact that groundwater recharge takes place through fractured crystalline bedrock, where a significant portion of the infiltration occurs through fractures (Figure 3-11). The time scale of infiltration through the fractures is therefore much shorter than through the matrix. The depth to which recharge water can penetrate will depend on a number of factors, such as watershed topography and density differences between recharge waters and deep saline groundwater recharge waters as well as the effect of glacial compression and uplift. Fracture water composition may be significantly different from the water composition in the rock matrix because recharge water can easily enter into the fractures, but not into the matrix. This will lead to geochemical interactions focused on the fracture–matrix interface and within the matrix material directly adjacent to the fracture. Previous studies have shown that the present day mineralogy in the fractures is very different from the mineralogical composition in the matrix, which supports this hypothesis. The different mineralogy reflects that water–rock interaction has been more significant in the fractures or in the matrix directly adjacent to the fracture. In general three zones can be identified: fracture filling consisting of secondary minerals, weathered matrix rock composed of primary minerals, but also containing secondary minerals, and relatively unweathered matrix rock that primarily consists of the initial mineral assemblage. Minerals typically encountered in fractures include chlorite, calcite, epidote, fluorite, quartz, iron-oxyhydroxides (hema-

tite/FeOOH, $Fe(OH)_2$(am)), pyrite, clay minerals (e.g. smectite and illite), prehnite, laumonite, and kaolinite /PUI 01/. Water–rock reactions may also cause changes in porosity within the fractures and in the matrix due to the dissolution of primary minerals and the formation of secondary phases (e.g. clays and Fe(III) oxides and hydroxides), which will subsequently cause permeability changes and will affect the groundwater flow regime /STE 98/, /SPY 03/. This is particularly important, because this process may lead to a self-sealing groundwater flow system, or to the formation of high permeability preferential flow channels. It is likely that the temperature of bedrock waters in the far-field will vary over the time scale of interest. In particular, microbially mediated reaction rates typically decrease significantly with decreasing temperature. Conversely in warmer water, an increase in microbial activity may enhance weathering and the formation of clay minerals. This is due in part to the fact that microbes access mineral phases for electron donors such as Fe(II) and S_2_, but also for nutrients, such as P and N.

On the one hand, the formation of clay minerals and Fe(II) oxides and hydroxides may increase the adsorption capacity of the media, which can limit the mobility of radionuclides. On the other hand, the formation of clay minerals may also result in the formation of mobile fine-grained particles (colloids) that may enhance the mobility of radionuclides /PUI 01/. Additional temperature changes will be caused by the heat emanating from the repository due to radioactive decay of the waste; however, this effect is expected to be limited to the region near the waste canisters and is not considered further in this review.

The present day redox conditions at proposed repository depths are reducing. The overall reduction capacity of the host rock depends on the presence of reduced species in solid and in dissolved form and the occurrence of primary and secondary redox reactions that consume oxygen. Primary redox reactions are defined as microbially mediated reactions that consume O_2 as an electron acceptor. Additional abiotic reactions that consume O_2 are also possible /HUN 98/. Electron donors include mineral phases that contain reduced species, and dissolved reduced species that are present in the matrix and which may interact with the infiltrating oxygen by means of diffusion. Present day oxygenated recharge waters tend to contain a significant amount of dissolved organic carbon, which is leached from the soil horizon. The reduction capacity of the recharge water may therefore exceed its oxidation capacity. For example, aerobic respiration of CH_2O (a simple representation of dissolved organic carbon) may lead to the consumption of dissolved oxygen and the production of CO_2: $CH_2O+O_2 \rightarrow CO_2+H_2O$. (1) In addition, anaerobic degradation of CH_2O by Fe(III)-containing mineral phases and SO_4 may take place, which leads to additional consumption of organic carbon, if oxygen is depleted.

These reactions may lead to the formation of reduced mineral phases such as pyrite or iron-monosulfides, which leads to an increase in reduction capacity in fractures:

$$Fe^{2+}+H_2S \rightarrow FeS+2H^+$$

However, the composition of recharge water during periods of glacial ice cover may be significantly different than currently observed. As depicted in Figure 3-11, it can be assumed that the soil horizon will be eroded away by glacial action. The input of organic carbon is therefore minimal during these periods. At the same time, dissolved O_2-concentrations may be significantly increased (by a factor of 3 to 5) during periods of melting caused by the elevated

pressure below the melting ice. Furthermore, recharge rates may be increased simultaneously due to an abundance of melt water /GUI 99/, /PUI 01/. The combination of these effects leads to infiltration of more recharge water with a higher oxidation capacity and a negligible reduction capacity. The infiltrating pore water will be of sub-neutral pH and undersaturated with respect to the rock forming minerals and fracture fillings and will promote mineral dissolution.

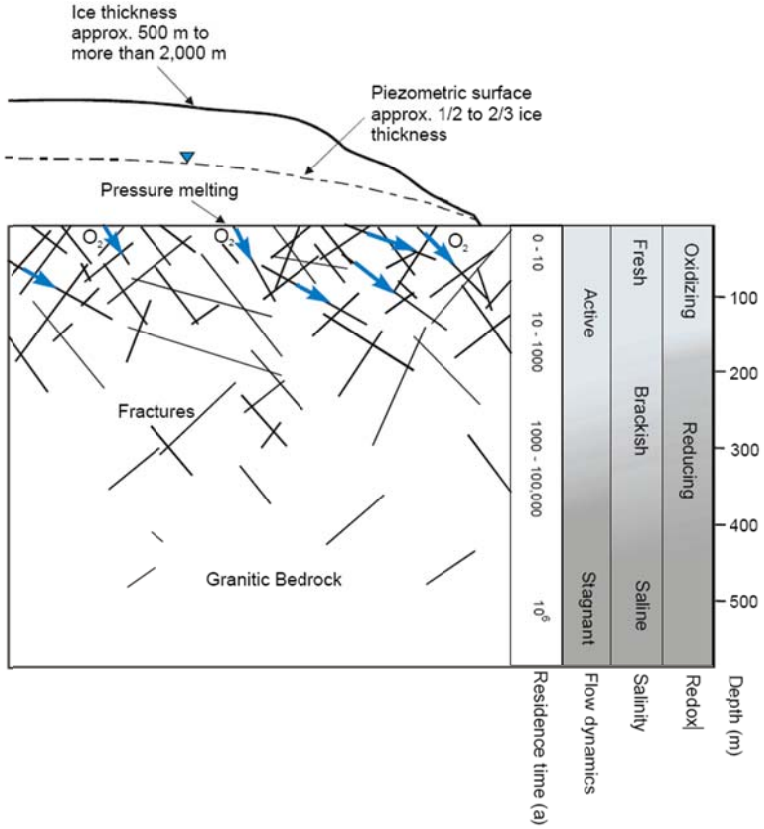

Figure 3-11 Conceptual view of surface and subsurface conditions during a glacial period, arrows indicate advective mass transport of recharge waters /KER 05/

In the reference frame of the proposed low- and intermediate-level radioactive waste repository at Wellenberg, the alteration of a fractured marl due to the circulation of hyperalkaline solutions derived from the degradation of cement has been studied by means of 2-dimensional reactive transport simulations /SOL 03/. A modified version of the GIMRT software package has been used for the reactive transport calculations. Both diffusive/dispersive and advective solute transport is taken into account. Mineral reactions are described by kinetic rate laws. The changes in porosity caused by mineral dissolution and precipitation are used to update the fluid flow field during the calculations. Flow fields are calculated using a separate finite difference code. Four different cases have been considered. These 4 cases are representative of the 2different types of groundwater ($NaHCO_3$-type and NaCl-type) present at Wellenberg and 2different stages in the process of degradation of cement (pH 12.5 and pH 13.5). Only the results for the NaCl-type groundwater have been shown. The results of the calculations show only small differences between the $NaHCO_3$ system and the NaCl

system. However, the results with the two different pH values are quite different. In both cases, the flow velocity in the fracture diminishes with time, due to a decrease in porosity. However, the decrease in porosity and flow velocity is much more pronounced in the lower pH case. Also, the extent of the zone of mineral alteration along the fracture is much more limited in the lower pH case (1–2m along the fracture after 20 000 a). For the higher pH case, mineral alteration affects the whole length of the flow domain along the fracture (6 m) after only 5000 a. One of the main mineral reactions in these systems is the dissolution of the dolomite initially present in the rock (fracture) and its replacement (partial or total) by calcite. A markedly advancing reaction front is defined by this reaction in the higher pH system. The Mg released by the dissolution of dolomite is taken up by the precipitation of brucite and sepiolite (a Mg-phyllosilicate). Brucite dominates near the fracture inlet and at earlier stages of the process. Sepiolite is the dominant Mg-containing phase further from the fracture inlet and also at later stages (brucite tends to dissolve and be replaced by sepiolite with time in the lower pH cases). Other secondary minerals that precipitate during the simulations are analcime and natrolite (zeolites) and tobermorite (a CSH phase). The amount of reaction affecting quartz (dissolution) and muscovite (dissolution and precipitation) is relatively minor. Since the biggest source of uncertainty for the reaction rates arises from the value of the surface areas used for the primary minerals, additional calculations making use of smaller values of these areas have also been performed. The results show that the smaller surface areas result in an overall smaller reactivity of the system and smaller porosity changes. These smaller porosity changes mean than porosities near the fracture inlet are larger than in the calculations with larger surface areas. The larger porosities translate into larger Darcy velocities along the fracture (less favourable for the performance of a repository), showing that the coupling between chemical reaction, which drives the changes in porosity, and fluid flow is very important. In summary, the results of the simulations suggest that the net result of the interaction of the high-pH solutions with the fractured marl is a reduction of porosity and water velocity along the fractures. This result would actually be highly beneficial for the performance of a repository hosted by the Valanginian marls at Wellenberg. The magnitude and scale (spatial and temporal) of this evolution is open to a large degree of uncertainty. However, the results of this modeling study are consistent in general terms (precipitation and nature of secondary phases, decrease in porosity/permeability) with the results from experimental work performed on comparable rocks and with the results from other modeling.

3.5.1 Interpretation of Modeling Results to Field Applications

If reactive transport models are going to be used to describe water–rock interaction and other processes like reactive contaminant transport, then they must be able to simulate natural, in situ reaction rates adequately. One possible approach is to use reaction rates and rate laws based on direct measurement in the field, in this way by passing the entire issue of how to interpret rates at a variety of scales. But this approach runs counter to the stated role of reactive transport modeling here, which is to use it to integrate fundamental, mechanistic descriptions of the various sub-processes that, coupled together, control the overall system reactivity. This is perhaps the first point to be mentioned, namely that reaction rates in field settings are not to be interpreted as strictly geochemical or microbiological quantities, but are the net result of all of the coupled processes that affect rates. A priori, there is no clear information on whether the rates are even limited by the intrinsic geochemical or microbiological reactivi-

ty, or whether the major limitation on rates is transport. Unfortunately, much of the discussion about the discrepancy between laboratory and field rates has ignored this crucial point for years, with physically and chemically heterogeneous systems treated effectively as well mixed flow through reactors. Reactive transport models cannot solve the problem of the apparent discrepancy between laboratory and field rates by themselves, but they can be used to rigorously evaluate the importance of individual processes, some of which can be constrained independently. In other cases, the reactive transport modeling can be used to narrow down the possible explanations for the overall rates observed in the field.

Probably the most significant problem on developing realistic models for reactive transport flow is the need to incorporate the multitude of spatial scales that are characteristic of natural subsurface environments. Spatial scales may range from nano scale surface chemistry, to pore and fracture apertures of millimeters to centimeters, to fracture spacing and matrix block sizes of tens of centimeters to meters, to reservoir or basin scales of kilometers to tens of kilometers. Even where a particular system can be discretized with a reasonable number of grid cells in a numerical model, it maybe those physical and chemical processes occur at much smaller sub-grid scales. These processes may include mass transfer-limited exchange between low and high permeability regions, or highly localized chemical micro-environments that are related to a heterogeneous distribution of reactive material. Under such conditions, gradients in concentration can develop at the pore to centimeter-scale, thus causing reaction rates to vary spatially at scales well below the numerical grid size that can be handled with reasonable computational efficiency.

The problem of up-scaling from the laboratory to the field-scale has been extensively discussed in the physical hydrology literature, particularly with regard to the scale dependence of macro dispersion /KAB 91/. A variety of mathematical approaches to up-scaling transport and reactive transport in porous media have

3.5.2 Thermodynamic Databank

The characterization of the chemical behavior of contaminants (actinides and long-lived fission products) is based on the knowledge about three distinct parameter categories:

- Solubility products of all relevant solubility limiting solid phases
- Equilibrium constants for the formation of the various aqueous complexes. The occurrence of stable aqueous complexes (with ligands such as OH^-, CO_3^{2-}, NO_3^-, SO_4^{2-}, ...) often drastically increases the solubility of nuclides
- Activity coefficients. They are necessary to assess the effects of ion-ion interactions at high ionic strengths in solution on equilibrium states.

Those thermodynamic data required for the characterization of aqueous speciation are often derived from experimental data in a coherent way. However, in many cases adequate experiments are still missing, introducing serious gaps and uncertainties into the thermodynamic data bases. Considering the high number of input values even when restricting to 25 °C a large number of thermodynamic parameters is necessary. Considerable efforts have to be provided on the data quality and internal consistency. Moving to higher temperatures and pressures, including the formation of solid solution and sorption phenomena, further increases the complexity of the underlying thermodynamic data base.

The proof of long term safety of a nuclear waste disposal is based on numerical simulations and geochemical calculations. These computations are taking into account all relevant processes releasing contaminants from the waste matrix into the biosphere. Quality assurance of such model calculations requires a significant understanding of homogeneous and heterogeneous reactions in aqueous solutions, together with a reliable parameterization of their thermodynamics. This is very important due to the fact that the maximum amount of contaminants expected to be released into the biosphere is governed by solubility limits. Because all geochemical modeling is based on thermodynamic data, the precision and trustworthiness of such computations is directly correlated to the quality of the underlying data base, as is the confidence in the final assessment of the long term safety of a waste disposal. Valid safety assessments are only possible using reliable thermodynamic data from a consistent and comprehensive database. Various databases providing the model constants have been developed in various industrial applications. A summary of these attempts that exhibit relevancy for geochemical modeling of repository issues can be cited as follows /ALT 04/:

3.5.2.1 CODATA

This is an initiative of international Committee on Data for Science and Technology (ICSU) with the aim of improving the quality of geochemical data and methods based on international cooperation on the issue. The thermodynamical properties of “key chemical substances” which are consistent with each other were determined and listed. These basic properties were selected as formation enthalpy and entropy at 298,15 °C. This is an important study because it is one of the first of such attempts.

3.5.2.2 OECD/NEA

The corresponding OECD/NEA project had the aim to search and compile all thermodynamical data of the components that are relevant for a nuclear repository. To be used in the performance assessment study of a nuclear repository, the databank is aimed to fulfil the following condition:

- The databank must consist of all data relevant for the safety analysis of the repository
- The documentation should be complete with auxiliary data
- The sources of the data should also be documented
- The databank should be self consistent
- All aqueous and solid phases of the elements should also be documented.

None of the previous databanks did fulfil these criteria and therefore the defined aims were reasonable. The works began at 1984 and a valuable and self consistent databank for repository studies step by step. The selection of the parameters was based on the need of the selected models, the general validity of the application and also the availability of the data.

The most of the geochemical models function by the use of equilibrium constants. Although the solubility and the equilibrium constants are the primary parameters, various models are using various thermodynamical data based on Gibbs Phase rule. To avoid the calculation of the selected equilibrium constants for all new set of components, the NEA data consisted of standard formation enthalpy, standard entropy and heat capacity at constant pressure and at

molar basis. The needed equilibrium constants are therefore available from these parameters for all aqueous and solid phases. With the aid of this concept the internal consistency of the selected thermodynamical parameters could be easily checked.

All these parameters are a function of the temperature. Therefore it is important to evaluate their temperature dependency with an empirical correlation of the following form:

$$F(T) = a + bT + cT^2 + dT^{-1} + eT^{-2} + f\ln T + gT\ln T + h\sqrt{T} + i\frac{1}{\sqrt{T}} + jT^3 + kT^{-3} \quad (3\text{-}2)$$

The most of the temperature dependencies can be defined with between 2 and 4 parameters (a, b, c, d).

3.5.2.3 FZK-INE Databank

In the framework of a project on modeling the near field of high activity disposal in Gorleben Repository conducted by INE for BGR, a thermodynamic databank for Thorium, Uran, Neptunium, Plutonium, Americium and Curium was developed. The databank compiled in this project offers some improvements in comparison with the NEA databank. It contains molar free standard formation enthalpies and equilibrium constants for solubility constants for solubility determining solids formation constants for aquatic complexes and for hydroxid, carbonate, silicate, chloride sulphate, phosphate and fluoride. The FZK-INE databank is developed primarily for the geochemical modeling in aquatic systems as expected for the German repository systems. Therefore the FZK-INE databank includes a comprehensive set of activity coefficients for actinitions after Pitzer Ion exchange model limited by 6 mol /kg H2O NaCl solutions.

3.5.2.4 NAGRA/PSI Databank

The Nagra/PSI databank was established, developed and improved in order to be used for the performance assessment studies of the planned repository sites in Switzerland. The study is focused mostly on the sorption and dissolution of the radionuclide. Thermodynamical data to model the geochemical milieu corresponding to groundwater in contact with waste and buffer material is also added to the databank. In the repository concept it is worth to note that the various cement/concrete and clay consisting buffer material play an important role. In this databank a significant emphasis to the consistency and applicability was given. The priority was given for hydroxide and carbonate as well as for fluoride, sulphate sulphite and phosphate.

3.5.2.5 WIIP databank

The databank compiled in the framework of the studies on “the Waste Isolation Pilot Plant (WIPP)”, a nuclear waste repository excavated in New Mexico is especially focused on the solubility data of actinides (1992). For WIPP it is decided that the solubility of the actinides is estimated with an equilibrium thermodynamic model which is based on the experimental data. This methodology differs from the determination of the solubilities directly from the experimental results. The databank was developed continuously as new data is available.

3.5.2.6 Yucca Mountain Project

In the framework of the “total system performance assessment” (TSPA) of Yucca Mountain nuclear repository project various applications were defined in which the use of a thermodynamical databank has been applied. The precipitation and salt model is based on the laboratory results and is intended to model the precipitation of the mineral phases if the water totally evaporated. The nature of the processes is dependent on various process and phase properties such as water composition, buffer material, resolubility etc. This databank comprises also a condensate water model in which the water composition of the condensate is calculated considering the effect of CO_2. The salt model for low and high humidity is also incorporated to describe the behavior of the salts at a relative humidity of various grades. Some problems and limitations are reported related to dew point pressure lowering, solubility of salts, the behavior of carbonates.

3.5.2.7 Pitzer Databank

This is a databank related to the Pitzer activity model used for the high activity aqueous solutions. The EQ3/6 code that makes the Pitzer activity model available offers also two Pitzer database: the HMW and PIT databases. The HMW database is self consistent; consist of 9 elements and 17 aqueous species. However some components such as Al, Fe, Si and F for the modeling of the repository conditions are not included. The database is only for 25°C available. The PIT database on the other hand is relatively more developed in comparison with HMW database. This is applicable for a temperature interval which is relevant for repository problems. Some inconsistency problems are reported and PT4 is developed to eliminate these problems. PT4 includes data from both database HMW and PIT for temperature interval of 20°C to 95°C. The PT4 all minerals and gases from PIT database as well as CO_2 (g) and corresponding number of carbonates, silicates and other mineral phases from the COM database.

3.5.2.8 THEREDA

THEREDA is the acronym of a project on THErmodynamic REference Database /THE 10/. The main objective is to establish a comprehensive and internally consistent thermodynamic reference database for the geochemical modeling of near-field and far-field processes occurring in the different rock formations currently under discussion in Germany to host a repository for radioactive waste. The project commenced in 2006 and is organized and conducted by the leading research institutes in the field of radioactive and (chemo) toxic waste disposal in Germany. More information on this recent effort to create a more reliable database for german cases can be found in /THE 10/.

3.6 Background – Basic Definitions

The aim is to remember and make an overview the basics and terminology of reactive flow and related geo-processes. The definitions were collected from the most complete and easily available sources mostly from internet sites and general books on the geochemistry.

Phase

In the physical sciences, a phase is a region of space (a thermodynamic system), throughout which all physical properties of a material are essentially uniform. Examples of physical properties include density, index of refraction, and chemical composition. A simple description is that a phase is a region of material that is chemically uniform, physically distinct, and (often) mechanically separable. When a substance undergoes a phase transition (changes from one state of matter to another) it usually either takes up or releases energy. The amount of energy required to induce the transition is more than the amount required to heat the water from room temperature to just short of boiling temperature, which is why evaporation is useful for cooling. See Enthalpy of vaporization. The reverse process, condensation, releases heat. The heat energy, or enthalpy, associated with a solid to liquid transition is the enthalpy of fusion and that associated with a solid to gas transition is the enthalpy of sublimation.

Corrosion

Corrosion is the disintegration of an engineered material into its constituent atoms due to chemical reactions with its surroundings. In the most common use of the word, this means electrochemical oxidation of metals in reaction with an oxidant such as oxygen. Formation of an oxide of iron due to oxidation of the iron atoms in solid solution is a well-known example of electrochemical corrosion, commonly known as rusting. This type of damage typically produces oxide(s) and/or salt(s) of the original metal. Corrosion can also refer to other materials than metals, such as ceramics or polymers, although in this context, the term degradation is more common.

In other words, corrosion is the wearing away of metals due to a chemical reaction.

Many structural alloys corrode merely from exposure to moisture in the air, but the process can be strongly affected by exposure to certain substances. Corrosion can be concentrated locally to form a pit or crack, or it can extend across a wide area more or less uniformly corroding the surface. Because corrosion is a diffusion controlled process, it occurs on exposed surfaces. As a result, methods to reduce the activity of the exposed surface, such as passivation and chromate-conversion, can increase a material's corrosion resistance. However, some corrosion mechanisms are less visible and less predictable.

Leaching

Removal of materials by dissolving them away from solids is called leaching. The chemical process industries use leaching but the process is usually called extraction, and organic solvents are often used. The theory and practice of leaching are well-developed because for many years leaching has been used to separate metals from their ores and to extract sugar from sugar beets. Environmental engineers have become concerned with leaching more recently because of the multitude of dumps and landfills that contain hazardous and toxic wastes. Sometimes the natural breakdown of a toxic chemical results in another chemical that is even more toxic.

Although many toxic materials have low solubility in water, the concentrations that are deemed hazardous are also very low. Furthermore, many toxic compounds are accumulated by living cells and can be more concentrated inside than outside a cell. This is why long-term exposure is a serious problem; encountering a low concentration of a toxic material a few

times may not be dangerous, but having it in your drinking water day after day and year after year can be deadly.

Precipitation

Precipitation is the formation of a solid in a solution or inside another solid during a chemical reaction or by diffusion in a solid. When the reaction occurs in a liquid, the solid formed is called the precipitate, and the liquid remaining above the solid is called the supernate.

Natural methods of precipitation include settling or sedimentation, where solid forms over a period of time due to ambient forces like gravity or centrifugation. During chemical reactions, precipitation may also occur particularly if an insoluble substance is introduced into a solution and the density happens to be greater (otherwise the precipitate would float or form a suspension). With soluble substances, precipitation is accelerated once the solution becomes supersaturated.

In solids, precipitation occurs if the concentration of one solid is above the solubility limit in the host solid, due to e.g. rapid quenching or ion implantation, and the temperature is high enough that diffusion can lead to segregation into precipitates. Precipitation in solids is routinely used to synthesize nanoclusters.

An important stage of the precipitation process is the onset of nucleation. The creation of a hypothetical solid particle includes the formation of an interface, which requires some energy based on the relative surface energy of the solid and the solution. If this energy is not available, and no suitable nucleation surface is available, supersaturation occurs.

Mineralization

Mineralization is the hydrothermal deposition of economically important metals in the formation of ore bodies or "lodes". The term can also refer to the process by which sediments replace organic material within the body of an organism that has died and was buried by sediments.

Hydrolysis

Hydrolysis is a chemical reaction during which molecules of water (H_2O) are split into hydrogen cations (H^+) (conventionally referred to as protons) and hydroxide anions (OH^-) in the process of a chemical mechanism. The most common hydrolysis occurs when a salt of a weak acid or weak base (or both) is dissolved in water. Water autoionizes into negative hydroxyl ions and positive hydrogen ions. The salt breaks down into positive and negative ions. For example, sodium acetate dissociates in water into sodium and acetate ions. Sodium ions react very little with hydroxyl ions whereas acetate ions combine with hydrogen ions to produce neutral acetic acid, and the net result is a relative excess of hydroxyl ions, causing a basic solution.

Complexation

This is a chemical reaction that takes place between a metal ion and a molecular or ionic entity known as a ligand that contains at least one atom with an unshared pair of electrons.

Colloid generation

A colloid is a substance microscopically dispersed evenly throughout another one. A colloidal system consists of two separate phases: a *dispersed phase* (or *internal phase*) and a *continuous phase* (or *dispersion medium*). A colloidal system may be solid, liquid, or gaseous. The dispersed-phase particles have a diameter of between approximately 5 and 200 nanometers. Such particles are normally invisible to an optical microscope, though their presence can be confirmed with the use of an ultra microscope or an electron microscope. Homogeneous mixtures with a dispersed phase in this size range may be called *colloidal aerosols*, *colloidal emulsions*, *colloidal foams*, *colloidal dispersions*, or *hydrosols*. The dispersed-phase particles or droplets are affected largely by the surface chemistry present in the colloid.

Cation Exchange Capacity

In soil science, cation exchange capacity (CEC) is the capacity of a soil for ion exchange of cations between the soil and the soil solution. CEC is used as a measure of fertility, nutrient retention capacity, and the capacity to protect groundwater from cation contamination. Cations can also be easier to understand by just adding the group number. The quantity of positively charged ions (cations) that a clay mineral or similar material can accommodate on its negatively charged surface is expressed as milli-ion equivalent per 100 g, or more commonly as milliequivalent (meq) per 100 g or cmol/kg. Clays are aluminosilicates in which some of the aluminium and silicon ions have been replaced by elements with different valence, or charge. For example, aluminium (Al^{3+}) may be replaced by iron (Fe^{2+}) or magnesium (Mg^{2+}), leading to a net negative charge. This charge attracts cations when the clay is immersed in an electrolyte such as salty water and causes an electrical double layer. The cation-exchange capacity is often expressed in terms of its contribution per unit pore volume, Q_V.

Redox

Redox (reduction-oxidation reaction) describes all chemical reactions in which atoms have their oxidation number (oxidation state) changed. This can be either a simple redox process, such as the oxidation of carbon to yield carbon dioxide or the reduction of carbon by hydrogen to yield methane (CH_4), or a complex process such as the oxidation of sugar in the human body through a series of complex electron transfer processes.

The term comes from the two concepts of reduction and oxidation. It can be explained in simple terms:

- Oxidation is the *loss* of electrons or an *increase* in oxidation state by a molecule, atom, or ion.
- Reduction is the *gain* of electrons or a *decrease* in oxidation state by a molecule, atom, or ion.

Though sufficient for many purposes, these descriptions are not precisely correct. Oxidation and reduction properly refer to *a change in oxidation number* — the actual transfer of electrons may never occur. Thus, oxidation is better defined as an *increase in oxidation number*, and reduction as a *decrease in oxidation number*. In practice, the transfer of electrons will always cause a change in oxidation number, but there are many reactions that are classed as "redox" even though no electron transfer occurs (such as those involving covalent bonds).

Non-redox reactions, which do not involve changes in formal charge, are known as metathesis reactions.

Sorption

Sorption refers to the action of both absorption and adsorption taking place simultaneously. As such it is the effect of gases or liquids being incorporated into a material of a different state *and* adhering to the surface of another molecule. Absorption is the incorporation of a substance in one state into another of a different state (e.g., liquids being absorbed by a solid or gases being absorbed by a liquid). Adsorption is the physical adherence or bonding of ions and molecules onto the surface of another molecule. Absorption, in chemistry, is a physical or chemical phenomenon or a process in which atoms, molecules, or ions enter some bulk phase - gas, liquid or solid material. This is a different process from adsorption, since molecules undergoing absorption are taken up by the volume, not by the surface (as in the case for adsorption). A more general term is sorption which covers adsorption, and ion exchange. Absorption is basically where something takes in another substance.[1]

If absorption is a physical process not accompanied by any other physical or chemical process, it usually follows the Nernst partition law:

"The ratio of concentrations of some solute species in two bulk phases in contact is constant for a given solute and bulk phases:

$$\frac{x_1}{x_2} = \text{constant} = \mathrm{K}_{\mathrm{N(x1,2)}} \qquad (3\text{-}3)$$

The value of constant K_N depends on temperature and is called partition coefficient. This equation is valid if concentrations are not too large and if the species "x" does not change its form in any of the two phases "1" or "2". In the case of gas absorption, one may calculate its concentration by using e.g. the Ideal gas law, c = p/RT. alternatively one may use partial pressures instead of concentrations.

4 MODELING TOOL; TOUGH2/TOUGHREACT

The study is performed based on numerical simulation using TOUGHREACT, a numerical reactive transport modeling code developed by the scientists of Lawrence Berkeley National Laboratory (LBNL), University of California, USA as an extension of TOUGH2.

4.1 TOUGH2

TOUGH2 is a numerical simulator for non-isothermal fluid flow of multi-component, multi-phase fluids in one, two, and three-dimensional porous and fractured media /PRU 87/. It was developed at LBNL and is continuously developed and maintained. The main applications for which TOUGH 2 was designed are in geothermal reservoir engineering, nuclear waste disposal, environmental assessment and remediation, and unsaturated and saturated zone hydrology. TOUGH2 is used world-wide by 152 institutes. Several different fluid property modules and enhanced process modeling capabilities exist. Several publications are available for applications and fundamentals /NIT 90/ /ADE 93/ /HOC 95/.

The source code has a modular architecture and can be easily modified for any user specific problem. TOUGH2 uses unstructured grids which enables the flow simulation in complex structures. Several numerical parameters (e.g. time step function or weighting) and different auxiliary functions for capillary pressure and relative permeability are available for an optimum adaptation to the physical problem. Fluid advection is described with a multiphase extension of Darcy's law; in addition diffusive mass transport in all phases is considered. Heat flow occurs by conduction and convection. Several modules for different fluid systems in non-isothermal multiphase flow exist. These are e.g. a module for the flow of tracers (e.g. radionuclides) including the effects of advection, diffusion, dispersion, adsorption, volatilisation and radioactive decay, a module for the system water-salt and a non condensable gas including the effect of precipitation and dissolution of salt, and another module for the flow of water-air and a volatile organic compound. A version ITOUGH for inverse modeling allows for the determination of model dependent hydraulic parameters such as e.g. permeability from flow measurements.

4.2 TOUGHREACT

TOUGHREACT is developed firstly by Xu and Pruess (LBNL; California Un.) by introducing reactive geochemistry into the framework of the existing multi-phase fluid and heat flow code TOUGH2 /XUT 99/. As TOUGH2 transport of aqueous and gaseous species by advection and molecular diffusion is considered in both liquid and gas phases. Any number of chemical species in liquid, gas and solid phases can be accommodated. Aqueous complexation, acid-base, redox, gas dissolution/exsolution, and cation exchange, are considered under the local equilibrium assumption. Mineral dissolution and precipitation can proceed either subject to local equilibrium or kinetic conditions. Linear adsorption and decay can be included.

TOUGHREACT is applicable to one-, two-, or three-dimensional geologic domains with physical and chemical heterogeneity. Temperature ranges from 0 °C to 300 °C, because the present most available geochemical database is up to 300 °C such as EQ3/6 /WOL 92/. Pressure can be from 1 bar (atmospheric pressure) to several hundred bars (at several thousand meter depth). Water saturation can range from completely dry to fully water saturated. In its

original form, the model can deal with low ionic strength and has three important features in terms of fluid flow and geochemical transport: (1) the gas phase is active for multiphase fluid flow, mass transport and chemical reactions, (2) not only porous media, but also reactive fluid flow and transport in fractured rocks is considered, (3) the effects of heat are considered, including heat-driven fluid flow, and temperature-dependent thermophysical and geochemical properties (such as fluid density and viscosity, and thermodynamic and kinetic data).

4.2.1 Governing Equations

The primary governing equations for multiphase fluid and heat flow, and chemical transport have the same structure, derived from the principle of mass (or energy) conservation. These equations are presented in Table 4.1. Major processes considered for non-isothermal fluid and heat flow are: (1) fluid flow in both liquid and gas phases occur under pressure, viscous and gravity forces; (2) interactions between flowing phases are represented by characteristic curves (relative permeability and capillary pressure), (3) heat flow occurs by conduction and convection. Aqueous (dissolved) species are subject to transport in the liquid phase as well as to local chemical interactions with the solid and gas phases. Transport equations are written in terms of total dissolved concentrations of chemical components, which are concentrations of the basis species plus their associated aqueous secondary species /XUT 01b/. If kinetically controlled reactions occur between aqueous species, then additional ordinary differential equations need to be solved to link the total concentrations of the primary species with the evolving concentrations of the secondary species. Kinetically controlled reactions between aqueous species are not considered. Advection and diffusion processes are considered for both the liquid and gas phases, and their coefficients are assumed to be the same for all species. The local chemical interactions in the transport equations are represented by reaction source/sink terms.

The primary governing equations must be complemented with constitutive local relationships that express all parameters as functions of fundamental thermophysical and chemical variables. Expressions for non-isothermal multiphase flow are given by Pruess, /PRU 87/. Mass conservation in the closed chemical system is written in terms of basis (component) species. The species distribution must be governed by the total concentrations of the components. As the manual is available the equations used in the chemical part are not given all in the report.

Table 4.1 Governing equations for fluid and heat flow as given in TOUGH2 manuals

General governing equations		$\frac{\partial M_\kappa}{\partial t} = -\nabla F_\kappa + q_k$
Water	$M_w = \phi(S_1\rho_1 X_{wi} + S_g\rho_g X_{wg})$	$F_w = X_{wi}\rho_l u_l + X_{wg}\rho_g u_g$
Air	$M_c = \phi(S_1\rho_1 X_{cl} + S_g\rho_g X_{cg})$ $q_c = q_{cl} + q_{cg} + q_{cr}$	$F_c = X_{cl}\rho_l u_l + X_{cg}\rho_g u_g$ $q_w = q_{wl} + q_{wg}$
Heat	$M_h = \phi(S_1\rho_1 U_l + S_g\rho_g U_g) +$ $(1-\phi)\rho_s U_s$	$F_h = \sum_{\beta=1,g} h_\beta\rho_\beta u_\beta - \lambda\nabla T$ $u_\beta = -k\frac{k_{r\beta}}{\mu_g}(\nabla P_\beta - \rho_g g))$
Chemical components in the liquid phase		
	$M_j = \phi\ S_l\ C_{jl}$	$F_h = u_1 C_{jl} - (\tau\phi S_l D_l)\nabla C_{jl}$ $q_c = q_{cl} + q_{cg} + q_{cr}$ $\tau_\beta = \phi^{1/3} S_\beta^{7/3}$

4.2.1.1 Chemical Reactions

In TOUGHREACT, as the case in other similar codes a subset of not condensable aqueous are selected as basis species (or component or primary species). All other species are called secondary species that include aqueous complexes, precipitated (mineral) and gaseous species. The number of secondary species must be equal to the number of independent reactions.

Aqueous complexation

These reactions are assumed to be at local equilibrium. By making use of the mass action equation to the dissociation of the i-th aqueous complex, concentrations of aqueous complexes can be expressed as functions of the concentrations of basis species:

$$c_i = K_i^{-1}\gamma_i^{-1}\prod_{j=1}^{Nc} c_j^{vij}\gamma_j^{v_{ij}} \qquad (4\text{-}1)$$

where c_i is molal concentration of the i-th aqueous complex, and c_j is molal concentration of the j-th basis species, γ_i and γ_j are thermodynamic activity coefficients and K_i is the equilibrium constant.

Equilibrium mineral dissolution/precipitation

The mineral saturation ratio is expressed with:

$$\Omega_m = X_m^{-1} \lambda_m^{-1} K_m^{-1} \prod_{j=1}^{Nc} C_j^{vmj} \gamma_j^{v_{mj}} \qquad m = 1,...N_p \tag{4-2}$$

where m is the equilibrium mineral index, X_m is the mole fraction of the m^{-th} mineral phase, λ_m is its thermodynamic activity coefficient (for pure mineral phases X_m and λ_m are taken equal to one), and K_m is the corresponding equilibrium constant. At equilibrium, following relationship is valid:

$$SI_m = \log_{10} \Omega_m = 0$$

where SI_m is called the mineral saturation index.

Kinetic mineral dissolution/precipitation

The kinetic precipitation (or dissolution) rate for minerals in TOUGHREACT is described by:

$$r_n = k_n \ A_n \ (1 - \Omega_n^{\theta})^{\eta} \tag{4-3}$$

where positive values of r_n indicate dissolution, and negative values precipitation, k_n is the rate constant (moles per unit mineral surface area and unit time) which is temperature dependent, A_n is the specific reactive surface area per kg H_2O, Ω_n is the kinetic mineral saturation ratio. The parameters θ and η must be determined from experiments; usually, but not always, they are taken equal to one.

For the temperature dependence of the reaction rate constant following equation is used:

$$k = k_{25} \ \exp\left[\frac{-E_a}{R}\left(\frac{1}{T} - \frac{1}{298{,}15}\right)\right] \tag{4-4}$$

where Ea is the activation energy, k_{25} is the rate constant at 25°C, R is gas constant, T is absolute temperature. The pH dependence of mineral precipitation and dissolution rates are taken into consideration with corresponding equations. The precipitation of a mineral can be suppressed up to a given, positive saturation index value, $\log(\Omega)_w$. Within this "supersaturation window", the mineral is not allowed to precipitate. The mineral precipitates if its saturation index $\log(\Omega) \geq \log(\Omega)_w$, and dissolves if $\log(\Omega) < 0$. The size of the window can be set to decrease exponentially with temperature as follows:

$$\log(\Omega)_{w,T} = \log(\Omega)_{1,T^0} \exp(-4{,}61(T - T^0)/(T_1 - T^0)) \tag{4-5}$$

where $log(\Omega)_{w,T}$ is the window at the current temperature T and $log(\Omega)_{w,T\,0}$ is the initial (input) window at temperature T^0. T_1 is the temperature at which the window is one hundredth the size of the initial window. Values of $log(\Omega)_{w,T\,0}$, T^0, and T_1 are provided as input parameters.

Gas dissolution/exsolution

Reactions involving aqueous and gaseous phases are usually assumed to be at equilibrium. According to the Mass-Action Law, the following equation is valid:

$$p_f \Gamma_f K_f = \prod_{j=1}^{N_c} c_j^{v_{fj}} \gamma_j^{vfi} \tag{4-6}$$

where subscript f is gas index, p is the partial pressure (in bar), Γ is the gas fugacity coefficient. For low pressures (in the range of atmospheric pressure), the gaseous phase is assumed to behave like an ideal mixture, and the fugacity coefficient Γ is assumed equal to one. At higher temperatures and pressures, such as boiling conditions in hydrothermal systems and CO_2 disposal in deep aquifers, the assumption of ideal gas and ideal mixing behavior is not valid, and the fugacity coefficients should be corrected according to temperatures and pressures /SPY 88/ /XUT 99/.

Cation exchange

Cation exchange takes place when free cations in solution exchange with interlayer cations. This process can be described as an equilibrium reaction between an exchangeable cation and an exchange site. The equilibrium constant is usually known as the exchange coefficient because its value depends on the ionic strength of the solution. A general expression for cation exchange reactions according to the Gaines-Thomas convention is given as /APP 94/:

$$\frac{1}{v_i} S_i + \frac{1}{v_j}(X_{vj} - S_j) \Leftrightarrow \frac{1}{v_i}(X_{vi} - S_i) + \frac{1}{v_j} S_j \tag{4-7}$$

where vi and vj are the stoichiometric coefficients (equal to their charges) of dissolved and interlayer cations, respectively; Si and Sj denote dissolved cationic species and $(X_{vj}\text{-}S_j)$ and $(X_{vi}\text{-}S_i)$ represent exchange sites or exchange interlayer cations. The equilibrium equation for cation exchange is obtained from the Mass Action Law:

$$K_{ij}^* = \frac{\overline{w_i^{1/vi}}.a_j^{1/v_j}}{\overline{w_j^{1/vj}}.a_i^{1/v_i}} \tag{4-8}$$

where K_{ij} is the exchange coefficient or selectivity, a_j is the activity of the j-th dissolved species and w_i is the activity of the i-th exchanged species. Activities of dissolved cations are related to concentrations as discussed in the following chapters. Activities of interlayer cations are approximated by their equivalent fractions of the number of exchange sites. The sum of concentrations of surface sites or interlayer cations is the so-called cation exchange capacity (CEC). Three cation exchange conventions are implemented in TOUGHREACT. These are Gaines-Thomas, Vanselow and Gapon /APP 93/. The related numerical basis is given in /XUT 99/.

4.2.1.2 Solution Method for Solute Transport Equations

Most chemical species are only subject to transport in the liquid phase. A few species is transported in both liquid and gas phases such as O_2 and CO_2. For the solution of the solute transport equations, the numerical formulation of reactive transport in the liquid phase is derived firstly. This is then extended to transport in the gas phases for some gaseous species. In the sequential iteration approach (SIA), the mass transport equations and chemical reaction equations are considered as two relatively independent subsystems. They are solved separately in a sequential manner following an iterative procedure. If reactions taking place in the liquid phase are assumed to be at local equilibrium, mass transport equations can be written in terms of total dissolved component concentrations. The concentrations of advective and diffusive flux terms for each chemical component in liquid phase, Cj are evaluated in each block implicitly which gives accumulation term in each block introducing the saturations. The linearization results in:

$$\left[S_{1,n}^{k+1}\phi_n^{k+1} + \frac{\theta\Delta t}{V_n}\sum_m A_{nm}\left(-u_{nm}^{k+1}\varepsilon_{nm} + \frac{D_{nm}}{d_{nm}} \right) \right] C_n^{(j),k+1,s+1/2} +$$

$$\frac{\theta\Delta t}{V_n}\sum_m A_{nm}\left[u_{nm}^{k+1}(\varepsilon_{nm} - 1) - \frac{D_{nm}}{d_{nm}} \right] C_n^{(j),k+1,s+1/2} =$$

$$\frac{(1-\theta)\Delta t}{V_n}\sum_m A_{nm}\left[u_{nm}^{k+1}(\varepsilon_{nm} - \frac{D_{nm}}{d_{nm}} \right] C_n^{(j),k} -$$

$$\frac{(1-\theta)\Delta t}{V_n}\sum_m A_{nm}\left[u_{nm}^{k+1}(\varepsilon_{nm} - 1) - \frac{D_{nm}}{d_{nm}} \right] C_n^{(j),k}$$

$$S_{1,n}^{k}\phi_n^{k} C_n^{(j),k} + q_n^{(j)k+1}\Delta t + R_n^{(j),k+1,s}\Delta t \qquad j = 1, NC \tag{4-9}$$

where n labels the grid block, j labels the chemical component, NC is the total number of chemical components, l labels liquid phase (for simplicity, the liquid phase index l is neglected), k labels the number of the time step, s labels the number of the transport-chemistry iteration, u_{nm} is the liquid volumetric flux or Darcy.s velocity (m/s), D_{nm} is the effective diffusion coefficient (including effects of porosity, phase saturation, tortuosity and weighting factors between the two grid blocks), d_{nm} is the nodal distance, R_n (j)k+1 are the overall chemical reaction source/sink terms. For the sequential iteration approach, the iteration index s is essential. A new transport-chemistry iteration consists of two parts, transport part denoted by, s+1/2, (it should be noted that ½ does not mean Δt/2), and chemistry part denoted by, s+1. The above given Equation for each chemical component j is linear if R(j),s is known, and has the same structure as the non-reacting (conservative) solute transport equation. The chemical reaction source/sink term R(j),s represents mass transfer of component j between aqueous and solid phases. The values of these source/sink terms at the new transport iteration, s+1/2, are evaluated at the previous chemistry iteration, s. The resulting new values of

C(j),s+ 1 2 , obtained by solving transport Equations, are substituted into chemical reaction subroutines and one can compute new values of R(j),s+1. Transport and chemical reaction equations are solved iteratively until prescribed convergence criteria are satisfied. The essence of this sequential iteration approach is therefore the sequential solution of two independent sets of equations: the transport equations and the chemical equations. The transport equations are solved on a component by component basis, whereas the chemical equations are solved on a grid block basis. These two sets of equations are coupled by updating chemical source/sink terms.

The mathematical treatment of adding Kd linear adsorption and first-order decay effects in the model follows the work by Oldenburg and Pruess /OLD 95/, but no gas phase partitioning is considered. The mass accumulation term for any species (for simplification, the species index is not appeared in the following equations) with Kd adsorption on the solid matrix is:

$$M = \phi S_l C + (1-\phi)\rho_s CK \qquad (4\text{-}10)$$

where ϕ is porosity, S_l is the liquid saturation, C is the aqueous concentration (mol/l), ρ_s is the solid density (kg/dm^3), K_d is the distribution coefficient (l/kg = mass/kg solid divided by mass/l solution) and is species-dependent. The accumulation term also can be written in terms of retardation factor. The first-order decay of a species is discretized based on /OLD 95/.

The transport in gas phase is considered in the same manner as the liquid phase. A similar equation is used. The concentration of the gaseous species is calculated based on the partial pressures with the following equation:

$$C_g = \frac{100}{RT} p_g \qquad (4\text{-}11)$$

where C_g are gaseous species concentrations (in mol/l), p_g is the gaseous species partial pressure (in bar), R is the gas constant (8,314 J.mol^{-1}.K^{-1}) and T is the absolute temperature.

4.2.1.3 Numerical Method for Mixed Equilibrium-Kinetics Chemical System

It is assumed that aqueous complexation and gas dissolution/exsolution proceed according to local equilibrium, while mineral dissolution/precipitation is subject to equilibrium and/or kinetic conditions. Only pure mineral phases are considered. Gas dissolution/exsolution is included in the model and treated in a similar way as equilibrium mineral dissolution/precipitation. The formulation is based on mass balances in terms of basis species as described in /PAR 80/ and /REE 82/ for the equilibrium chemical system. The kinetic rate expressions for mineral dissolution/precipitation are included in the equations along with the mass balances of basis species /XUT 99/. The solution of the reaction system requires knowing initial total concentrations of basis species j in the equilibrium system (aqueous and mineral) and the time step Δtr. Adding kinetic mineral dissolution/precipitation processes does not require additional primary equations, because the reaction rate is a function of the concentrations of the basis species. Once the concentrations of the basis species are obtained, all other secondary variables can be computed in a straightforward manner.

4.2.2 Effects of Mineral Precipitation/Dissolution on Hydrologic Properties

Porosity changes in matrix and fractures are directly related to the volume changes as a result of mineral precipitation and dissolution. The molar volumes of minerals created by hydrolysis reactions (i.e., anhydrous phases, such as feldspars, reacting with aqueous fluids to form hydrous minerals such as zeolites or clays) are often larger than those of the primary reactant minerals; therefore, constant molar dissolution precipitation reactions may lead to porosity reductions. These changes are taken into account in the code as follows:

The porosity of the medium (fracture or matrix) is given by:

$$\phi = 1 - \sum_{m=1}^{nm} fr_m - fr_u \tag{4-12}$$

where nm is the number of minerals, fr_m is the volume fraction of mineral m in the rock ($V_{mineral}/V_{medium}$, including porosity), and fr_u is the volume fraction of nonreactive rock. As the fr_m of each mineral change, the porosity is recalculated at each time step. The porosity is not allowed to go below zero.

4.2.2.1 Fracture Permeability Change

Fracture permeability changes can be approximated using the porosity change and an assumption of plane parallel fractures of uniform aperture as done in cubic law /STE 94/ Steefel and Lasaga, 1994. The modified permeability, k, is then given by where k_i and φ_i are the initial permeability and porosity, respectively. This law yields zero permeability only under the condition of zero fracture porosity. In most experimental and natural systems, permeability reductions to values near zero occur at porosities significantly greater than zero. This generally is the result of mineral precipitation in the narrower interconnecting apertures. The hydraulic aperture, as calculated from the fracture spacing and permeability (as determined through air-permeability measurements) assuming a cubic law relation, is a closer measure of the smaller apertures in the flow system. Using the hydraulic aperture, a much stronger relationship between permeability and porosity can be developed. This relationship can be approximated as follows:

The initial hydraulic aperture $b_{0,h}$ (m) is calculated using the following cubic law relation:

$$b_{0,h} = (12 k_0 s)^{1/3} \tag{4-13}$$

where k_0 is the initial fracture permeability (m^2) and s is the fracture spacing (m). The permeability (k') resulting from a change in the hydraulic aperture, is given by

$$k' = \frac{(b_{0,h} + \Delta b)^3}{12 s} \tag{4-14}$$

where Δb is the aperture change resulting from mineral precipitation/dissolution.

The aperture change resulting from a calculated volume change can be approximated by assuming precipitation of a uniform layer over the entire geometric surface area of the fracture, assuming also that this area as well as the fracture spacing remains constant. The ac-

tual distribution of mineral alteration is much more heterogeneous and depends on many processes that are active at scales much smaller than the resolution of the model; however, the combined effect of the initial heterogeneities and localized precipitation processes can only be treated through model sensitivity studies and experiments.

The initial aperture available for precipitation (b_g, the geometric, rather than the hydraulic, aperture) can be calculated from the ratio of the initial fracture porosity ($\varphi_{f,0}$) to the fracture surface area (A_f), as follows:

$$b_g = \frac{\phi_{f,0}}{A_f} \tag{4-15}$$

For a dual permeability model, changes in the fracture porosity are calculated based on the porosity of the fracture medium, so that Δb can be approximated by

$$\Delta b = \frac{(\phi'_{fm} - \phi_{fm,0})}{\phi_{fm,0}} b_g \tag{4-16}$$

Equations (4-15) and (4-16) were implemented in TOUGHREACT with input parameters of b_g and s.

4.2.2.2 Matrix Permeability Changes

Matrix permeability changes are calculated from changes in porosity using ratios of permeabilities calculated from the Carman-Kozeny relation, and ignoring changes in grain size, tortuosity and specific surface area as follows:

$$k = k_i \frac{(1-\phi_i)^2}{(1-\phi)^2} \left(\frac{\phi}{\phi_i} \right)^3 \tag{4-17}$$

The simple cubic law (Eq. 4-13) and Kozeny-Carman (Eq. 4-17) porosity-permeability equations may not reflect complex relationship of porosity and permeability in geologic media that depends on a interplay of many factors, such as pore size distribution, pore shapes, and connectivity /VER 88/. Laboratory experiments have shown that modest reductions in porosity from mineral precipitation can cause large reductions in permeability /VAU 87/. Detailed analysis of a large set of field data also indicated a very severe dependence of permeability on small porosity changes. This is explained by the convergent-divergent nature of natural pore channels, where pore throats can become clogged by precipitation while disconnected void spaces remain in the pore bodies /VER 88/. The permeability reduction effects depend not only on the overall reduction of porosity but on details of the pore space geometry and the distribution of precipitate within the pore space. These may be quite different for different media, which makes it difficult to achieve generally applicable predictions. To evaluate the effects of a more sensitive coupling of permeability to porosity, we also implemented an improved porosity permeability relationship presented by /VER 88/.

$$\frac{k}{k_i} = \left(\frac{\phi - \phi_c}{\phi_i - \phi_c} \right)^n \tag{4-18}$$

where φ_c is the value of critical porosity at which permeability goes to zero, and n is a power law exponent. Parameters φ_c and n are medium-dependent.

4.2.2.3 Mineral Reactive Surface Area

Fracture

In the dual permeability method, the porosity of the fracture medium can be taken as 1.0. However, for modeling of mineral dissolution and precipitation, there would then be no rock to dissolve. Because the dissolution rates of many minerals are quite small at temperatures below 100°C, only a small volume of rock adjoining the open space of the fracture needs to be considered as the starting rock fraction. Reactive surface areas of minerals on fracture walls were calculated from the fracture-matrix interface area/volume ratio, the fracture porosity, and the derived mineral volume fractions. These areas can be calculated based on the fracture densities, fracture porosities, and mean fracture diameter. The wall of the fracture is treated as a surface covered by mineral grains having the form of uniform hemispheres. The grain diameter and spatial density are not included in this calculation, so that the area is actually only marginally greater than the fracture geometric surface area. An alternative method to approximating the surface area in excess of the geometric area would be to include a roughness factor. The geometric surface area of the fracture wall can be approximated by:

$$A_r = \frac{\pi \, A_{f-m}}{2 \, \phi_{f-m}} \tag{4-19}$$

where A_r is the reactive surface area, $A_{f\text{-}m}$ is the fracture-matrix interface area/volume ratio, and $\varphi_{f\text{-}m}$ is the fracture porosity of the rock. $A_{f\text{-}m}$ is the surface area used as input (in FLOW.INP) to the model simulations as a proximation of the reactive surface area. This model for the fracture surface area considers that the areal coverage is approximately equivalent to the mineral volume fraction. A further modification, which was implemented in TOUGHREACT, relates the 3-D cross-sectional area to the 2-D surface area in the fracture, which yields a factor of 3/2, i.e. an increase of 50 % in the reactive surface area. The reactive surface area of each mineral (in units of m / kg) that is used in geochemical calculations is then given by:

$$A_m (m^2 / kg_{water}) = \frac{A_r f_m}{\rho_w \phi_f} \tag{4-20}$$

where f_m is the volume fraction of the mineral in the mineral assemblage, ρ_w is the density of water (in kg/m3) and φ_f is the porosity of the fracture medium, as opposed to the fracture porosity of the rock. This is the surface area/water mass ratio for a mineral in a liquid-saturated system. To provide the correct rock/water ratio in an unsaturated system, the form of this surface area can be written as:

$$A_m(m^2/kg_{water}) = \frac{A_r f_m}{\rho_w \phi_f S_w} \tag{4-21}$$

where S_w is the water saturation. However, as S_w goes to zero, the reactive surface area would tend to infinity. Clearly, at a very low liquid saturation, the surface area of the rock contacted by water is likely much smaller than the total area. Two methods have been implemented to address this phenomenon. The first method considers that the surface area contacted by water diminishes proportionately to the saturation. This yields the saturated surface area. The second method employs the active-fracture-model concept /LIU 98/ modified to consider water-rock reactions taking place below the residual saturation /LIU 98/. The form of the active fracture parameter for reaction is then given by the following set of equations:

$$S_{ar} = (S_w - S_m)/(1 - S_m)$$

$$a_{fnr} = S_{arr}^{(1+\gamma)} \tag{4-22}$$

where S_m is the minimum liquid saturation for which water-rock reactions are considered and S_{ar} is the effective saturation for reaction. The active fracture parameter, γ, is obtained from the calibrated hydrological property set. The factor that reduces the surface area contacted by the water phase is given by a_{fmr}. In all simulations S_m is set to the very small saturation of 1x10-4, to ensure that reactions take place until virtually no water is left (e.g., during dryout via ventilation or heating). Finally, the reactive surface area, using this modified form of the active fracture model, is given by:

$$A_m(m^2/kg_{water}) = \frac{A_r a_{fmr}}{\rho_w \phi_f S_w} \tag{4-23}$$

calculated in this way is applicable only to reactions taking place in the fracture medium, and is used directly. Note that this area is not the input surface area.

Matrix (porous medium)

Mineral surface areas in the rock matrix (or porous medium) were calculated using the geometric area of a cubic array of truncated spheres that make up the framework of the rock /SON 94/. Clay minerals are considered as coatings of plate-like grains. The mineral surface areas of framework grains (truncated spheres) in contact with the open pore space are calculated using an initial grain diameter, followed by successive truncation of the grains in the vertical direction until the porosity of this system is close to the measured porosity of the rock. The abundance of secondary phases (i.e., those that formed as alteration products or low-temperature coatings on the primary assemblage), such as clay minerals, is used to reduce the free surface area of the framework grains. The surface areas of the secondary phases are calculated assuming a tabular morphology. The full details of the geometric calculations are given in /XUT 04/. Note that the surface area calculated by the above method for the matrix is an input parameter in chemical.inp file.

4.2.3 Phase Properties; Equation of State Modules

The TOUGH2 code uses separate modules to model the fluid phase properties; a list of these modules is given in Table 4.2. The modules EOS5 and ECO2N are used in the project as coupled EOS modules.

Table 4.2 Equation of state modules introduced to TOUGH2 family and modelled phases

Module	Capability, phases modelled
EOS1	Water, water+tracer
EOS2	Water, CO2
EOS3	Water, air
EOS4	Water, air, with vapor pressure lowering
EOS5	Water, hydrogen
EOS7	Water, brine, air
EOS7R	Water, brine, air, parent-daughter radionuclides
EOS8	Water, dead-oil, non-condensable gas
EOS9	Variably-saturated isothermal flow according to Richards Eq.
EWASG	Water, salt, H_2, CO2 with precipitation of NaCl,
ECO2N	Improved form of EWASG with some new options

More information on TOUGH2 and its EOS modules can be found in related manuals. The simulation work conducted in the framework of the project is essentially based on the use of EOS packages EOS5 and ECO2N.

4.2.3.1 EOS Module EOS5

The EOS5 Module was developed to model the behaviour of groundwater systems in which hydrogen releases is taking place. The assignment and handling of primary thermodynamic assignement of secondary parameters as follows: Density of gaseous hydrogen is modelled from the ideal gas law. Viscosity and water solubility of hydrogen are interpolated from the tabulated experimental data. The input controlling is the same as similar EOS modules i.e. EOS3 with air replaced by hydrogen /PRU 99/

4.2.3.2 EOS Module ECO2N

The ECO2N is one of the latest developments in TOUGH2 project /PRU 05/. It is a fluid property module for the TOUGH2 simulator (Version 2.0) that was designed for applications to geologic sequestration of CO_2 in saline aquifers as well as other H_2O-CO_2 systems like geothermal reservoirs. It can be also applied to the underground repository systems if they include CO_2 as free gas and/or as dissolved in water/brine. The module includes a comprehensive description of the thermodynamics and thermophysical properties of H_2O - NaCl - CO_2 mixtures, that reproduces fluid properties largely within experimental error for the temperature, pressure and salinity conditions of interest (10 °C < T < 110 °C; P < 600 bar; salinity up to full halite saturation). Flow processes can be modelled isothermally or non-isothermally, and phase conditions represented may include a single (aqueous or CO2-rich) phase, as well as two-phase mixtures.

TOUGH2/ECO2N represents fluids as consisting of two phases: a water-rich aqueous phase, herein often referred to as "liquid," and a CO_2-rich phase referred to as "gas." In addition, solid salt may also be present. The only chemical reactions modelled by ECO2N include equilibrium phase partitioning of water and carbon dioxide between the liquid and gaseous phases, and precipitation and dissolution of solid salt. The partitioning of H_2O and CO_2 between liquid and gas phases is modelled as a function of temperature, pressure, and salinity, using the recently developed correlations of Spycher and Pruess, 2005, /SPY 05/. Dissolution and precipitation of salt is treated by means of local equilibrium solubility. Associated changes in fluid porosity and permeability may also be modelled. All phases - gas, liquid, solid - may appear or disappear in any grid block during the course of a simulation. More information on the details and use of ECO2N is found in /PRU 05/.

4.2.4 Input - Output

The input-output organisation of TOUGH2 is applied in TOUGHREACT too. Because of the need of more input to characterize the chemical structure of the present phases two additional input data files are required for TOUGHREACT. As the original TOUGH2 input file (flow.inp) the other files are also user-specified. The input file names have been fixed in the program (i.e. names cannot be specified by the user). Descriptions of these input files are given below.

Flow.inp - Flow input. This file mainly includes rock properties, time-stepping information, geometric grid information, initial and boundary conditions, and data related to multi-phase fluid and heat flow simulation. The flow input is the same as the original TOUGH2 V2, with an additional data block REACT.

Solute.inp - Transport and other run parameters. This file contains various flags and input parameters for calculations of reactive transport, such as diffusion coefficients, tolerance limits for convergence of transport and chemical iterations, printout flags for mineral and aqueous species, and the configuration of model zones with different chemical composition (the composition of each zone, however, is defined in the following file CHEMICAL.INP).

Chemical.inp - Geochemical parameters and properties. This file is used to define the geochemical system (i.e. the type and number of aqueous component species, minerals, gases, and sorbed species considered in the simulation). It also includes the initial compositions of

water, mineral, and gas zones configured in file solute.inp, and kinetic data for minerals (rate constants, surface areas, etc.). In addition to the above mentioned three input files, the program needs a thermodynamic database file. The file name is specified in solute.inp file. This file contains reaction stoichiometries, dissociation constants (log(K)), and regression coefficients of log(K) as a function of temperature.

Changes made in these input data to introduce the Pitzer and other improvements are given and discussed in Chapter 6.

4.3 Modeling Algorithm and Planned Improvements

The computation algorithm and planned improvements are described in the algorithm given in Figure 4-1. In the Figure EOS abbreviates the changes performed in the EOS modules used. The DB is for the improvements in the database used. CONV is used for the convergence implementation. The Pitzer ion-interaction module is the most important implementation being worked and is abbreviated in the Figure as PITZER. The Pitzer implementation was already performed by the scientists of LBNL and at the planning phase of the project a co-operation was agreed with Mr. Zhang, the developer of Pitzer Version of TR. However, due to some unexpected events (moving of Mr. Zhang to Shell and the preparation of TOUGHREACT 2.0 including the Pitzer as an option by the scientists of LBNL for Department of Energy, USA), this agreement did not take place. The other implementation work consists of the convergence, swelling and some changes in EOS module. The related work is given in following chapters.

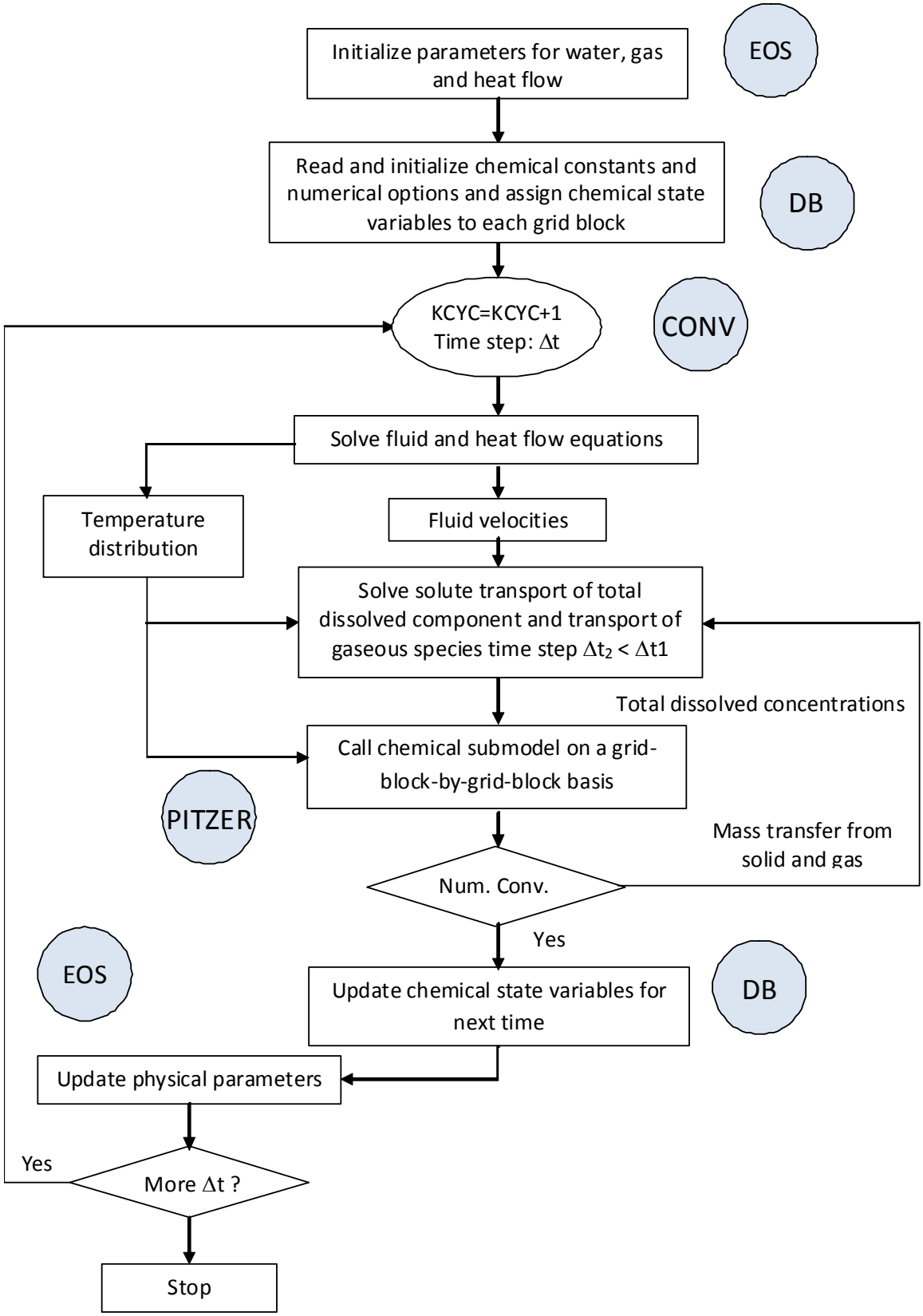

Figure 4-1 The computation algorithm of TOUGHREACT and realized modifications

5 CODE IMPROVEMENT; IMPLEMENTATION, VALIDATION

5.1 Background: Pitzer Ion Activity Model

As indicated in previous sections the activity coefficients of charged aqueous species are computed in original TOUGHREACT using an extended Debye-Hückel equation and parameters derived by Helgeson et al. (HKF) /HEL 69/. The assumption is made that the dominant cation and anion in solution are sodium and chloride, respectively, so that HKF Equation can be used directly. Concentrated aqueous solutions are significantly different from dilute solutions not only in terms of geochemical behavior (e.g., water activity and ionic activity coefficients far from unity), but also in terms of flow and transport because of elevated density and viscosity and it is well known that the Debye-Hückel model may not model the activity behaviour of such solutions. The Pitzer ion-interaction model is implemented in TOUGHREACT for more reliable calculations of the high salinity solutions.

The original plan of the project was scheduled to provide the Pitzer version of TOUGHREACT from LBNL of University of California. An agreement for this scientific cooperation was made prior to the launch of the project. This intention was confirmed by Mr. Zhang from LBNL, the developer of TOUGHREACT-PITZER, in his visit to Germany on spring 2008. However Mr. Zhang leaved LBNL to join Shell Co. unless delivering the required module and the agreement was not realized by LBNL with the argument that the version has not been officially released yet. As the succeeding correspondence did not give any finalizing results, it was decided to make the necessary programming, implementation and calibration work internally within the project. For this attempt, in order to avoid more delay in the deadline of the project, the methodology applied for the LBNL Pitzer module is applied /ZHA 06/. The work performed is given in the following.

In a given aqueous solution, the thermodynamic activity of a dissolved species is a function of the solution excess free energy which is, in turn, a function of temperature, pressure, chemical composition of the solution, and the thermodynamic properties of the solutes. In the solution, ions with opposite signs attract and interact with each other. Some of the ions with opposite signs are bound by their ionic charges, leading to aqueous complexes. Meanwhile, some of the ions tend to depart from each other, leading to the existence of free ions in the solution. The ratio of the bounded ions and free ions is a constant under given composition, temperature and pressure conditions, and is quantified in the thermodynamic equilibrium theory. The thermodynamic activity of any ion in the attraction-repulsion processes is determined by (1) the abundance of that ion in the solution and (2) the non-ideal behavior of the ion in solution. The abundance of that ion is the concentration of the free ion. Non-ideality, evaluated using an ionic activity coefficient, is a complex function of temperature, pressure, and concentrations. Dilute solutions (typically with ionic strength, I, < 0.1 molal) are considered quasi-ideal solutions. The non-idealities of such solutions are minor and are mainly attributed to long distance ionic interactions, which can be quantified using ionic strength. The activity coefficients of species in those solutions can be calculated with simple models, such as the Debye-Hückel model and its variations, in which only solution ionic strength and ionic properties are accounted for in the calculation. The effects of interactions among individual ions are neglected.

The non-idealities in concentrated solutions (ionic strength *I* > 0.1 molal, and especially *I* > 1 molal) are significant because the distances between ions are much shorter than those in dilute solutions. Most ions in such solutions are neither completely dissociated nor tightly associated, because of the short distance and strong interactions among ions in the solutions. Instead, ions engage in attraction-repulsion interactions with other ions. Ionic activity is mainly attributed to such interactions. Activity models that apply to dilute solutions, such as the Debye-Hückel model and its extensions, are no longer suitable in such concentrated solutions. To calculate ionic activities, one needs to consider interactions among different individual ions. A quantitative description of how ion interactions affect the ionic activities in concentrated aqueous solutions is given in /PIT 73a/ and /PIT 73b/. Pitzer's model formulates the ionic activity as a function of each individual ionic interaction, i.e., the interactions among each cation-anion pair, cation-cation pair, anion-anion pair, and various ternary ionic combinations and other possible interactions. Like-sign pairs and ternary ionic combinations result from multiple salt contributions (also referred to as mixing terms). The Pitzer model evaluates the ionic activity of a solution as a function of solution ionic strength (long-distance interaction), interaction terms (short-distance interaction), temperature, and pressure. The model formulation consists of several virial equations, sometimes called specific interaction equations, Pitzer equations, or phenomenological equations. These equations can adequately express the thermodynamic properties of the concentrated solution over a wide range of concentrations and temperatures. The Pitzer model is based on a virial expansion that essentially reduces to the Debye-Hückel equation at low ionic strength /PIT 91/. This virial expansion involves summations over all possible binary and ternary short-range interaction terms, as well as mixing terms. A generally accepted form of the Pitzer model was formulated by Harvie et al. and referred to as the HMW formulation /HAR 80/. This formulation has been adopted in several computer codes, such as PHRQPITZ, GMIN, and BIO-CORE. In EQ3/6, Wolery and Jarek (2003) use Pitzer's original formulation but also make use of interaction parameters for the HMW formulation by mapping these parameters into the formulation implemented in the code /WOL 03/.

The HMW formulation is often preferred to Pitzer's original formulation because it is more convenient for numerical implementation. Also, parameters for the HMW formulation are often more readily available from the literature than parameters for Pitzer's original formulation. The implementation of the Pitzer model allows TOUGHREACT to deal with concentrated solutions, with limits on ionic strength, temperature, and pressure depending on the types and validity range of ion-interaction parameters in the thermodynamic database. The Pitzer model implemented in TOUGHREACT allows the water activity of concentrated solutions to be accurately calculated, such that vapor-pressure lowering, and its subsequent effects, can be properly simulated.

The fugacities (and partial pressures) of volatile gases such as HCl, HF, and HNO_3 over dilute solutions are generally quite low at low temperatures (typically < 10^{-15} bar). However, when these solutions become heated and highly concentrated, the fugacities of these gases increase significantly. The fugacities of these gases over highly concentrated solutions can be calculated using the Pitzer model. However, computing the diffusive and advective transport of these gases

In numerical simulations of boiling or evaporation under rapidly drying conditions, a model gridblock can “dry out” between two sequential time steps (i.e., evolve from partially wet to dry conditions, with liquid saturation sharply dropping from a non-zero value to zero or almost zero). In this case, capturing the rapid chemical evolution of the drying solution is important for predicting the precipitation sequence of solid phases, the accompanying gas volatilization, and the composition of the remaining brine. Modeling such a rapid process is extremely challenging. For this purpose, the localized iterative algorithm (LIA) developed by LBNL is used. The algorithm proposes that the water is removed gradually from drying model gridblocks until the water activity of the remaining brine reaches equilibrium with the prevailing air relative humidity (i.e., until equilibrium is established between the brine and the vapor phase in contact with it). The LIA enables TOUGHREACT to deal locally with rapid drying processes in simulations that involve otherwise much larger time frames to accurately predict the evolution of the aqueous, solid, and gas phases upon evaporation. The LIA is invoked if (1) the temperature is higher, or equal to, the boiling point, and (2) the water activity is higher than the prevailing air relative humidity (such that the water can be concentrated and thus its activity lowered until equilibrium is reached at the prevailing relative humidity).

5.1.1 Implementation

The implementation of Pitzer model is performed based on the formulation proposed by Harvie et al. (1984). This is a generally accepted form of the Pitzer model has been implemented in TOUGREACT. In the HMW model, water activity is formulated as:

$$Ln(a_{H_2O}) = -\frac{m_w}{1000}(\sum_{i=1}^{N} m_i)\phi \tag{5-1}$$

where a_{H2O} is water activity, m_i is molality of species i, w_m is molecular weight of water, N is the number of species in the system, and ϕ is the osmotic coefficient, defined as:

$$\sum_{i=1}^{N} m_i(\phi - 1) = 2(-\frac{A^{\Phi} I^{\frac{2}{3}}}{1+1.2\sqrt{I}}) + \sum_{c=1}^{N_c}\sum_{a=1}^{N_1} m_c m_a (B_{ca}^{\Phi} + ZC_{ca}) +$$

$$\sum_{c}\sum_{c'=c+1} m_c m_{c'} (\Phi_{cc'}^{\phi} + \sum_{a=1} m_a \Psi_{cc'a}) + \sum_{a}\sum_{a'=a+1} m_c m_{c'} (\Phi_{aa'}^{\phi} + \sum_{a=1} m_c \Psi_{aa'c}) +$$

$$\sum_{n=n+1}^{N_n}\sum_{c=1}^{N_c} m_c m_{c'} \lambda_{nc} \sum_{n=n+1}^{N_n}\sum_{c=1}^{N_c} m_n m_a \lambda_{na} + \sum_{n=n+1}^{N_n}\sum_{c=1}^{N_c}\sum_{a=1}^{N_a} m_n m_c m_{c'} \zeta_{nca} \tag{5-2}$$

where I is the ionic strength, defined as $I = -\frac{1}{2}\sum_{i=1}^{N} z_k^2 m_i$ and z_k is the electrical charge k. The subscripts c, a, and n denote cations, anions, and neutral species, respectively. The activity coefficients of cations (γ_M), anions (γ_X), and neutral species (γ_N) are respectively calculated as:

$$Ln\gamma_M = Z_M^2 F + \sum_{c=1}^{N_c} m_a (2B_{Ma} + ZC_{Ma}) +$$

$$\sum_c m_c (2\Phi_{Mc} + \sum_{a=1} m_a \Psi_{Mca}) + \sum_a \sum_{a'=a+1} m_c m_{c'} \Psi_{aa'M} +$$

$$|Z_M| \sum_{c=1}^{N_c} \sum_{a=1}^{N_a} m_n m_c m_{c'} \zeta_{nca} + 2 \sum_{n=1}^{N_n} m_n \lambda_{nM}$$

$$Ln\gamma_X = Z_X^2 F + \sum_{c=1}^{Nc} m_c (2B_{cX} + ZC_{cX}) +$$

$$\sum_c m_c (2\Phi_{Xa} + \sum_{a=1} m_c \Psi_{Xca}) + \sum_c \sum_{c'=c+1} m_c m_{c'} \Psi_{cc'X} +$$

$$|Z_M| \sum_{c=1}^{N_c} \sum_{a=1}^{N_a} m_c m_a C_{ca} + 2 \sum_{n=1}^{N_n} m_n \lambda_{nX}$$

$$Ln\gamma_N = \sum_{a=1}^{N_a} m_a (2\lambda_{na}) + \sum_{c=1}^{N_c} m_c (2\lambda_{na})$$

$$+ \sum_{c=1}^{N_c} \sum_{a=1}^{N_a} m_n m_c m_{c'} \zeta_{Nca} \qquad (5\text{-}3)$$

Where F is given by:

$$F = -A^{\Phi} \frac{\sqrt{I}}{1+1.2\sqrt{I}}) + \frac{2}{1+1} \ln(1+1.2\sqrt{I})) +$$

$$\sum_c \sum_{c'=c+1} m_c m_{c'} \Phi_{cc'}^{\phi} + \sum_a \sum_{a'=a+1} m_c m_{c'} (\Phi_{aa'}^{\phi}$$

$$\sum_{n=n+1}^{N_n} \sum_{c=1}^{N_c} m_c m_{c'} B'_{nc} \qquad (5\text{-}4)$$

C_{MX} is derived from C_{MX}^{Φ} as:

$$C = \frac{C^{\Phi}_{MX}}{2\sqrt{|z_M z_X|}} \tag{5-5}$$

And Z is calculated as

$$Z = \sum_{k=1}^{N} |z_k| m_k \tag{5-6}$$

The Pitzer virial coefficients, $^{\Phi MX}B$, ^{MX}B , $^{'MX}B$, $^{MX}\alpha$, ^{MX}C , $^{NC}\lambda$ and $^{NA}\lambda$ in Equation (5-2) through (5-3) are described below.

$$g'(x) = -2(1 - 1 + x + \frac{x^2}{2})e^{-x}) / x^2 \tag{5-7}$$

and *x* denoting α_{MX} or $\alpha^{MX}\alpha'$, respectively.

For any salt containing a monovalent ion, $^{MX}\alpha$ = 2

$$g'(x) = -2(1 - 1 + x)e^{-x}) / x^2$$
$$B_{MX} = \beta^{(0)}_{MX} + \beta^{(1)}_{MX} g(\alpha_{MX}\sqrt{I}) + \beta^{(2)}_{MX} g(\alpha_{MX}\sqrt{I}) \tag{5-8}$$

With function g'(x) defined as:

$$g'(x) = -2(1 - (1 + x + \frac{x^2}{2})e^{-x}) / x^2 \tag{5-9}$$

and denoting $\alpha_{MX}\sqrt{I}$ or $\alpha'_{MX}\sqrt{I}$ respectively.

For any salt containing a monovalent ion, α_{MX}=2 $\alpha_{MX} = 2$ and $\alpha'_{MX} = 12$ for 2-2- electrolytes $\alpha_{MX} = 1{,}4$ and $\alpha'_{MX} = 12$; for 3-2,4-2 and higher valence electrolytes $\alpha_{MX} = 2$ and $\alpha_{MX} = 50$

It should be noted that Φ'_{cc} Φ'_{ac} Φ_{cc} Φ_{ac} are interaction parameters for like sign pairs (mixing terms). They are temperature and ionic strength dependent*:*

Terms $^{E}\theta_{ij}(I)$ and $^{E}\theta'_{ij}(I)$ are functions of the ionic charges between the pair and solution ionic strength. These functions are defined in /PIT 91/ and can normally be ignored in moderately concentrated solutions of ionic strength less than 10 molal. Also θ'_{ij} are temperature dependent fitting parameters with $^{E}\theta_{ij}(I)$ and $^{E}\theta_{i'j}(I)$ calculated according to Pitzer. Ψcca and Ψcaa are the temperature dependent interaction coefficient of ternary terms ξacc is the temperature dependent interaction coefficient of neutral cation-anion terms. Normally this term is ignored.

To implement the above given equations two subroutines were essentially created and in TOUGHREACT implemented. The subroutine PITZPAR deals with the calculation of Pitzer parameters (β,θ,λ,ψ). The subroutine PITZ-HMW, on the other hand, calculates the activity coefficients of water and other species based on the above given HMW methodology. The main subroutine PITZER.f consists of these both routines. A second main routine called IN-

ICHM.f is introduced to the programme to initiate and read the required data from the database. The TZF.f and NEWTON.f original routines of TOUGHREACT were changed accordingly. The MOPR(9) and MOPR(10) in TZF are used as control parameters for applying Pitzer module or not (selecting the Debye-Hückel method). The list of the created and changed subroutines is given in Table 5.1 with their function.

Table 5.1 Introduced and changed subroutines for TOUGHREACT-Pitzer

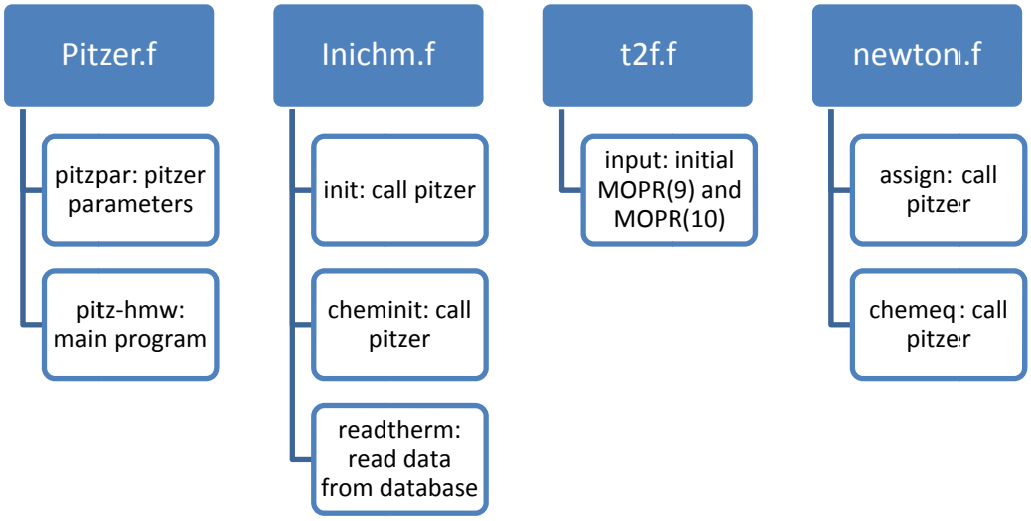

5.1.2 Validation

For the validation various attempts were made basically following the TOUGHREACT Pitzer version /ZHA 06/. The activity coefficients of NaCl, KCl, $CaCl_2$ are predicted with ISTec implementation and compared with experimental data as well as with the predictions of the LBNL version. As can be shown in Figure 5-1 to Figure 5-5 the predictions match generally well with the experimental data. A significant difference between the ISTec version and LBNL version was the increasing deviation from the measured values after 100 °C. This deviation was corrected in some degree by changing the coefficient of the related correlation for adjusting the effect of the temperature after cooperation with the LBNL co-workers however a negligible deviation remained in spite of all correction measures. This deviation is commented as acceptable thing that the temperature ranges encountered in nuclear repositories.

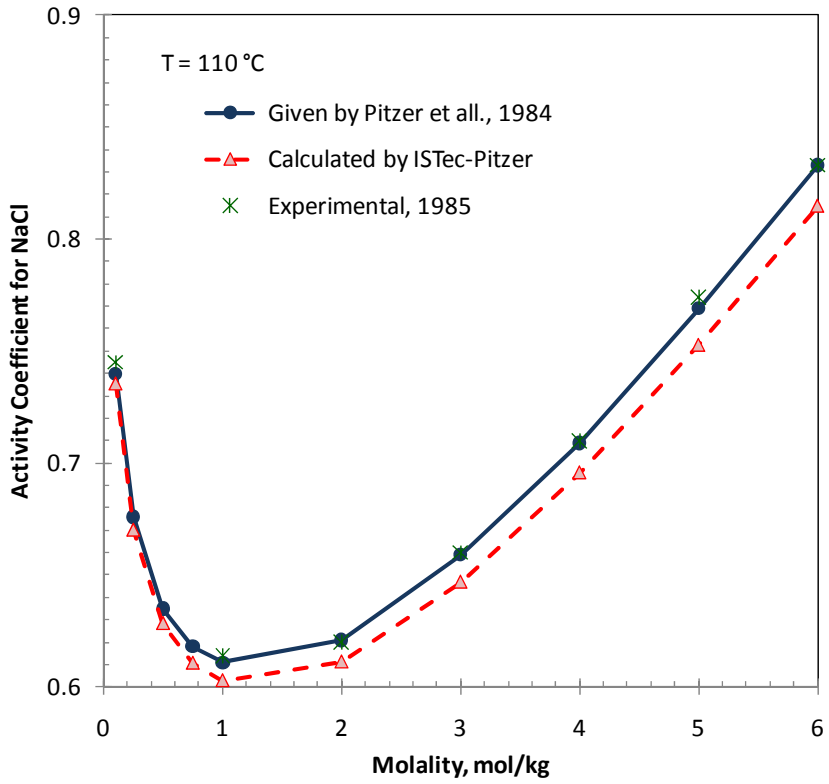

Figure 5-1 Prediction of the activity coefficient of NaCl and comparison with LBNL Pitzer and experimental values.

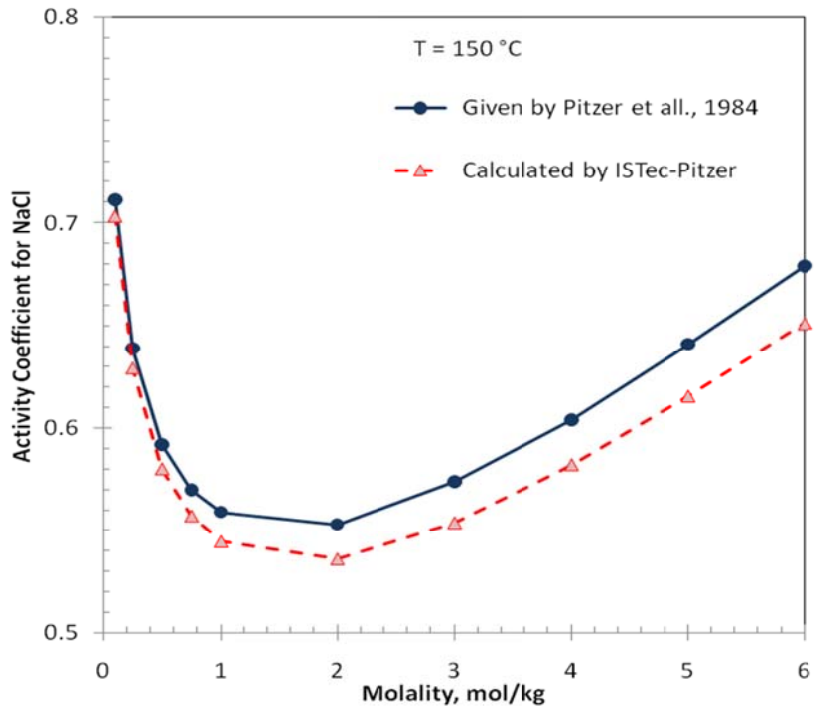

Figure 5-2 Prediction of the activity coefficient of NaCl and comparison with LBNL Pitzer predictions.

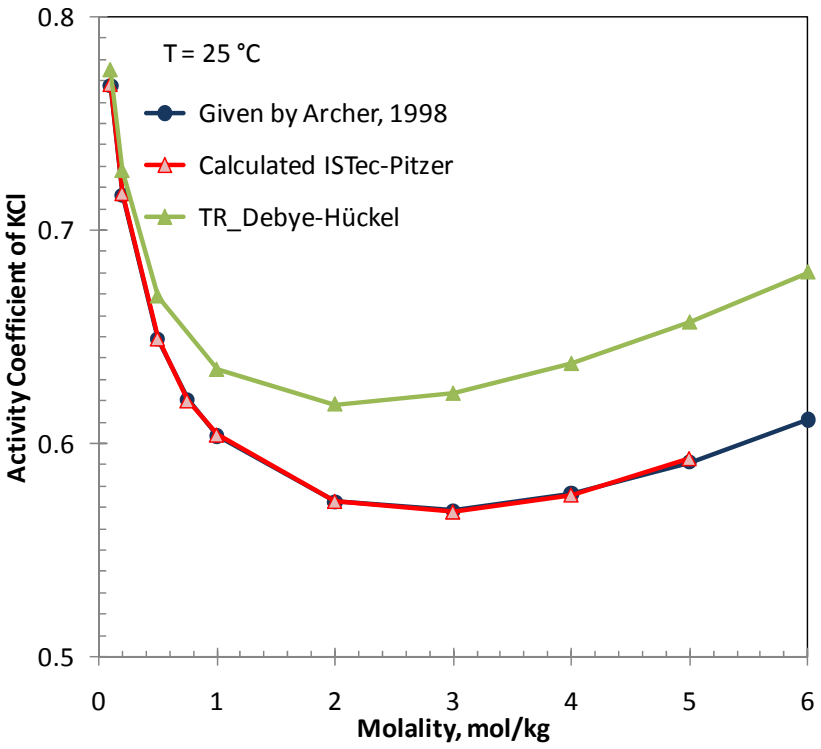

Figure 5-3 Prediction of the activity coefficient of KCl and comparison with experimental values and the prediction with Debye-Hückel activity model

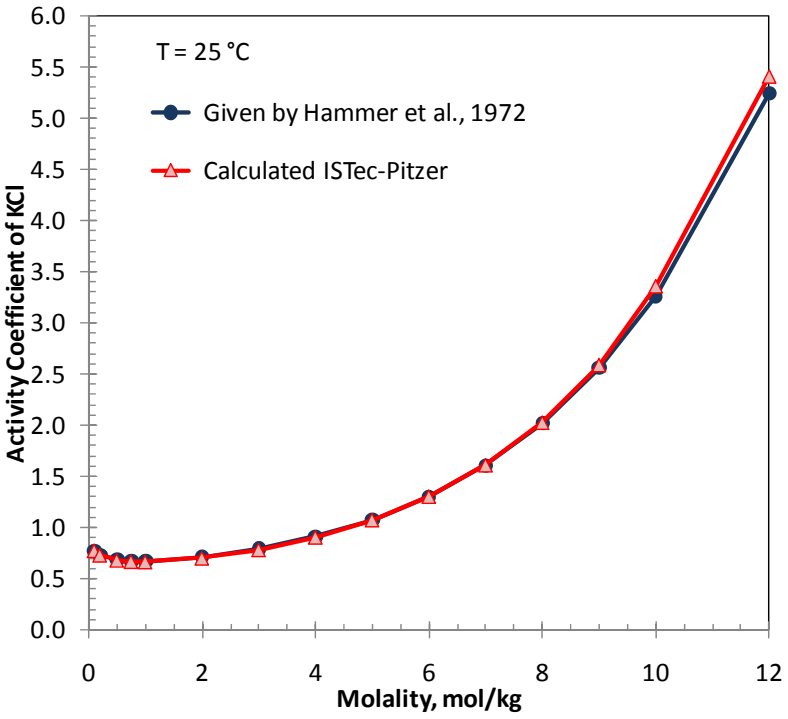

Figure 5-4 Prediction of the activity coefficient of KCl and comparison with experimental values.

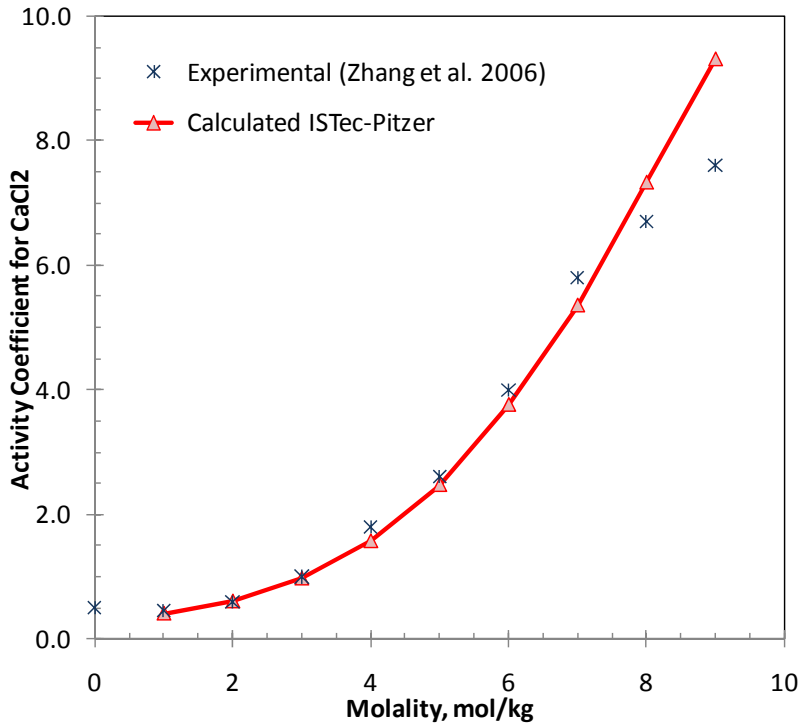

Figure 5-5 Prediction of the activity coefficient of CaCl2 and comparison with experimental values.

5.1.3 Thermodynamic Databank

For the calculation the same database as used in TOUGHREACT is used. This means the EQ3/6-formatted database *data0.ypf* of TOUGHREACT-PITZER provided by LBNL /WOL 04/ is applied for both Pitzer ion-interaction parameters and thermodynamic equilibrium constants. These parameters are temperature-dependent. The previous TOUGHREACT-formatted thermodynamic database is also required to provide mineral molal volumes and gas molecular diameters, in case these data are not available in *data0.ypf*. The interpolation and extrapolation equations, as a function of temperature, for various thermodynamic properties of aqueous solutions, for binary and ternary systems, and for multiple component mixtures within the Pitzer formulation is performed with the following equation as proposed /WOL 04/ and used in /ZHA 06/ :

$$P(T) = a_1 + a_2\left(\frac{1}{T} - \frac{1}{T_0}\right) + a_3 \ln\left(\frac{T}{T_0}\right) + a_4(T - T_0) \qquad (5\text{-}10)$$

Where P(T) represents Pitzer parameters $\beta^{(0)}$, $\beta^{(1)}$, $\beta^{(2)}$, α, Φ, Ψ and C_{MX} *at temperature T (absolute* temperature); and T_0 is the reference temperature (298,15 K is used in the database).

These data are generally good up to at least 90°C and were derived specifically for the Yucca Mountain Project. The dependency of the Pitzer parameters on pressure is not considered in the present model, because the effect of pressure is much less significant than the effect of temperature within the current temperature range considered. In addition to the EQ3/6-formatted Pitzer database, the code can also use the regular TOUGHREACT-formatted

thermodynamic database and an unformatted database for Pitzer ion interaction parameters from Zhang et al. /ZHA 06/. The unformatted database is easy to extend and modify, and could be useful for users who develop their own parameters. Users can read the parameters from either database by simply assigning different option parameters in the input file (MOPR(12)).

Because the effect of ion pairing and aqueous complexations (forming secondary aqueous species) is generally taken into account by the ion-interaction parameters, much care must be taken to avoid “double counting”. Such an occurrence can be avoided by including in simulations only those secondary species that were specifically included in the fits of experimental data used to determine the ion-interaction parameters used in the simulation.

5.2 Convergence- Compaction

The creep behavior (convergence) of the rock salt that can result in the closing of the caverns with time is one of the critical parameter of long term safety analysis for rock salt. Because of the compaction of rock salt the pore volume is expected to reduce, the pressure at the pore may increase locally which can act as an additional impulse for flow to the boundaries of the repository volumes. The change of the porosity results in the change of the permeability as well as in capillary pressure that are vital parameters of the transport processes. Therefore the numerical modeling attempts of the multi-phase flow in repository conditions should be modified according the changes related to compaction.

A convergence model was implemented into TOUGHREACT based on previous ISTec studies and related porosity-permeability-capillary pressure changes were also revisited. The implementations performed are given in the following chapters.

5.2.1 Background

The objective of the numerical implementation is the modeling of the pore volume changes through creeping of the rock salt. The convergence rate $\dot{\varepsilon}$ is defined with the change of the total pore volume with time:

$$\dot{\varepsilon} = \frac{d\phi}{dt} \tag{5-11}$$

Where ϕ the porosity and t is the time. In the following the crushed salt is considered as backfill material and its compaction is calculated. The main mechanisms following the compaction of the crushed salt are given by /ZHA 93/ as follows:

- Grain destruction
- Dislocation
- Grain deformation at the contact surfaces oft he grains as the result of dislocation
- Pressure dissolution in solutions
- Recrystallisation and dissolution

Based on microscopical as well as macroscopical observations the effect of these mechanisms in a saline solution is dependent on the pressure, temperature and fluid saturation. A generalized definition of the compaction of the crushed salt is given in the following relation:

$$F(\varepsilon_v, \dot{\varepsilon}_v, \sigma, T, S) = 0 \qquad (5\text{-}12)$$

where

- ε_v volumetric compaction (dimensionless),
- σ effective hydrostatic stress (Nm^{-2}),
- T temperature (K) and
- S material parameter

The effective stress is a mechanical parameter. Therefore the implementation of the convergence is a kind of coupling of mechanical to the fluid dynamical parameters in a limited sense. Here two methods can be distinguished: In the first one the convergence is modelled based on geomechanical parameters and so the modeling of fluid dynamics is performed. In the second one the stress is coupled to fluid dynamic directly based on the constitutive relationships. The first one gives a better evaluation of the compaction however needs a more difficult and time consuming modeling effort because of the non-linear coupling of stress and fluid pressure. The second one is based on an empirical expression in which the corresponding parameters should be determined experimentally.

5.2.1.1 Modeling with Geomechanical Parameters

The generalized form of this approach is:

$$\dot{\varepsilon} = f_1(\sigma, S_1) \cdot f_2(T, S_2) \cdot f_3(\varepsilon_v, S_3) \qquad (5\text{-}13)$$

With S_1, S_2, S_3 as material dependent parameters. Based on the formulation developed by /ZHA 93/ the following equation is used:

$$\dot{\varepsilon} = A \cdot e^{-\frac{Q}{RT}} \cdot \left(\frac{\sigma}{\sigma_0}\right)^n \cdot \left(\ln\left(\frac{\phi_0(1-\phi)}{\phi(1-\phi_0)}\right)\right)^{-m} \qquad (5\text{-}14)$$

In this equation R is the universal gas constant (8,314 10^{-3} kJ mol^{-1} K^{-1}), Q is the activity energy (kJ mol^{-1}), σ_0 reference stress and ϕ_0 is the reference porosity. A, n und m are material specific parameters.

Experimental values for the parameters A, n and m are published for six various salt and experimental conditions /ZHA 93/.

5.2.1.2 Modeling with Fluid Dynamic Parameters after /PSE 85/

A similar approach to Eq. (5-14), is given by the following equation with the application of the fluid pressure p instead of mechanical stress σ /PSE 85/:

$$\dot{\varepsilon} = \dot{\varepsilon}_0 \cdot f_1(T) \cdot f_2(p) \cdot f_3(\phi) \cdot f_{\mathrm{Re}d} \qquad (5\text{-}15)$$

with $\dot{\varepsilon}_0$ as the time independent initial convergence rate of the cavity and $f_{\mathrm{Re}\,d}$ as reduction factor.

5.2.1.3 Modeling after /PRI 91/

Another formulation is given by /PRI 91/ with the following:

$$\dot{\varepsilon} = \dot{\varepsilon}_n(\tau, n) \cdot \dot{\varepsilon}_0 \qquad (5\text{-}16)$$

where $\dot{\varepsilon}_n(\tau, n)$ is the normalized convergence rate, n is a coefficient related to second Norton-Law and τ is the normalized time defined as:

$$d\tau = E \cdot A_0 \cdot \exp\left(-\frac{Q}{RT}\right) \cdot (\alpha \cdot p_e)^{n-1} \quad dt \qquad (5\text{-}17)$$

In this equation E is the Young's Module for rock salt, A_0 is the creep constant, p_e is the effective pressure and α is a factor for the consideration of the geometry.

The obvious difference between the models of /PRI 91/ and /PSE 85/ is the relation of the time dependent convergence of an open cavern or wellbore with the compaction behaviour of the crushed salt.

5.2.1.4 Pressure-Time-Porosity Line Interpolation Method

A synthesis of both methods for modeling the convergence is based on the principle proposed in /FRE 95/; the parameter variations of the convergence computations is performed with a geomechanical program using following formulation for the porosity:

$$\phi = f(p, t) \qquad (5\text{-}18)$$

Based on this value the numerical simulations for two-phase flow can be performed. In these calculations the porosity is corrected based on the geomechanical calculations which mean that the pressure and time dependence will be included to the convergence calculations.

5.2.1.5 Boundary-Back Stress-Method

With this method the creep behaviour of salt is calculated directly /FRE 95/. The rock salt is modelled as a fluid phase with high viscosity. The properties of this fluid must be selected properly in order to simulate the total closing of the cavity. To apply this method the empirical parameters in terms of fluid properties should be calibrated based on experimental data.

5.2.2 Comparison and Selection of the Convergence Model

The comparison and selection of the method to be used for the implementation is made based on /LOR 99/. Models based on the geomechanic parameters need more complex algorithms and higher computer times. Based on this reason these are not applied in the current project. These models can be used if the coupling between stress and fluid pressure can be described in form of analytical relationships. Models based on the description of pore volume with pressure, temperature and fluid saturation are suitable to be used in TOUGH2 and its derivatives. Both convergence models were tested and compared in a case study in /GOM 97/. After this study the model of /PRI 91/ shows better results with a better evaluation of the physical interactions. However this approach necessitates higher number of input parameter that should be determined experimentally. In contrast the model affirmed by /PSE 85/ exhibits a more robust, practical and applicable method with less calibration parameters. For a case study material specific parameters are available.

The modeling work necessary for an implementation is determined to be relatively less; the convergence rate is implemented as an additional „constitutive relationship“ as alternative to the model of /PRI 91/ proposing a time dependent formulation The models “pressure-time-porosity line interpolation-Method” and “boundary-backstress-Method” have been applied both for the safety analyze of WIPP /FRE 95/. Both methods need however considerable computer time therefore for example the results of geomechanical computations of the methods should be extrapolated for an application in TOUGH2 for related calculation time. On the other hand the temperature dependency was not taken into account in both methods. In a probable implementation this would certainly lead to an additional computer time. Therefore in TOUGH2 implementation these two methods were not considered.

Based on the determined criteria the model described in /PSE 85/ (Eq. 5-15) has been decided to be implemented. The model is relatively simple to implement and needs lower computer time and experimental parameters specific to the materials used. Another advantage is that it has been tested and validated for several cases. /RÖH 97/, /JAV 97/, /JAV 98/.

5.2.3 Definition of the Implemented Convergence Model

For a complete definition of the convergence model the main basic equations is given in the following: The rock convergence $\dot{\varepsilon}$ is defined as the time dependent change of the cavity as given in Eq. (5-12) and Eq. (5-13). The terms for pressure, temperature and porosity dependence as well as for the reduction factor are given with the following expressions:

$$f_1(T) = \frac{1}{1+a} \cdot \left[\exp\left(\frac{Q_1}{R} \cdot \left(\frac{1}{T_G} - \frac{1}{T} \right) \right) + a \cdot \exp\left(\frac{Q_2}{R} \cdot \left(\frac{1}{T_G} - \frac{1}{T} \right) \right) \right] \tag{5-19}$$

$$f_2(p) = (1 - p_{Fluid} / p_{Rock})^m , \tag{5-20}$$

$$f_3(\phi) = \begin{cases} \phi \cdot \left(1 - \frac{\phi}{\phi_0}\right) \cdot \left[\left(1 - \frac{\phi}{\phi_0}\right)^2 + \phi \cdot \left(1 - \frac{\phi}{\phi_0}\right)^{1/S}\right]^{-S} & if \quad \phi < \phi_0 \\ 1 & if \quad \phi \geq \phi_0 \end{cases} \tag{5-21}$$

$$f_{red} = f_d + (f_w - f_d) \cdot \frac{V_B}{V_p} = f_d + (f_w - f_d) \cdot S_L \tag{5-22}$$

where

Q_1 und Q_2 activity energy for secondary creep (J),

R gas constant (J/K),

T_G reference temperature of rock salt based on equilibrium temperature (K),

a dimensionless temperature (-),

p_{Fluid}, p_{Rock} fluid and lithostatic pressure (Pa),

m, S dimensionless exponent (-),

ϕ_0 reference porosity (-),

f_d , f_w constants for the consideration of the convergence rate for dry (d) and wet (w) crushed salt $(f_{d,w} \leq 1)$,

V_B, V_p Brine and pore volume (m³),

S_L brine saturation in crushed salt (-)

Based on above given formulations the porosity may reach to limit value of 0 which is meaningless from a physical point of view. Therefore the convergence rates smaller than minimum porosity ϕ_{min} is set to zero; the same is applied for the fluid pressure greater than the lithostatic pressure. Following these considerations the convergence rate is changed as follows:

$$\dot{\varepsilon} = \begin{cases} G\,\mathrm{lg.}\ (5) & wenn \quad (\phi > \phi_{\min} \quad oder \quad p_{Fluid} < p_{Rock}) \\ 0 & wenn \quad (\phi \leq \phi_{\min} \quad oder \quad p_{Fluid} \geq p_{Rock}) \end{cases} \tag{5-23}$$

For the implementation in TOUGH2 time and porosity changes are discretised in the first order.

Table 5.2 Input parameters used in the study

Parameter	**Gorleben** /RÖH 97/	**ERAM** /JAV 97/, /JAV 98/
$\dot{\varepsilon}_0$ [a^{-1}]	-0.01	$-5\cdot10^{-5}$ ($-1\cdot10^{-4}$ bis $-1.1\cdot10^{-5}$)
P_{Rock} [MPa]	10	10,7
T_G [K]	310 (311.6)[1)]	f1(T) = 1 (isothermal calculations)
Q_1/R [K]	6500	
Q_2/R [K]	13000	
a	0.029	
ϕ_0	0,3 (0,36)	0,3
ϕ_{min}	-	0,005
M	4	4
S	4	4
f_{Red}	1	1

The input data provided by /RÖH 97/ und /JAV 97/, JAV 98/ were applied for associated simulations. The function for the reduction factor takes the various convergence rates of dry and wet crushed salt. This should be applied with caution when it is implemented to TOUGH2 for two-phase flow because there is no linear dependency between convergence rate and fluid saturation as the Eq. 5-22 implicitly denotes. Generally the effect of the humidity is very strong for saturation values up to 2%. For this reason in previous studies the calculation were performed without reduction (d.h. $f_{Red} = 1$) which means that the convergence corresponds to wet crushed salt /JAV 97/, /JAV 98/, /RÖH 97/.

As suggested and applied in previous studies a constant reduction factor of 1 is applied in the current implementation, however it is possible that the parameters f_d and f_w are smaller than 1. An experimental confirmation of the function does not exist.

Based on Eq. (5-21) and (5-23) for the time dependent porosity the convergence rate change exhibits a discontinuity on the vicinity of minimum porosity ϕ_{min}. The porosity changes for constant pressure, temperature and f_{Red} based on $\dot{\varepsilon} = \dot{\varepsilon}_0 \cdot f_3(\phi)$. On $\phi = \phi_{min} = 0{,}1$ the curve decreases stepwise as given in Figure 5-6.

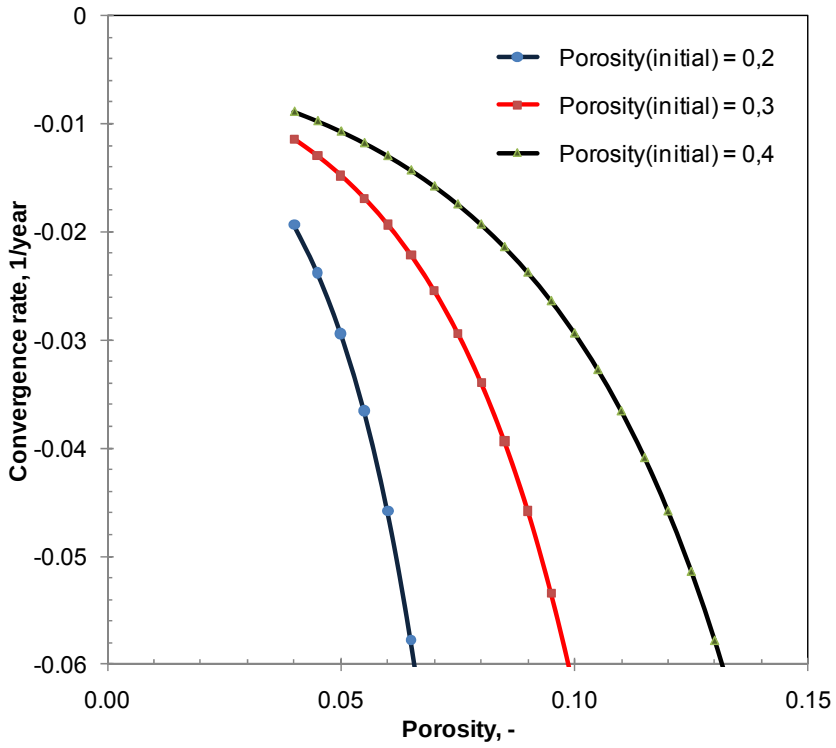

Figure 5-6 Calculated convergence rate as function of porosity

($\dot{\varepsilon} = \dot{\varepsilon}_0 \cdot f_3(\phi)$, S = 4, ϕ_{min}= 0.05, ϕ_0 = 0,5, $\dot{\varepsilon}_0$ = -0,05 a^{-1},) $f_{\mathrm{Re}\,d} = 1$

5.2.3.1 Permeability – Porosity – Capillary Pressure Relationship

TOUGH2 and its derivative TOUGHREACT provide various porosity-permeability relationships to be used in the above given convergence model. In addition to these relationships an improved form of the Kozeny-Carman relation is implemented in order to consider the effect of the pore geometry on the change of petrophysical properties better. Following type of equation is also preferred to estimate the permeability of the crushed salt and clay departing from the porosity:

$$k = A \cdot \phi^n \qquad (5\text{-}24)$$

with A and n as case specific parameters to be determined experimentally. For crushed salt determined values are given in Table 5.3. These parameters are valid for the porosities greater than 0,3 %. This relation was also implemented in the related part of the TOUGHREACT. Other porosity-permeability relationships available in TOUGHREACT can also be used to model the permeability of the buffer material.

Table 5.3 Parameters for A and n of Equation (5-24) as given in /MÜL 99/

State	log(A)	A	n	Δlog(A)	Δn
Dry	-9,885	$1{,}303 \cdot 10^{-10}$	3,841	0,217	0,151
Wet	-8,127	$7{,}464 \cdot 10^{-9}$	5,253	0,952	0,553
All	-9,561	$2{,}540 \cdot 10^{-10}$	4,175	0,251	0,166

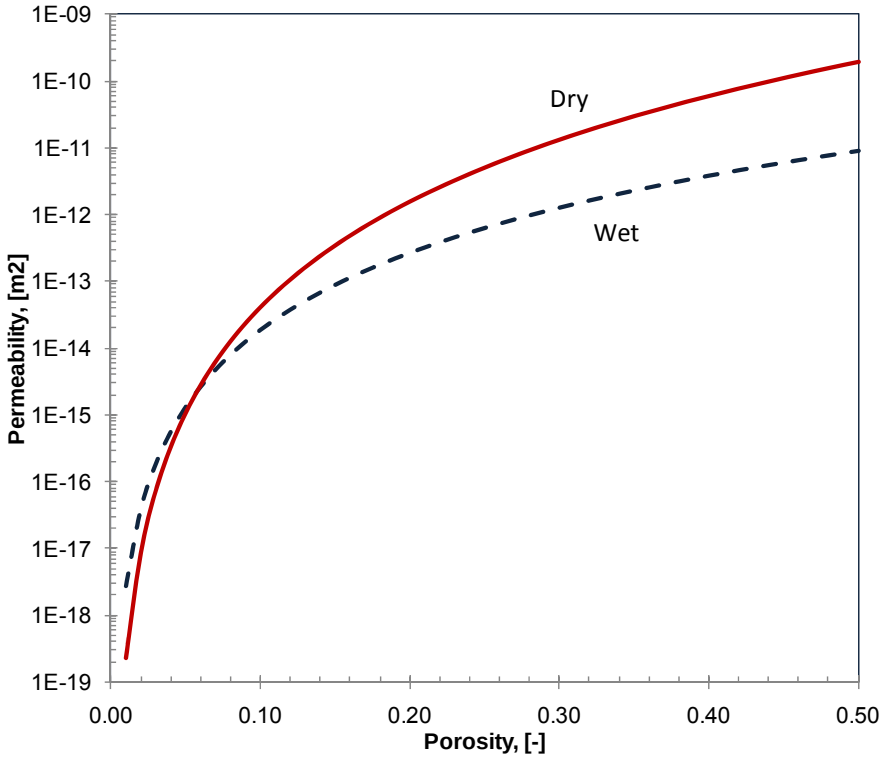

Figure 5-7 k-ϕ-relationship as given in Eq. with given parameters in Table 5.3

The values given in Table for wet crushed salt are valid for a wet content of 0,04 up to 0,1 in wgt. Therefore these values are suggested for wet crushed salts.

Capillary Pressure $P_c(S_W, \phi, k)$

In the case of two-phase flow the change in porosity and permeability would also change the capillary pressure which is expected to affect the transport behavior considerably. To take this variation into account in TOUGHREACT the dimensionless expression of /LEV 41/ could be basically used:

$$J(S_W) = p_c(S_W) \cdot \frac{\sqrt{k/\phi}}{\gamma \cos\theta} \qquad (5\text{-}25)$$

This equation gives the dependency of the capillary pressure to the saturation $p_c(S_W)$ for constant porosity and permeability. In the equation γ is the surface tension and θ is the wettability angle. This capillary pressure function is due to a capillary network or in a porous me-

dium with the same type and it does not depend on the fluid. The applicability of the Leverett-Function for rocks of various types of rock was tested for different porosity and permeabilities with success. /BRO 51/. The capillary pressure can be defined based on e.g. according to Corey-Brooks /BRO 64/ or Van Genuchten /GEN 80/.

If the porosity, permeability and the capillary function for these values are experimentally known, the capillary function for different porosity and therefore permeability values can be calculated with the following equation with the condition that the surface tension and wettability remain the same:

$$p_c(S_W, k, \phi) = p_c(S_W, k_0, \phi_0) \cdot \sqrt{\frac{k_0}{\phi_0} \cdot \frac{\phi}{k}} \qquad (5\text{-}26)$$

The application and validity interval of the Leverett Function for the repository conditions were tested in /LOR 99/ For this purpose the above given Eq. is transformed into the following with inserting the related porosity-permeability relationship:

$$p_c(S_W, k, \phi) = p_c(S_W, k_0, \phi_0) \cdot A^{-\frac{1}{2n}} \cdot \sqrt{\frac{k_0}{\phi_0}} \cdot k^{\left(\frac{1}{2n} - \frac{1}{2}\right)} \qquad (5\text{-}27)$$

With the values for n given in Table 5.3 for the exponents of k one obtains the values of the Table 5.4.

Table 5.4 Exponents (1/2n-1/2) in Eq.(5-27) for various values of n

Value n	**Exponent (1/(2n)-1/2) in Eq.(18)**
3.841 (dry crushed salt)[1)]	-0.3698
5.253 (wet crushed salt) [1)]	-0.4048
4.175 (all) [1)]	-0.3802

[1)] Value for n from Table 5.3 for crushed salt

After /DAV 95/, for the salt formations of WIPP an average value of exponents for „consolidated lithologies“ with an exponent for k of –0.346 can be applied (the range is between –0.336 bis –0.369). The difference for the suggested values for wet crushed salt reaches 15% in numerical simulations. Therefore the applicability of the Leverett Function on crushed salt is verified with an acceptable level of reliability.

5.2.4 Implementation

For very low porosities ($\phi \rightarrow 0$), the capillary pressure may have very high values. These values can be accounted as physically plausible however the application on the numerical

values is not practicable. In such form the salt can be commented as impermeable because the required capillary pressure remains above the formation pressure. Because of this for the implementation in TOUGH2 a maximum capillary pressure is allowed so that for the capillary pressure dependency the following relationship would be valid:

$$p_c(S_W, k, \phi) = \begin{cases} G\,\text{lg.} \quad (17) & wenn \quad p_c \le p_{c,\max} \\ p_{c,\max} & wenn \quad p_c > p_{c,\max} \end{cases} \qquad (5\text{-}28)$$

TOUGH2/TOUGHREACT allows the selection and use of various capillary pressure curves for constant porosity and permeability. The implementation of the variable capillary pressure TOUGH2 allows optional dependency fort he capillary curves p_c = f(S_w) for constant porosity and permeability /PRU 87/.

To implement the above mentioned compaction calculation method, two separate subroutines (Compac.f and Conver.f) were created and implemented in TOUGHREACT. A common block including all necessary parameters was included in TOUGHREACT. The related data were changed by introducing subroutines (Indata and out) to read and write the input and output parameters. The structure of the improvements are schematically shown in Table 5.5

Table 5.5 Structural changes performed in TOUGHREACT for the implementation of convergence

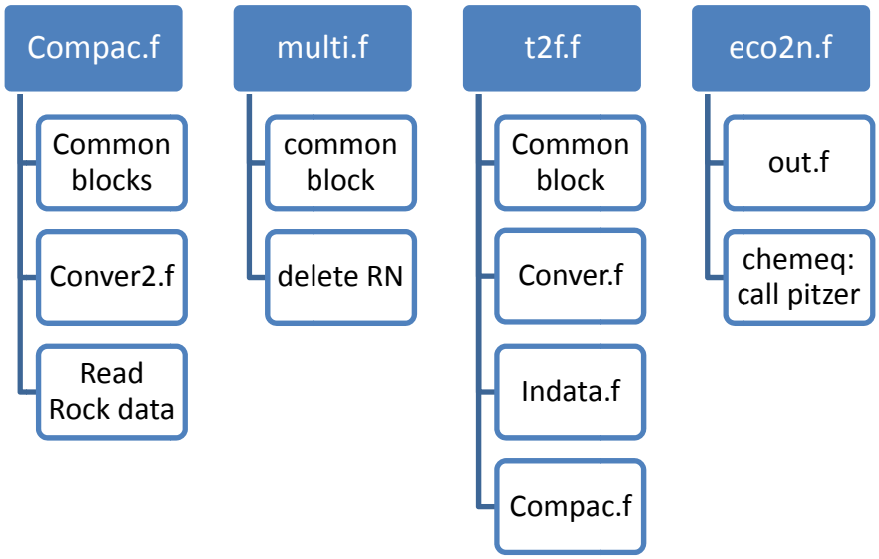

5.2.5 Validation

As the validation of the method is previously in /LOR 99/ performed, the only validation effort remained as the revisitation and the investigation of these validation tests.

5.3 Swelling

5.3.1 Background

The function of buffer material is to create lower permeability zone around the containers to isolate the containers. The buffer material can be produced by pre-compacting bentonite and (or) sand–bentonite mixtures in a plant and inserted into the space between the containers and host rock. The swelling characteristics of the buffer material are expected to result in the filling of the spaces mentioned above and the generation of a better seal around high-level radioactive wastes. For the corresponding characteristics such as dry density, sand–bentonite mass ratio, and dimensions, of buffer material from the viewpoint of self-sealing, the swelling characteristics of compacted bentonite and sand–bentonite mixtures must be evaluated quantitatively.

A good thermophysical description of the swelling of the clay buffers is given in /TRI 04/. Clay particles carry negative charges at their surfaces due to the isomorphous substitution in the crystal lattice. Exchangeable cations in the clay media are attracted to these negative charges. In a clay–water electrolyte system, the adsorbed cations near the surface of the clay particles produce a much higher concentration as compared with the ion concentration in solution away from the surfaces. Because of the difference in ion concentration in solution near the surfaces and away from the surfaces of the clay particles, the cations near the surfaces of the particles try to diffuse away to equalize the concentration throughout. Their tendency to do so, however, is opposed by the negative electric field originating in the particle surfaces. The tendency of the ions to diffuse away and the opposing electrostatic attraction lead to ion distribution adjacent to a clay particle in suspension. The charged clay surface and the distributed charge in the adjacent phase are together termed the diffuse double layer.

Volume change in clays is due to the clay–water–cation interaction. The Gouy–Chapman diffuse double layer theory has been the most widely used approach to relate clay compressibility to basic particle–water–cation interaction. According to this theory, the interaction force between two double layers depends on the ion concentration at the mid plane between two adjacent parallel clay platelets and is given by the osmotic pressure in that plane. Therefore, for any given separation distance between two clay platelets the osmotic pressure can be determined from the theory by knowing the concentration of the ions in the central plane between the platelets. Similarly, for any given osmotic pressure and known concentration of the ions in the central plane between two clay platelets, the separation distance between the clay platelets can be determined from the theory.

Many researchers have attempted to use the Gouy–Chapman diffuse double layer theory for determining the swelling pressure of clays /YON 92/ /SRI 02/. It is pointed out that some differences between experimental data and relationships derived theoretically from the diffuse double layer theory. There is not much evidence in the literature, however, showing the differences between the experimental and theoretical swelling pressures for the case of compacted clays. The difference between the theoretical and experimental results was attributed to many factors: (i) poorly developed or partially developed diffuse double layer, (ii) deviation of soil structure and fabric from the parallel plate concept, (iii) surface hydration forces at close particle distances, (iv) direct mechanical effect of water in tension, (v) non-uniform size

of clay plates, (*vi*) existence of electrical attractive forces, (*vii*) presence of multivalent cations, (*viii*) effect of ion size, (*ix*) anion adsorption, (*x*) particle size, and (*xi*) expulsion of diffuse double layer water in the case of application of high compressive stresses. One of these factors or a combination of several of these factors may contribute to the difference between the theoretical and experimental results depending on the initial stress state of clay. The diffuse double layer can be expected to be completely developed for clays at their slurry state. In /BOL 56/ it was suggested, however, that even for slurried clays the structure and fabric deviate slightly from those of the parallel plate concept, at least during the first compression stage.

In the case of compacted clays, the initial water saturation influences the swelling pressure. For dry compacted clay, the hydration of ions near the surfaces of the clay particles may contribute significantly to volume change. The swelling of clays due to hydration of ions is governed by the crystalline swelling resulting from the sorption forces and is associated with the matrix potential. For a compacted clay with an amount of water but still unsaturated, however, the swelling upon wetting is a result of the repulsive forces developed between adjacent clay particles and can be determined from the diffuse double layer theory. The swelling of clays due to interlayer or interlamellar swelling occurs beyond the crystalline swelling and stems from the interactions described by the osmotic potential. Various approaches have been proposed in the past for determining the swelling pressure of clays to overcome some of the factors that have not been considered in the original Gouy–Chapman diffuse double layer theory. The limited swelling of Ca-montmorillonite and the behaviour of highly compacted clays cannot be explained by the theory, however. Low and Margheim suggested an empirical exponential relationship between dry density and swelling pressure for Na-montmorillonite clays /LOW 79/. Sridharan and Choudhury (2002) proposed a swelling-pressure equation for Na-montmorillonite while analysing the compression data of slurried samples of Na-montmorillonite /SRI 02/.

An attempt was made by Komine and Ogata (1996) to use the diffuse double layer theory for determining the swelling strain and swelling pressure of a highly compacted bentonite /KOM 96/. New equations were suggested based on the equations for single clay platelets. However it is stated that the use of single-platelet equations to determine mid plane potential function is valid only for large diffuse double layer thickness (e.g., slurried clays). For compacted bentonites, the double layer thickness is less, and hence the equations proposed by Komine and Ogata are not tenable.

The literature review indicates that, although the Gouy– Chapman diffuse double layer theory has been successfully utilized to explain the compressibility behaviour of slurried clays, very little information is available with regard to the use of the theory for determination of the swelling pressure of compacted clays. Also, the alternative approaches proposed by various researchers which have a theoretical background are only for homoionized clays with monovalent and bivalent cations and are not valid for clays with a mixture of several types of ions. This paper presents and discusses the determination of swelling pressure of compacted bentonites from the consideration of the Gouy–Chapman diffuse double layer theory. The reported experimental swelling pressures of several bentonites proposed for use as barrier materials in storing high level radioactive waste in many countries are considered in the study. The reported experimental swelling pressures of the bentonites and the swelling pressures de-

termined from the theory are compared, and new equations are proposed to determine the swelling pressures of the compacted bentonites which have theoretical support.

Although swelling of the bentonite is the most important parameter to be considered, a small part of the published works deals with swelling in high salinity solutions. /COL 86/ /HER 99/ /HER 06/. The most of these works considers the NaCl concentration without taking the geochemical aspects of others components into considerations. Some reports of recent GRS projects try to put this aspect of bentonite as buffer material into consideration. In /HER 02/ the role of smectite on the swelling of Bentonite is discussed. It is well known that the smectite can swell with various mechanisms even in high salinity solutions. It is affirmed that the swelling pressure is directly dependent on the Mg content of the solutions, the K content of the solution on the other hand inversely. With a constant concentration of Mg ions the swelling pressure decreases with increasing K ion concentration. On the other hand it is also determined that the compacted bentonite behaves like a semi-impermeable membrane for salt solutions by retention of considerable amount of salts. This means that the measured pressures reflect not only swelling pressures but also crystallization pressures of the salts which are dependent on the salt content of the solutions. This also means that as the result of the decreasing salt concentration of the solution results in a higher swelling.

The effect of the temperature on the swelling properties is also one of the themes which are not well understood; the results of existing studies are contradictory. Zhang et al. /ZHA 93/ report on the swelling of Montmorillonit in 10^{-4} molar NaCl solution and mention that the distance oft he interlayers decreases with increasing temperature. A conflicting result is affirmed by /COL 86/ for up to 5 molar NaCl solutions with no significant changes with increasing temperature. Bucher et al. /BUC 89/ studied the swelling pressures of bentonit-iron mixtures at room temperature, 80 °C and 150 °C in low salinity solutions. It is reported that 5 of 6 tests resulted in lower swelling pressures with increasing temperatures.

It is well known that salt solutions reduces the swelling capacity of bentonite and no swelling pressure will obviously develop if the capacity is reduced to an extent where the actual volume is not filled by the maximum swollen clay. Thermodynamic models to predict the swelling behavior match with laboratory data well with laboratory data. However for very high salt content solutions a conservative use of the thermodynamic models predict a total loss of swelling pressures which is not in accordance with laboratory results /KAR 98/.

The swelling-pressure determination is an important aspect of all high-level radioactive waste disposal projects and the swelling properties of bentonite and sand–bentonite mixtures have been reported in various publications /OSC 90/, /PUS 82/; /KEN 92/, /DIX 96/, /KOM 99/, /ZHA 04/. The swelling-pressure tests have been conducted for the confined situation, where volume of the specimen was held constant. Models of the swelling characteristics of bentonite were also proposed. A simplified model of the swelling characteristics and a new parameter (swelling volumetric strain of montmorillonite), which were able to evaluate the swelling characteristics of compacted bentonite, were proposed by /KOM 94/. A double porosity model, which is believed to be especially relevant when simulating expansive soils, is proposed to characterize the water transfer mechanism /NAV 00/. Another relevant feature of the framework developed is the incorporation of a consistent elastoplastic model to describe stress-strain relationships in unsaturated soils. In a recent study, the isolated aggregates of raw and cation exchanged bentonite were directly observed at different relative humidity in

an ESEM chamber /MON 05/. A visual evaluation of these observations allows for the calculation of the swelling–shrinkage potential (%) of bentonite taking the geochemical transformations including cation exchange into account. Finally, a kinetic model of first order was tested to fit the kinetic experimental data of swelling–shrinkage potential.

In /HER 06/ the results of experimental studies on the effect of the salinity on swelling capacity of bentonites are reported. This can be summarized as follows:

- Bentonites have a certain swelling capacity even in contact with brines. The resulting swelling pressures are in general rather low. They do not exceed 10 bars. The relative standard deviation is up to 50 %.
- Swelling pressures are strongly dependent on the raw density. Between 1,55 and 1,7 g/cm³ the increase is flat and gets steep between 1,7 and 1,8 g/cm³. A maximum pressure of 50 bars was reached at a density of 1,8 g/cm³. With increasing compaction, the scatter of the results increases.
- The differences between swelling pressures with different brine compositions are less than expected.
- The most reliable swelling pressure values were obtained for MX-80 bentonite of 1,6 g/cm³ raw density with NaCl solution and IP21 solution. The swelling pressures with these two solutions are very similar in spite of their large difference in chemical composition. 11 bars were recorded with bentonite IP21 and 10 bars with NaCl solution.
- However, small but systematic differences were measured with different brines of the six-component-system Na-K-Ca-Mg-Cl-SO_4. The swelling pressures increased with increasing Mg content of the solutions. K in solutions decreases the swelling pressure. In order to estimate the swelling pressure with given brine, the K/Mg ratio is more important than the K content of the solution. High K/Mg ratios lead to low swelling pressures and vice versa.
- A short-term contact of bentonites with high pH brines has no significant impact on swelling pressures compared to those with brines of intermediate pH. But as high pH brines induce mineralogical changes in the bentonites giving rise to a decrease in water uptake capacity, reduced swelling pressures after longer reaction times are to be expected. Higher temperatures lead to higher swelling pressures. MX-80 of 1.6 g/cm³ raw density with IP21 solution develops 11 bars swelling pressure at room temperature, 18 bars at 70 °C and 20 bars at 75 °C. Also at higher temperatures the swelling pressures with NaCl and IP21 solution are very similar, but always the pressure with IP21 is slightly higher.
- Sample size and geometry do not seem to influence the swelling pressure.
- The measured swelling pressures are not pure swelling pressures but a combination of real swelling pressure and crystallization pressure. It is not clear which part of the total pressure is higher. The crystallization pressure is due to the water uptake of the Bentonite. This leads to an over-saturation of the brine and the crystallization of large amounts of salt minerals in the pore space of the compacted Bentonite.

Some problems encountered in the experiments are also reported. The reproducibility of the measurements is not satisfying. The scatter is too high for the intended correlation between swelling pressure and chemical composition of brines. A mathematical model could not be established. Only a complete and homogeneous flooding, i.e. the full saturation of the pore

space leads to the maximum swelling of the compacted Bentonite with a given brine composition. The full saturation of the pore space was reached only in a few experiments. This explains part of the scatter of the measured values. It must be pointed out however that no other method guarantees better results. Furthermore the boundary conditions during the construction of large scale dam in-situ are less well defined than in our laboratory experiments. Therefore the uncertainties recorded in this project must be taken into account for practical purposes. The multitude of measurements performed in this project has rendered results with high practical value:

- Bentonites are swelling even in contact with high saline brines. Compacted bentonites may thus be used as sealing materials in salt formations. The resulting swelling pressures, however, are rather low. A successful sealing with compacted bentonites can not be guaranteed. In 30 % of the laboratory experiments, no self sealing was reached when the fluid pressure exceeded the swelling pressure. The order of magnitude of the swelling pressures which can be expected in salt formations is known and reliable.
- The differences of swelling pressures with different brines are very low. For practical purposes a mathematical model for the prediction of these small differences is not needed.
- Calcigel is more predictable than MX-80.

A correlation is proposed to estimate the effect of the brine salinity on swelling pressures /HER 06/:

$$\ln P_s = A\frac{m_{Na}}{m_K} + B\frac{m_{Na}}{m_{EA}} + C\frac{m_K}{m_{EA}} + D\rho_{red} + Ew \qquad (5\text{-}29)$$

Where mi is the molarity of the species in the solution (EA=Earth alkali metals, $m_{EA}=m_{Mg}+m_{Ca}$), ρ_{red}=dry density, w=water content total and E and A regressed parameters.

Several mechanisms are considered to possibly change the long-term properties and thus degrade the isolation properties of the bentonite buffer. The first one is the oxidation mechanism. Atmospheric oxygen entrapped in the deposition hole during the excavation of the repository is small and will either be depleted by reaction with the reducing components in the near field, or escape by mass transport, mainly diffusion. Radiolytically generated oxidants can however last for a longer time and possibly react with (oxidize) the pyrite and the organics in the bentonite either directly, or by first oxidizing uranitite in the spent fuel to release hexa-valent uranium as oxidant. The radiolytically generated oxidant will not be released until the canister is damaged. Even under rigorous quality control of canisters a small probability by manufacturing such as defect welding, a small hole or a crack in the canister wall may end with escaping of the oxidant generated by water radiolysis.

Another mechanism that affects the long-term properties of bentonite is the alteration to other minerals. Montmorillonite in the bentonite buffer can be converted to non-expanding hydrous mica (typically illite). This conversions result in a considerable decrease in swelling pressure and stiffness and an increase in the permeability. The alteration due to dissolution likely occurs in a final repository.

The third mechanism is the ion-exchange mechanism. The bentonite used in the buffer material will be Na-bentonite. Sodium cations incorporated in the interlamellar sites of montmorillonite can be replaced by calcium cations through cation-exchange. Some investigations showed that this mechanism does not significantly alter the physical properties of smectite buffer high density. In some projects however, the ion exchange of sodium for calcium is considered to be probably the most important chemical alteration of the bentonite buffer, resulting in a loss of plasticity and to a limited extent, of swelling ability.

5.3.2 Implementation

5.3.2.1 Model

Several methods are published to model the swelling behaviour of the bentonit or bentonite-sand mixtures to be used as backfill material in geological repositories. A prediction method dealing with the influences of pore-water chemistry and temperature that can be applied to the swelling characteristics of compacted bentonite only was presented by Komine and Ogata /KOM 96/. However, it is difficult to apply this method to the sand–bentonite mixtures because it does not consider the influences of the mass ratio of sand and bentonite. A new method for predicting the swelling characteristics, which can apply to the sand–bentonite mixtures and can evaluate the effects of exchangeable-cation compositions in detail, is therefore necessary to predict the swelling behavior of buffer material /KOM 03/. This methodology is selected in this project to model the swelling of bentonite because it proposes the consideration of the chemical interactions which are modelled in the framework of the present project.

To evaluate the relationship between the swelling characteristics of compacted bentonite and sand–bentonite a new parameter “swelling volumetric strain of montmorillonite, ε_{sv} (%)” is proposed /KOM 99/. The authors assumed the composition of buffer material, i.e., voids, montmorillonite minerals, component minerals excluding montmorillonite, and sand as given in Figure 5-8. The new parameter ε_{SV} is the percentage volume increase of swelling deformation of montmorillonite when dry and is defined by:

$$\varepsilon_{SV} = \frac{V_v + V_{sw}}{V_m} \qquad (5\text{-}30)$$

where V_m is the volume of montmorillonite in the buffer material, V_v is the volume of voids shown in Figure 5-8 in the buffer material, and V_{sw} is the maximum swelling deformation of the buffer material at constant vertical pressure ($V_{sw}\,\varepsilon\,0$).

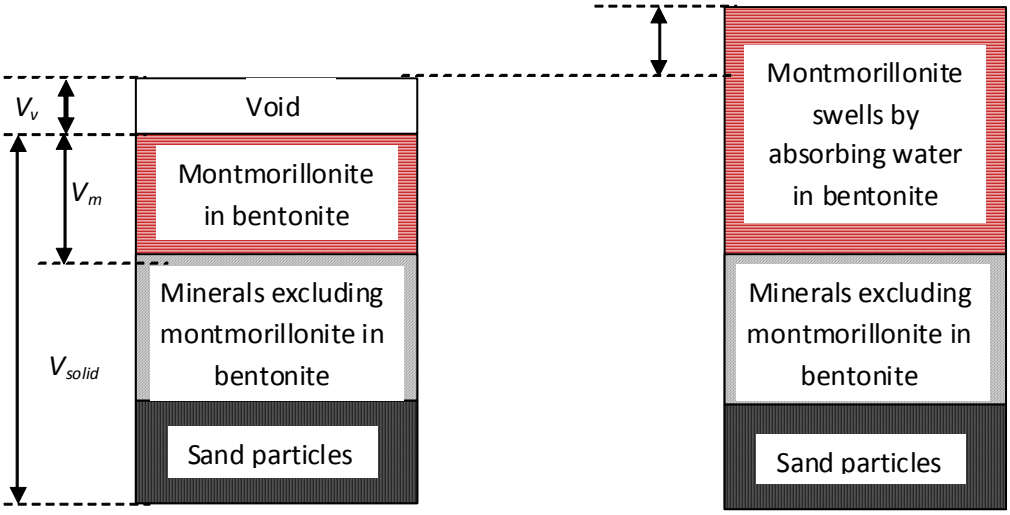

Figure 5-8 Schematized swelling behavior of bentonite in the bentonite-buffer material (bentonite content 50%) /KOM 03/.

From the observed results in SEM (scanning electron microscope), it was found that the voids in the material were completely filled by swelling deformations of bentonite absorbing water. The swelling processes of buffer material are described as shown in Figure 5-8. Equation (5-31) of the parameter ε_{sv}* are obtained by expanding previous attempts on swelling processes.

$$\varepsilon_{sv} = \left[e_0 + \frac{\varepsilon_{s\max}}{100}(e_0+1) \right] x \left[1 + \left(\frac{100}{C_m} - 1 \right) \frac{\rho_m}{\rho_{nm}} + \left(\frac{100}{\alpha} - 1 \right) \frac{100}{C_m} \frac{\rho_m}{\rho_{sand}} \right] x 100$$

$$e_0 = \frac{\rho_{solid}}{\rho_{d0}} - 1 \qquad (5\text{-}31)$$

$$\rho_{solid} = \frac{\frac{100}{C_m}\frac{100}{\alpha}\rho_m}{\left[1 + \left(\frac{100}{C_m} - 1 \right) \frac{\rho_m}{\rho_{nm}} + \left(\frac{100}{\alpha} - 1 \right) \frac{100}{C_m} \frac{\rho_m}{\rho_{sand}} \right]} \qquad (5\text{-}32)$$

where $\sum_{smax}$ is the maximum swelling strain (%) of buffer material, e_0 is the initial void ratio of the materials, C_m is the content (%) of montmorillonite in the bentonite by percentage mass, ρ_{d0} is the initial dry density (Mg/m³) of the materials, α is the content (%) of bentonite in the materials by percentage mass, ρ_m is the particle density (Mg/m³) of montmorillonite, ρ_{nm} is the particle density (Mg/m³) of component minerals excluding montmorillonite in the bentonite and $\sum_{sand}$ is the particle density (Mg/m³) of sand in the materials. The parameter $\sum_{sv}$* can also be evaluated from the swelling deformation of a montmorillonite mineral. A model-simulated deformation of a montmorillonite mineral was produced, and an equation was proposed for evaluating the relationship between the parameter $\sum_{sv}$* and the distance $2d$ between two parallel montmorillonite layers /KOM 96/. The study proposed the model of montmorillonite

mineral shown in Figure 5-9 on the basis of the structure of montmorillonite mineral. When the montmorillonite mineral is in an absolute dry condition with no water between each interlayer, the distance between two parallel montmorillonite layers is considered to be equal to the nonhydrated diameter of the exchangeable cations that exists between two layers. Thus, the structure of a montmorillonite mineral can be modelled as shown in Figure 5-9 when there is no water between each interlayer. The structure of a montmorillonite mineral after swelling can be modelled as shown in Figure 5-9. Therefore, the relationship between $\sum_{sv}$* and d can be evaluated by Eq. (5-33) which can be derived from the thickness increment of a montmorillonite mineral when the distance between each interlayer is 2d as shown in Fig. 5b.

$$d = \frac{\varepsilon_{sv}}{100}(t + R_{ion}) + R_{ion} \tag{5-33}$$

where d is half the distance between two parallel montmorillonite layers (m), t is the thickness of the montmorillonite layer (m), and R_{ion} is the nonhydrated radius of exchangeable cations between two layers (m). Equations (5-31)–(5-33) can be used to evaluate the relationship between the maximum swelling strain of buffer material and half the distance between two parallel montmorillonite layers through the intermediary of the parameter $\sum_{sv}$* .

The theories of repulsive and attractive forces between two parallel montmorillonite layers are expanded to consider the influence of the exchangeable-cation composition of bentonite. A montmorillonite mineral expands by absorbing water in the interlayers. The swelling pressure and deformation of bentonite containing montmorillonite minerals are considered to be caused by the repulsive forces occurring between the two layers. The Gouy–Chapman theory of the diffuse double layer says the repulsive pressure between two parallel montmorillonite layers can be calculated from the following equations:

$$f_r = 2nkT(\cosh\ u - 1)x10^{-3} \tag{5-34}$$

$$u = 8\tanh^{-1}\left[\exp(-\kappa d)\tanh\left(\frac{z}{4}\right)\right] \tag{5-35}$$

$$\kappa = \sqrt{\frac{2nv^2e^2}{\varepsilon\ k\ T}} \tag{5-36}$$

$$\varepsilon_s = \frac{H_1 - H_0}{H_0} = \frac{d - R_{ion}}{t + R_{ion}}.100 \tag{5-37}$$

$$z = 2\sinh^{-1}\left(96{,}5\frac{CEC}{S}\sqrt{\frac{1}{8\varepsilon kT}}\right) \tag{5-38}$$

where f_r is the repulsive pressure (kPa) between two parallel montmorillonite layers, montmorillonite layers, v is the ionic valence, e' is the electronic charge (C), k is the Boltzmann constant (J/K), T is the absolute temperature (K), n is the ion concentration in pore water (number/m^3), ε is the static permittivity of pore water, CEC is the cation exchange capacity (mequiv./g) of bentonite, S is the specific surface (m^2/g) of bentonite, and κ is the double-

layer parameter (m^{-1}). The constant, 96.5 (C/mequiv.) in eq. [6*d*] is used to convert the unit (C) from the unit (mequiv.). It is well-known that attractive forces act between two layers if they come extremely close to each other. London's theory for attractive energy between a pair of molecules was extended to explain the attractive energy between two parallel layers /CAS 48/. The attractive pressure known as the van der Waals forces, is given by Eq. (5-29).

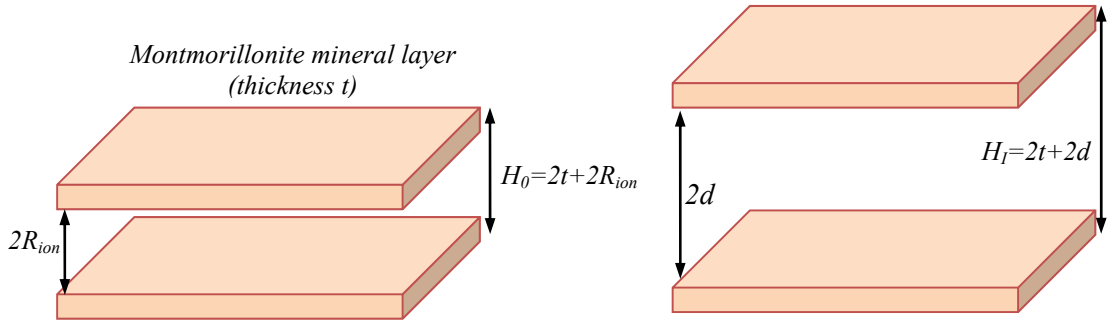

Figure 5-9 Formulation of the swelling volumetric strain of montmorillonite eSV (%) from the viewpoint of the behavior of montmorillonite mineral /KOM 03/.

$$f_a = \frac{A_h}{24\pi}\left[\frac{1}{d^3} + \frac{1}{(d+t)^3} - \frac{2}{\left(d+\frac{t}{2}\right)^3}\right] x10^{-3} \qquad (5\text{-}39)$$

where f_a is the attractive pressure (kPa) between two parallel montmorillonite layers, and A_h is the Hamaker constant (J). The above equations evaluate the relationship between half the distance between two parallel montmorillonite layers and the pressure acting between them. Some kinds of exchangeable cations exist on the surface of the montmorillonite layer. Therefore, the influence of the exchangeable-cation composition of bentonite must be considered when calculating the pressures acting between two montmorillonite layers.

In /KOM 03/ a calculation method for pressures acting between two montmorillonite layers allowing for the influence of Na^+, Ca^{2+}, K^+, and Mg^{2+}, the main exchangeable cations of bentonite is proposed. Figure 5-10 shows the concept of the calculation method described above. In this proposition, the influences of the exchangeable cations are evaluated by the weighted average of repulsive and attractive pressures caused by Na^+, Ca^{2+}, K^+, and Mg^{2+}, using the exchange capacities of each ion. Therefore Eqs. (5-40)–(5-43) are derived by expanding Eqs. (5-37) to (5-39).

$$p = \frac{1}{CEC}\sum_{i=Na^+,Ca^{2+},K^+,Mg^{2+}}\{EXC_i[(f_r)_i - (f_a)_i\} \qquad (5\text{-}40)$$

$$(f_r)_i = 2nkT(\cosh u_i - 1)x10^{-3} \qquad (5\text{-}41)$$

$$u_i = 8\tanh^{-1}\left[\exp(-\kappa_i d_i)\tanh\left(\frac{z_i}{4}\right)\right] \tag{5-42}$$

$$\kappa_i = \sqrt{\frac{2nv_{i^2}^2 e^2}{\varepsilon\, k\, T}} \quad z_i = 2\sinh^{-1}\left(96{,}5\frac{EXC_i}{S}\sqrt{\frac{1}{8\varepsilon kT}}\right) \tag{5-43}$$

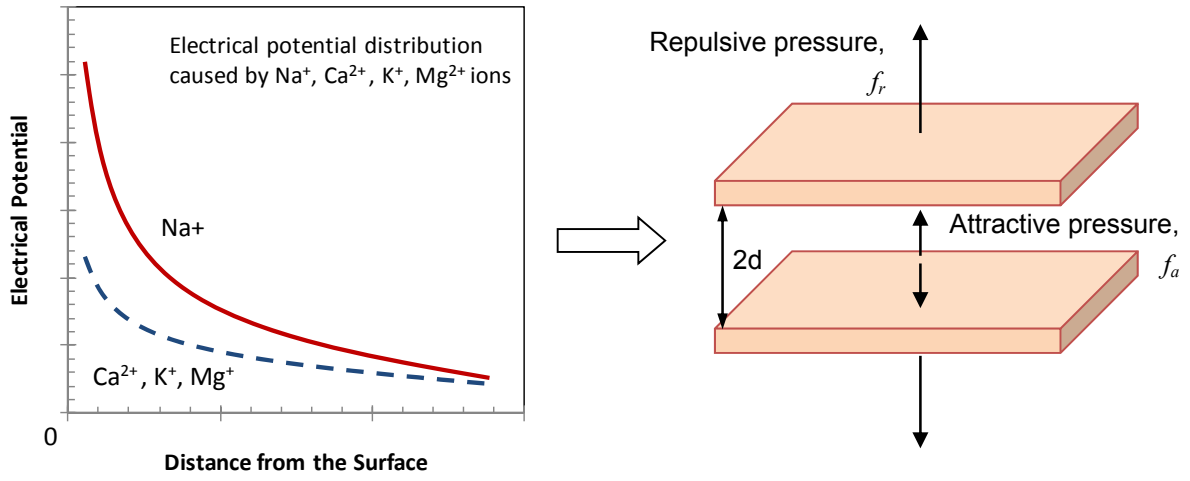

Figure 5-10 Schematized description of new calculation Method for pressure acting two montmorillonite layers

$$(f_a)_i = \frac{A_n}{24\pi}\left[\frac{1}{d_i^3} + \frac{1}{(d_i + t)^3} - \frac{2}{\left(d_i + \frac{t}{2}\right)^3}\right] x10^{-3} \tag{5-44}$$

where p is the pressure of the buffer material (repulsion: positive), $(f_r)_i$ is the repulsive pressure between two parallel montmorillonite layers that is caused by the exchangeable cation i (i denotes either Na_+, Ca_{2+}, K_+, or Mg_{2+}), $(f_a)_i$ is the attractive pressure between two parallel montmorillonite layers that is caused by the exchangeable cation i, $|_i$ is the double- layer parameter (m^{-1}) of the exchangeable cation i; EXC_i is the exchange capacity of i (mequiv./g), and $\}_i$ is the ionic valence of the exchangeable cation i. Following the above discussions, Eq. (5-45) is developed to allow for the influence of the exchangeable cation of bentonite.

The expanded equation is as follows:

$$d_i = \frac{\varepsilon_{sv}}{100}\{(t + R_{ion})_i\} + (R_{ion})_i \tag{5-45}$$

where d_i is the half distance between two montmorillonite layers (m) at the exchangeable cation i, and $(R_{ion})_i$ is the nonhydrated radius of the exchangeable cation i (m).

It is known that both the ion concentration of pore water and the specific surface of bentonite significantly influence the swelling characteristics of soils. Equations for evaluating the influences of pore-water chemistry and the specific surface of bentonite are needed, in addition to the preceding equations, to predict the swelling behavior of buffer material. Additional equations for evaluating the influences of pore-water chemistry and the specific surface of bentonite are proposed by /KOM 99/. The concentration of ions in pore water is thought to be dependent on the number of montmorillonite minerals per unit volume of pore water. The concentration of ions in pore water is constant provided the number of montmorillonite minerals per unit volume of pore water is unchanged; hence the concentration decreases as the volume of montmorillonite mineral increases with water absorption. Following equation can be used the actual ion concentration in pore water n:

$$n = \frac{n_0 N_A}{1 + \frac{\varepsilon_{sv}}{100}} \tag{5-46}$$

where N_A is Avogadro's number, and n_0 is the ion concentration (mol/m3) in pore water. The specific surface of bentonite S in Eq. (5-43) is evaluated from the composition of bentonite with the following equation as given in Figure 5-11:

$$S = \frac{C_m}{100} S_m + \left(1 - \frac{C_m}{100}\right) S_{nm} \tag{5-47}$$

where S_m is the specific surface (m^2/g) of montmorillonite, and S_{nm} is the specific surface (m^2/g) of component minerals excluding montmorillonite in the bentonite. Figure 5-12 shows an example of the flow chart used to predict the swelling characteristics of buffer material. The proposed method of prediction is founded on (*i*) the swelling models shown in Figure 5-8; (*ii*) the theories of diffuse double layer; and (*iii*) the van der Waals forces. The swelling models shown in Figure 5-8 were proposed on the basis of the experimental results reported in /KOM 96/ /KOM 99/. These experiments measured the swelling behavior of buffer material absorbing water from air-dried material. The above given method of prediction can be applied to predict the swelling characteristics of buffer material saturated from air-dried material.

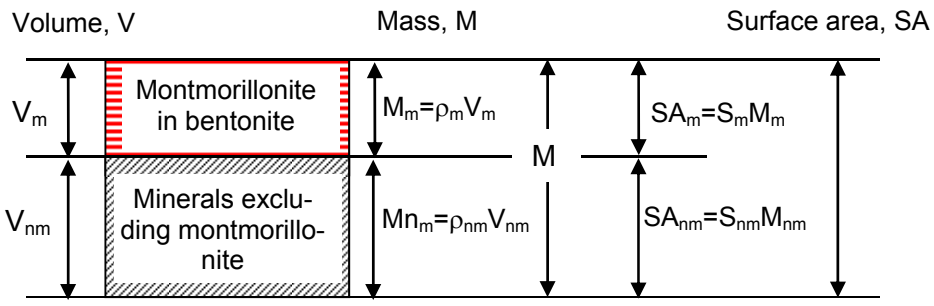

Figure 5-11 Surface area–volume–mass relationships for bentonite

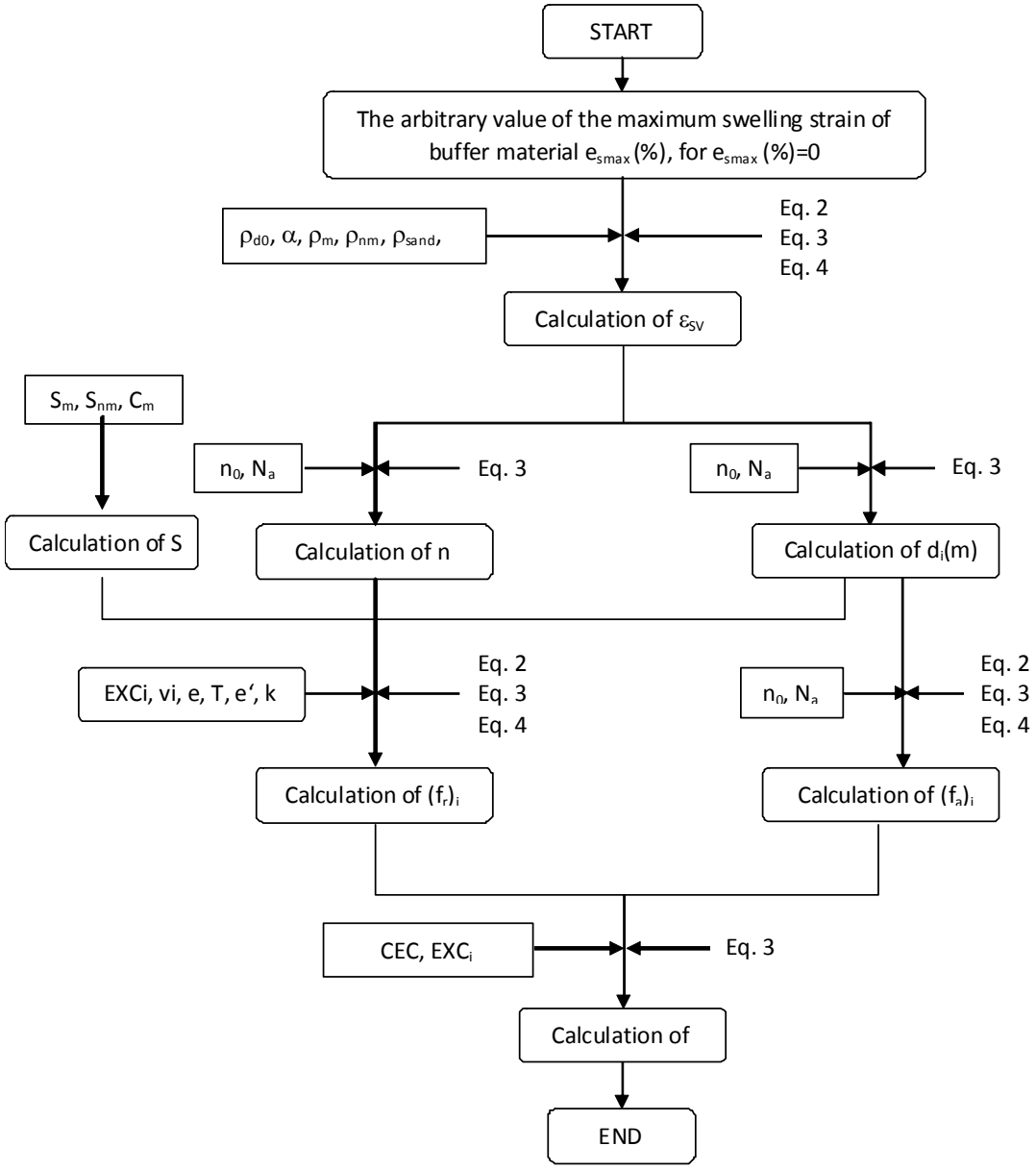

Figure 5-12 Schematic description of the implementation structure for bentonite swelling after /KOM 03/

5.3.3 Validation

The implemented model has been tested first with a Japanese bentonite as given in /KOM 03/. The first aim is to validate the programmed algorithm of the model as given in the source. Therefore instead of matching the experimental values given in /KOM 03/ the calculated values of the same references were tried to match. A second validation effort was made based on the properties of MX-80 bentonite which is used for German applications. The properties of both bentonites, Kunigel-VI and MX-80 used in the validation studies are given in Table 5.6.

Table 5.6 Typical properties of the bentonites used in validation studies.

Property	**Kunigel_VI /KOM 03/**	**MX-80 /GOM 10/**
Type	sodium	sodium
Particle density, Mg/m^3	2,79	2,81
Montmorillonite content, %	48	88
ρ_m, Mg/m^3	2,77	
ρ_{nm}, Mg/m^3	2,81	
ρ_{sand}, Mg/m^3	2,66	
S_m, m^2/g	810	750
S_{nm}, m^2/g	0	0
CEC, meq/g	0,732	0,730
EXC of Na+, meq/g	0,405	0,624
EXC of Ca2+, meq/g	0,287	0,074
EXC of K+, meq/g	0,009	0,040
EXC of Mg2+, meq/g	0,030	0,002
(R_{ion})Na+, nm	0,098	0,102
(R_{ion})Ca2+, nm	0,115	0,101
(R_{ion})K+, nm	0,133	0,130
(R_{ion})Mg2+, nm	0,083	0,072
l, m	$9{,}6.10^{-10}$	1.10^{-10}

The results of validation of efforts are given in Figure 5-13 and Figure 5-14. The match with published results of /KOM 03/ is of acceptable level. The deviation from the measured value is higher for MX-80. This can be caused by the uncertainties of the input data collected from various sources. However the deviation is of acceptable level and with this result the main part of the implementation can be accepted as validated.

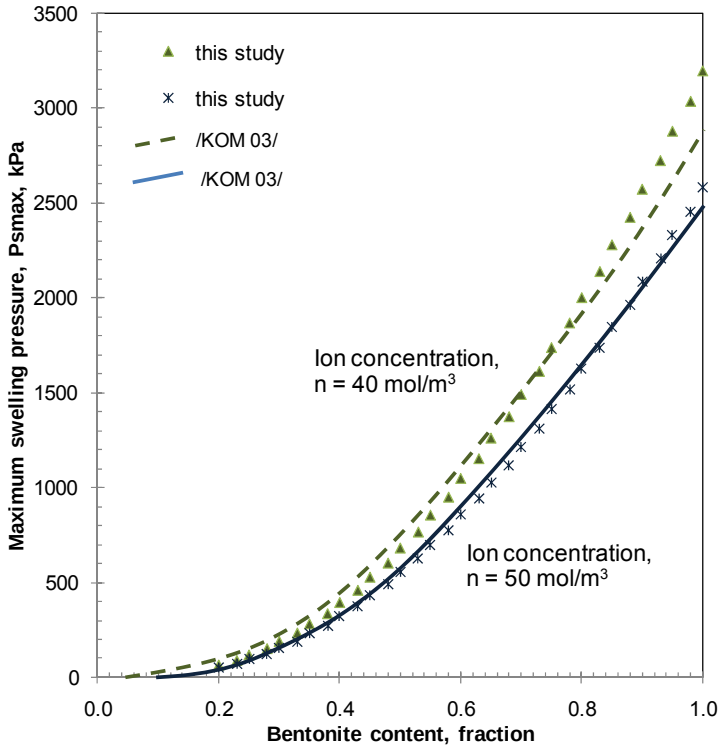

Figure 5-13 Validation runs for swelling implementation performed with the data of Kunigel VI, ρ_{di}=1,97 Mg/m3

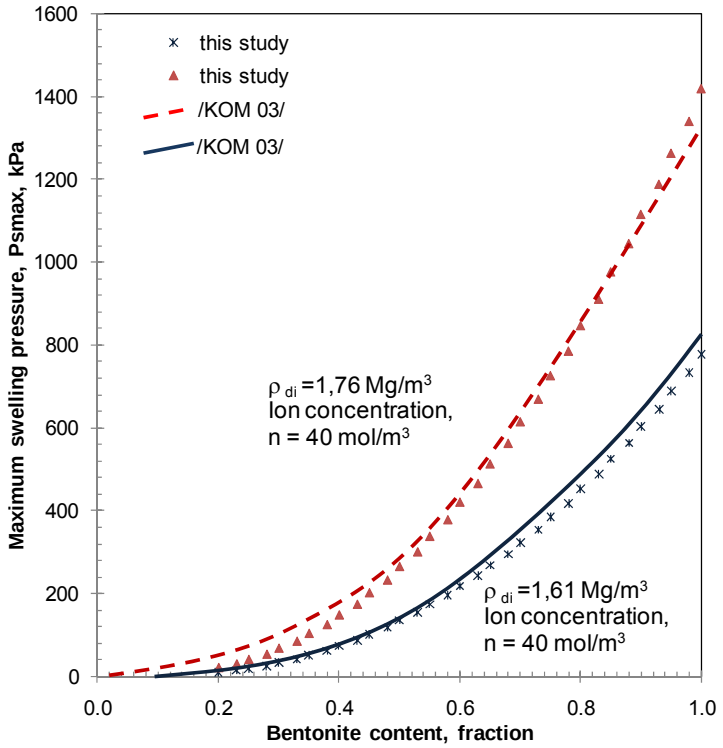

Figure 5-14 Validation runs for swelling implementation performed with the data of Kunigel VI

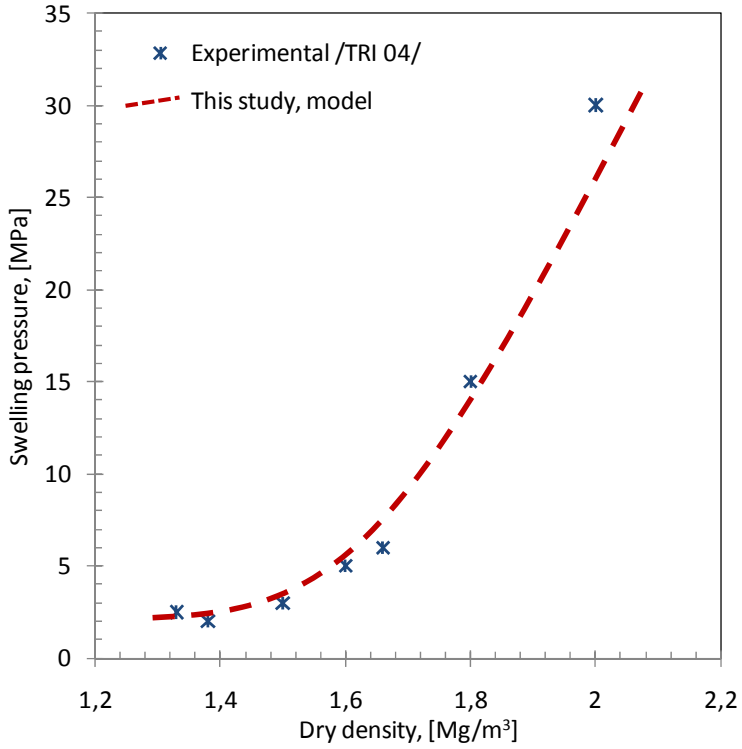

Figure 5-15 Validation runs for swelling implementation performed with the data of MX-80

6 MODELING WORK

6.1 Models; Conceptual and Numerical

Generic models for HAW as well as MAW/LAW repository in salt were created based on related studies. The properties of individual components of the system were selected due to published data with a special care to simplicity. Two concepts were considered; in the first one the HAW waste containers are emplaced in a borehole as described in Figure 6-1 and in the second one MAW/LAW are emplaced in a drift as shown in Figure 6-2.

6.1.1 Geometrical Models; Discretisation and Initialization

The borehole model was applied for salt and clay host rock separately with related components. The following dimensions were taken as basis without any up-scaling.

Related to the selected geometry the total of the borehole is divided as the active borehole of 15 m, with a distance of 2 m to the gallery to the top; an additional distance to the bottom is also considered. The distance between the containers is equal to 1,80 m assuming 6 containers disposed along the borehole. The borehole diameter consists of the container diameter and buffer material being equal to 1,75 m. The schematic description and the geometry of the borehole model as well as the cross sections of the containers with the discretisation applied in modeling are given in Figure 6-3 and Figure 6-4.

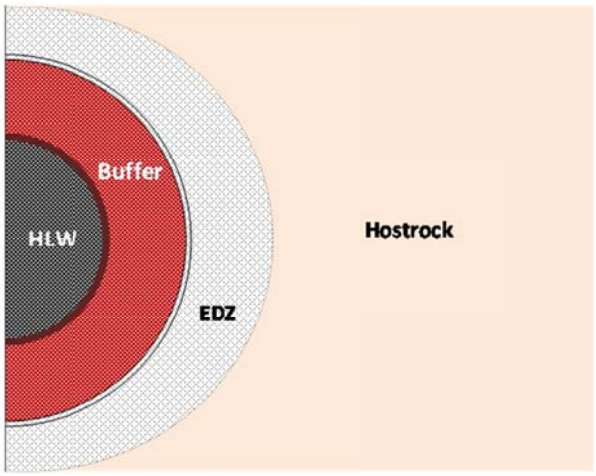

Figure 6-1 Horizontal cross section of the borehole repository concept applied in the study

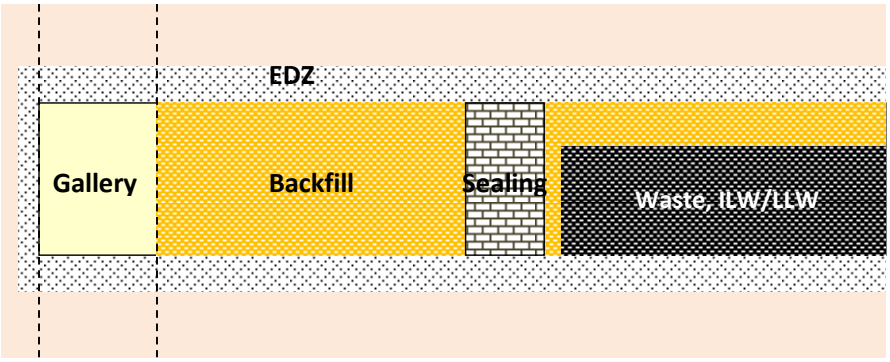

Figure 6-2 Vertical cross section of the drift repository concept applied in the study

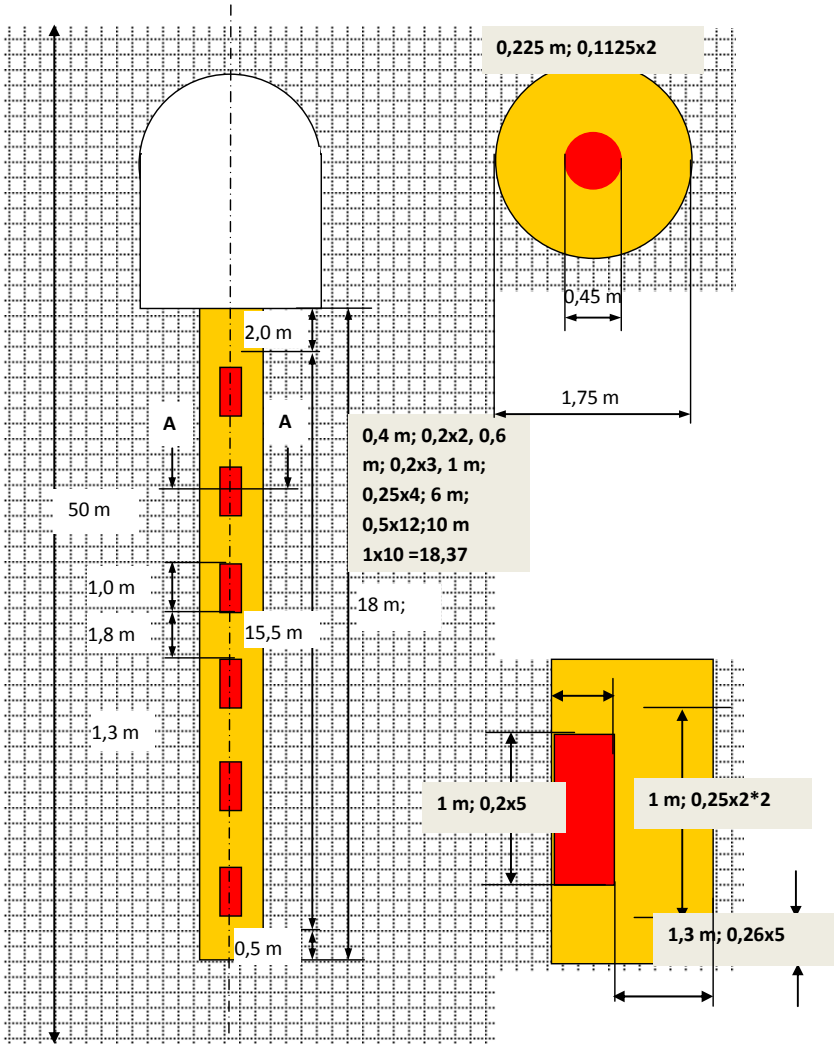

Figure 6-3 Geometry and dimensions of the borehole model applied in the study

As can be concluded from the discretisation an axisymetrical, two-dimensional model is applied. The symmetry axis is the borehole axis. This is consistent to the repository concept applied.

The model grid network consists of 38x204 blocks; this means a total of 7752 blocks is applied with various geometry in an r-z geometry. From the theoretical and practical stand point it is well known that the discretization may have a considerable effect on the reliability of the numerical computation results. This study focuses especially on the THMC behaviour of the near field therefore special emphasize was given on the selection of detail discretization around the containers therefore before the decision on the discretization was taken, some runs were performed with various gridding of the near field and the basic hydraulical parameter (temperature/pressure) were compared with each other. As the result of these sensitivity runs the final discretization was decided. The discretization given in Figure 6-4 was run for determining mainly the thermal-hydraulic-mechanical basic parameters basically. As the chemical issues requires a time consuming computation the model was reduced only to one container with encountering blocks with increasing dimensions in order to assure the boundary conditions.

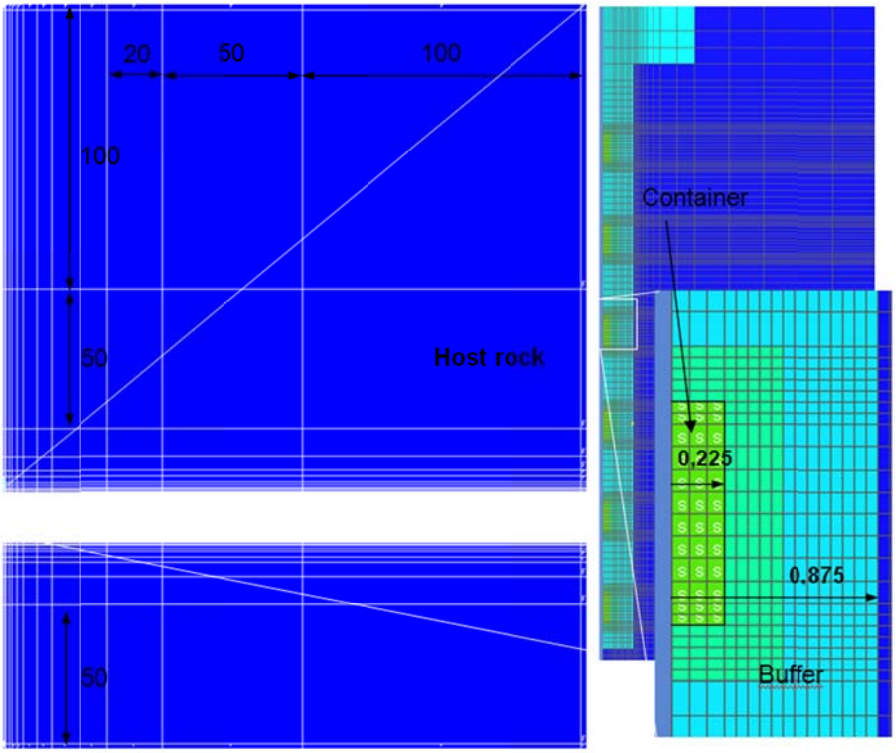

Figure 6-4 Discretization of the borehole model (units in m)

The boundary conditions were determined as „Dirichlet“. To minimize the effect of the constant boundary conditions on the calculations the block dimensions and the discretization of the model were adapted. The thermodynamic conditions were held constant in the last block with assigned smaller width. In addition, except the last blocks, the geometry of the blocks out of the finer discretization area was increased gradually up to 100 m (Figure 6-4).

Similar principles were also applied for modeling the drift repository model. A simplified rectilinear 2D grid model was used; finer discretization was applied in the near field. A total volume of 40 m^3 was assigned for backfill material, and four source terms were located in the model chamber. For the determination of the source term, a waste volume of 60 m^3 was assumed, based on a volume ratio of 0,60 for waste to total excavated volume. The schematic of the model applied is depicted in Figure 6-5.

In both models the parameters were introduced according to the cases studied.

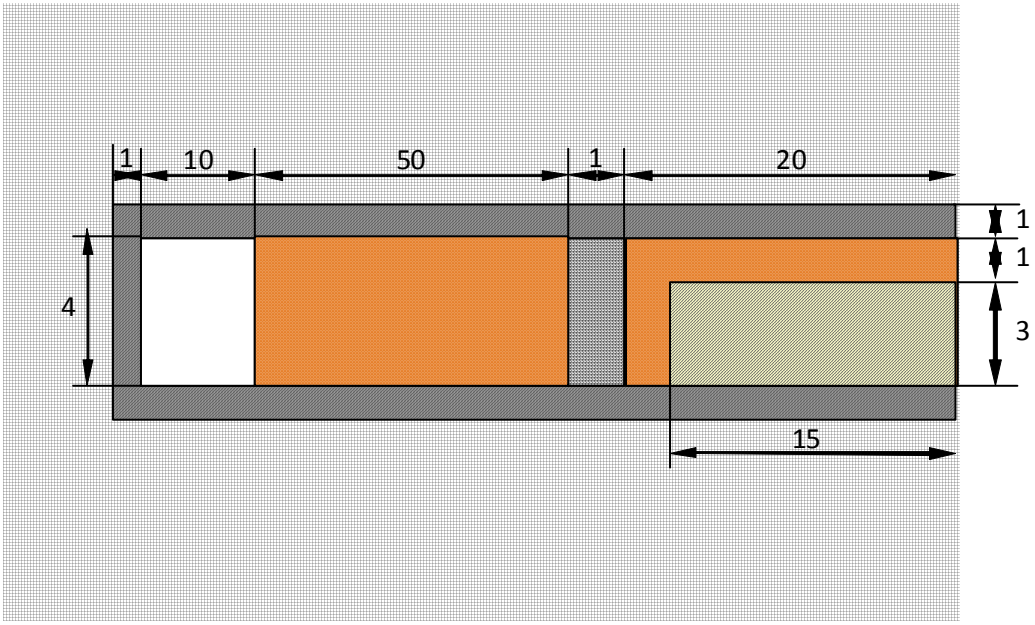

Figure 6-5 Geometry of the drift model applied in the study

6.1.2 Model Parameters

For all components of the models the physical, petrophysical, thermal and chemical parameters were introduced based on published data. They are described in the following.

6.1.2.1 Physical/Petrophysical Parameters

The physical/petrophysical parameters to be used in the model were selected according to previous studies. As buffer in clay case a bentonite-sand mixture of 75/25 is used. The initial density, porosity and permeability of this mixture were provided from /MIE 03/. To define the effect of the compaction on the porosity and successively on the permeability of the bentonite following equation proposed is used:

$$k = 4{,}86x10^{-9}\phi^{4{,}367} \qquad (6\text{-}1)$$

where the porosity is in fraction and permeability in m^2. For determining the permeability of crushed salt under compaction the information given in the chapter 5.2 is referred. The two-phase parameters (relative permeability, capillary pressure) of the buffer materials were used

referring to published data. The gas entry pressure, p_t for bentonite was estimated from following equation as function of the permeability /PUS 87/:

$$p_t = 5{,}874x10^{-6}\left[\frac{1}{k}\right]^{0,33} \quad (6\text{-}2)$$

For crushed/compacted salt the entry pressure was entered as function of the permeability and porosity with the following correlation /CIN 06/

$$p_t = 5{,}99x10^{-8}\left[\frac{1}{k.\phi}\right]^{0,36} \quad (6\text{-}3)$$

For the entry pressure of both type of host rock a value of 1 MPa was introduced. The grain radius and surface area of the backfill minerals were given as 1 mm and 10 cm^2/g for crushed salt and 0,1 mm and 100 m^2/g for bentonite successively. Other parameters applied in basic case are given in Table 6.1.

Table 6.1 Physical/petrophysical parameters applied in basic case models for various materials applied

Property/Rock	Rock salt	Clay Rock	Buffer Bentonite	Compac. Salt/Mg-Depot	EDZ (for all cases)	Sealing
Density [kg/m^3],	2180	2700	2100	2165	Same as the host	2500
Heat conductivity [W/(m ·K)]	2,35	2,10	2,10	2,00	Same as the host	1,90
Specific Heat capacity , [J/(kg.K)]	950	960	1050	900	Same as the host	1000
Porosity, [%]	0,1	1,0	20,0	30,0	1,0	15,0
Permeability, [m^2]	1.10^{-22}	1.10^{-21}	1.10^{-14}	1.10^{-13}	1.10^{-16}	1.10^{-15}
Relative Permeability/ Capillary Pressure (after Genuchten-Mualem Model)	P_t = 0,5 MPa λ= 0,45 P_{max}= 10^2 MPa	P_t = 1 MPa λ= 0,45 P_{max}= 10^2 MPa	P_t = 0,1 MPa λ= 0,45 P_{max}= 10^4 MPa	P_t = 0,05 MPa λ= 0,73 P_{max}= 10^2 MPa	P_t = 0,1 MPa λ= 0,45 P_{max}= 10^2 MPa	P_t = 0,05 MPa λ= 0,50 P_{max}= 10^2 MPa

6.1.2.2 Heat Source

A heat source representing the heat generating from HAW containers is introduced based on precious studies /ALK 07/. The heat generation is due to HAW waste and exhibit higher heat activity at the beginning of the repository time being equal to approximately 2500 W/m^2 and after about 200 years the heat generation decreases below 10 W/m^2 that means no more relevance for the numerical modeling. Following equation based on the correlated data presented in Figure 6-6 is used as the heat source from the HAW containers:

$$Q = 2379\, e^{-0{,}026.t} \tag{6-4}$$

where Q is obtained as W per volume of container (m^3) by introducing t as years. The corresponding heat source is calculated considering the volume of the containers (0,16 m^3). The total heat source was assigned in the container model considering the number of blocks given for the model.

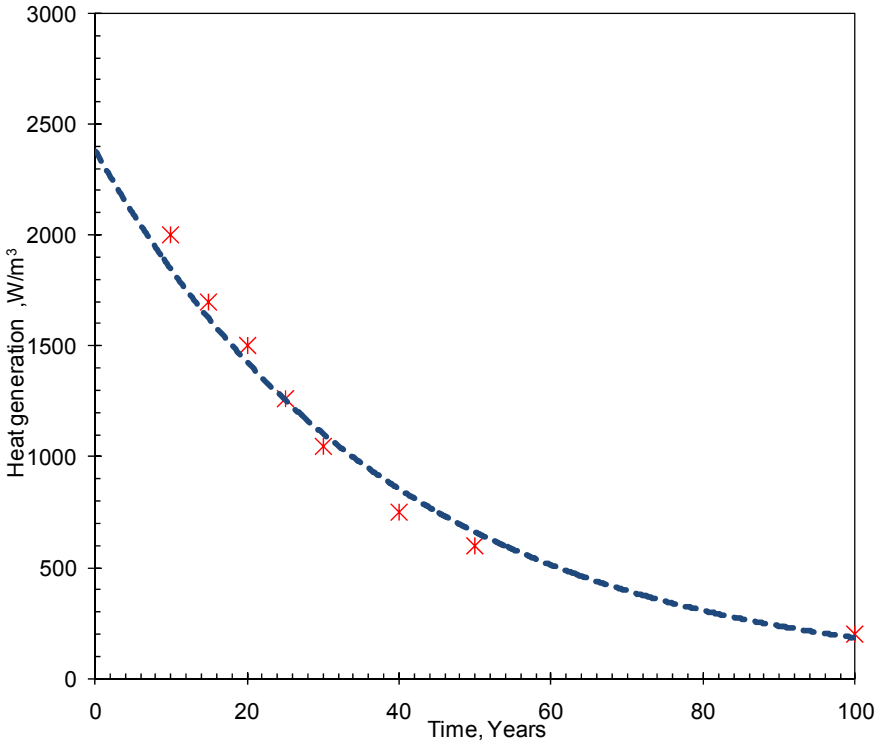

Figure 6-6 Heat source applied in the model as function of time.

6.1.2.3 Gas Generation Rate

The effect of the temperature on corrosion rate is well known from the related research /ROD 99/. The corrosion rate from HAW containers was estimated based on the Arrhenius-Diagram as represented in Figure 6-7 for various container metals in NaCl (N) and $MgCl_2$ (Q)

brines. The measured and estimated data are shown in the same Figure and the corrosion rate is correlated to temperature according to the following relationship:

$$\dot{q} = a \cdot e^{-\frac{Q}{T}} \tag{6-5}$$

which can be reformulated as:

$$\ln \dot{q} = \ln a - \frac{Q}{T} \tag{6-6}$$

With this relationship the correlation of the represented points results in a line for both brine types with parameters of

Q = 4847 1/K and a = 1,93.10^6 μm/a for N brine and

Q = 3157 1/K and a = 1,49.10^5 μm/a for Q brine

The correlation function repeats the measured data with acceptable deviation. The differences from experimental values could be explained with varying experimental conditions. These two corrosion rates were used to calculate the gas generation rate in corresponding solutions according to the following reaction:

$Fe+H_2O \rightarrow FeO+H_2$

The effects of other chemical and related issues (i.e. the effect of pH) on gas generation rate are neglected. The actual gas generation rate is introduced to the model based on the container volume and number of blocks assigned. The CO_2 generation for the ILW models in a drift repository was approximated from previous studies as 9.10^{-11} kg/s per m^3 of waste with the assumption of a transformation of the organic carbon to CO_2 /BRA 03/.

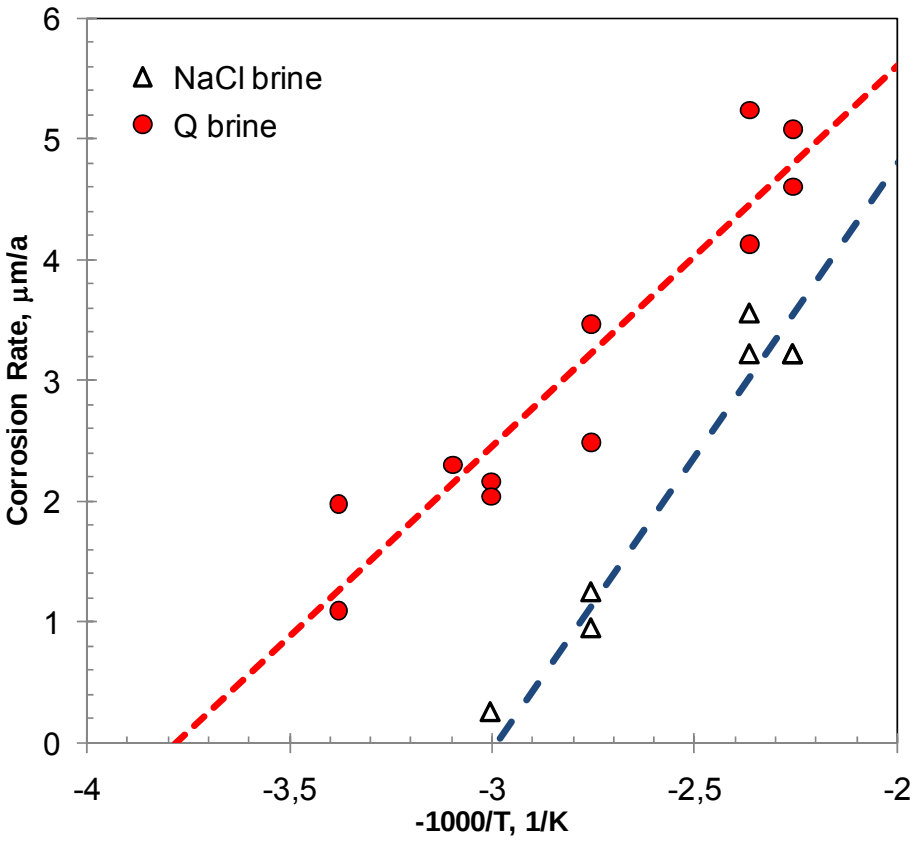

Figure 6-7 Arrhenius representation for the determination of the corrosion rate in dependency of the temperature

6.1.2.4 Initialization and General Assumptions

The initialization of the model and model parameters were performed according to the general knowledge on deep geological repository. Data given in Table 6.2 were used for determining the initial set-up of the model.

Some general assumptions of the modeling study in addition to the assumptions made for individual implementations are as follows:

- The effects of the temperature and water saturation on the petrophysical and thermal parameters (porosity, permeability, thermal conductivity, etc.) are negligible.
- No free or dissolved gas is allowed at the start of the model.
- The pore volume of the repository and the host rock is assumed to be initially saturated with the fluid.
- The EDZ properties are assumed constant throughout the width of EDZ.
- The self-healing of the EDZ zone is neglected this means the properties of EDZ is assumed constant.
- The dissolution and precipitation of any mineral is represented as volume change of these mineral.

Table 6.2 Initial parameters of the models used in the study

Parameter	Value
Depth of the repository [m]	700
Temperature gradient [K/m]	0,038
Hydraulic pressure gradient [Pa/m]	11000
Temperature @ (-700 m) [°C]	31,5
Hydraulic pressure @ (-700 m) [MPa]	7,8
Water saturation [-]	1,0

6.1.3 Chemical Input

Two different fluid systems were used in the simulations performed for rock salt; solution N based on NaCl content and solution Q based on $MgCl_2$ content. For clay system a pore water solution representing the similar cases as published in the literature was used. The compositions of the model brines are given in Table 6.3. The compositions were selected consisting of only main components in order to sake the simplicity in the evaluations and also to reduce the computing time. A backfill material consisting mainly of brucite ($Mg(OH)_2$) is considered to be most suitable for a robust, long-term geochemical environment. Experimental as well as numerical modeling studies support the performance of brucite as backfill material, confirming its ability to limit/decrease the dissolved carbonate content and to stabilize the pH of the system. The mineralogical composition of the clay as host rock was given based on the composition of the Opalinus Clay /ZHA 04/. The exchange ion capacity of bentonite was introduced based on the data given in Table 5.6 for the bentonite MX-80. The composition of the container was introduced as consisted of iron and only for the surrounding blocks of container.

Table 6.3 Initial solution compositions used in the model, g/l

Species	Solution N	Solution Q	Solution Clay
NaCl	230	-	6
$MgCl_2$	-	190	1
$MgSO_4$	-	20	-
KCl	-	10	0,1
$CaSO_4$	10	1	0,1
$CaCl_2$			1,2

Table 6.4 Mineral compositions used in the study, volume fraction

Minerals	Rock Salt	Buffer Salt /Cement, C	Clay Rock	Bentonite, MX80	Mg-Depot, B	Container
Halite	1	0,40	-	-	0.25	-
Portlandite	-	0,50	-	-	-	-
Quartz	-	0,08	0,20	0,05	0,04	-
Iron	-	0,01	-	0,01	0,01	1
Brucite	-	-	-	-	0.70	-
Dolomite	-	0,01	0,05	-	-	-
Anhydrite	-	-	-	-	-	-
Kaolinite	-	-	0,35	-	-	-
Illite	-	-	0,25	-	-	-
Montmorillonite	-	-	-	0,90	-	-
Calcite	-	-	0,15	0,01	-	-
Albite	-	-	-	0,03	-	-

6.1.4 Other Modeling Considerations

The runs were performed for maximum 5000 years. If necessary and sufficient, runs were performed for earlier times too. The basic discretizations represented in related chapters were changed if necessary in terms of time and space considerations. The input data were prepared based mainly on the related facilities disseminated by the developers of TOUGH2, LBNL. The keywords required for the improvements made in the framework of this study were added to the standard input files as described in previous chapters. The evaluation of the outputs was performed mainly by using the Tecplot for two and three dimensional description of the results. In some cases other periphery software such as Microsoft EXCEL or Petrasim were also used. In order to perform more rapid runs, various solving schemes were applied for reactive flow. With the same reason ct of the precipitation/dissolution on the flow were omitted in most of the runs. The runs were basically coded according to the case studied. The simulation runs for clay host rock were named as CLAY; the runs for salt as host rock were named SALT. The simulation of the drift type repository for medium-low level wastes containing organic components were named as DRIFT. The suffixes separated with a line were used to describe the runs specific to the parameter or property studied.

6.2 Clay as Host Rock

The model described in section 6.1.1 as borehole model was used by introducing the component compositions and other required physical and petrophysical parameters. The initial chemical composition of the model consists of HLW container, bentonite as buffer material and clay as host rock. The disposal of heat generating waste case was considered to investigate the thermal effects. The EOS module EWASG was mainly used for the runs. The chemical parameters are assumed as being given in data files of TOUGHREACT-Pitzer. To assure a better isolation of the chemical coupling the simulation runs were performed by adding the mechanical and chemical options successively to thermal-hydraulic computations. The results are given in the same order.

6.2.1 Thermal-Hydraulic Issues

The runs with basic model, CLAY-basic, without mechanical-chemical option provides the effect of the heat and gas generation on the hydraulic aspects contributing the transport of radionuclides towards the host rock. The temperature profile of the basic run performed with initial data is given for after 1 and 1000 years in Figure 6-8. As can be concluded from the figures the temperature is as high as 190 °C in the repository after one year whereas it decreases beyond 50 °C in the vicinity of the containers after 1000 years. It should be noted that the maximum temperature reflects the temperatures in container blocks. The temperature profile after 1 year of disposal is given in Figure 6-9 with a higher resolution for near vicinity of one container. The temperature in the buffer near the container reaches approximately 130 °C after 1 year and decreases with increasing distance from the container. The evolution of the temperature with time is given in Figure 6-10 for two blocks, the first one in the boundary container-buffer and the second in the boundary buffer-host rock both on a horizontal line crossing the middle of the container. The Figure is redrawn in for the first 10 years of the disposal in Figure 6-11.

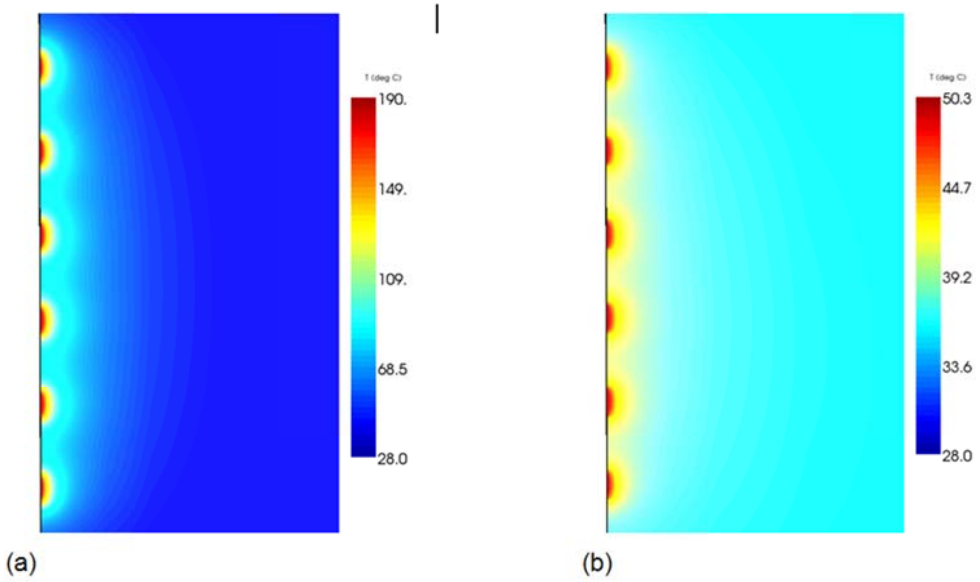

Figure 6-8 Calculated temperature profile of the case Clay-Basic after one (a) and 1000 (b) years.

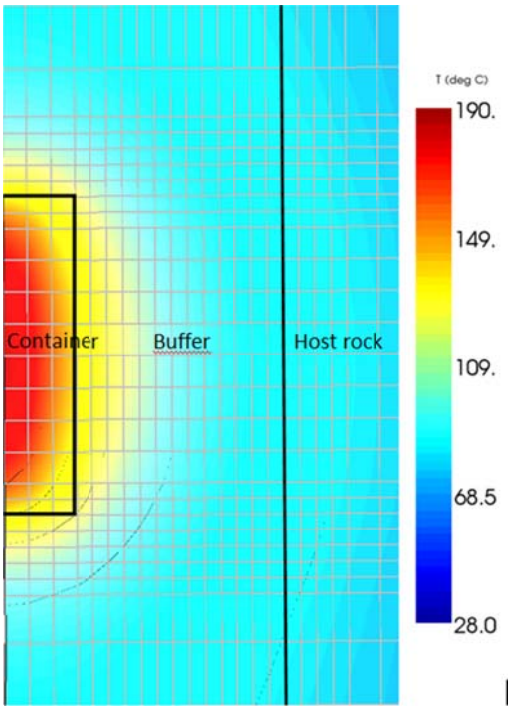

Figure 6-9 Calculated temperature profile in the near vicinity of a container for the case Clay-Basic after one year of disposal.

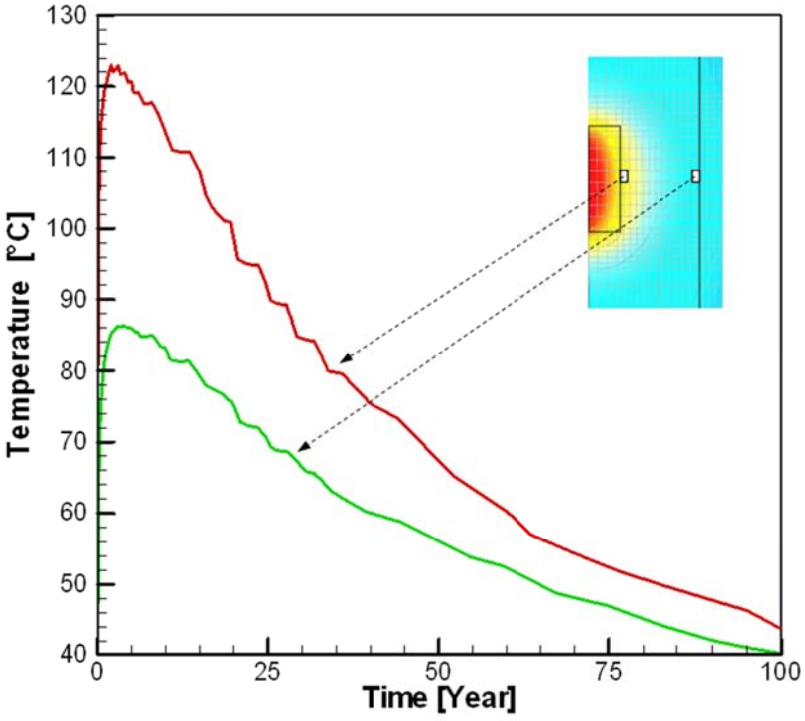

Figure 6-10 Change of the temperature with time at the near container-buffer and buffer-host rock blocks

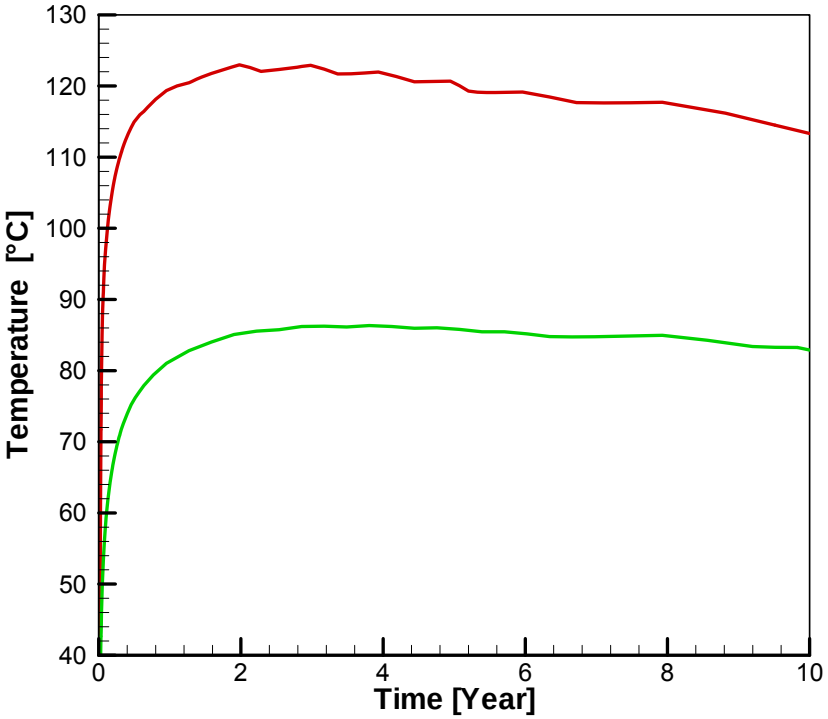

Figure 6-11 Change of the temperature with time for the near container-buffer and buffer-host rock blocks for the 10 years after the disposal

As expected the maximum temperature is calculated in the first years and after approximately 2 years the temperature begins to decrease. This thermal behaviour is conforming to experimental/laboratory studies to investigate the temperature distribution around the heat generating radioactive wastes /BUR 06/.. It is worth to note that the maximum temperature reached after the disposal as well as the temperature profile is strongly dependent on the thermal and hydraulic parameters assumed for the model. The parameters assumed for the host rock are defined well in the literature. The parameters for the buffer material on the other hand originate from various sources and shows variations after the measurement equipment, methodology and material used. Higher heat conductivity f.i. would have a positive effect in terms of heat dissipation towards the host rock and therefore causing a lower temperature profile. A run with a heat conductivity of 2,5 [W/(m ·K)] instead of 2,1 [W/(m ·K)] was performed in order to test the effect of the heat conductivity on temperature profile. This resulted in a reduction of approximately 5°C on the maximum temperature being reached at the near container block which can be very important in term of long-term buffer performance. A lower porosity on the other hand would be preferred because of the lower heat conductivity of gases.

Another aspect of the heat generation is the thermal effects on the hydro-mechanical behaviour. Difference in thermal expansion between pore water and solid particles in water saturated buffer and clay constitutes an additional driving force. If the very low permeability host rock does not permit water to dissipate towards the formation the pore pressure should increase in the buffer region. With a realistic permeability of 1.10^{-21} m^2 set in the model, this is the case in the simulations. An excess pressure of approximately 6 MPa is calculated immediately after the beginning of the simulation within the weeks showing the effect of the high

heat generation rate. After the maximum value pressure decreases rapidly and tends to reach a constant value of approximately 3,5 MPa after 30 years. The effect of the buffer and host rock permeability on the pressure built-up is significant and this will be discussed in the following chapter.

As a second simulation series the gas generation (H_2) was switched on to observe the effect of the gas generation on thermo-hydraulic issues. In this run named "Clay-gas" a diffusion coefficient of 5.10^{-9} m^2/s is used for the diffusion of gas in liquid. No free gas phase is observed; all of the gas generated dissolves in water instantaneously, therefore no significant changes are expected in pressure built-up behaviour. The H_2 generation case is expected to make no relevant impact on the chemical issues. It should be repeated that the pressure behaviour is strongly related to the petrophysical data most of all on the permeability of the materials used.

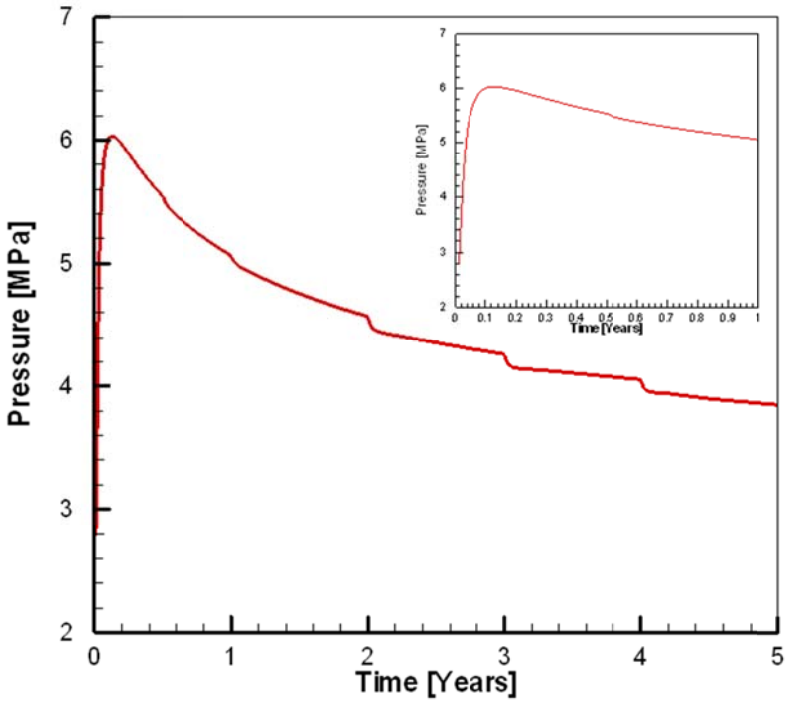

Figure 6-12 Evolution of pore pressure in buffer blocks with time as the result of heat generation.

6.2.2 Thermal-Hydraulic-Mechanical Issues

An increase in the pore pressure may cause hydrodynamical heterogeneities in host rock as well as in the buffer material. This effect is accelerated in the case where the geological materials exhibit stress and petrophysical anisotropies. The formation of excavation damaged zones is very well known example of the deviatoric stress conditions in the host rock. The sudden and high increase of the pore pressure, p_{fluid} may also contribute on the formation of heterogeneities by fracturing the surrounding formations according the following relation:

$$\Delta p_{excess} = p_{fluid} - \sigma_{\min} \quad (6\text{-}7)$$

where σ_{min} is the minimum stress component acting on the formation. In the case of the generation of gas, the pressure caused by the gas will affect the pore pressure so that it can get a higher value than the minimum stress resulting in a fracturing of the surrounding formation. In the case of the pressure built-up due to gas generation or thermal expansion in a bentonite buffer the excess pressure Δp_{excess} is obviously dependent on the swelling pressure. In other words, the swelling pressure should contribute on the frac-strength of the buffer material. After /HOR 99/ the effective stress is directly equal to the swelling pressure comparing it with “gas entry” or “capillary threshold” pressure.

In this study, as the bentonite is assumed to be fully saturated with the “solution clay” which has lower ionic strength it is expected that the swelling occur in a short time. The CLAY-Swell calculates the swelling pressure according to the data given in Table 5.6 for MX-80 bentonite. The calculated swelling pressure reaches 32 MPa for the data assumed for the case studied. This value is higher than the pore pressure calculated in previous chapters. This swelling pressure is also higher than the expected frac-strength of the surrounding host rock which is calculated between 17-19 MPa.

Another issue that may affect the thermal-hydraulical-mechanical considerations is the formation and the presence of an EDZ. This zone having a higher porosity and permeability reduces the pressure built-up in the buffer by compensating high thermal and hydraulic gradients.

One of the results of the swelling of the bentonite buffer is the decrease on the porosity and therefore on the permeability. This variation of the petrophysical parameters may have additional effects on the mechanical response of the repository barriers. Some additional runs were performed in order to evaluate extreme cases in terms of pressure built-up and its effect on mechanical behaviour. These runs consider the swelling of bentonite and EDZ formation into the model both separately and together as CLAY-Swell, CLAY-Edz and CLAY-Swell-Edz. The models being developed based on the data of Table 6.1 are described in Table 6.5. In all models gas generation was also considered. The permeability of the host rock was not changed considering that this is realistic and conservative at the same time.

Table 6.5 Runs performed in order to evaluate the variations in mechanical and relate petrophysical parameters.

Run Name	**Description**
CLAY_swell	Bentonite with swelling, ϕ= 5%, k = 1.10^{-18} m^2
CLAY_swell_bent	Bentonite-sand mixture 25-75%, swelling, ϕ= 10%, k = 1.10^{-16} m^2
CLAY_swell_EDZ	Bentonite with swelling, ϕ= 5%, k = 1.10^{-18} m^2, EDZ as given
CLAY_swell_bent_EDZ	Bentonite-sand mixture 25-75%, swelling, ϕ = 10%, k = 1.10^{-16} m^2, EDZ

The comparison of the runs is compared in Figure 6-13. In all cases the pore pressures are lower than the calculated swelling pressure that are 32 MPa for bentonite case and 15 MPa for bentonite sand mixture. The presence of an EDZ is particularly important for the bentonite swelling case and it reduces the pore pressure from app. 10,2 MPa to app. 6 MPa. In all cases the pressure increases within weeks and than reduces in two years near 5 MPa staying afterwards approximately constant.

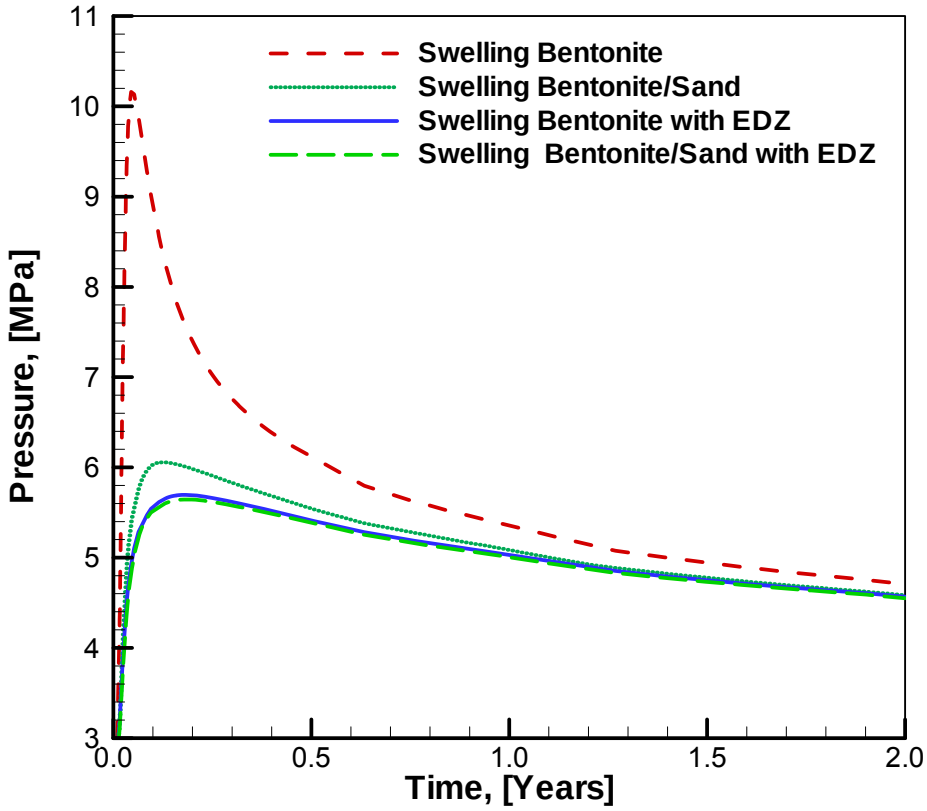

Figure 6-13 Comparison of the pore pressure for swelling bentonite cases

6.2.3 Reactive Coupling

The reactive issues were introduced in the model by the activation of the chemical part of the model. This was realized by using the necessary data input provided and modified in the framework of this work.

6.2.3.1 Input Data

The input data was given from the compositions given in Table 6.3. The secondary minerals were chosen based on the possible reactions suggested by similar studies. They are listed in Table 6.7. The kinetic constants were given as provided in the literature. The fluid initial compositions were introduced from the Table 6.3 for both the bentonite and the clay as host rock. The temperature dependency of the related coefficients was assumed as given in the data set based on the discussions of the Chapter 4. The partial pressure of CO_2, P_{CO2} was

fixed to 2.10^{-4} Bar initially. The initial pH was calculated to be 7,6 considering a temperature of 100 °C. The activation energy, E_a and kinetic rate constant, k_{25} for the following dissolution rate approach were chosen according to previous studies. The cation exchange capacity for buffer and host rock were entered according to data given in previous chapters.

$$k = k_{25} Exp\left[\frac{-E_a}{R}\left(\frac{1}{T} - \frac{1}{298{,}15}\right)\right] \tag{6-8}$$

The initial porosity and permeability of the bentonite and host rock were introduced as given in previous chapters. The two-phase properties namely relative permeability and capillary pressure were also entered although no two-phase flow was expected.

The grain radius and effective surface area for the calculation of precipitation and its effect on porosity and permeability were entered as 0,1 mm - 0,001 mm and 10 - 100 cm^2/g successively for non clay and clay minerals. Finally, it was also assumed that only 10% of the total mineral surface area participated as reactive surface area (S_{meff}=0,1S_{mT}). Evidently, these assumptions are rough, but this estimation of reactive surface area of mineral phases is still discussed in the literature.

The transport of solutes into the clay barrier was considered to be a pure diffusion process in a saturated medium. The initial effective diffusion coefficients used in the simulations were given as 10^{-11} and 10^{-10} m^2/s. These values were selected based on published data for compacted MX-80 /LEH 96/.

Many successive runs were performed to have a better understanding of the reactive transport phenomena in the systems where clay is assigned as host rock. Three main runs given in Table 6.6 were taken as essential for the discussion performed in the following. The run named “CLAY_plus reactive” is used to couple all of the improvements performed in this study. However this data set could be run under restricted time and space conditions which conclude one of the main limitations of the model improvements of the project. The main discussion was performed based on the CLAY_reactive and CLAY_reactive_EDZ.

Table 6.6 Runs performed in order to evaluate the reactive transport phenomena

Run Name	**Description**
CLAY_plus_reactive	THMC coupling as aimed at the project
CLAY_reactive	THC coupling to better isolate the chemical effects
CLAY_reactive_EDZ	THC coupled taking the formation of EDZ with 1 m width.

Table 6.7 Secondary minerals used in the model and simulations “CLAY”

Mineral	Chemical Formula
Montmorillonite-Na	$[(Si_{3.98}Al_{0.02}O_{10})(OH)_2]$ $(Al_{1.55}Mg_{0.28}FeII_{0.08}FeIII_{0.09})Na_{0.18}Ca_{0.1}$
Montmorillonite-Ca	$[(Si_{3.96}Al_{0.04}O_{10})(OH)_2](Al_{1.52}Fe^{III}_{0.18}Mg_{0.27})Ca_{0.2}$
Siderite	$Fe^{II}CO_3$
Anhydrite	$CaSO_4$
Magnetite	$Fe^{III}_2Fe^{II}O_4$
$Chlorite_{FeAl}$	$[Si_2Al_2O_{10}(OH)_2](Fe^{II}Al_2)(Fe^{II}_3)(OH)_6$
$Chlorite_{MgAl}$	$[Si_2Al_2O_{10}(OH)_2](MgAl_2)(Mg_3)(OH)_6$
$Saponite_{Fe(II)}$	$[(Si_{3.67}Al_{0.33}O_{10})(OH)_2](FeII_3)Na_{0.33}$
Gypsum	$CaSO_{4d}$ $2H_2O$
Microcline	$KA^{I}Si_3O_8$
Hematite	$Fe^{III}_2O_3$
Brucite	$Mg(OH)_2$
Fayalite	Fe_2SiO_4
Magnesite	$MgCO_3$
Forsterite	Mg_2SiO_4
Jarosite	$KFe^{III}_3(SO_4)_2(OH)_6$
Pyrite	FeS_2

6.2.3.2 Observed Processes

The bentonit barrier is subjected to temperature variations (up to 120 °C) as modelled and discussed in previous chapters. As expected the temperature gradient must be a function of time and space. Considering the temperature gradient given and the long term evolution of the system, the mineralogical transformations have been considered as being more important than the surface and ion exchange reactions. As a consequence, these reactions were neglected in most of the runs. The most important conclusion of the “CLAY_plus_reactive” which takes the swelling into account is the strong and rapid decrease

of the porosity around the container. The variation in porosity is due to firstly swelling and secondly to the precipitation/dissolution of the minerals where the swelling is a more rapid process causing the reduction in pore volume. The Figure 6-14 shows the porosity distribution around one container for the cases “CLAY_plus_reactive” and “CLAY_reactive” after 10 years of simulation. As can be seen the porosity reduction is concentrated in the vicinity of the container whereas an overall porosity reduction is observed in the whole of the barrier volume. The porosity is calculated as low as 0,001 which reflects a decrease of more than 100 fold from its original value although a rate of dissolution of some minerals is also calculated for buffer zone. This confirms the effect of swelling on porosity reduction as discussed in earlier chapters. The effect of the dissolution is apparent for the “CLAY_reactive” with a small increase in porosity. The heterogeneous distribution of the porosity reduction is obviously a result of mineral the dissolution. The dissolution of the bentonite is resulted in an increase in Si, Al, Mg, K, Ca, and Na contents in the interaction fluid. The very low concentration in iron in the interaction fluid indicates chlorite precipitation in the system. This phenomenon is controlled by the silicate minerals dissolution and by the corrosion of iron container.

The swelling bentonite buffer is considered as initially saturated with an equilibrated solution. It is observed that chemical parameters like pH and Eh are significantly changed. The consequences on mineralogy are significant and the buffer may lose its initial thermodynamic stability. The pH decreases particularly in the vicinity of the container with increasing temperature influencing the corrosion process considerably.

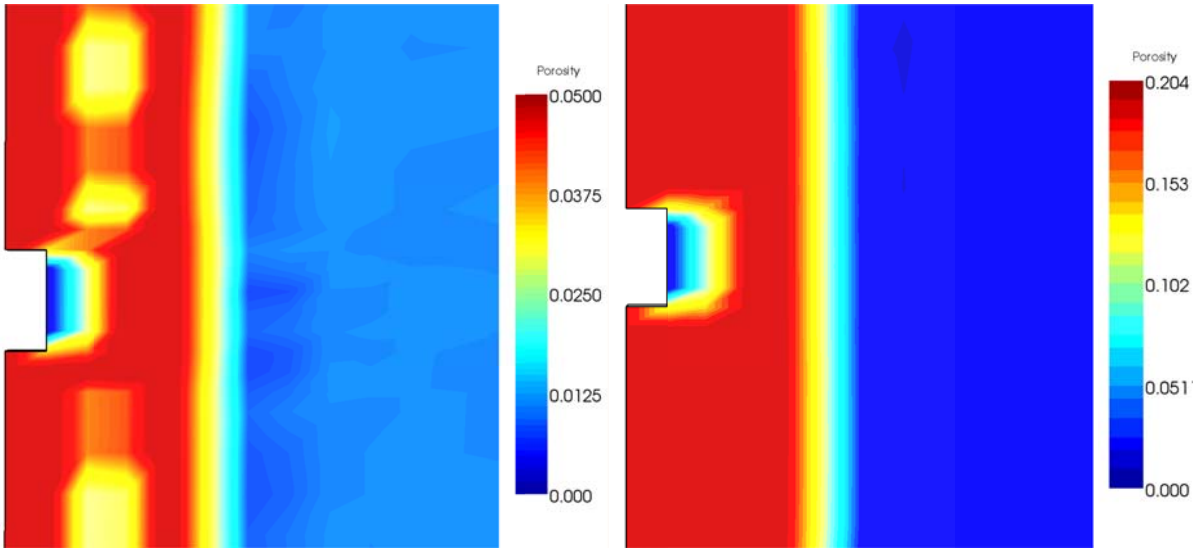

Figure 6-14 Comparison of the porosities around the container calculated with “CLAY_plus_reactive” and “CLAY_reactive”

6.2.3.2.1 Corrosion

The metallic corrosion provides Fe^{+2} which are incorporated in ferrous minerals mainly near the cell of the steel container corrosion. A massive formation of smectites occurs that reduces the pore volume. This is the cause of the intensive porosity reduction given above. Chlorites appear in a zone more distant from the container (after the precipitation zone of $Fe_{II}Al$

chlorite). Chlorites are precipitated at temperatures over 100 °C. The magnetite is found as the main corrosion product of the iron; it is oversaturated in the cell of the bentonite and stays directly in contact with the container. Due to the kinetic control of the growing phase extracted from experiments in homogeneous phase rather than heterogeneous phases, the precipitated volume of magnetite is limited.

The swelling clay buffer is considered as initially saturated with an equilibrated solution. During modeling time, chemical parameters like pH and Eh are considerably modified. The consequences on mineralogy are significant and the composition may lose its initial thermodynamic stability. The pH of the groundwater is 7,3 at a temperature of 25 °C. If the temperature of this fluid increases to 100 °C, the pH decreases to about 6,2 (see Figure 6-15). At the end of the simulation, this pH value tends to be imposed to the whole profile. Eh decreases with increasing pH. As for pH, the redox potential in the bentonite barrier is significantly influenced by the groundwater diffusion process. The corrosion process goes together with a release of hydroxide ions. These ions migrate into the bentonite under the influence of the effective diffusion (D), and generate an increase of pH value at the interface between the buffer and the steel. After 5000 years, the porosity plugging significantly decreases the mass transport by molecular diffusion. Then the migration of hydroxide ions decreases as a function of time, and the clay chemical conditions, at 100 °C, tend to be imposed in the buffer. In the cell which models the steel overpack corrosion, the chemical conditions remain quite unchanged.

In order to model the bentonite alteration in contact with the steel, a cell simulates the iron corrosion. In that cell, only siderite and magnetite formations are kinetically processed. The alteration profile of the steel container overpack is shown Figure 6-16. As already highlighted magnetite is the main corrosion product in reducing conditions. Siderite precipitates but the corresponding volumes are low and cannot be distinguished. The siderite precipitation is limited by the CO_2 partial pressure which was not imposed at a given value during modeling. The radioactive waste disposal cell is isolated from the atmosphere and the geochemical system is supposed to exhaust its CO_2 reserve. This is particularly true near the iron/clay interface where the porosity and the permeability are decreasing and make any renewal of aqueous CO_2 impossible: magnetite and siderite are taking more volume in the pore space than the initial massive steel. Figure 6-17 shows the volume change around the container due to the magnetite precipitation (iron + magnetite). The simulated decrease of the corrosion rate with time can be explained by high values of pH (around 11) and iron concentrations developed with time, as well as by a weak accumulation of hydrogen in the cell, modeling the steel overpack alteration. The availability of hydroxide and ferrous ions as well as hydrogen is also linked to the porosity reducing at the iron/clay interface.

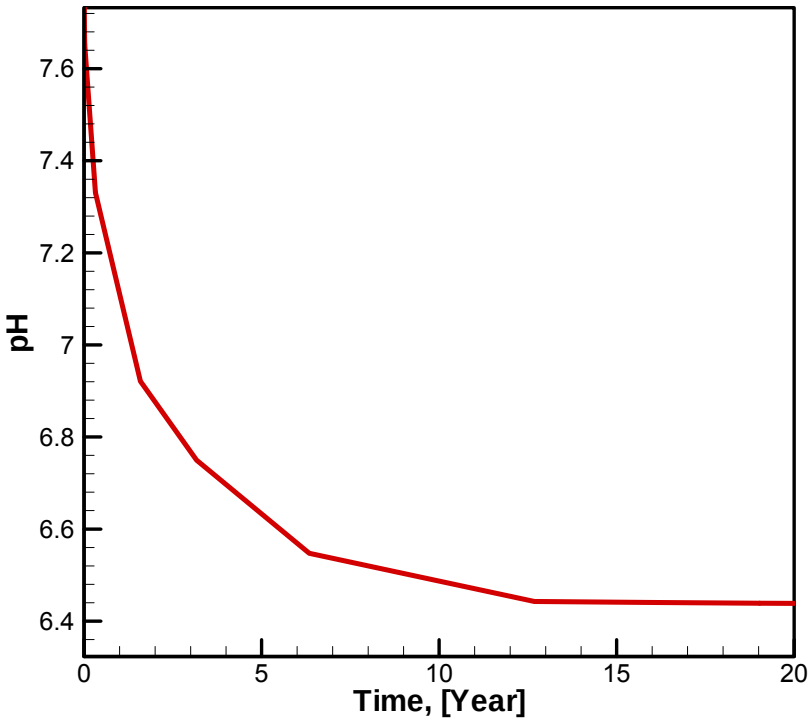

Figure 6-15 Change of pH around the container at the first years of the simulations, “CLAY_reactive”

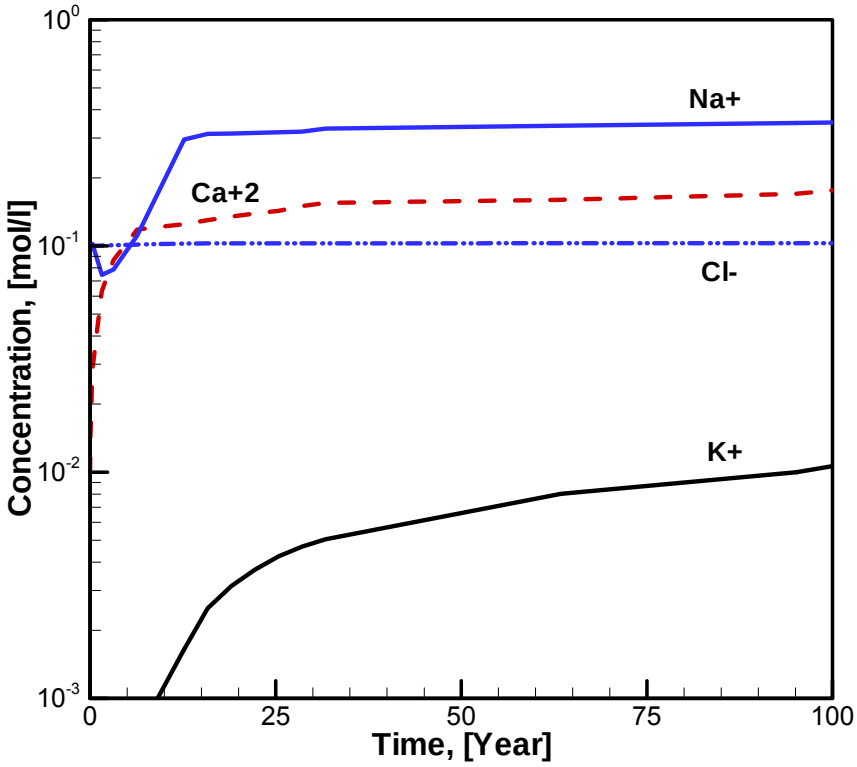

Figure 6-16 Change of ion concentration in the bentonit buffer around the container, “CLAY_reactive”

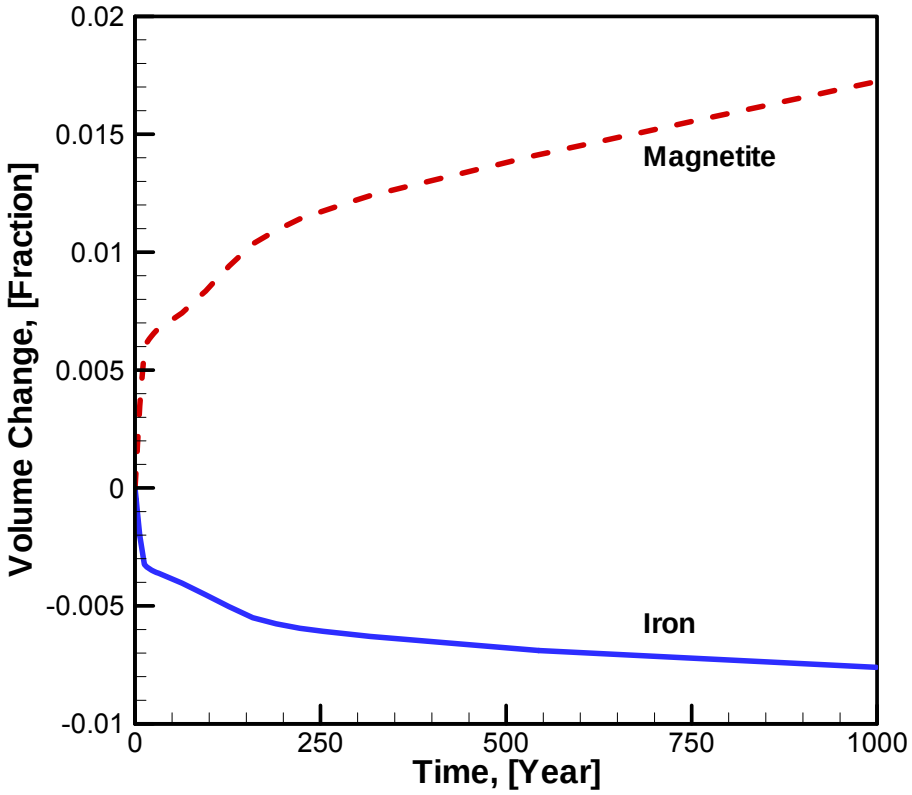

Figure 6-17 Corrosion of the steel containers and its products observed in buffer around the container, “CLAY_reactive”.

6.2.3.2.2 Mineralogical Alterations in Buffer

The Na/Ca–montmorillonite-to-illite conversion is reported as a potential chemical process for a bentonite barrier in the radioactive waste repository because of high concentration potassium in the geological fluid. Illite production can be assumed negligible, but, this phenomenon is effectively more significant when the potassium concentration increases in the interacting fluid. As a result, it is normal to predict that the montmorillonite-to-illite conversion depends on the reaction temperature and on the geological fluid concentration, particularly on the potassium concentration. In the present study, this chemical process is not significant after 1000 years of reaction and transport.

The montmorillonite-to-chlorite conversion is considered as a potential chemical process for bentonite barrier in the radioactive waste repository because of the iron concentration in the geological fluid and also because of the iron excess by the container corrosion (see Figure 6-18). As expected high iron concentration favors the Na/Ca–montmorillonite dissolution. In fact, the Na/Ca–montmorillonite dissolution is calculated to be more significant near the iron container. In addition, the high iron concentration also favours the montmorillonite-to-chlorite conversion. For example, this chemical process constitutes about 10% of the Na/Ca–montmorillonite dissolution near the container then this value decreases until about 8% in the bentonite barrier. It is clear that a montmorillonite-to-chlorite conversion will limit the swelling property of a bentonite barrier.

The present study has shown that the Na/Ca–montmorillonite-to- Ca–montmorillonite conversion is the most significant chemical transformation, i.e., the chemical transformation from medium-swelling clay to low-swelling clay (see Figure 6-19). Here, the Ca–montmorillonite formation increases proportionally with the Na/Ca–montmorillonite transformation.

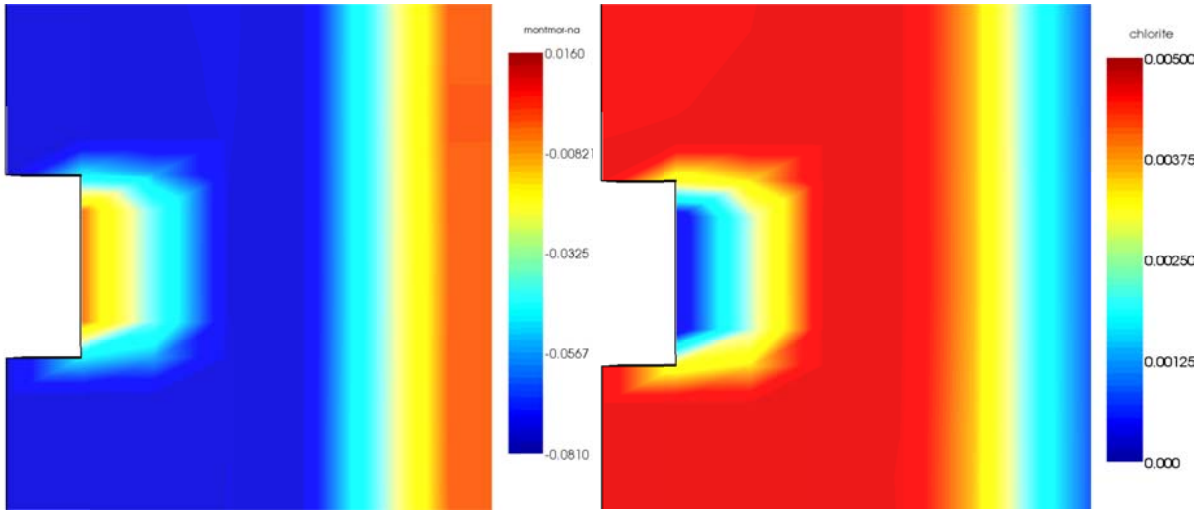

Figure 6-18 Calculated volume changes of Na-montmorillonite and chlorite around the container after 100 years of simulation, “CLAY_reactive”

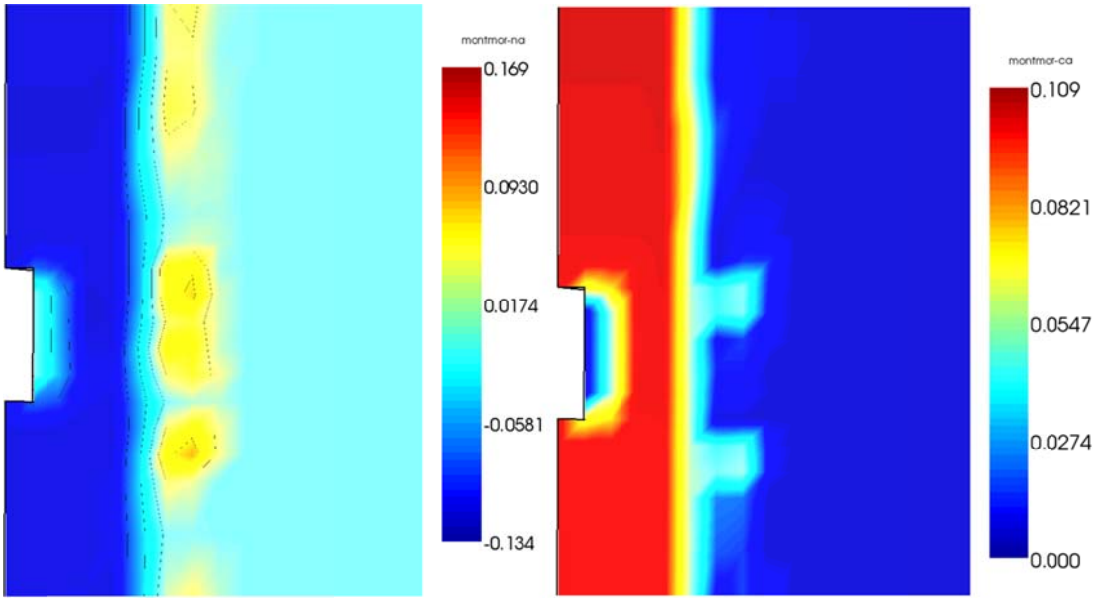

Figure 6-19 Calculated Na-montmorillonite to Ca-montmorillonite conversion around the container after 1000 years of simulation

6.2.3.2.3 Effect of EDZ on Reactive Transport

The most important result of the run carried out by activating the EDZ option together with swelling is given in Figure 6-20. As given in Table 6.1 the EDZ with a width of 1 m has the same porosity with the clay host rock but a permeability of 1.10^{-16} m^2 which is considerably higher than the permeability of the clay host rock. As the result of this difference the porosity of the zone beyond the EDZ in host rock is observed to be increased. Figure 6-20 compares the porosities in buffer zone, in EDZ and a short distance in the host rock beyond the EDZ. The porosity in buffer begins to decrease due to the swelling in a short time. After 1000 years the porosity is smaller than 0,05 in most of the buffer. In EDZ the porosity remains approximately in its original value but a slight increase in porosity in host rock beyond the EDZ is apparent. The porosity increases up to 0,015-0,02 and this is due to dissolution of the some clay minerals by the protection fluid advancing through the formation via higher permeability EDZ. The transformation of Na-montmorillonite to Ca-montmorillonite and illite yields probably more pore volume in the clay host rock.

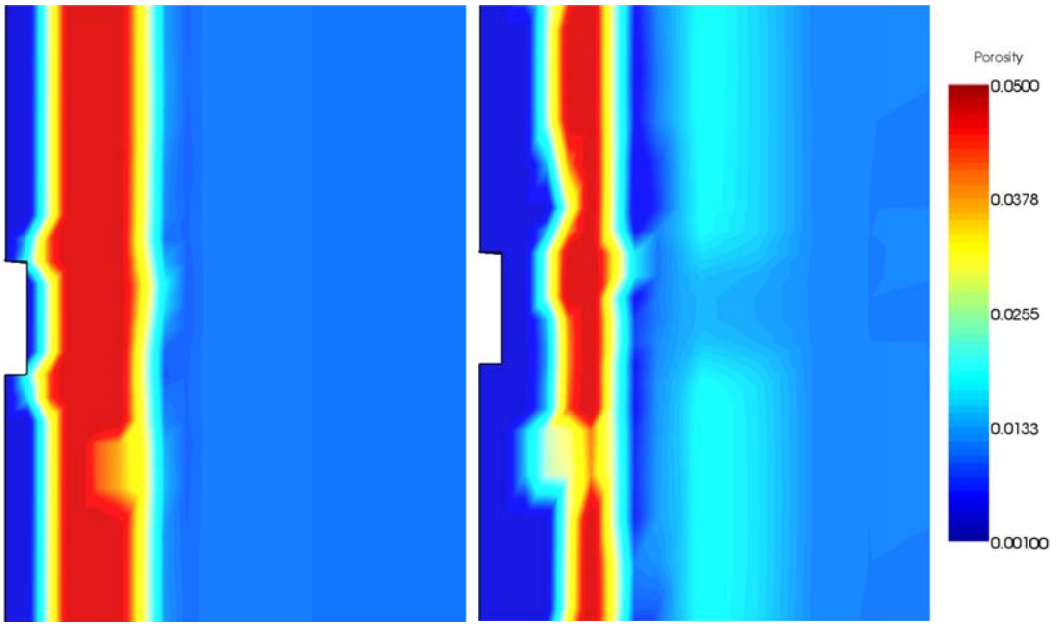

Figure 6-20 Effect of the EDZ zone on the porosity distribution around the container after 10 and 1000 years of simulation (CLAY_reactive_EDZ)

6.3 Rock Salt as Host Rock

In this model the rock salt is introduced as host rock. The source terms to model heat and gas generation were entered the same as clay rock. The compositions of the solid and aqueous phases were selected from the Table 6.3 and Table 6.4 successively. Two various models were applied in this case; borehole model for HAW and drift model for MLW/LLW.

6.3.1 Borehole Model

The geometry and initial set-up of the borehole model used in the case clay host rock was not changed for rock salt case. The EOS module EWASG was used for the runs. The model

runs performed in this chapter are listed in the Table 6.8. In this model two buffer types were introduced: the bentonite with N solution as the formation fluid and the brucite based material with Q solution as the protection fluid as the compositions are given in Table 6.3 and Table 6.4. The run “SALT_plus_reactive” aims at maximizing the THMC coupling that can be reached in this study which means the consideration of bentonite swelling together with rock salt compaction and reactive issues. To isolate the effect of the chemical issues the mechanical issues were switched off in a further run called “SALT_reactive_EDZ”. As the “SALT_plus_reactive” exhibits properly running difficulties because of timing and discretization problems the geomechanical issues were essentially commented on a run “SALT_reactive_BufferB_Q” that includes the ED zones in addition to swelling and compaction issues. In this run the brucite based material and Q solution were introduced as buffer properties. The H_2 is selected as the gas phase in EWASG and were given properly in the container blocks as the source with previously indicated generation rate.

Table 6.8 Runs performed in order to evaluate the reactive transport phenomena

Run Name	Description
SALT_plus_reactive	THMC coupling as aimed at the project
SALT_reactive	THC coupling to better isolate the chemical effects
SALT_reactive_BufferB_Q	THC with buffer B and solution Q as given in related chapter
SALT_reactive_B+Q_EDZ	THC coupled with “SALT_reactive_BufferB_Q” taking the formation of EDZ with 1 m width into consideration.

6.3.1.1 Thermal-Hydraulic-Mechanical Issues

The challenging part of these calculations is the coupling of the compaction of the rock salt. Figure 6-21 shows the porosity changes as the result of the compaction with and without taken the gas generation into account. As expected the compaction is stronger in the case “without gas generation” because no additional pore pressure is present. To couple this thermal-hydraulical-mechanical calculation to the chemical issues under the run SALT_plus_reactive was not possible because of the unsolved compatibility problems.

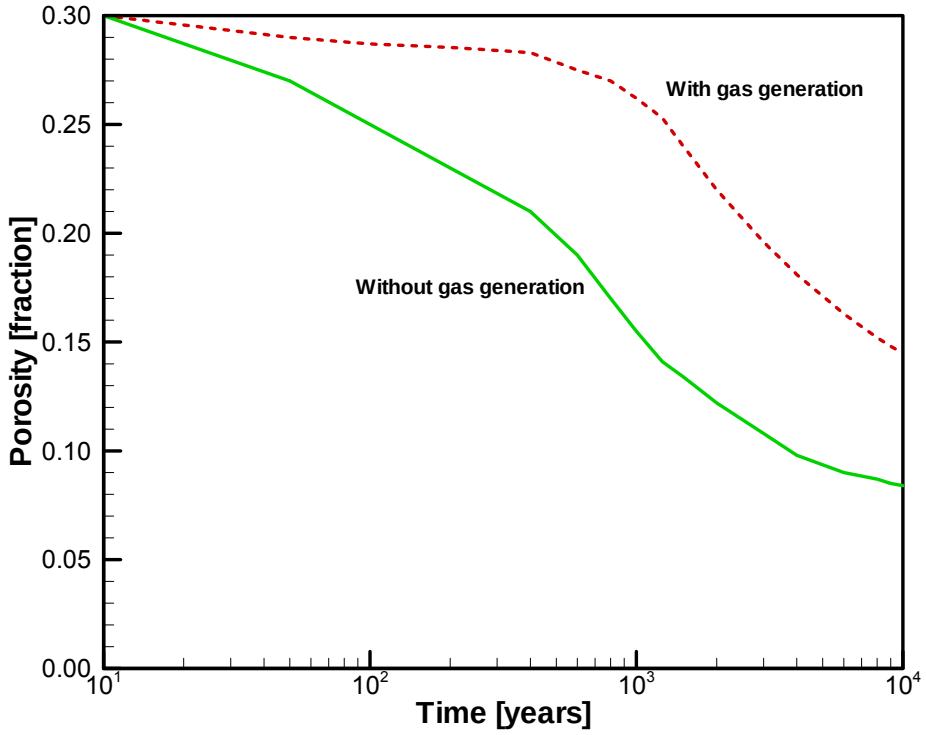

Figure 6-21 Variation of porosity due to compaction for various cases with "SALT" runs

6.3.1.2 Reactive Coupling

As indicated the reactive coupling were run based on the use of bentonite and brucite based buffer materials with corresponding protection fluids. In "SALT_reactive" any buffering effect is lacking and the pH increases within a very short time (few days) up the values 12. The calculated pH around the container in the case of NaCl solution for various times of simulation is shown in the Figure 6-22.

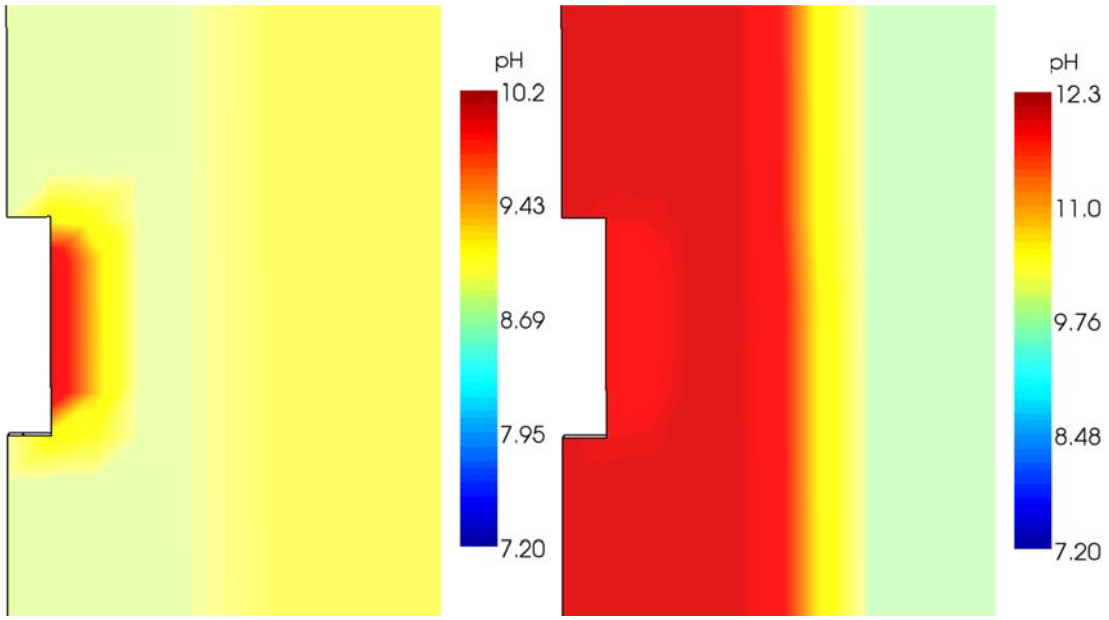

(a) (b)

Figure 6-22 Calculated pH distribution around the container for the case "SALT_reactive" after (a) 1 hr. (b) 10 days of simulation time

A comparison of the iron dissolution gives the advantage of using brucite buffer with Q solution clearly. Figure 6-23 shows the comparison of the corrosion rates between the two cases for the same initial conditions. As can be concluded the corrosion stability of this buffer combination is higher than previous case. After 1000 years the dissolution of iron in the protection fluid reaches 0,4 % of the initial iron concentration. The pH increase shortly after the simulation start to a level of 7,30 and remains at this value constant. This value stays constant as long as magnesium level is sufficiently high for buffering the pH and brucite $MgOH_2$ precipitates. The mineral precipitation around the container is of particular level. The precipitation of calcite, pyrite, fayalite, magnetite and magnesite especially around the container with the effect of increasing temperature causes a reduction in pore volume which directly affects the permeability. As shown in Figure 6-24 the porosity around the container decrease as low as 0,05. The effect of this decrease of porosity on the permeability is given on the right hand side of the same figure; the permeability decreases approximately to 1.10^{-15} m^2 that may cause a considerable reduction in convective transport of the contaminants.

The effect of a probable formation of EDZ around the borehole was investigated with "SALT_reactive_B+Q_EDZ". A similar effect as has been observed for clay was also observed for salt namely the interaction of the fluid in the buffer with the host rock, salt. A slight dissolution of halite in EDZ is remarkable which in turn causes an increase in porosity and permeability.

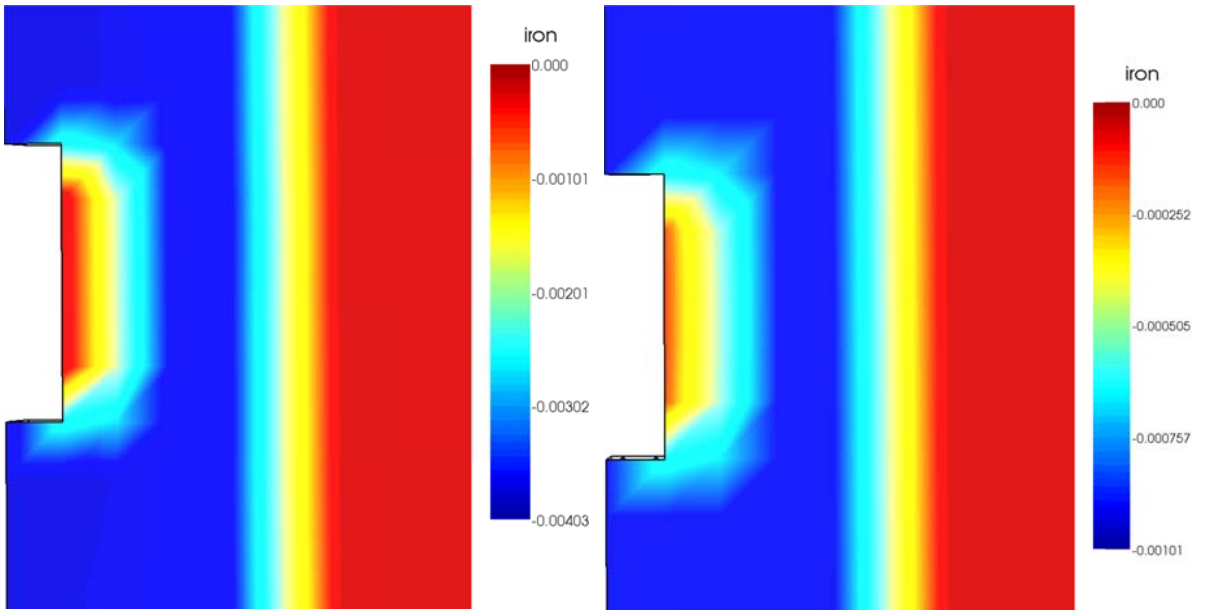

(a) (b)

Figure 6-23 Comparison of the corrosion between bentonite buffer (a) with “SALT_reactive” and brucite based buffer (b) with “SALT_reactive_BufferB_Q” with corresponding protection fluid around the container (after 1000 years of simulation).

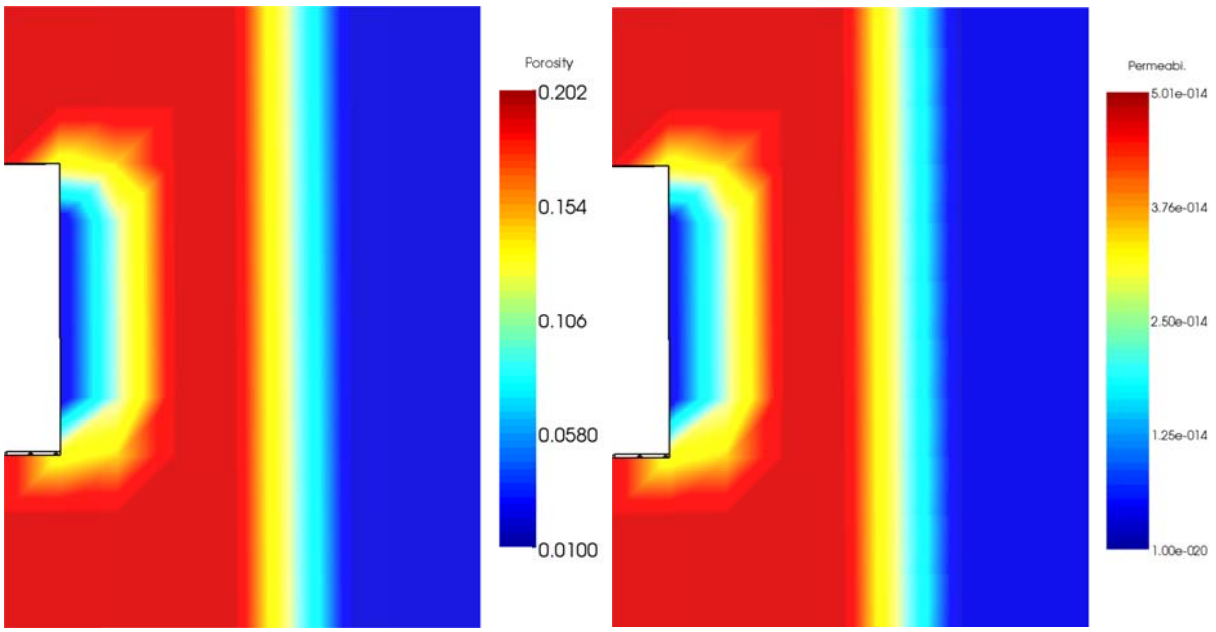

Figure 6-24 Decrease of porosity and permeability around the container due to mineral precipitation

6.3.2 Drift Model

The aim of creating and studying this model is to investigate the gas generation as a result of microbial degradation of organic components. The radioactive waste is emplaced within the excavated volumes. The remaining portion of the volume is consumed with a backfill material, and the pore volume is assumed to be saturated with a suitable brine solution. The schematic of the model is provided in Figure 6-5. The gallery is also backfilled to delay the transport of potential contaminants to the far field and/or directly to the biosphere. In the emplacement chamber gas (mainly CO_2, CH_4, or H_2) is generated. The gas may be dissolved in solution or available in a free gas phase. Pressure may increase over time in the emplacement chambers, as a result of gas generation and rock convergence. This increased pressure may squeeze the gas and/or solution to the upper parts of the mine. A potential region of damage can be created, in the near vicinity of the cavern walls, caused by excavation (thus described as an excavated damaged zone, or EDZ). In addition, natural pathways, galleries and drifts can each provide potential pathways for contaminant transport, both as gas and solution. This attempt is similar to the simulation given in /ALK 06/ with the main and important introduction of the high salinity chemistry via Pitzer activity module. This introduction fulfills the deficiency of the previous models originated from the use of Debye-Hückel activity model that is limited only for lower salinity solutions.

In this model, the gas generation rate was approximated from previous studies to be 9×10^{-11} kg/(s.m^3 waste), assuming a transformation of the organic carbon to CO_2. Mineral composition of the rock salt was set to as given in Table 6.4. Two different compositions of backfill materials were applied. The first one represented standard backfill material used with waste disposal in rock salt (Backfill C, C=Cement), consisting mainly of halite (40%) and portlandite (50%). The second one is brucite-based backfill material, also called Mg-Depot (Backfill B, B=Brucite). In previous studies, it was concluded that this backfill material has advantages over cement based backfill materials for setting up a robust geochemical environment and hydraulics. A small amount of iron was included in each composition to simulate dissolved steel from waste containers. Secondary phases, likely to exist in the backfill, were also added to the composition.

The chemical activity of CO_2 is known to be very high in comparison to the other gases present in the emplacement tunnel - chambers and when CO_2 is generated in an emplacement chamber, three mechanisms contribute to the gas dissolution rate in the solution:

(1) The molecular diffusion of the CO_2 within the aqueous phase.
(2) Reactions of dissolved gas and the host mineralogy, with dissolving or precipitating carbonate minerals possibly changing the dissolution capacity of the aqueous phase.
(3) Convective mixing, resulting from the density of the brine saturated with CO_2 being ~1% greater than the unsaturated brine11. When the layer of saturated brine becomes thick, instability sets in, and plumes of brine saturated with CO_2 migrate downwards, slowly becoming diluted.

To study how molecular diffusion affects the CO_2 dissolution rate, a modeling run omitting molecular diffusion was performed. In the previous runs, the diffusion coefficient of CO_2 in the aqueous phase was set to be 3.10^9 m^2/s. The effect of omitting the molecular diffusion

between the gas and aqueous phases results in a delay in CO_2 diffusion to the distance of the protection fluid. The volume of dissolved CO_2 increases first in the vicinity of the source term blocks. After local saturation of the dissolved gas in the solution, CO_2 goes out the solution forming a free gas phase.

6.3.2.1 Thermal-Hydraulic Issues

The basic run performed using the NaCl solution as pore fluid. As the salinity of the fluid is higher than 1 M, the ECO2N module was applied as the EOS module. Using TOUGHREACT, the solubility of CO_2 in salt solution is modelled according to Spycher and Pruess /SPY 05/. In this model, the salinity is expressed as NaCl equivalent molality. This reveals that the phase behavior module ECO2N is not fully coupled to the reactive code, in which the ionic strength is calculated based on the components of the aqueous phase. Using an $MgCl_2$-based aqueous phase in reactive transport modeling, and then modeling the phase behavior with NaCl-equivalent salinity in this model, poses potential consistency problems. However, the approach is acceptable as long as the physical properties and (respectively) the solubility properties of both systems are comparable. In the present model, a 6M NaCl (app. 0,26 mass ratio, kg/kg) solution is used for representing the phase behavior of a 4M $MgCl_2$-based aqueous system. Figure 6-25 compares the solubility of CO2 in the solutions of 2M NaCl and 4M $MgCl_2$, according to the following model of Duan et al. /DUA 03/, /DUA 06/:

$$\ln(m_{CO2}) = \ln y_{CO2}\phi_{CO2}p - \mu_{CO2}/RT - 2\lambda_{CO2-Na}(m_{Na}+m_K+2m_{Ca}+2m_{Mg})$$

$$-\zeta_{CO2-Na-Cl}m_{Cl}(m_{Na}+m_K+m_{Mg}+m_{Ca})+0.07m_{SO4} \quad (6\text{-}9)$$

where T is absolute temperature in Kelvin, p represents the total pressure of the system in bar, R is the universal gas constant, m is the molality of components dissolved in water, y_{CO2} is the mole fraction of CO_2 in vapor phase, ϕ_{CO2} is the fugacity coefficient of CO_2, μ_{CO2} is the standard chemical potential of CO2 in liquid phase, λ_{CO2}–Na is the interaction parameter between CO_2 and Na+, and $\zeta_{CO2-Na-Cl}$ is the interaction parameter between CO_2 and Na+, Cl-. The fugacity coefficient of CO2, ϕ_{CO2}, is calculated as a function of temperature and pressure, as proposed in the same study.

This CO_2 dissolved in water or in salt solutions results in the enrichment of the CO_2 related ions in water namely CO_3^{-2} and HCO_3^-. The carbonate ions is the main cause of reactive activity in the case of CO_2 generation from the organic waste, this will be studied later.

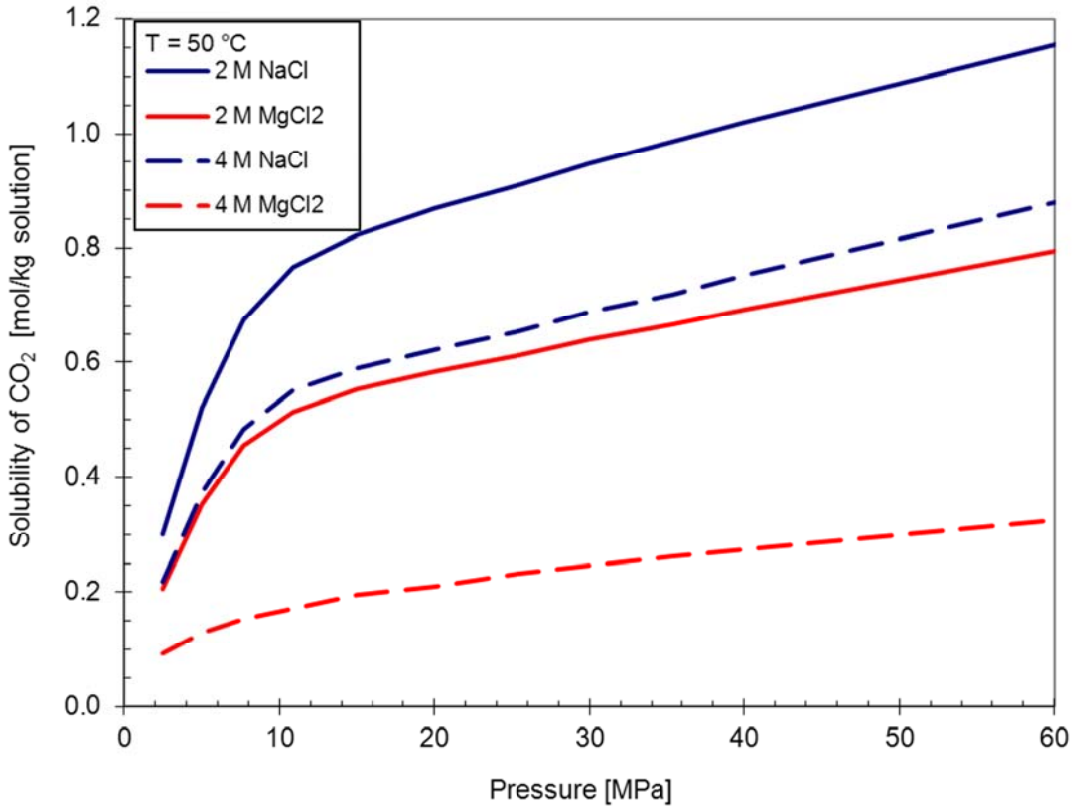

Figure 6-25 Comparison of the CO_2 solubility in solutions with various salinities

The calculated pressure distribution in and around the emplacement chamber after 100 years is given in Figure 6-26. As shown in the Figure the assumed gas generation rate is high enough to create a pressure excess of approximately 2 Bar in the emplacement chamber compared to drift gallery. After 1000 years, the pressure in the emplacement chamber reaches 20 MPa, showing a decreasing but uniform distribution around the drift as seen in Figure 6-28. Note that the figure shows the pressure created by CO_2 dissolved in water after 1000 years of simulation omitting the diffusion of CO_2 in water. Figure 6-28 shows on the other hand the pressure distribution around the emplacement chamber and drift after 1000 years by assuming the diffusion of CO_2 in water and an EDZ around the drift. The introduction of an ED zone of 1 m thickness around the gallery makes a slight difference on the pressure distribution around the emplacement. Figure 6-29 depicts the dissolved CO_2 concentration around the emplacement chamber. As can be observed the maximum pressure reaches only about 14 MPa and a wider distribution of the CO_2 in water is observed around the drift. The distribution of the CO_2 dissolved in water in and around the drift is shown in Figure 6-29. The maximum CO_2 dissolved in water is only about 1,4% as mass ratio. This is low compared to the maximum dissolution of CO_2 in water (pure water), however expected because of the high salinity of the water and lower solubility of CO_2 in high salinity brines than in pure water. From the safety point of view the diffusion of CO_2 containing radioactive traces in the water is essential; based on the worst case calculations performed dissolved CO_2 reaches approximately 50 m away from the drift after 5000 years. It should be noted that this result is due to the assumption that the host rock mass is homogeneous and no higher permeability pathways exists.

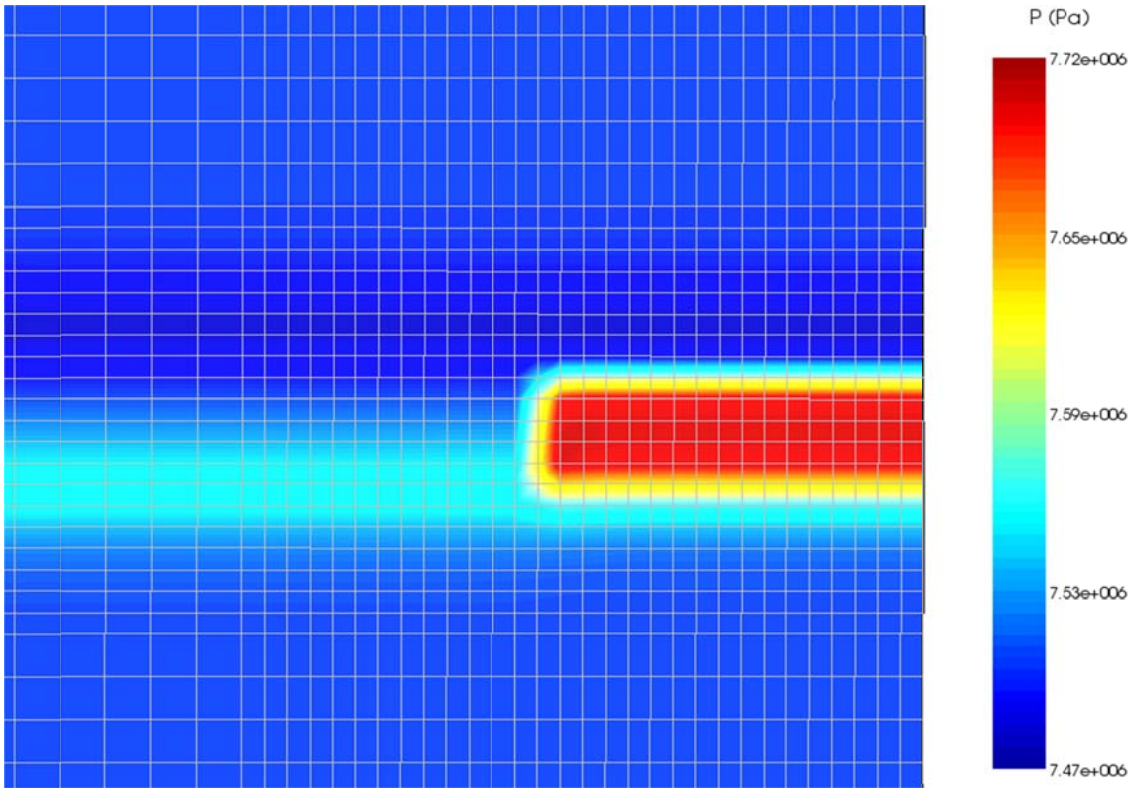

Figure 6-26 Pressure profile around and in the emplacement chamber after 100 years of simulation.

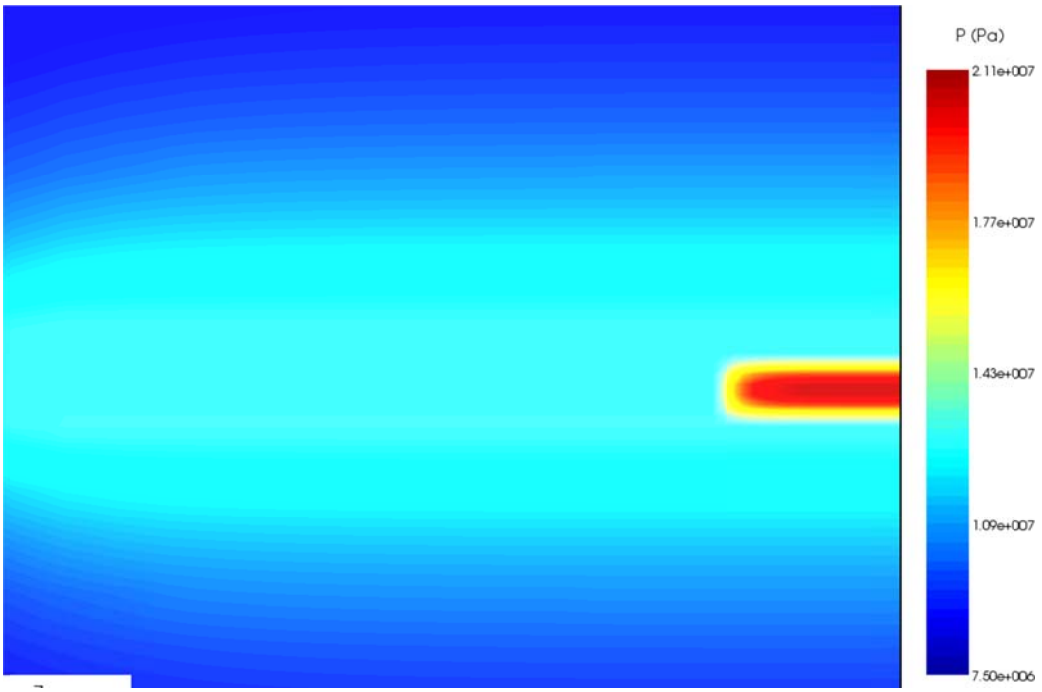

Figure 6-27 Pressure distribution around the drift after 1000 years of simulation.

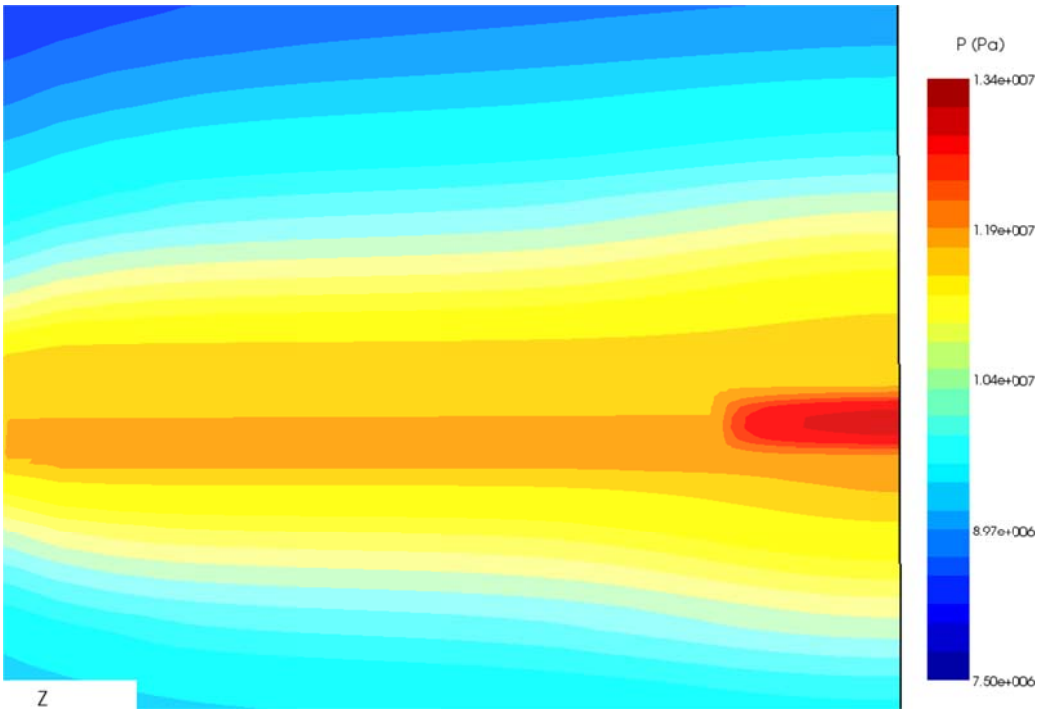

Figure 6-28 Pressure distribution around the drift after 1000 years (assuming the CO_2 diffusion in water and an EDZ of 1 m around the gallery)

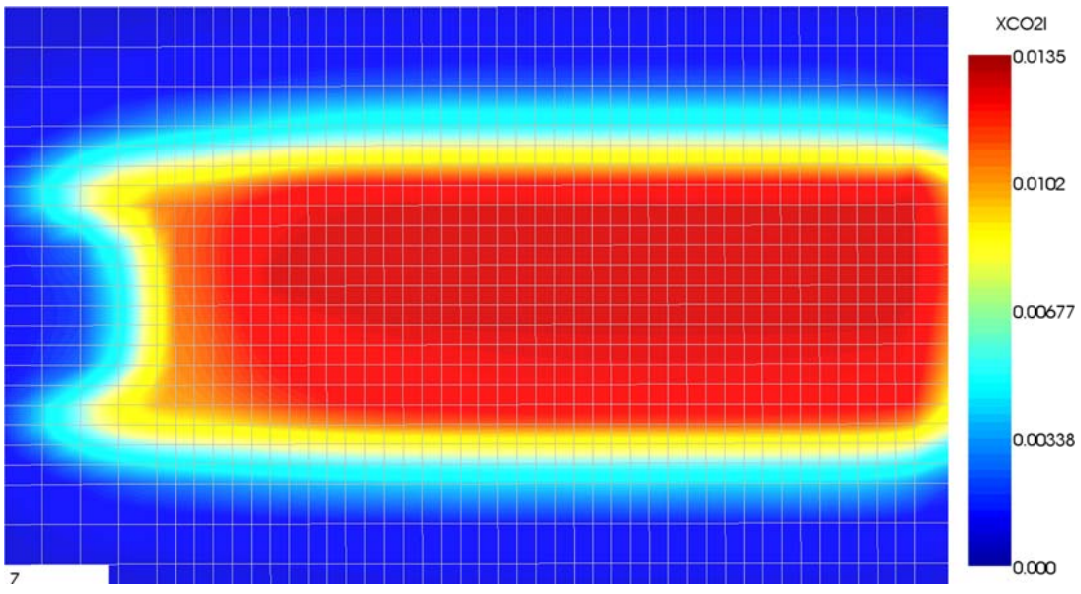

Figure 6-29 Dissolved CO_2 concentration around the drift after 1000 years (assuming the CO_2 diffusion in water and an EDZ of 1 m around the gallery).

Free gas was observed firstly after 500 years approximately. The free gas distribution after 2000 years is shown in Figure 6-30. After 2000 years maximum gas saturation reaches 0,20 approximately and is limited mainly in the emplacement chamber with an accumulation on the top of the chamber. Here it should be noted that the free gas amount accumulated and gas saturation is strictly dependent on the gas generation scenario given as input.

The formation of free gas is especially important taking the two-phase conditions into account. In this case due to the its higher mobility, gas being generated moves more rapidly towards the lower pressure areas, i.e. to the upper parts of the repository namely to the direction of biosphere. The flow of the gas is obviously dependent on the petrophysical parameters in particular on two-phase properties such as relative permeability and capillary pressure which in turn influenced by many factors. One of these factors is the chemical interactions as the case given in the following.

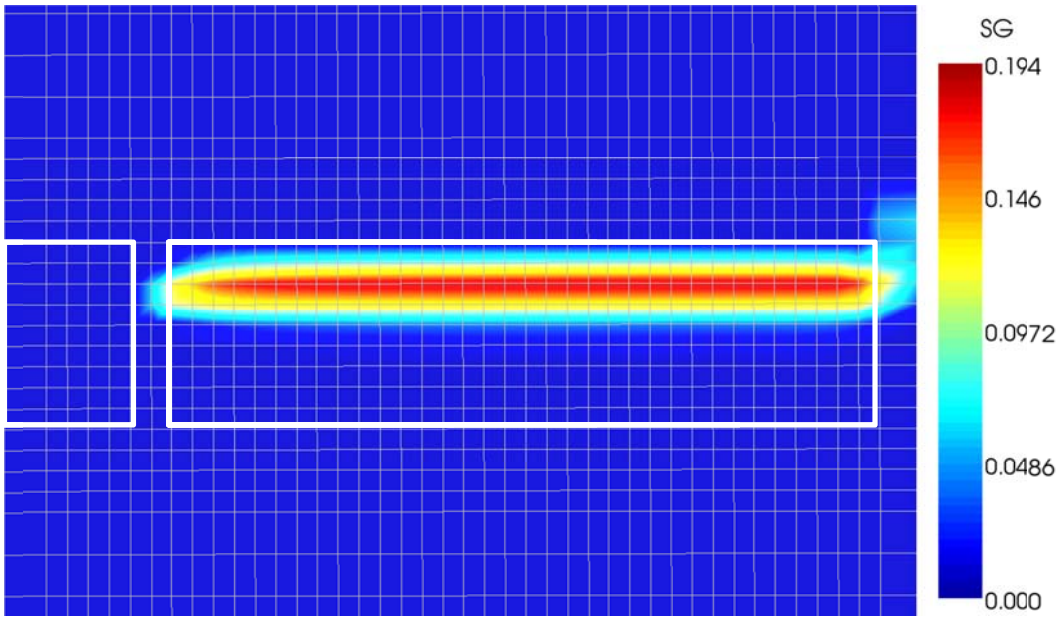

Figure 6-30 Distribution of free gas in the emplacement chamber after 2000 years of simulation.

6.3.2.2 Reactive Coupling

Reactive modeling is especially important for the case of MLW disposal containing organic material as the reactivity of CO_2 generated from organic wastes may have major effects on the transport properties of radioactive traces with gas or fluid mowing to the upper parts of the repository. Four main modeling cases were studied based on realistic scenarios mentioned in previous sections. Related runs are listed in Table 6.9. Additional runs were also performed to study the sensitivity of the simulation results to process parameters such as gas generation rate and dissolution characteristics. The runs were initialized according to the cases studied and performed for a time period of up to 5,000 years. The main output parameters were phase saturations and mineral abundances, porosity-permeability values, geochemical data such as pH, aqueous and solid phase compositions.

Table 6.9 Runs performed in order to evaluate the reactive transport phenomena

Run Name	Description
DRIFT_BufferC_N	Buffer C, solution N
DRIFT_BufferC_Q	Buffer C, solution Q
DRIFT_BufferB_Q	Buffer B, solution Q
DRIFT_BufferB_Q_Comp_EDZ	Buffer B, solution Q with compaction and EDZ

Case 1: Backfill C, Solution N

The first modeling run was performed for Solution N with standard backfill material, C. After 1000 years of simulation, the CO_2 mass ratio (kg/kg) in solution in the emplacement chamber remained below 0,02 due to limited solubility in high salinity brine. The highest gas saturation after 1000 years remained below 0,05. Because of the CO_2 dissolution in brine, the salinity of the brine decreased a small portion in the location where the CO_2 accumulation is highest. The most important aspect is the decrease in the pH of the protection fluid due to the dissolution of CO_2 causing an enhancement of the bicarbonate ions in the solution. However, the low precipitation of the carbonate minerals yields high CO_3^{2-} concentrations in solution, which can increase concentrations of radionuclide elements. This decrease of pH is expected to enhance the corrosion and the dissolution rate of some minerals such as portlandite, fosterite and calcite. The dissolution (oxidation) of iron was apparent, with a reduction of approximately 0.05% of the free volume. The iron based minerals such as fayalite, magnesite and hematite on the other hand tend to precipitate. Some dissolution of halite is also observed which can be related to the change in the composition of the brine because of the increase of some ions. As a result of the precipitation-dissolution interactions, changes in the porosity of the buffer take place. This is apparent by a slight decrease in the emplacement chamber. . This reduced porosity also implies a decrease in permeability in this region, causing a lower conductivity for the CO_2-containing fluid to the upper parts of the repository.

Case 2: Backfill C, Solution Q

In the second case, modeling was carried out using Solution Q with Backfill C (DRIFT_BufferC_Q). In addition to the cases reported by /ALK 07/, the composition given in Table 6.3 is used to model the mentioned case fully. The material compositions were identical to the previous case (DRIFT_BufferC_N). Similar secondary phases as listed in Table 6.7 are given in this simulation case.

The main issue in this run is the decrease of the pH below 5. As a result of the CO_2 forming carbonic acid, the pH value decreases to 4,6 in the emplacement chamber. This yields a higher corrosion rate from the first hand. This result, while in agreement with previous experimental studies, is not desirable, since the solubility of the radioactive elements is increased

at low pH values. No free gas is present in the system, and the porosity increases slightly because of the increasing mineral dissolution in the emplacement chamber.

Case 3: Solution Q, Backfill B

Backfill B was introduced to investigate how the brucite-based backfill would affect the geochemical environment of the system and its stability. This case is relevant with its effect on the pH of the system. A comparison of the pH's of the system studied is given in Figure 6-31 As seen from the figure the pH is lower for the case DRIFT_BufferC_Q as indicated in previous section. The pH for the case DRIFT_BufferB_Q remains at a relatively higher level even after 1000 years because of the buffering effect of the brucite. Figure 6-32 shows on the other hand the distribution of the pH in the drift for the cases DRIFT_BufferB_Q and DRIFT_BufferC_Q. The difference on pH is apparent and especially drastic in emplacement chamber. As discussed in previous chapters, a decrease in pH has at least two important impacts on the transport phenomena in the repository. Firstly it increases the corrosion rate and secondly it causes the dissolution of minerals increasing the porosity thus the permeability.

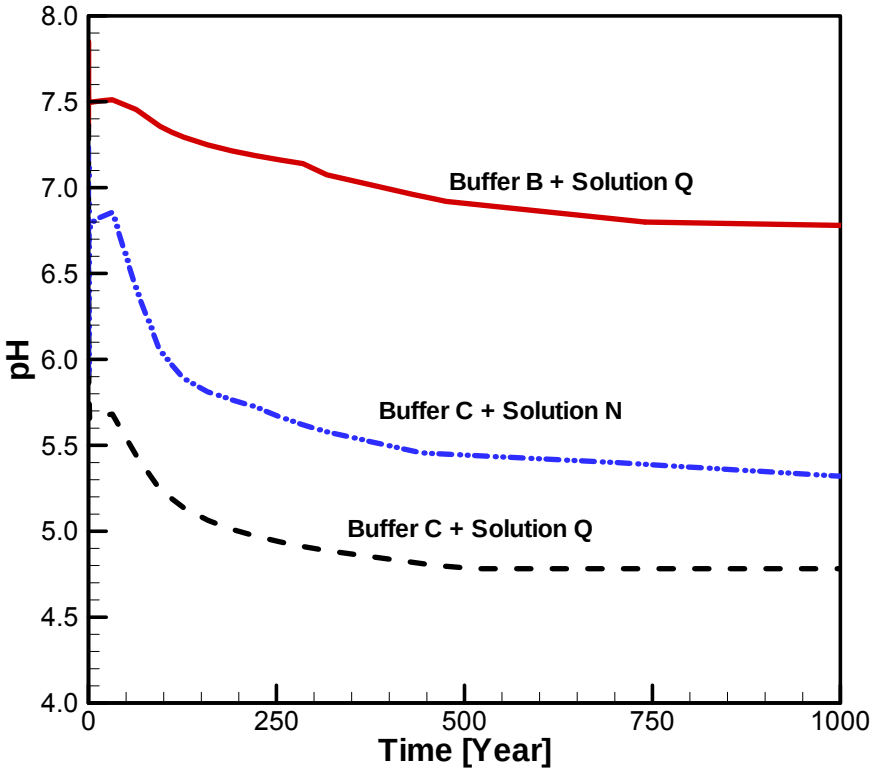

Figure 6-31 Calculated change of the pH for 1000 years in the emplacement chamber for various runs

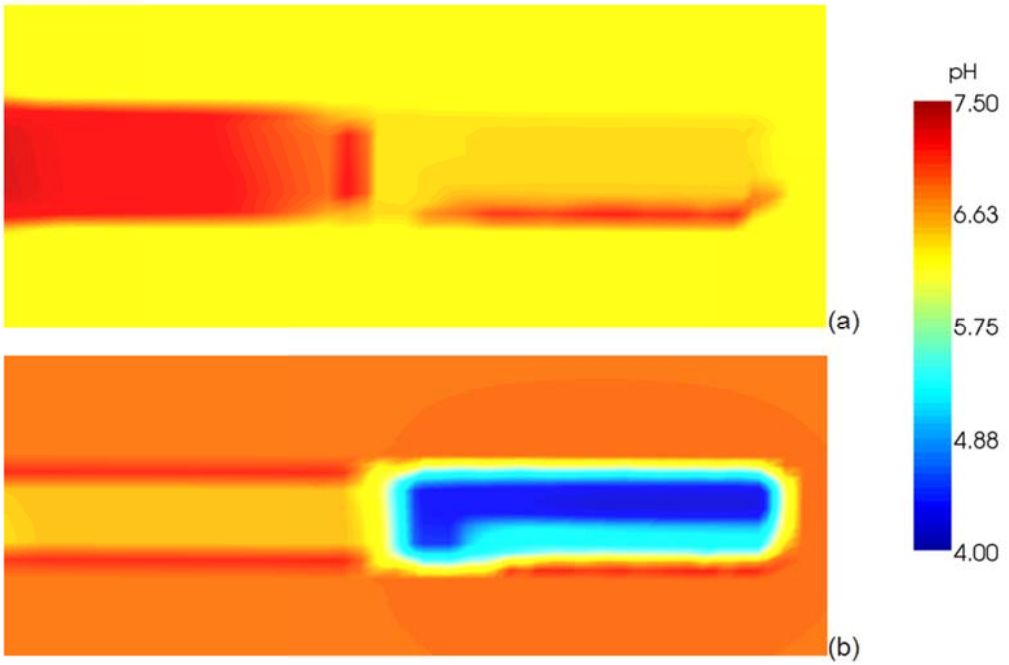

Figure 6-32 pH distribution in the drift after 1000 years of simulation for the cases DRIFT_BufferB_Q (a) and DRIFT_BufferC_Q (b)

The corrosion of the metal containers is observed as the decrease in iron volume as given in Figure 6-33 resulting in an increase in the volume (precipitation) of the iron based minerals such as magnesite and fayalite. The changes in volume of some minerals given as input are depicted in Figure 6-34. As can be seen the volume of calcite, brucite, pyrite were increased causing a decrease in the porosity. The decrease in porosity and permeability is favorable in terms of transport of the contaminants. The decrease in porosity due to chemical interactions is considerably higher for the case of brucite buffer as can be concluded in Figure 6-35. This offers an obvious advantage in terms of the transport of the radionuclides by reducing the permeability.

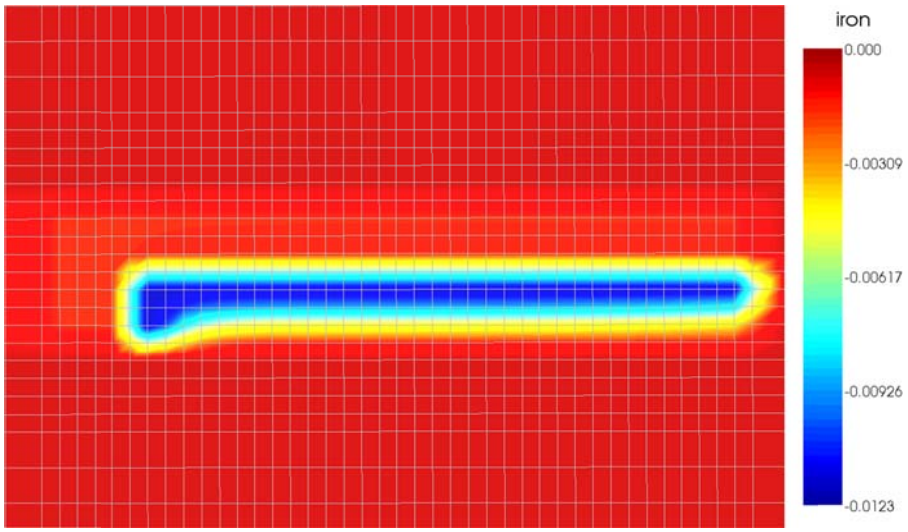

Figure 6-33 Decrease in volume (dissolution) of iron as the result of the corrosion

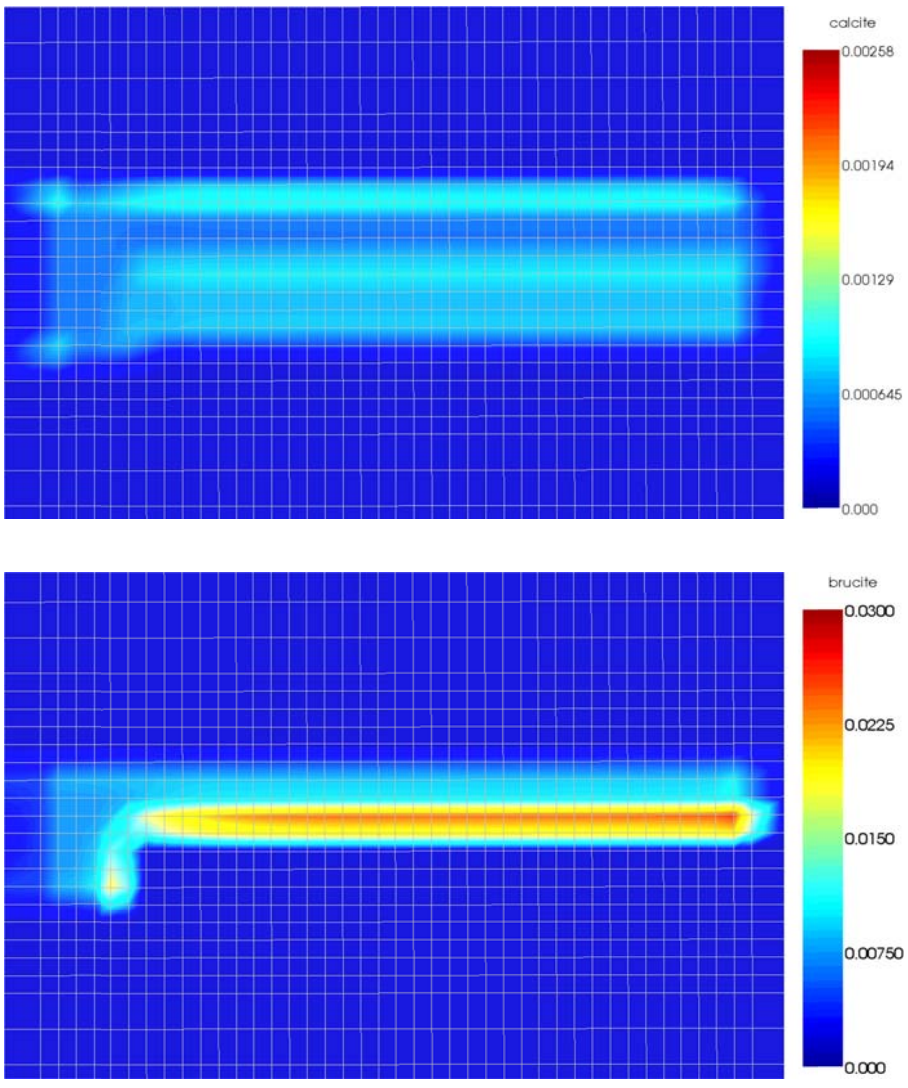

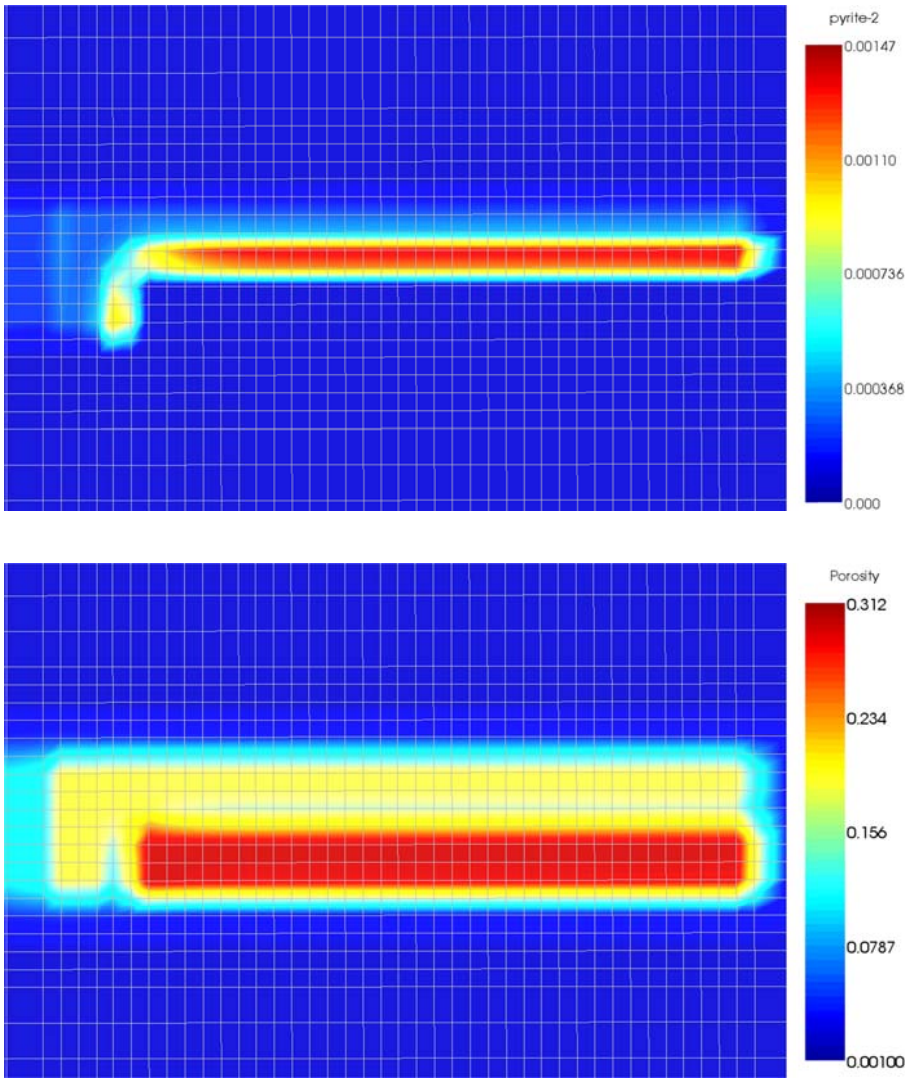

Figure 6-34 Increase in volume of the some minerals (precipitation) yielding a decrease in the repository chamber and resulting porosity at the end of 1000 years simulation DRIFT_BufferB_Q

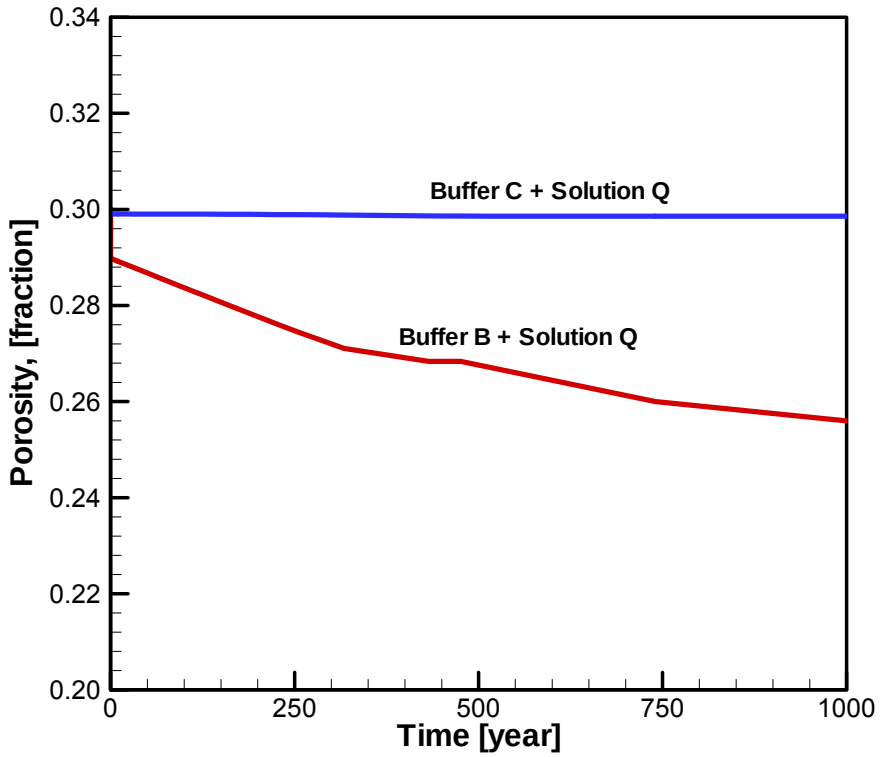

Figure 6-35 Change in porosity in the emplacement chamber with various models

7 REMARKS AND CONCLUSIONS

The improvements in TOUGHREACT planned in the framework of the project "BMWi-02E10467" were performed. These consist of the implementations of Pitzer activity model for a more realistic simulation of the high salinity geosystems, the implementation of a swelling model for bentonite-sand mixtures as buffer material to be used in radioactive repositories and the implementation of a compaction model for rock salt. These implementations were validated, tested and studied. The resulting program was used for modeling the reactive flow in various cases which can basically distinguished as salt and clay as host rocks for underground HLW and MLW disposal. Various runs were conducted to discuss the performance of the improvements performed as well as the implications of THMC issues on safety conditions in the repository. Following general remarks can be made:

1. The Pitzer Activity Module had to be programmed, implemented, tested and validated by internal possibilities. This activity which was not originally planned in the project caused two main difficulties:
    a. A time gap of at least 6 months was occurred in respect of the original time schedule.
    b. The testing and validation of the module needed additional efforts. To reduce these efforts, the methodology and validation cases of Lawrence Berkeley National Laboratory (LNBL), University of California were principally followed. To reduce the knowledge and experience gap between the developers of TOUGHREACT a visit of approximately 2 months co-financed by Alexander von Humboldt Foundation was planned and realised. This visit was served to discuss and solve some problems related the implementation and validation of Pitzer Activity Module.
    c. The databank proposed by LNBL was basically used. Only some limited changes were performed.
    d. A 2th version of TOUGHREACT including the Pitzer Activity Module as an option has been prepared by LBNL for a release by Department of Energy, USA. This version that is due to an immense work on the subject should be provided for further projects on the reactive transport phenomena in underground radioactive repositories.
2. The modeling and implementation of the salt compaction was performed based on the previous studies of ISTec on the subject as proposed originally in the project. A review and further improvement of the methodology is required.
3. The swelling of the bentonite/sand mixtures was simulated with a model for which the validity in higher salinity systems should be further studied.
4. The time consuming numerical modeling process by using Pitzer Activity Module has been one of the main problems during the study. This necessitated the limiting of the size and the discretisation of the numerical models which also somehow limits the consideration of the effect of the boundary conditions on the results. The necessity of the use of the finer grid blocs for reliable results in reactive modeling is another limiting factor. The use of more powerful computers would be a solution to this problem. Another solution can be the optimisation of the algorithms and the programs by software specialists.

5. The present study also implies the importance of a cooperative work for conducting such software development projects as the case for other projects of nuclear repository issues. The cooperation of engineers and physicians is especially important as the problem is rather an optimisation issue of the safety requirements in one hand and the realistic and validated prognosis of the reactive transport parameters on the other hand.

Besides of these remarks, following conclusions can be drawn based on the numerical applications performed in clay and salt as host rock for HLW and MLW with organic content:

1. Numerical evaluations were performed based on three models basically; i. Clay as host rock in a borehole repository concept, ii. Salt as host rock in a borehole repository concept, iii. Salt as host rock in a drift repository concept. The swelling of bentonite as well as the compaction of salt were introduced to thermal-hydraulic and chemical issues in each model. Pitzer module was used for all cases.
2. The modeling of heat generation for a HWL container shows that temperatures as high as 130 °C may occur in the repository in the vicinity of the containers after one year of repository whereas it decreases beyond 50 °C after 1000 years. It should be noted that the maximum temperature reflects the temperatures around the container blocks.
3. The most important conclusion of the “CLAY_plus_reactive” which takes the swelling into account is the strong and rapid decrease of the porosity around the container. The variation in porosity is due to firstly swelling and secondly to the precipitation/dissolution of the minerals where the swelling is a more rapid process causing the reduction in pore volume. The metallic corrosion provides iron which is incorporated in ferrous minerals mainly near the cell of the steel container corrosion.
4. As already highlighted magnetite is the main corrosion product in reducing conditions. Siderite precipitates but the corresponding volumes are low and cannot be distinguished. The siderite precipitation is limited by the CO_2 partial pressure which was not imposed at a given value during modeling.
5. The montmorillonite-to-chlorite conversion was observed also as a potential chemical process for bentonite barrier in the radioactive waste repository because of the iron excess by the container corrosion. As expected high iron concentration favors the Na/Ca–montmorillonite dissolution. In fact, the Na/Ca–montmorillonite dissolution is calculated to be more significant near the container.
6. In “SALT_reactive” any buffering effect is lacking and the pH increases within a very short time (few days) up the values 12. A comparison of the iron dissolution gives the advantage of using brucite buffer with Q solution clearly. In the latest case corrosion stability of this buffer combination was higher than previous case. The pH increases shortly after the simulation start to a level of 7,30 but remains at this value constant. This value is calculated to be constant as long as magnesium level is sufficiently high for buffering the pH and brucite $MgOH_2$ precipitates.
7. The drift modeling attempt is similar to the simulation given in /ALK 07/ with the main and important introduction of the high salinity chemistry via Pitzer activity module.

This introduction fulfills the deficiency of the previous models originated from the use of Debye-Hückel activity model that is limited only for lower salinity solutions.

8. The main issue in the run performed with cement buffer with Q solution is the decrease of the pH below 5. As a result of the CO_2 forming carbonic acid, the pH value decreases to 4,6 in the emplacement chamber. This yields a higher corrosion rate from the first hand and higher solubilities of the radionuclides in the pore fluid.
9. Backfill B was introduced to investigate how the brucite-based backfill would affect the geochemical environment of the system and its stability. This case is relevant with its effect on the pH of the system. The pH is higher at the level of approximately 6,7 for this case and stays stabile even after 1000's years. So it offers lower corrosion rates and lower solubilities of the radionuclides. The calculated precipitation of carbonates is another advantage for lower mobility of the contaminants.

8 REFERENCES

/ADE 93/ Adenekan, A.E., Patzek, T.W., Pruess, K.
Modeling of multiphase transport of multicomponent contaminants and heat in the subsurface-numerical model formulation, Water Resources Research, vol. 29, no. 11, 1993, pp. 3727-3740

/ALK 06/ Alkan, H., Bracke, G., W. Müller
TOUGHREACT/ECO2 on reactive transport modeling of CO_2 in a geological repository, Proceedings TOUGH Symposium 2006, Lawrence Berkeley National Laboratory, Berkeley, California, May 15–17, 2006

/ALK 07/ Alkan H., Müller W.
Untersuchungen zur Behälterkorrosion, der daraus resultierenden Gasbildung sowie deren Wirkung auf die Bentonitummantelung, ISTec-A–129, December 2007.

/ALT 04/ Altmaier, M., Brendler, V., Bosbach, D., Kienzler, B., Marquart, C., Neck, V., Richter, A.
Geochemische Prozesse bei der Ausbreitung von Schadstoffen aus einem Endlager für Radioaktive Abfälle, FZK-INE 002/04, 2004

/APP 93/ Appelo, C. A. J., Postma, D.,
Geochemistry, groundwater and pollution, Rotterdam, The Netherlands, Balkema, 1993, 536 pp.

/APP 94/ Appelo, C.A.J.,
Cation and proton exchange, pH variations, and carbonate reactions in an aquifer, Water Resource Res. 30, 1994, 2793– 2805.

/ARC 03/ Arcos, D., Bruno J., Karnland O.,
Clay Microstructure. Geochemical model of the granite–bentonite–groundwater interaction at Äspö HRL (LOT experiment) Applied Clay Science Volume 23, Issues 1-4, August 2003, 219-228

/BER 80/ Berner R.A.
Early Diagnosis: A Theoretical Approach, Princeton Univ. Press, 1980, p. 241 ff

/BER 92/ Berner U.R.
Evolution of pore water chemistry during degradation of cement in a radioactive waste repository environment, Waste Manag. 12, 1992, pp 201–219,

/BOL 56/ Bolt G.H.
Physico-chemical analysis of the compressibility of pure clays. Géotechnique, 6(2), 1956, pp 86–93

/BRA 03/ Bracke G., Müller W.
Modeling the Gas Generation of Intermediate and Low Level Radioactive Wastes, Proceedings ICEM ’03 „9th International Conference on Radioactive Waste Management and Environmental Remediation“, Oxford England, September 21 – 25, 2003

/BRE 08/ Brennecke, P., Kugel, K., Möller, K.
Mengen, Konditionierung, Zwischen-und Endlagerung radioaktiver Abfälle-Sachstandbericht zum 30. April 2008, Fachbereich Sicherheit nuklearer Entsorgung

/BRO 51/ Brown, H.W.
Capillary Pressure Investigations
Trans. AIME 192, 67, 1951

/BRO 64/ Brooks, R.H., Corey, A.T.
Hydraulic Properties of Porous Media
Hydrology Papers of Colorado State University, No. 3, 1964

/BRU 02/ Brun, A., Engesgaard, P., Christense, T.H., Rosbjerg, D.
Modeling of transport and biogeochemical processes in pollution plumes: Vejen landfill, Denmark, J. Hydrol. 256, 2002, pp 228– 247,

/BUC 89/ Bucher F., Müller-Vonmoos, M.
Bentonite as a containment barrier for the disposal of highly radioactive wastes, Appl. Clay Sci. (4), 1989, pp 157-177

/BUR 06/ Burnol A., Blanc P., Xu T., Spycher N., Gaucher E.C.
Uncertainty In The Reactive Transport Model Response To An Alkaline Perturbation In A Clay Formation Proceedings, Tough Symposium 2006 Lawrence Berkeley National Laboratory, Berkeley, California, May 15–17, 2006

/CAS 48/ Casimir H.B.C., Polder, D.
The influence of retardation of the London–van der Waals forces. Physical Review, 73, 1948, p. 360 ff

/CLA 02/ Claret, F., Bauer, A., Schäfer T., Griffaut, L., Lansion, B.
Experimental investigations of the interactions of clays with high pH solutions: a case study from the collovo-oxfordian formation, Clays and Clay Minerals, 50, 5, 633-646, 2002

/CIN 06/ Cinar, Y., Pusch, G., Reitenbach, V.
Petrophysical and capillary properties of compacted salt, Transport in Porous Media, 64 (2), 2006, pp. 199-228.

/COL 86/ Colten, V. A.
Hydration states of smectite in NaCl brines at elevated pressures and temperatures, Clays Clay Min. (34,4), 1986, pp 385-389

/DAI 06/ Dai, Z., Samper, J.
Inverse modeling of water flow and multicomponent reactive transport in coastal aquifer systems. JHydrol 327(3–4) 2006, pp 447–461

/DAV 95/ Davies, P. et al. .
Using a multiphase flow code to model he coupled effects of repository consolidation and multiphase brine and gas flow at the WIPP, SAND95-2244C, 1995

/DIX 96/ Dixon, D.A., Gray, M.N., Graham, J.
Swelling and hydraulic properties of bentonites from Japan, Canada and the USA. In Proceedings of the 2nd International Congress on Environmental Geotechnics, Vol. 1, 1996, pp. 43–48

/DUA 03/ Duan, Z., Sunc, R.
An Improved Model Calculating CO2 Solubility in Pure Water and Aqueous NaCl Solutions from 273 To 533 K and from 0 To 2000 Bar", Chemical Geology 193, 2003, pp 257– 271

/DUA 06/ Duan, Z., Sun, R., Zhu, C., Chou, I-M.
An Improved Model for the Calculation of CO2 Solubility in Aqueous Solutions Containing Na+, K+, Ca2+, Mg2+, Cl_, and SO42_, Marine Chemistry, 98, 2006, pp 131-139

/ENG 96/ Engesgaard P., Traberg R.
Contaminant transport at a waste residue 2. Geochemical transport modeling, Water Resource, Res.32, 1996, 939– 951,

/FAN 98/ Fanghanel, Th., Weger, H.T., Konnecke, Th., Neck, V., Paviet-Harmann, P., Steinle, E., Kim, J.I.
Thermodynamics of Cm (III) in concentrated electrolyte solutions: carbonate complexation at constant ionic strength. Radiochem. Acta 82, 1998, pp 47–53

/FER 06/ Fernandez F., Cuevas, J., Sanchez L., Villa R.
Reactivity of the cement–bentonite interface with alkaline solutions using transport cells, Applied Geochemistry 21, 2006, 977–992

/FRE 95/ Freeze, G.A., Larson, K.W., Davies, P.B.
A Summary of Methods for Approximating Salt Creep and Disposal Room Closure in Numerical Models of Multiphase Flow
SAND94-0251, Albuquerque, Sandia National Laboratories, 1995

/GEN 80/ van Genuchten, M.Th.
A Closed-Form Equation for Predicting the Hydraulic Conductivity of Unsaturated Soils
Soil. Sci. Soc. A.J. 44, pp.892-898, 1980

/GOM 97/ Gomit, J.M., Hirsekorn, R.P., Martens, K.-H., Prij, J.
Evaluation of Elements Responsible for the effective Engaged dose rates associated with the final Storage of radioactive waste: Everest project – Volume 3b: Salt formation, sites in France and the Netherlands and common conclusions on salt, EUR 17449/3b EN, ISSN 1018-5593, 1997

/GOM 10/ Gómez-Espina, R., Villar, M.V.
Geochemical and mineralogical changes in compacted MX-80 bentonite submitted to heat and water gradients, Applied Clay Science 47, 2010, 400–408,

/GRA 90/ Grambow, B., Muller, R.
Chemistry of glass corrosion in high saline brines. Mat. Res. Soc. Symp. Proc. Vol. 176, 1990, pp 229–240,

/GUI 99/ Guimera,` J., Duro, L., Jordana, S., Bruno, J.,
Effects of icemelting and redox front migration in fractured rocks of low-permeability. Svensk Karnbranslehantering AB. Report no. TR-99-19. 1999.

/HAR 80/ Harvie, C.E., Weare, J. H.
The Prediction of Mineral Solubilities in Natural Waters:The Na–K–Mg–Ca–Cl–SO4–H2O System from Zero to High Concentration at 25°C, Geochimica, et Cosmochimica Acta, 44, ((7)), Pergamon Press, New York, New York 1980, pp 981-997

/HEL 68/ Helgeson H.C.
Evaluation of irreversible reactions in geochemical processes involving minerals and aqueous solutions: I. Thermodynamic relations, Geochim. Cosmochim. Acta 32, 1968, pp 853–877.

/HEL 69/ Helgeson H.C., Garrels R.M., MacKenzie F.T.
Evaluation of irreversible reactions in geochemical processes involving minerals and aqueous solutions: II. Applications, Geochim.Cosmochim. Acta 33, 1969, pp 455– 482.

/HER 99/ Herbert, H.-J., Moog, H. C.
Cation exchange, interlayer spacing and water content of MX-80 bentonite in high molar saline solutions, Engineering Geology 54, 1999, pp 55-65

/HER 02/ Herbert, H-J., Kasbohn, J., Venz, C., Kull H., Moog, H., Sprenger, H. Langzeitstabilität von Tondichtungen in Salzformationen, GRS-185, Juni 2002

/HER 06/ Herbert, H.-J.,
Modellentwicklung zur Quellung hochkompaktierter Bentonite: Bentonite im Kontakt mit Lösungen unterschiedlicher Salinität im Temperatur Bereich von 25 – 120°C, GRS-211, November 2006

/HOC 95/ Ho, C.K., Dunn, E., Sobolik, S.R.
"Ventilation and Vapor-Phase Transport Near the ESF Tunnel," Proceedings of the Sixth Annual International Conference on High Level Radioactive Waste Management, American Nuclear Society and American Society of Civil Engineers, Eds., Las Vegas, NV, May 1-4, 1995

/HOR 99/ S.T. Horseman, J.F. Harrington, P. Sellin
Gas Migration in Clay Barriers, Engineering Geology, 54 139-149, 1999

/HUN 98/ Hunter, K.S., Wang, Y., Van Cappellen, P.
Kinetic modeling of microbially-driven redox chemistry of subsurface environments:coupling transport, microbial metabolism and geochemistry.J. Hydrol. 209, 1998, pp 53–80

/JAV 97/ Javeri, V.
Vergleichende Analysen zum Nuklidtransport in einem vereinfachten Grubengebäude eines Endlagers im Salinar, GRS - A - 2411, 1997

/JAV 98/ Javeri, V.
Combined Gas and Nuclide Transport in a Two Dimensional Repository Considering Variable Rock Convergence
TOUGH Workshop ’98, Lawrence Berkeley Laboratory (LBNL), LNBL-41995 Berkeley, May 4-6, 1998

/JON 94/ Johnson, T.M., DePaolo, D.J.
Interpretation of isotopic data in groundwater–rock systems—model development and application to Sr isotope data from Yucca Mountain, Water Resour. Res. 30, 1994, pp 1571–1587

/KAB 91/ Kabala, Z.J., Sposito, G.
A stochastic model of reactive solute transport with time-varying velocity in a heterogeneous aquifer, Water Resour. Res. 27, 1991, pp 341– 350,

/KAR 98/ Karnland, O.
Bentonite Swelling pressure in strong NaCl solutions, Posiva 98-01, Helsinki, Finland 1998

/KAU 09/ Kaufhold, Dohrmann, R S.
Stability of bentonites in salt solutions | sodium chloride, Applied Clay Science, v 45, n 3, p 171-177, July 2009

/KEN 92/ Kenny, T.C., van Veen, W.A., Swallow, M.A., Sungaila, M.A.
Hydraulic conductivity of compacted bentonite–sand mixtures. Canadian Geotechnical Journal 29, 1992, pp 364–374

/KER 05/ Kerry MacQuarrie, T.B., Mayer, K. U.
Reactive transport modeling in fractured rock: A state-of-the-science review, Earth-Science Reviews 72 189–227, 2005

/KIE 98/ Keinzler, B., Vejmelka, P.
Geochemische Modellierung der Korrosion von Zementierten Abfallprodukten in Salzlösungen, FZKA 6046, Karlsruhe 1998

/KIM 99/ Kim J.I., Grambow, B.
Geochemical assessment of actinide isolation in a German salt repository environment, Engineering Geology 52, 1999, pp 221–230

/KOM 94/ Komine H., Ogata N.
Experimental study on swelling characteristics of compacted bentonite, Canadian geotechnical journal, Canadian Geotechnical Journal 31, 1994, pp 478–490.

/KOM 96/ Komine, H., Ogata, N.
Prediction for swelling characteristics of compacted bentonite. Canadian Geotechnical Journal 33, 1996, pp 11–22

/KOM 99/ Komine H., Ogata, N.
Experimental study on swelling characteristics of sand–bentonite mixture for nuclear waste disposal. Soils and Foundations, 39(2), 1999, pp 83–97

/KOM 03/ Komine H., Ogata N.
New equations for swelling characteristics of bentonite-based buffer materials, Can. Geotech. J. 40, 2003, pp 460–475

/LEH 96/ Lehikoinen, J., Carlsson, J., Muurinen, A., Olin, M., Salonen, P.
Evaluation of factors affecting diffusion in compacted bentonite, Mat. Res. Soc. Symp. Proc. 412, 1996, 675– 682

/LEV 41/ Leverett, M.C.
Capillary Behavior in Porous Solids
AIME Transactions 142, 1941, pp. 152 – 169

/LIC 85/ Lichtner, P.C.,
Continuum model for simultaneous chemical reactions and mass transport in hydrothermal systems, Geochim. Cosmochim. Acta 49, 1985, pp 779–800.

/LIC 88/ Lichtner P.C
The quasi-stationary state approximation to coupled mass transport and fluid–rock interaction in a porous medium, Geochim. Cosmochim. Acta 52, 1988, pp 143– 165.

/LIC 96/ Lichtner, P.C., Seth, M.
Multiphase-multicomponent nonisothermal reactive transport in partially saturatedporous media. Proceedings of the 1996 International Conference on Deep Geological Disposal of Radioactive Waste, Sept. 16–19. Canadian Nuclear Society, Winnipeg, Manitoba 1996, pp. 133–142

/LIU 98/ Liu, H. H.; Doughty, C., Bodvarsson, G. S.
An Active Fracture Model for Unsaturated Flow and Transport in Fractured Rocks, Water Resour. Res. 1998, v. 34, p. 2633-2646,

/LOR 99/ Lorenz, S., Müller, W,
Modellierung von Zweiphasen-Strömungen in kompaktierendem Salzgrus unter Einbeziehung der Konvergenz
ISTec-A-343, 1999

/LOW 79/ Low, Philip F., Margheim, James F., Walsh, L. M.
The swelling of clay; I, Basic concepts and empirical equations, *Soil Science Society of America Journal*, 43, 3, 473-481

/LUC 04/ Luckscheiter, B., Kienzler, B., Bosbach, D.
Literaturstudie zum Korrosionsverhalten von HAW-Gläsern in Ton: Tongestein und Versatz-Material Forschungszentrum Karlsruhe - Wissenschaftliche Berichte – FZKA 7068, Dezember 2004

/MAH 04/ Maher, K., DePaolo, D.J., Lin, J.C.F.,
Rates of silicate dissolution in deep-sea sediment: in situ measurement using U-234/U-238 of pore fluids, Geochim. Cosmochim. Acta 68, 2004, pp 4629–4648.

/MAL 04/ Malmstrom, M.E., Destouni, G., Martinet, P.
Modeling expected solute concentration in randomly heterogeneous flow

systems with multicomponent reactions, Environ. Sci. Technol. 38, 2004, 2673– 2679.

/MIE 03/ Miehe, R., Kröhn, K-P., Moog, H.,
Hydraulische Kennwerte tonhaltiger Mineralgemische zum Verschluss von Untertagedeponien, GRS-193, November 2003

/MOL 06/ Molinero, J., Samper, J.
Modeling of reactive solute transport infrastructure zones of granitic bedrocks, J Cont. Hydrol 82, 2006, pp 293–318

/MON 05/ Montes-H G.
Swelling–shrinkage measurements of bentonite using coupled environmental scanning electron microscopy and digital image analysis, Journal of Colloid and Interface Science 284, 2005, 271–277

/MOO 02/ Moog, H. C., Kühle T., Buhmann D., Herbert H.-J.
Coupling of transport processes and geochemical processes - a new feature in the EMOS-code, EUROSAFE 2002 - International Forum for Nuclear Safety, vol.3, 2002, p. 9 ff

/MOO 07/ Moog, H.C., Keesmann, S.M.
Modellierung des reaktiven Stofftransports im Nahfeld eines Endlagers, GRS-225, Februar 2007

/MÜL 99/ Müller-Lyda, I., Birthler, H., Fein E.,
Ableitung von Permeabilitäts-Porositätsrelationen für Salzgrus, GRS 148, BMWi 02E 8855-2, Juli 1999

/NAV 00/ Navarro, V., Alonso, E.E.
Modeling swelling soils for disposal barriers, Computers and Geotechnics 27, 2000, p. 19-43

/NEA 91/ NEA Workshop
on gas generation and release from radioactive waste repositories, Aix-en-Provence, 1991

/NIT 90/ Nitao, J.
"Increasing the Efficiency of the TOUGH Code for Running Large-Scale Problems in Nuclear Waste Isolation," Proceedings of the TOUGH Workshop, Report LBL-29710, Lawrence Berkeley Laboratory, Berkeley, CA, pp. 143--148, September 1990, 13-14

/NIT 97/ Nitao, J.
Thermohydrochemical alteration of flow pathways above and below the re-

pository. In: Hardin, E.L. (Ed.), Near-Field Altered Zone Models Report. Lawrence Livermore National Laboratory, Livermore, CA. YMP Milestone SP3100M4, 1997, Chapter 5.6, pp. 57– 67

/NOV 93/ Novak, C.F.,
Modeling mineral dissolution and precipitation indual-porosity fracture-matrix systems* *Journal of Contaminant Hydrology,* 13, 1993, 91-115

/OLD 95/ Oldenburg, C. M., Pruess, K.,
EOS7R: Radionuclide transport for TOUGH2, Lawrence Berkeley National Laboratory Report LBNL-34868, Berkeley, California, 1995

/OSC 90/ Oscarson, D.W., Dixon, D.A., Gray , M.N.
Swelling capacity and permeability of an unprocessed and a processed bentonitic clay, *Engineering Geology,* 28, 1990, p. 281-289

/PAR 80/ Parkhurst, D. L., Thorstenson, D. C., and Plummer, L. N.
PHREEQE: A computer program for geochemical calculations, US Geol. Surv. Water Resour. Invest. 174, 1980, pp.80-96

/PIT 73a/ Pitzer, K. S.
Thermodynamics of electrolytes, I. Theoretical basis and general equations, J. Phys. Chem., 77, 1973, 268– 277

/PIT 73b/ Pitzer, K. S., Mayorga, G.
Thermodynamics of electrolytes. II. Activity and osmotic coefficients for strong electrolytes with one or both ions univalent. J. Phys. Chem. 77, 1973, pp. 2300-2307

/PIT 91/ Pitzer K.S.
Activity Coefficients in Electrolyte Solutions, CRC Press, Boca Raton, 1991

/PRI 91/ Prij, J.
An improved model for the convergence of an excavation in rock salt SMiRT 11 Transactions Vol. L, Paper L19/5, Tokyo, 1991

/PRU 87/ Pruess, K.
TOUGH User's Guide,
Nuclear Regulatory Commission Report NUREG/CR-4645, Lawrence Berkeley Laboratory Report LBL-20700, March 1987

/PRU 99/ Pruess, K., Oldenburg, C., Moridis, G.,
TOUGH2 User's Guide, Version 2, Lawrence Berkeley Laboratory Report LBL-43134, November 1999

/PRU 05/ Pruess K.,
ECO2N: A TOUGH2 Fluid Property Module for Mixtures of Water, NaCl, and CO2 LBNL-57952 Earth Sciences Division, Lawrence Berkeley National Laboratory, August 2005

/PSE 85/ Projekt Sicherheitsstudien Entsorgung (PSE)
Abschlußbericht, Fachband 15, Hahn Meitner Institut für Kernforschung, Berlin, Januar 1985

/PUI 01/ Puigdomenech, I., Gurban, I., Laaksoharju, M., Luukkonen, A., Lofman, J., Pitkanen, P., Rhen, I., Ruotsalainen, P., Smellie, J., Snellman, M., Svensson, U., Tullborg, E.-L., Wallin, B., Vuorinen, U., Wikberg, P.
Hydrochemical stability of groundwaters surrounding a spent nuclear fuel repository in a 100,000 year perspective. Posiva Report No. 2001

/PUS 82/ Pusch, R.
Mineral–water interactions and their influence on the physical behavior of highly compacted Na–bentonite. Canadian Geotechnical Journal, 19: 381–387

/PUS 87/ Pusch, R., Hokmark, H., Borgesson, L.
Outline of Models of Water and Gas Flow through Smectite Clay Buffers. Swedish Nuclear Fuel and Waste Management Co., SKB Tech. Rept. TR 87-10, Stockholm, 1987

/REE 82/ Reed, M. H.,
Calculation of multicomponent chemical equilibria and reaction processes in-systems involving minerals, gases and aqueous phase, Geochim. Cosmochim. Acta, v. 46, 1982, p.513-528

/ROD 99/ Rodwell, W.R., Harris, A.W., Horseman, S.T., Lalieux, P., Müller, W., Amaya L.O., Pruess K.
Gas Migration and Two-Phase Flow trough Engineered and Geological Barriers for a deep Repository for Radioactive Waste, AENNEA, EUR 19122, 1999

/ROM 95/ Romero, L.; Moreno, L.; Neretnieks, I.
Movement of a redox front around a repository for high-level nuclear waste Source: *Nuclear Technology*, v 110, n 2, 238-49, May 1995

/RÖH 97/ Röhlig, K.-J., Becker, A., Fischer, H., Hofer, E., Kloos, M., Krzykacz, B., Martens, K.-H.,
Evaluation of Elements Responsible for the effective Engaged dose rates associated with the final Storage of radioactive waste: Everest project – Vol-

ume 3a: Salt formation, site in Germany, EUR 17449/3a EN, ISSN 1018-5593, 1997

/ROT 10/ Rothfuchs, T., Buhmann, D., Zhang C. L.
Long-term safety analysis and model validation through URL research Journal of Rock Mechanics and Geotechnical Engineering. 2010, 2 (1): 32–38

/RÜB 07/ Rübel, A.
Gase in einem HAW-Endlager in Salz – Die Perspektive der Langzeitsicherheitsanalyse, GRS-Gas-Workshop, Berlin, 2007

/SAF 03/ Radioactive Waste Management SAFIR 2:
Belgian R&D Program on the Deep Disposal of High-level and Long-lived Radioactive Waste: An International Peer Review, OECD Publishing, 2003

/SAM 03/ Samper, J, Yang, C, Montenegro, L.
User's manual of CORE2D version 4: A Code for groundwater flow and Reactive solute transport. Universidad de A Corun˜ a, A Corun˜a, Spain 2003

/SAM 06a/ Samper, J, Zhang, G, Montenegro, L.
Coupled microbial and geochemical reactive transport models in porous media: formulation and application to synthetic and in situ experiments. J IberGeol 32(2):211–217(2006)

/SAM 06b/ Samper, J, Yang, C.
Stochastic analysis of transport and multicomponent competitive monovalent cation exchange in Aquifers. Geosphere 2:102–112, 2006

/SAV 02/ Savage, D, Noyb, D, Miharac, M.
Modeling the interaction of bentonite with hyperalkaline fluids. Appl Geochem 17, 2002, p.207–223

/SMA 02/ Smailos, E., Cuiiado, M.A., Azkarate, I., Kursten, B., Marx, G.
Long-Term Performance of Candidate Materials for HLW/Spent Fuel Disposal Containers FZKA 6706, Forschungszentrum Karlsruhe GmbH, Karlsruhe 2002

/SOL 03/ Soler, J. M.
Reactive transport modeling of the interaction between a high-pH plume and a fractured marl: the case of Wellenberg Applied, Geochemistry 18, 2003, p. 1555–1571

/SON 94/ Sonnenthal, E., Ortoleva, P. J.
Numerical simulations of overpressured compartments in sedimentary Basins, *Basin Compartments and Seals*. Ortoleva, P.J., ed., AAPG Memoir v.

61, p. 403-416, Tulsa, Oklahoma, American Association of Petroleum Geologists, 1994

/SON 01/ Sonnenthal, E.L., Spycher, N.F., Apps, J., Conrad, M.
A Conceptual Model for Reaction-Transport Processes in Unsaturated Fractured Rocks at Yucca Mountain: Model Validation using the Drift Scale Heater Test, LBNL-48292 Abs. Eleventh Annual V.M. Goldschmidt Conference, Hot Springs, Virginia, May 19– 24.Lawrence Berkeley National Laboratory, Berkeley, CA, 2001

/SPY 88/ Spycher, N. F., Reed, M. H.
Fugacity coefficients of H2, CO2, CH4, H2O and of H2O-CO2- CH4 mixtures: A virial equation treatment for moderate pressures and temperatures applicable to calculations of hydrothermal boiling, *Geochim. Cosmochim. Acta*, v. 52, 1988, p. 739- 749

/SPY 03/ Spycher, N.F., Sonnenthal, E.L., Apps, J.A
Fluid flow and reactive transport around potential nuclear waste emplacement tunnels at Yucca Mountain, Nevada Journal of Contaminant Hydrology 62–63, 2003, p. 653– 673

/SPY 05/ Spycher, N., Pruess, K.
CO2-H2O Mixtures in the Geological Sequestration of CO2. II. Partitioning in Chloride Brines at 12–100 °C and up to 600 bar, Geochim. Cosmochim. Acta, Vol. 69, No. 13, 2005, pp. 3309–3320, doi:10.1016/j.gca., 2005.01.015

/SRI 02/ Sridharan, A., Choudhury, D.
Swelling pressure of sodium montmorillonites, Source: *Geotechnique*, v 52, n 6, August 2002, p. 459-462,

/STE 94/ Steefel, C. I., Lasaga, A. C.
A coupled model for transport of multiple chemical species and kinetic precipitation/dissolution reactions with applications to reactive flow in single phase hydrothermal system, *Am. J. Sci.*, v. 294, 1994, p. 529-592

/STE 98/ Steefel, C.I, Lichtner, P.C.
Multicomponent reactive transport indiscrete fractures: II: infiltration of hyperalkaline groundwater at Maqarin, Jordan, a natural analogue site. J Hydrol 209:200–224, 1998

/STE 05/ Steefel, C. I., DePaolo, D. J., Lichtner, P.C.
Reactive transport modeling: An essential tool and a new research approach for the Earth sciences, v 240, n 3-4, December 15, 2005, p. 539-558

/TAU 00/ Taubald, H., Bauer, A., Schäfer, H., Geckeis, H., Satir, M., Kim, J., Experi mental investigations of the effect of high-pH solutions on the opalinus shale and the Hammerschiemiede Smectite, Clay Minerals, 35, 515-524, 2000

/THE 10/ http://www.thereda.de, 2010

/TRI 04/ Tripathy, S., Sridharan, A., Schanz, T.
Swelling pressures of compacted bentonites from diffuse double layer theory Can. Geotech. J. 41, 2004, p. 437–450

/VAL 81/ Valocchi, A.J., Street, R.L., Roberts, P.V.
Transport of ion-exchanging solutes in groundwater: chromatographic theory and field simulation, Water Resour. Res. 17, 1981, p. 1517– 1527

/VAU 87/ Vaughan, P. J.
Analysis of permeability reduction during flow of heated, aqueous fluid through Westerly Granite, in C.F. Tsang (ed.), Coupled processes associat-ed with nuclear waste repositories, , Academic Press, New York, 1987, pp. 529-539

/VER 88/ Verma, A., Pruess, K.
Thermohydrological Conditions and Silica Redistribution Near High-Level Nuclear Wastes Emplaced in Saturated Geological Media
Journal of Geophysical Research, 93 (B2),1988, pp. 1159 – 1173

/WOL 92/ Wolery, T.J
EQ3NR, A Computer Program for Geochemical Aqueous Speciation Solubili-ty Calculations: Theoretical Manual, Version 7.0, Sept 1992

/WOL 03/ Wolery, T.J., Jarek, R.L.
EQ3/6, Version 8.0, Software User's Manual, Software Document Number 10813-UM-8.0-00, *U.S. Department of Energy*, Office of Civilian Radioactive Waste Management, Office of Repository Development, 1261 Town Center Drive, Las Vegas, Nevada 89144, 2003

/WOL 04/ Wolery, T., Jove-Colon, C., Rard, J., Wijesinghe, A.
Pitzer Database Development: Description of the Pitzer Geochemical Ther-modynamic Database data0.ypf. Appendix I in In-Drift Precipitates/Salts Model (P. Mariner) Report ANL-EBS-MD-000045 REV 02. Bechtel SAIC Company, Las Vegas, Nevada, 2004

/XUT 99/ Xu, T., Pruess, K., Brimhall, G.
An improved equilibrium-kinetics speciation algorithm for redox reactions in variably saturated flow systems, *Computers & Geosciences,* v. 25, 1999, p. 655-666

/XUT 01a/ Xu, T., Sonnenthal, E., Spycher, N., Pruess, K., Brimhall, G., Apps, J.
Modeling multiphase non-isothermalfluid flow and reactive geochemical transport in variably saturated fractured rocks: 2. Applications to supergene copper enrichment and hydrothermal flows. Am. J. Sci. 301, 2001, p. 34– 59

/XUT 01b/ Xu, T., Pruess, K.
Modeling multiphase fluid flow and reactive geochemical transport invariably saturated fractured rocks: 1. Methodology, *Am. J. Sci.*, v. 301, 2001b, p. 16-33

/XUT 04/ Xu, T., Sonnenthal, E., Spycher N., Pruess K.
Toughreact User's Guide, Berkeley National Laboratory, Berkeley, Calif. 2004

/YAB 98/ Yabusaki, S.B., Steefel, C.I., Wood, B.D.
Multidimensional, multicomponent subsurface reactive transport in nonuniform velocity fields: code verification using an advective reactive stream tube approach, J. Contam. Hydrol. 30, 1998, p. 299– 331

/YAN 08/ Yang, C., Samper, J., Montenegro, L.
A coupled non-isothermal reactive transport model for long-term geochemical evolution of a HLW repository in clay Environ Geol. 53, 2008, p. 1627–1638

/YEH 89/ Yeh, G.T., Tripathi, V.S.
A critical evaluation of recent developments in hydrogeochemical transport models of reactive multichemical components, Water Resour. Res. 25, 1989, p. 93– 108

/YON 92/ Yong, R.N., Mohamed, A.M.O.
A study of particle interaction energies in wetting of unsaturated expansive clays, Canadian Geotechnical Journal, 29, 1992, p.1060–1070

/ZHA 93/ Zhang, F.; Zhang, Z. Z.; Low, P. F.; Roth, C. B.
The effect of temperature on the swelling of montmorillonite, Clay Min. (28), 1993, 25-31:

/ZHA 04/ Zhang, C.L., Rothfuchs, T., Moog, H., Dittrich, J., Müller, J.
Thermo-Hydro-Mechanical and geomechanical behaviour of the callovo-oxfordian argillite and the Opalinus clay, GRS-202 Report, June 2004

/ZHA 06/ Zhang, G., Spycher, N., Xu, T, Sonnenthal, E., Steefel, C.
Reactive Geochemical Transport Modeling of Concentrated Aqueous Solutions: Supplement to TOUGHREACT User's Guide for the Pitzer Ion-Interaction Model, LBNL 62718, December 2006

VERTEILER

ISTec

Geschäftsführer	(WUR)	1 x
Abteilung 112	(GRD, MUW)	je 1 x
KIT		4 X
Gesamtauflage		**7 Exemplare**